Quantifying the OH radical by global scale NMHC measurements from the NOAA – ESRL cooperative flask sampling network

Dissertation zur Erlangung des Grades
“Doktor der Naturwissenschaften”

Am Fachbereich: Chemie, Pharmazie und Geowissenschaften
der Johannes Gutenberg – Universität in Mainz

Jan Pollmann

geboren am 29.März 1978 in Osnabrück

Mainz den 25.6.2007

Table of Contents:

1 Introduction

The overall aim of this thesis is to improve our understanding of the global distribution of non-methane hydrocarbons (NMHC) in the atmosphere and study implications for the global oxidation chemistry. Particular emphasis is placed on assessing the global distribution of the main atmospheric oxidant: the hydroxyl radical (OH). This work focuses on reactive, non-oxygenated C2-C7 atmospheric NMHC. These compounds can yield insight into various atmospheric processes such as transport, source structure and oxidative chemistry. However, the global meridionally varying background distribution of most NMHC has been largely unknown. Therefore, the scientific understanding of the earth's atmosphere can be significantly enhanced by the knowledge of the global distribution of the most important NMHC.

In this section we present a detailed overview of the current knowledge on atmospheric trace gases relevant to this thesis. The main sources of anthropogenic volatile organic compounds to the atmosphere are presented. We then describe the main atmospheric oxidation mechanisms and their implication for the NMHC budget. Furthermore, we describe the NOAA cooperative air sampling network which provided us with the air samples. Subsequently, a novel technique, based on the variability lifetime-relationship to estimate the 24 h average OH mixing ratio an air sample was exposed to during transport, is presented. Finally, the specific research aims and the outline of this thesis are detailed.

1.1 Non-methane hydrocarbons in the atmosphere

1.1.1 Sources

The natural to anthropogenic emission ratio for NMHC to the atmosphere was estimated to be approximately 2 (van Aardenne et al., 2001). However, biogenic emissions were mostly characterized by unsaturated, highly reactive species with lifetimes on the order of a couple hours (Guenther et al., 1999). Therefore, these species mostly have local effects on atmospheric chemistry. Anthropogenic NMHC emissions are usually dominated by saturated short-chained compounds with lifetimes on the order of several days (hexane) to months (ethane) (Atkinson, 1994). These species can impact atmospheric chemistry on a regional to hemispheric scale. The following sections will exclusively focus on the atmospheric chemistry of the long-lived anthropogenic C2-C7 organic trace gases since one of the primary scientific aims of this thesis is to determine the global distribution of these compounds.

The global anthropogenic non-methane hydrocarbon (NMHC) emissions to the atmosphere are dominated by fossil fuel usage, notably their evaporative loss and incomplete combustion. Natural and technical combustion processes such as internal combustion engines or furnaces are always incomplete to a certain degree. Reasons may include the lack of oxygen, low combustion temperatures or the residence time in the burning zone being too short. Minor emissions develop from fossil fuel exploitation and production, biofuel use as well as from anthropogenic biomass burning, the latter considering that most fires are human-induced (Singh et al., 2000). However, these minor processes may dominate the source structure of atmospheric NMHC in remote regions. A brief summary of NMHC emission sources to the atmosphere is shown in table 1.1. The main source regions for anthropogenic NMHC emissions are located in the mid-northern latitude region (30-60 °N) as the vast majority of industrialized countries are located. The emissions in this region are dominated by incomplete combustion of fossil fuels. Significant NMHC emissions from fossil fuel exploitation can be expected in the Arctic region as well as near the latitudinal region of the Tropic of Cancer (23.5 °N). Large biomass burning emissions periodically occur in the Arctic regions (Siberia, Canada and Alaska) as well as in tropical regions and Australia (Riano et al., 2007). Biofuel burning for energy production

becomes an important emission source for the developing countries mostly located south of the Tropic of Cancer. The dominant sink for all these species is reaction with the hydroxyl radical and is detailed in a later section.

Table 1.1: anthropogenic NMHC emission sources to the atmosphere

Compounds	Source	Reference
Acetylene and ethene	biomass burning	Singh et al., 2000
Acetylene	flaming combustion	Blake et al., 1996
C2-C5 alkanes	flare emissions	Kim et al., 2005
Ethane	natural gas cobustion	Na and Kim, 2001
Ethane	biofuel burning	Bertschi et al., 2003b
Ethane, propene	residual smoldering combustion	Bertschi et al., 2003a
Ethane, propane	leakage liquefied petroleum gas	Sahu and Lal, 2006
Ethane, propane	gas leakage	Yang et al., 2005
Ethane, propane	refinery	Kim et al., 2005
C2-C5 NMHC	motor vehicle exhaust	Kim et al., 2005
Ethene and 1,3-butadiene	fresh biomass burning plumes	Blake et al., 1996
Propane	fossil fuel production	Olivier et al., 1996
Propane	smoldering combustion	Blake et al., 1996
Propane	biomass burning	Gros et al., 2003, 2004
Propane, butane	natural gas burning	Mugica et al., 2001
Butane isomers	solid waste incineration	Leach et al., 1999
Butane isomers	gasoline evaporation	Lee et al., 2006
Isopentane	fossil fuel evaporation from cars	Hopkins et al., 2005
Isopentane	traffic	Tsai et al., 2006
Pentane isomers, butane	traffic	John, 1997
Pentane isomers, hexane	nontailpipe, evaporative loss	Lee et al., 2006
hexane and aromatics	traffic	Batterdam et al., 2002
Alkanes	long range pollution from oil exploration	Blake et al., 1992
Aromatic hydrocarbons	urban areas, gasoline usage	Christensen et al., 1999
Aromatic hydrocarbons	urban areas, gasoline usage	Derwent et al., 2000

1.1.2 Global distribution of NMHC

The current knowledge of the atmospheric distribution of NMHC is based on an integrated approach over a few long term NMHC measurements (e.g.: Gautrois et al., 2003, Hakola et al., 2006) and intensive field campaigns such as TOPSE (Blake et al., 2003). Rudolph (1995) compiled all available ethane data into a global meridionally and temporally resolved 3-D distribution. It was found that the global background distribution of reactive anthropogenic NMHC in the lower troposphere is dominated by two factors: 1. a large north-south gradient and 2. a distinct seasonal cycle anticorrelated to the seasonality of the hydroxyl radical (see section 1.2) which is hemispherically inversed (Rudolph, 1995, Gautrois et al., 2003).

Most anthropogenic NMHC are emitted in the northern hemisphere since the main part of the global energy consumption occurs in this region (see also table 1.1). Significant mixing ratios even for short-lived compounds were observed at very remote sampling stations e.g.: the Arctic (Gautrois et al., 2003). This source distribution was found to cause a large north south interhemispheric gradient (Rudolph, 1995, Bonsang and Boissard, 1999). This gradient was found to be higher for shorter-lived species such as pentane isomers than for longer-lived species such as ethane (e.g.: Gautrois et al., 2003, Rudolph, 1995). Rudolph (1995) found that a significant source of longer-lived NMHC in the southern hemisphere is interhemispheric transport smoothing the interhemispheric gradient for these species. In the month of December, interhemispheric ratios of 20 (ethane) and 30 (propane) were observed (Boissard et al., 1996).

The seasonal cycle of atmospheric NMHC was linked exclusively to the seasonality of the hydroxyl radical distribution (Goldstein et al., 1995). Northern hemispheric maximum NMHC mixing ratios were observed during late winter and minimum mixing ratios during late summer (Gautrois et al., 2003, Hakola et al., 2006). The seasonal amplitude (latitudinal maximum/minimum) was highest in the mid northern latitudes and lowest near the equator (Bonsang and Boissard, 1999). The southern hemispheric seasonal amplitude compared to the northern hemisphere was lower due to the presence of less continental sources and the existence of some interhemispheric transfer (Rudolph, 1995).

However, the understanding of NMHC distribution is limited; no coherent datasets with high regional and temporal resolution are available. Researchers to date have to rely on several individual datasets and need to account for instrumental and calibration bias (Apel et al., 2003, Plass Dülmer et al., 2006). A global NMHC sampling network relying on a single instrumental and calibration method was therefore desired to further investigate the atmospheric distribution of NMHC as well as the contribution of these species to atmospheric oxidation chemistry (Krol and Lelieveld, 2003, WMO report, 1995).

1.2 Atmospheric oxidation chemistry

Reaction with the hydroxyl radical (OH) is the dominant sink for light, saturated atmospheric NMHC. This section describes the atmospheric chemistry of the OH radical and its global distribution. The atmospheric chemistry of other oxidants (nitrate and halogen radicals as well as ozone) will also be presented.

1.2.1 Hydroxyl radical chemistry

The OH radical formation is initiated by the photolysis of ozone and subsequent reaction of the oxygen radical with water vapor (rct. 1.1 a, b).

$$O_3 \xrightarrow{h\nu} O(^1D) \qquad \text{rct. 1.1a}$$

$$O(^1D) \xrightarrow{H_2O} OH \text{ ; yield: < 10\%} \qquad \text{rct. 1.1b}$$

The $O(^1D)$ radical is very instable and the majority of $O(^1D)$ radicals is quenched to the ground state $O(^3P)$ by air molecules to reform O_3 (Lelieveld et al., 2004). The OH yield of reaction 1b is therefore strongly dependent on atmospheric humidity. Additional minor sources include the ozonolysis of unsaturated NMHC such as pentene, methylcyclohexene or biogenic VOC with OH fractional yields close to 1 (Atkinson and Aschmann, 1993, Atkinson et al., 1995, Faloona, 2001). Further radical sources develop from the photolysis of ketones such as acetone (Atkinson et al., 1989). The atmospheric cycle of the hydroxyl radical is presented in figure 1.1. The atmospheric oxidation of methane by reaction with the hydroxyl radical (Ehhalt et al., 1991) is shown exemplarily in rct. 1.2a – f.

$$CH_4 + \cdot OH \xrightarrow{O_2} CH_3O_2 \cdot + H_2O \qquad \text{rct. 1.2a}$$

$$CH_3O_2 \cdot + NO \longrightarrow CH_3O \cdot + NO_2 \qquad \text{rct. 1.2b}$$

$$CH_3O \cdot + O_2 \longrightarrow HCHO + HO_2 \cdot \qquad \text{rct. 1.2c}$$

$$HO_2 \cdot + NO \longrightarrow \cdot OH + NO_2 \qquad \text{rct. 1.2d}$$

$$2(NO_2 \xrightarrow{h\nu} NO + O) \qquad \text{rct. 1.2e}$$

$$2(O + O_2 + M \longrightarrow O_3 + M) \qquad \text{rct. 1.2 f}$$

$$CH_4 + 4O_2 + 2h\nu \longrightarrow HCHO + 2O_3 + H_2O \qquad \text{net}$$

The OH radical reacts with carbon monoxide, methane and NMHC to water and an organic peroxy radical (rct. 1.2a). The peroxy radical forms an oxygenated radical via reaction with NO (rct. 1.2b). The methane oxidation product is formaldehyde which is formed by oxidation of the oxygenated radical with molecular oxygen under the formation of HO_2 (rct. 1.2c). The conversion of HO_2 to OH occurs via reaction of HO_2 with ozone or NO (rct. 1.2d).

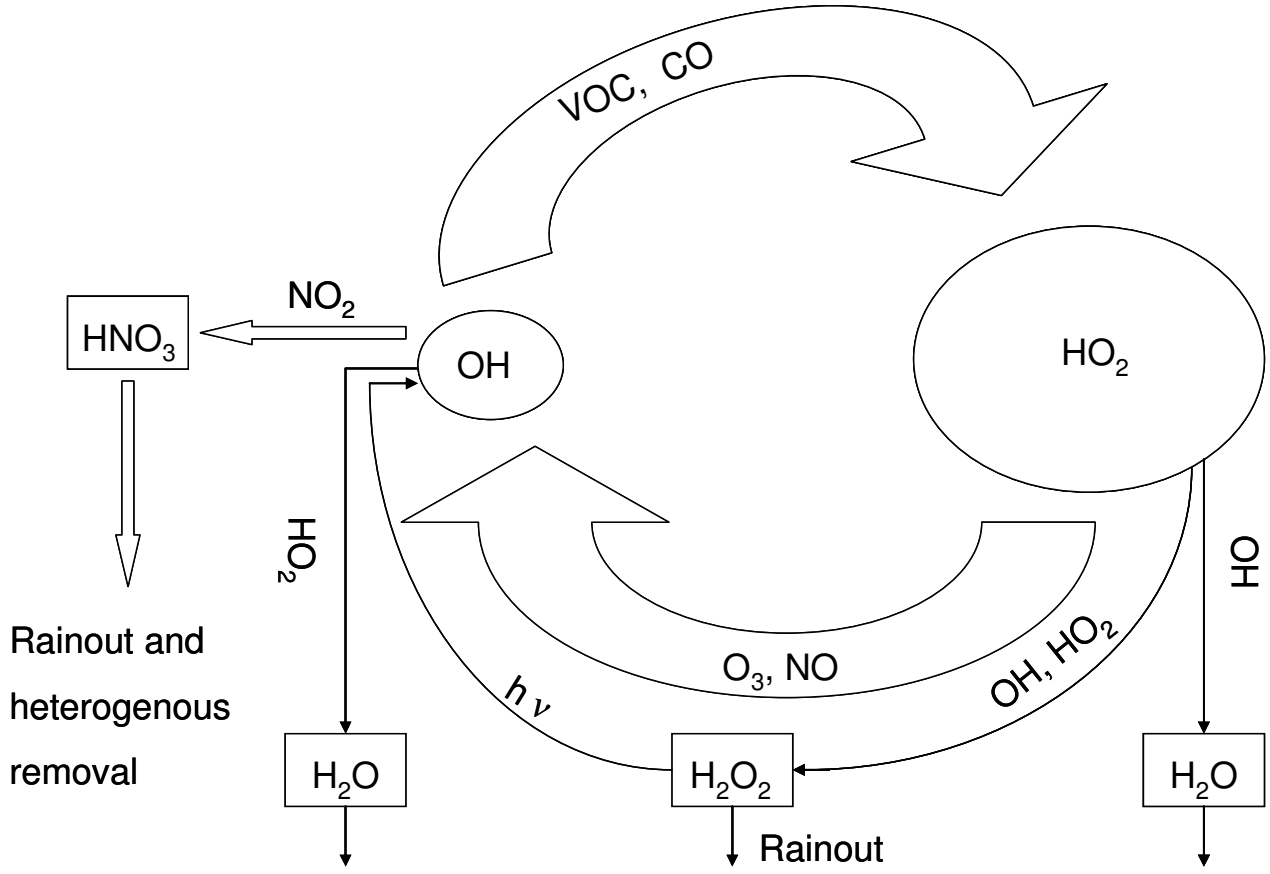

Figure 1.1: atmospheric OH cycle (Ehhalt et al., 1991). Thick arrows represent dominant processes; small arrows minor processes; OH formation by reactions 1a, b is not shown to improve figure readability

Atmospheric OH is in equilibrium with HO_2 with HO_2 being more abundant by approximately a factor of 100. The net atmospheric oxidation products of methane in the presence of NO are formaldehyde and two ozone molecules. Further formaldehyde oxidation leads to additional ozone production and ultimately the oxidation of methane to CO_2. Similar oxidation pathways over the respective aldehydes (e.g.: propane oxidation product is acetone) are expected for most NMHC. The mean lifetime of OH with respect to reaction 1.2a was estimated to be on the order of 1s (Atkinson et al., 1994). The more stable peroxy radical represents the atmospheric reservoir for the hydroxyl radical.

1.2.2 OH distribution

Direct OH measurements are very elaborate and therefore expensive (Heard and Pilling, 2003). The global average OH mixing ratio was thus mostly determined by model calculations based on the removal of methyl-chloroform (CH_3CCl_3) from the atmosphere (Krol et al., 1998, 2003, Spivakovsky et al., 2000, Prinn et al., 2001). Local OH mixing ratio was found to be a direct function of photolytic active (actinic) radiation under conditions that are neither water- nor ozone-limited (Rohrer and Berresheim, 2006). OH formation is thus believed to be highest in tropical regions due to the high solar zenith angle and the reduced absorption of the actinic radiation by the ozone layer (Lelieveld et al., 2004). OH mixing ratios were shown to decline towards the polar region proportional to the available actinic radiation. Concentrations during polar summer and winter were estimated at ~ 5 10^5 molec cm^{-3} and < 10^5 molec cm^{-3} respectively.

Several direct measurements, taken during intensive field campaigns, generally confirm the model derived OH distribution by Spivakovsky et al. (2000) (see also chapter 4). However, tropical OH mixing ratios appear to be underestimated by the model compared to direct OH measurements (Brauers et al., 2001, Tan et al., 2001a). Additionally, atmospheric effects (e.g.: strong pollution → high NO) can significantly impact local OH mixing ratios. Polluted regions often exhibit elevated OH mixing ratio as high NO_x mixing ratios push the OH - HO_2 equilibrium towards high OH mixing ratios and contribute to ozone formation (George et al., 1999). Since global models integrate over large regions a high NO background is assumed over industrialized areas. In contrast, intensive field campaigns are usually conducted in remote regions (low NO → lower OH). Significant

differences between modeled and measured OH can be expected in these regions. Similarly, higher OH mixing ratios than predicted by the model (Spivakovsky et al., 2000) were discovered at Amundsen Scott South Pole station (Mauldin et al., 2001, 2004). These large OH mixing ratios were correlated to surprisingly high surface concentrations of NO. The NO build-up was probably related to a very shallow boundary layer at approximately 100 m above ground and very stable, stratified air. This effect cannot be reproduced by global models and may explain the differences between observations and model calculations.

The global average OH mixing ratio of approximately 10^6 molec cm^{-3} (Spivakovsky et al., 2000) is fairly well constrained. However, possible atmospheric trends in the hydroxyl radical distribution are currently disputed (Prinn et al., 2001, 2005, Lelieveld et al., 2004, 2006). The fundamental question appears to be the sensitivity of the OH budget (as presented in figure 1.1) towards anthropogenic or natural perturbations such as El Niño events, large volcanic eruptions and global climate change (Bousquet et al., 2005, Lelieveld et al., 2006).

1.2.3 Other oxidative reactions (nitrate, ozone, halogens)

The nitrate radical (NO_3) is produced by the reaction of NO_2 with ozone and is in equilibrium with nitrogen pentoxide (rct. 1.3a, b).

$$NO_2 + O_3 \longrightarrow NO_3 + O_2 \qquad \text{rct. 1.3a}$$

$$NO_2 + NO_3 \rightleftharpoons \qquad \text{rct. 1.3b}$$

However, this radical is photolyzed rapidly and reacts with NO (rct. 4a-c) so that typical daytime NO_3 mixing ratios are below 1 pptv (Atkinson, 1991, Platt and Heintz, 1994).

$$NO_3 + h\nu(\lambda < 700nm) \longrightarrow NO + O_2 \qquad \text{rct. 1.4a}$$

$$NO_3 + h\nu(\lambda < 580nm) \longrightarrow NO_2 + O \qquad \text{rct. 1.4b}$$

$$NO_3 + NO \longrightarrow NO_2 \qquad \text{rct. 1.4c}$$

NO_3 24h average mixing ratios were found to be up to 2 orders of magnitude higher than OH during parallel measurements of OH and NO_3 radicals at a marine boundary layer site in Crete (Vrekoussis et al., 2004). However, the reaction of nitrate with saturated NMHC is typically 5 orders of magnitude slower than the reaction with OH (Atkinson, 1994). Consequently nitrate chemistry can probably be considered negligible compared to NMHC oxidation by OH, especially in remote NO_x-poor environments.

The third major atmospheric oxidant is ozone. Ozone chemistry is limited to reactions of ozone with unsaturated NMHC and even these reactions are generally significantly slower than the reaction with OH and therefore negligible (Atkinson, 1994). However, tropospheric ozone formation is closely related to the availability of atmospheric VOC (volatile organic carbon) (presented in a simplified mechanism in rct. 1.5a-d).

$$NO_2 + h\nu \longrightarrow NO + O \qquad \text{rct. 1.5a}$$

$$O + O_2 + M \longrightarrow O_3 + M \qquad \text{rct. 1.5b}$$

$$O_3 + NO \longrightarrow NO_2 + O_2 \qquad \text{rct. 1.5c}$$

$$RO_2 \cdot + NO \longrightarrow NO_2 + RO \cdot \qquad \text{rct. 1.5d}$$

The conversion of NO to NO_2 as shown in rct. 1.5d (and also rct. 1.2b) limits the removal of ozone by reaction with NO. Rapid ozone production as seen for industrialized, urban areas is only possible under high NO_x and high VOC conditions.

Bromine and chlorine radicals play an important role in the arctic troposphere during the period of the polar sunrise (Jobson et al., 1994). It was suggested that photolabile halogen species (particularly Br_2 and BrCl) are emitted to the atmosphere from sea ice at the onset of the arctic summer. Significant decrease of NMHC mixing ratios was observed (e.g. Ramacher et al., 1999, Boudries and Bottenheim, 2000). However, further research indicated that this depletion is only of importance in coastal areas and therefore no significant effect on the global NMHC distribution is expected (Swanson et al., 2003). In contrast, it was suggested that Cl radical chemistry may have significant impact on the atmospheric oxidation of NMHC comparable to OH (Pszenny et al., 2007, Arsene et al., 2007).

1.3 NOAA – ESRL cooperative air sampling network

The Global Monitoring Division (GMD) of NOAA – ESRL (National Oceanic and Atmospheric Administration – Earth Systems Research Laboratory) operates a global flask sampling network to provide essential constrains to our understanding of the global carbon cycle. In addition to the flask network four in-situ observatories as well as several routine aircraft projects are in progress. Measuring NMHC from the network flasks could generate the regional and temporally resolved measurements desired by the WMO report, 1995 and Krol and Lelieveld, 2003. In this section a first description of the cooperative sampling network is given. Details on the quantification of the individual flask samples are given in chapter 5.

The NOAA cooperative flask sampling program began in 1967 with regular flask sample collection at the Niwot Ridge high altitude research side (lat: 40.02 °N, long: 105.34 °W, alt: 3345 m asl). The number of cooperative flask sampling stations has increased to 69 since then. Most network stations are located in remote regions. However, a few stations can be found in polluted regions of the continental United States, central Europe and in the People's Republic of China. Flask samples are only taken under pre-defined clean air conditions. The sampling of freshly polluted air is therefore highly unlikely and the datapoints are generally expected to represent meridionally representative background mixing ratios.

NMHC are currently quantified from air samples collected at 40 individual stations (figure 1.2). Of these stations 37 were considered for this work; three were added too recently (2 locations in Mexico and Easter Island). The selection of the stations was performed following recommendations by the WMO report, 1995. Particular attention was also placed on achieving a good latitudinal coverage (from 82°N, Alert, Canada to 90°S Amundsen Scott Station, South Pole) see also figure 1.3.

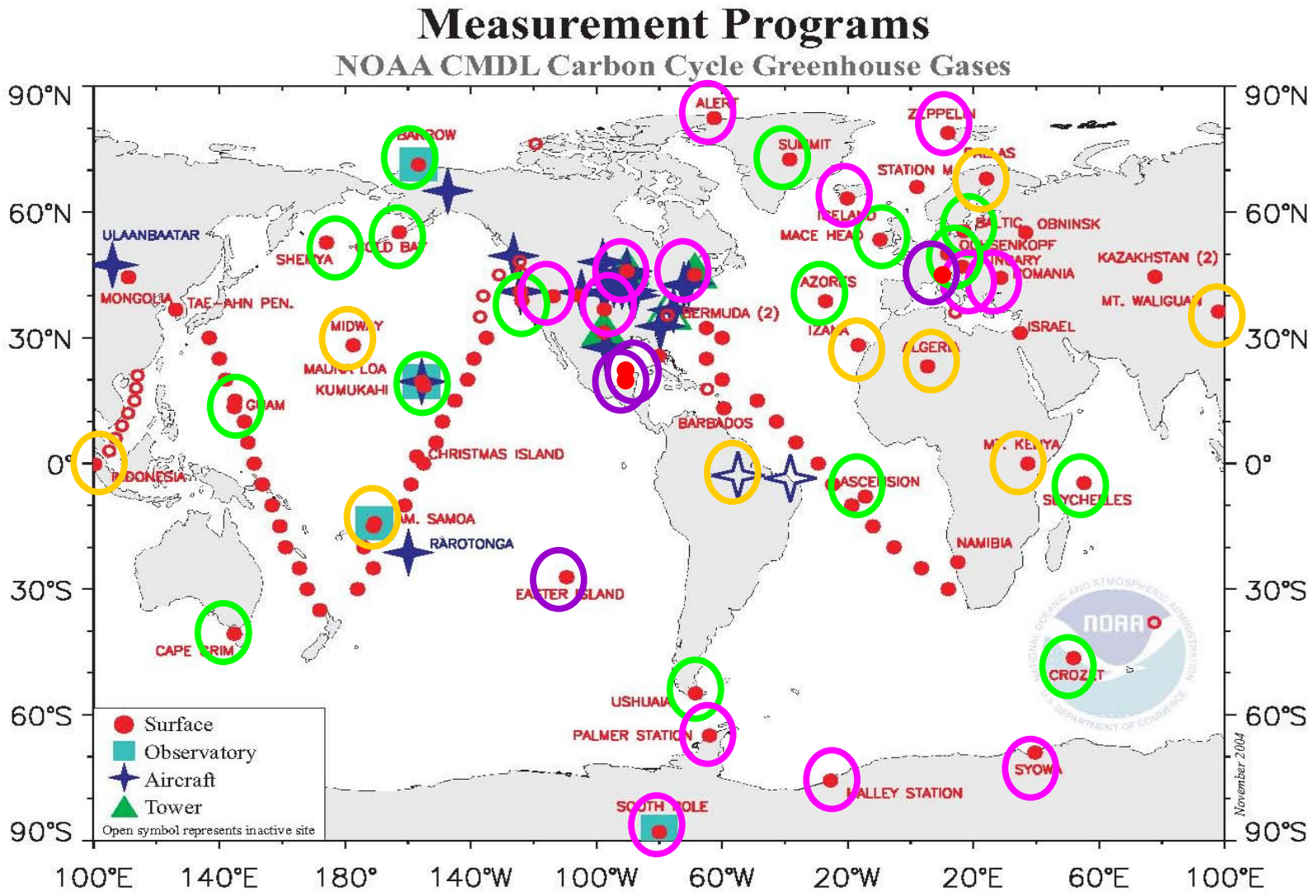

Figure 1.2: the NOAA cooperative air sampling network, red points: flask sampling sites; circled points NMHC measurements, green circles: NMHC measurements since March 2005; pink circles: since November 2005; orange circles: sampled since February 2006; purple circles: added May 2006

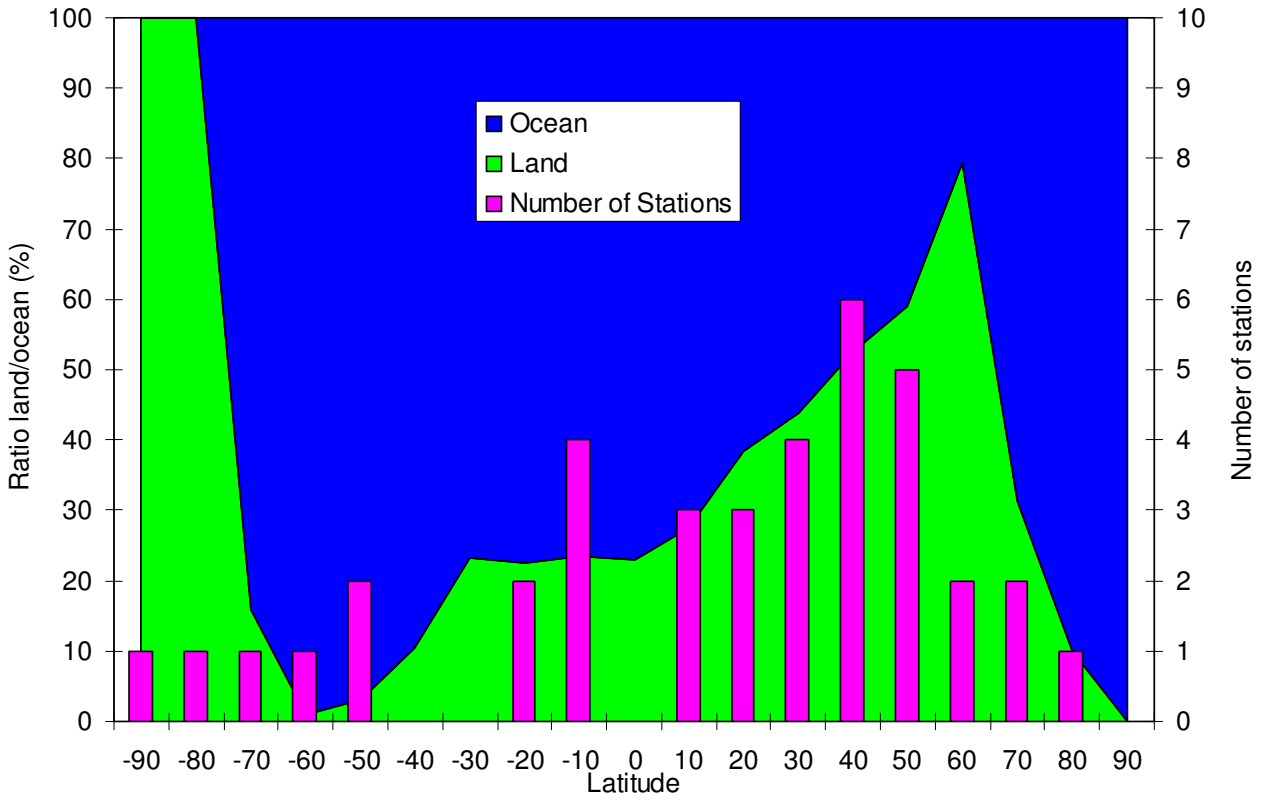

Figure 1.3: Latitudinal distribution of sampling stations, purple bars: number of sampling stations, blue area: percentage of sea, green area: percentage of landmass

1.4 Variability analysis

The relationship between the lifetime of atmospheric trace gas and their mixing ratio variability was first recognized by Junge (1974). He described this relationship with an empiric equation:

$$RSD = 0.14\ \tau^{-1} \qquad \text{eq 1.1}$$

where RSD is the relative standard deviation and τ is the atmospheric residence time in years. This equation was successfully applied to estimate the atmospheric lifetimes of long-lived trace gases (e.g.: Panshin and Hites, 1994, Thornton et al., 1996). In a model study on Junge's work Hamrud (1983) concluded that the τ^{-1} relationship was only approached

for very long-lived species and that shorter lived species follow a $\tau^{-0.72}$ dependence. However, this work demonstrated that a different equation is necessary to evaluate the variability lifetime relationship for short lived species such as NMHC. Initial improvements regarding this problem were achieved by considering the statistics of an exponentially decaying function for the atmospheric evolution of the hydrocarbons (Jaenicke, 1982 and Slinn, 1988). However, a clear relationship was not found until Jobson et al. (1998) substituted the relative standard deviation with the standard deviation of the natural logarithms of all data points: σ(ln(X)).

Hydrocarbon mixing ratios in a given air sample decline with respect to OH oxidation according to

$$\ln\left(\frac{X_t}{X_0}\right) = -\frac{t}{\tau} \qquad \text{eq. 1.2}$$

With *t* the time between emission and sampling, τ, the 1/e lifetime and X_0, the initial mixing ratio. When regarding a hydrocarbon data set sampled at the same location under the assumption of constant source (constant X_0) and variable *t* the variance over the long term is given by

$$\sigma_y^2 = \left(\frac{\partial}{\partial t}\ln\left(\frac{X_t}{X_0}\right)\right)^2 \sigma_t^2 = \left(\frac{-1}{\tau}\right)^2 \sigma_t^2 \qquad \text{eq. 1.3}$$

Assuming that the lifetime **T** is constant over the transport path the equation reduces to

$$\sigma_y = s_{\ln x} = \frac{1}{\tau}\sigma_t \qquad \text{eq. 1.4}$$

It can be seen that the *ln*-transformed standard deviation over the data set is inversely proportional to the 1/e lifetime under chemical kinetic conditions. An empirical comparison with measurement data from multiple campaigns showed that equation 5 solves the relationship (Jobson et al., 1998).

$$\sigma(\ln(X)) = A\,\tau^{-b} \qquad \text{eq. 1.5}$$

with: σ(ln(X)), the standard deviation over the natural logarithm of all measurement, τ, the atmospheric lifetime, *A* and *b*, proportionality factors.

A similar relationship was also found by Ehhalt et al. (1998) based on model calculations. Further research (Jobson et al., 1998, 1999) showed a clear relationship between the variability – lifetime relationship and the remoteness of the measurement station from pollution sources. A graphic explanation of this behavior is displayed in figure 1.4a, b.

In case of a measurement station in close proximity to local emission sources such as an urban site no relation between atmospheric lifetime and variability can be found (figure 1.4a). The atmospheric variability is completely dominated by the sources and not proportional to the atmospheric lifetime. The *b* factor from equation 1.5 is then close to 0.

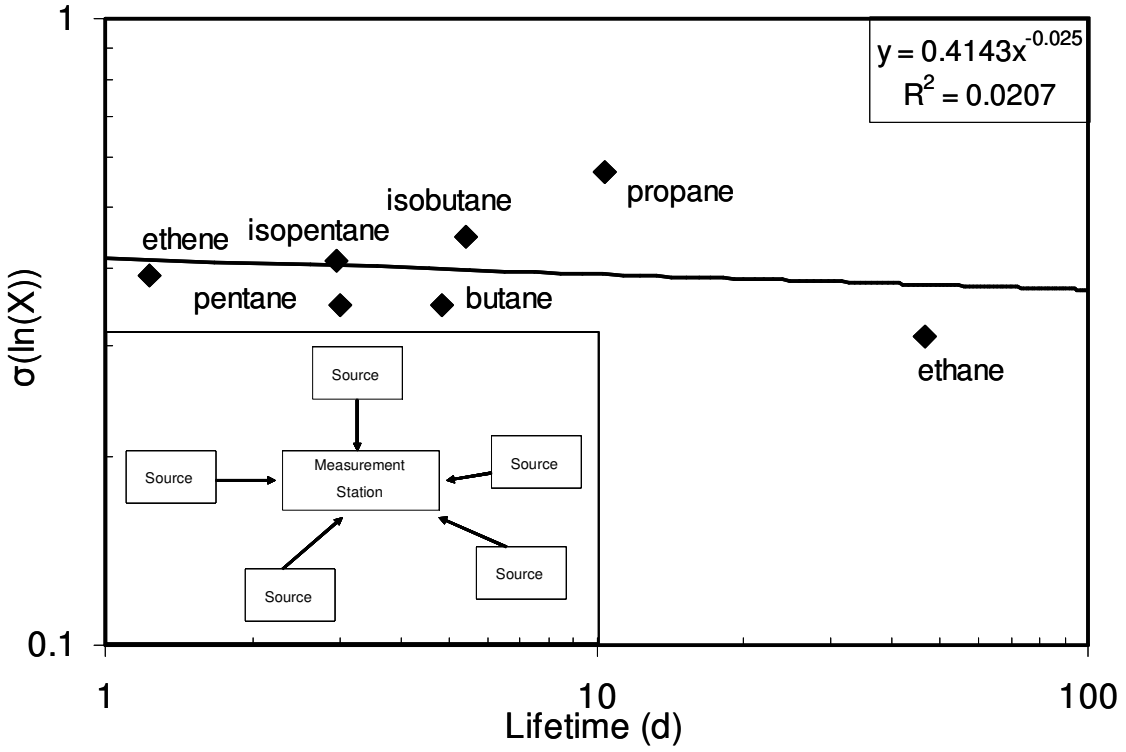

Figure 1.4a: Typical variability – lifetime plot for the inset urban source distribution

In contrast, the variability at a remote measurement station (figure 1.4b) is dominated by the chemical sink i.e. reaction with the OH radical for NMHC. Compounds with high reactivity towards OH (pentane isomers) are therefore usually found at a higher variability than longer lived species (ethane). Several measurement and model studies (Jobson et al., 1998, 1999, Ehhalt et al., 1998) found that remote stations are characterized by a *b* factor of 0.5 or higher.

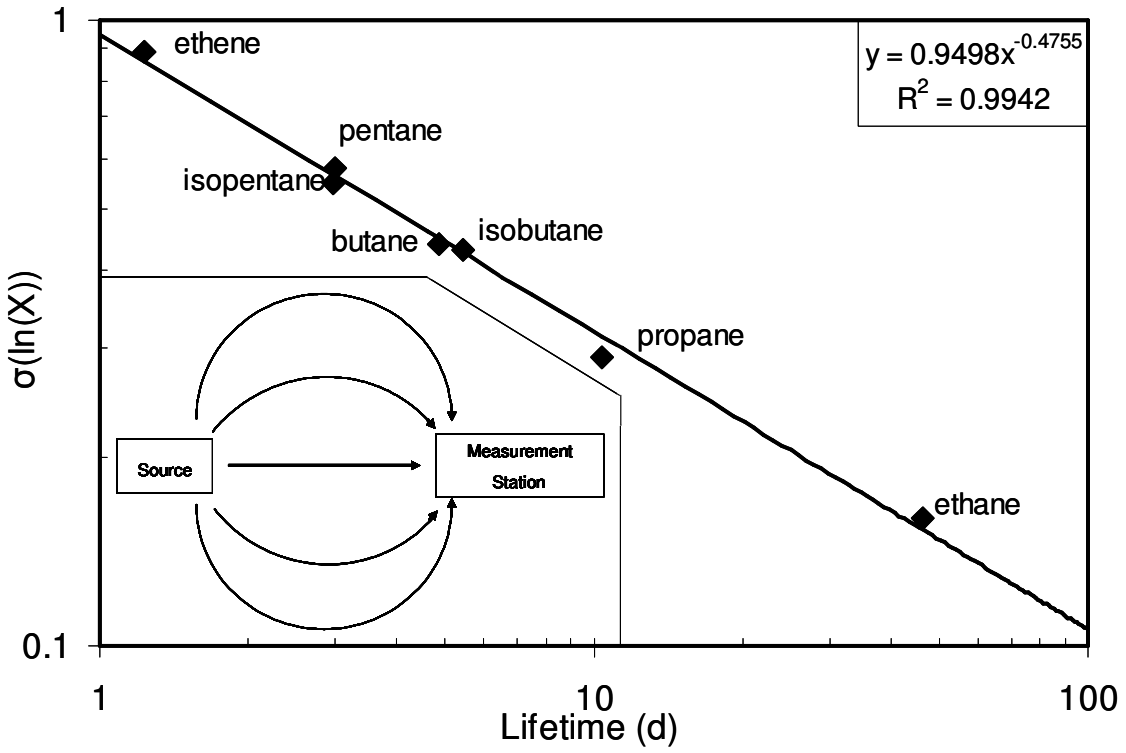

Figure 1.4b: typical variability – lifetime plot for the inset remote source distribution

The *A* factor has not yet been thoroughly understood. However, Karl et al. (2001) linked this proportionality factor to the age range of an airmass. A high *A* factor was thought to represent sampled air of vastly different photochemical ages and a low *A* factor would represent an airmass that was subject to homogenous age distribution.

In addition to the above described application, one can use the variability analysis to assess the average OH mixing ratio an air sample was exposed to (Williams et al., 2000, Karl et al., 2001, Bartenbach et al., 2007). The variability – lifetime relationship for two sets of gases needs to be known to successfully apply this method: 1, the variability of several

compounds with an atmospheric sink solely depending on OH (e.g. NMHC); 2, the variability of at least one compound with similar sources but an independent atmospheric sink. The atmospheric lifetime of the compounds needs to be known with high accuracy. Williams et al. (2000) and Karl et al. (2001) used photochemically active trace gases (e.g. acetone and methyl-vinyl ketone), which are removed from the atmosphere by both photolysis and reaction with OH. Williams et al. (2001) used Rn at a remote marine boundary layer site. Radon is emitted from the lithosphere and is removed from the atmosphere by radioactive decay.

The method is further detailed here using the example of Williams et al. (2001). The variability – lifetime relationships of an OH independent compound (Rn) is calculated. This relationship is then calculated for all NMHC (OH dominant sink) assuming arbitrary OH mixing ratios. The data can then be plotted as shown in the inset of figure 1.4 b assuming arbitrary lifetimes and the well known literature lifetime for Rn. A regression function according to eq. 1.5 can then be derived.

The OH mixing ratio is then modified, changing the NMHC lifetime, consequently shifting the variability – lifetime ratios for NMHC along the X axis. However, the Rn variability – lifetime relationship remains unchanged as its lifetime does not depend on OH. This change in NMHC lifetime will result in a different data point distribution and hence a different function. Statistical methods such as the least square method can then be used to determine the function with the least discrepancy of the function to the observed data. The OH mixing ratio corresponding to these NMHC lifetimes can thus be estimated to represent the average OH mixing ratio a sample was exposed to during the transport to the measurement station. Similar to Rn other compounds with OH independent sinks can be used in this method e.g.: photolytically active compounds, CFCs or sulfur hexafluoride (this study).

This method was validated by comparison of the variability derived OH mixing ratios with literature data by Spivakovsky et al. (2000). Generally good agreement (better than 50%) given the limitations of this method was found (Karl et al., 2001, Williams et al., 2001). Bartenbach et al. (2007) compared their variability derived OH mixing ratio with in-situ OH measurements at the same station. Again good agreement between both methods was found (<40%). These comparisons suggest that OH determination by variability analysis is a valid method as long as the limitations are taken into account (see also

chapter 5). The derived OH mixing ratio does not represent the local OH concentration but rather the diel average mixing ratio a sample was exposed to during its transport.

1.5 Thesis outline

The focus of this work is to examine the global distribution of non-methane hydrocarbons (NMHC). This knowledge is subsequently applied to improve our understanding of atmospheric oxidation chemistry and particularly on the global distribution of the hydroxyl radical. To meet this aim we were given access to flask samples collected by the NOAA-GMD (National Oceanic and Atmospheric Administration-Global Monitoring Division) cooperative air sampling network. These samples were made available after the routine greenhouse gas and stable isotope measurements were completed. Several challenges had to be overcome to utilize the remaining air left in the sampling flasks. At the time the flasks are available to us they contain only a limited volume of air at subambient pressure. Turnaround time of the flask samples was expected to be low as the flask logistics of the cooperative air sampling network should not be affected. A high sample throughput was expected after an initial test-phase and expensive consumables such as liquid nitrogen were to be avoided. The distinct research objectives were:

1. The development of a gas-chromatographic flame – ionization (GC – FID) system capable to meet the above challenges, especially focusing on designing a highly automated system with high sample throughput at low operational costs.

2. Evaluate potential analytical interferences by other trace gases particularly ozone and atmospheric water vapor

3. The establishment of a reproducible calibration for this instrument and the evaluation of analytical parameters (accuracy and precision) with particular emphasis on intercomparisons with other laboratories

4. Obtaining a full year of NMHC measurements from the network flasks with extensive meridional coverage to assess the global distribution of the most important NMHC

5. Evaluate the measurements with respect to atmospheric oxidation chemistry applying analytical techniques such as the variability analysis

In chapter 2 we address the first research objective, the instrumental development. Here we present the instrumental development with the focus on evaluating adsorbent materials for the cryogen free analysis of C2-C6 non-methane hydrocarbons, meeting one of the key analytical challenges described above. Nine solid adsorbents were investigated for their ability to trap and release C2-C6 NMHC in atmospheric samples with subsequent GC-FID quantification. Two options were found either a three – stage, multi – adsorbent trap (Carboxen 1016, Carboxen 563, Carbosieve SIII) or a single stage trap (Carboxen 1000). A detection limit of 3 pptC and a linear response over a wide volatility and sample volume range was obtained.
Water was found to cause major interference in the solid adsorption and subsequent chromatographic processes addressing research objective 2. A method to selectively remove water vapor from the sampling air was developed. This trap allowed for quantitative and reproducible results for all compounds at all investigated humidity conditions. Further investigation of major analytical interference is found in chapters 3 and 4.

In chapter 3 we investigate analytical techniques utilizing solid adsorbents for the quantification of biogenic volatile organic compounds (BVOC) with particular emphasis on ozone interference. Substantial analyte losses of 90% or more were discovered when co-sampling BVOC with ozone onto solid adsorbents. These loss rates were used to estimate the gas-phase reaction rate constants with ozone for 8 compounds and are the only known estimates to date. Four ozone mitigation techniques were tested and BVOC loss rates were reduced to less than 10% for most compounds. It was found that ozone interference is proportional to the number of double bonds in a molecule and therefore no substantial analytical interferences of ozone are expected when analyzing saturated C2-C6 NMHC, addressing the second major component of research objective 2.

Chapter 4 focuses on research objective 3. The analytical parameters accuracy and precision are investigated in depth and compared to the data quality objective presented by the World Meteorological Organization - Global Atmospheric Watch program (WMO-GAW; WMO report, 2007). We demonstrate that saturated C2 – C5 NMHC can be analyzed with a repeatability of 10 – 20% or better over more than one year. Samples were stable in the network flasks with mixing ratio changes of less than 5% over a period of one year. A significant overestimation of hexane could be associated to coelution of this compound with dichloromethane. A 4-month intercomparisons campaign with the in-situ GAW station at Hohenpeissenberg showed good agreement between both methods with 87% of all data comparison falling into the GAW data quality objective. The median measurement precision over all measurements was found at 0-5% for mixing ratios above 100 pptv and 0-10% for mixing ratios below 100pptv. Overall, approximately 88% of the data met the data quality objective for precision.

In chapter 5 we show the results of approximately 1.5 years of NMHC measurements from NOAA network flasks, addressing objective 5. The global background distribution of C2 – C4 saturated NMHC is presented in a 3-D grid with temporal and latitudinal resolution. These are, to our knowledge, the first distribution profiles derived with a single instrument for ethane and propane and the first ever profiles to be presented for isobutane and butane. This data was combined with trace gas measurements by NOAA CMDL to analyze the atmospheric variability – lifetime relationship. This relationship is then explored in a novel approach utilizing the variability of sulfurhexafluoride to determine the global distribution of the hydroxyl radical. Good agreement between our estimate and model calculations by Spivakovsky et al. (2000) and available direct OH measurement are found outside the tropical regions. Tropical OH concentrations estimated by the variability analysis appear to be significantly higher than available model calculations but agree well with direct OH measurements.

Finally, in chapter 6, the main conclusions of this work are summarized and an outlook onto future work with this dataset is given.

2 Evaluation of Adsorbent Materials for Cryogen – Free Trapping – GC Analysis of Atmospheric C2 - C6 Non-Methane Hydrocarbons

Abstract

Nine commercial solid adsorbent materials (ordered by decreasing surface areas: Carboxen 1000, Carbosieve S III, Molecular Sieve 5A, Molecular Sieve 4A, Silica Gel, Carboxen 563, Activated Alumina, Carbotrap and Carboxen 1016) were investigated for their ability to trap and release C2 to C6 non-methane hydrocarbons (NMHC) in atmospheric samples for subsequent thermal desorption GC-FID analysis. Recovery rates for 23 NMHC and methyl chloride (CH_3Cl) were determined. A three-adsorbent microtrap, containing Carbosieve S III, Carboxen 563 and Carboxen 1016 was found to allow for the analysis of the widest range of target analytes. A linear response over a wide range of volatilities and sample volumes, at a detection limit of approximately 3 pptC in a 600 ml sample was determined for this trap. Water vapor in the sample air was found to cause interference in sample trapping and subsequent chromatographic analysis of light NMHC. A peltier-cooled, regenerating water trap inserted into the sample flow path was found to mitigate these problems and to allow quantitative and reproducible results for all analytes at all tested humidity conditions.

This article was published in *Journal of Chromatography* with D. Helmig, J. Hueber, D. Tanner and P. Tans as co-authors

2.1 Introduction

Non-methane hydrocarbons (NMHC) have received growing interest in atmospheric research, as their concentrations and ratios can yield valuable insight into air mass transport, hydroxyl radical concentrations and photochemical ozone production (McKeen and Liu, 1993, William et al., 2000, Parrish et al., 2004). NMHC and NMHC ratios were also identified as tracers for pollution sources such as automobile traffic, fossil fuel exploration and biomass burning (Blake et al., 1992, Blake et al., 1996, Goldan et al., 1997, Parrish et al., 1998, Cardenas et al., 1998, Christensen et al., 1999, Hewitt, 1999, Derwent et al., 2000, Singh et al., 2000). These interests have motivated activities towards the establishment of a network of remote automated background stations to monitor NMHC over a long period of time (WMO Report, 1995). Ideally, NMHC monitors to be used for this purpose would have to require low maintenance and be operable without an external supply of cryogen, hydrogen or zero-air. Hydrogen and zero-air, which are needed for NMHC gas chromatography instruments, can be generated on-site with commercially available gas generators. A preconcentration step is typically required to increase NMHC concentrations from their low atmospheric concentrations to levels that allow analysis by GC-FID. A common technique is the freeze-out of NMHC in a cold trap that is cooled with a cryogen (such as liquid nitrogen). The supply of liquid nitrogen is cumbersome and can be a substantial expense for longterm monitoring purposes especially at remote locations. These constraints make it desirable to use a NMHC focusing and injection system that does not rely on liquid cryogen techniques. Furthermore, one-stage trapping/injection systems are preferable because of their simplicity and reduced design and operational cost. A one-stage system typically requires a low volume microtrap (internal volume < 1 cm^3) to ensure rapid sample desorption and narrow chromatographic peak shape. However, the internal diameter of the adsorbent trap needs to be large enough to reduce flow resistance thereby providing reasonable flow rates during the sampling step. Another limiting factor on the microtrap volume is that the trap has to be able to hold the required amount of adsorbent. Previous studies have shown that the use of strong adsorbent materials in combination with moderate cooling (down to – 30 ºC) by thermoelectric coolers can quantitatively trap selected volatile organic compounds down to the C2 to C4 range (Millet et al., 2004, Millet et al., 2005, Goldstein et al., 2004).

The ability of an adsorbent to retain NMHC is typically proportional to its surface area. A review on the physical properties and the production processes of many different adsorbent materials was published by Dettmer and Engewald (2002). The retention of compounds on solid adsorbents is generally inversely correlated with their volatility. Secondly, molecular structure and the abundance of unsaturated carbon-carbon bonds were found to affect adsorption efficiency. This made it especially challenging to quantitatively trap highly volatile compounds, such as C2 hydrocarbons (ethane, ethene and acetylene). Saturated compounds (e.g. ethane, propane) were found to be retained better on carbon molecular sieve adsorbents than unsaturated compounds (ethene, propene) (Tang et al., 1996). In agreement with this study, Badol et al. (2004) found that acetylene was the most difficult compound to retain quantitatively (despite a higher boiling point than ethane or ethene) on Carbosieve SIII. Approximately 110 mg of this adsorbent was needed to increase the breakthrough volume to > 600 ml at – 30 ºC trapping temperature.

Carbon molecular sieves such as Carbosieve and Carboxen materials were found to provide the highest adsorption efficiency for C2-C4 compounds, while heavier analytes in the C5 to C6 range were most often trapped by surface adsorption on carbon blacks. For instance, hydrohalocarbons and halocarbons were best retained on Carbosieve SIII, followed by Carboxen 1000 and 1001, while molecular Sieve 5A was a fairly weak adsorbent (Sturges and Elkins, 2000). Similar results where reported by Betz and Supina (1989), who evaluated 10 different solid adsorbents (including: Carbosieve S III, Carbosieve S II, Carboxen 563, 564 and 569 and activated charcoal) and found that Carbosieve S III was the strongest material for ethane retention. Among the Carboxen product line Carboxen 1000 was the strongest adsorbent (O'Doherty et al., 1992).

The temperature required to release analytes from the adsorbent bed depends both on the adsorbent strength and analyte volatility. Decomposition reactions became more probable at higher temperatures (e.g.: Sanchez et al., 2005). Weaker adsorbents placed in front of a stronger adsorbent in a multi-layer adsorbent trap can be used to ensure complete thermal desorption at lower temperatures (Helmig and Greenberg 1994).

The trapping efficiency of adsorbent traps increases exponentially with decreasing temperature. However, the increasing co-adsorption of atmospheric water vapor and

carbon dioxide at subambient temperatures can cause sampling and chromatographic interferences. Water vapor can affect the trapping procedure in several ways. First, the adsorption efficiency for organic analytes, especially for light NMHC (propene), can be reduced (Sturges and Elkins, 1993, Fabbri et al., 1987). These studies suggested that a monolayer of adsorbed water was formed on the surface of the adsorbent material when air with high water vapor content was sampled. The water monolayer was then responsible for the induced filling of a significant fraction of the micropores with water. The adsorption efficiency decreased as these pores were no longer available for the adsorption of VOC. The volume of carbon molecular sieve micropores was found to be proportional to the volume of adsorbed water (Gawlowski et al., 1999). Gawrys et al. (2001) determined a threshold relative humidity of 35% R.H. at 30 ºC for Carboxen 569, Carboxen 1001 and Carbosieve S III, above which the micropores were slowly filled with water and the recovery of VOC was reduced. The threshold for Carboxen 1000 was 45% R.H. at 30 ºC sampling temperature.

Secondly, focusing traps were also found to become plugged due to freeze-out of atmospheric water vapor while sampling at sub-zero temperatures. Chromatographic and detection interferences could subsequently arise in the chromatography process (Sturges and Elkins, Helmig et al., 1990). Carbon molecular sieve type adsorbents were found to exhibit the highest water retention (Betz and Supina, 1989, Helmig and Vierling, 1995).

These results underline the necessity to selectively remove water vapor from the sampling air prior to the adsorption step. Different types of water traps and water managing techniques were used to mitigate these problems (Kurdziel, 1998, Dewulf and van Langenhove, 1999, Helmig, 1999, Namiesnik and Wardencki, 1999, Parrish and Fehsenfeld, 2000, Karbiwnyk et al., 2002, Clemitshaw, 2004). An increasingly popular technique is to lower the sample dewpoint by freezeout of water vapor (Millet et al., 2005, Goldan et al., 2004, Jobson et al., 1994). Typically, the sample is drawn through a section of thermoelectrically cooled tubing. The trap is subsequently heated and the retained water is removed by applying a vacuum or by purging the trap with a dry gas. It was proven that this technique required little maintenance and did not interfere with the sampling of C2-C10 NMHC. These water traps can be operated automatically over a long period of time and are favorable approaches for long-term, remotely operated sampling projects (Tanner et al., 2006).

Most of this previous research investigated the use of a particular adsorbent for a narrow range of applications, e.g. for a few targeted compounds. Our goal was to characterize readily available adsorbents for their applicability over a wide range of analyte volatilities. This research was conducted in the context of instrument development for light NMHC monitoring at a remote sampling location and for continuous, automated and unattended analysis of a large series of flask samples on a laboratory instrument. Commercially available adsorbent materials which were previously reported in the literature and appeared to be suited for volatile NMHC preconcentation were systematically investigated for the cryogen-free trapping of C2-C6 NMHC. The susceptibility of the analysis towards water vapor in the sampling stream was studied in detail and a freeze-out water trap, suitable for automated long-term single stage adsorption -thermodesorption applications was thoroughly tested.

2.2 Instrumental

Inlet System: The experiments were performed using a custom-made inlet system coupled to a commercial gas chromatograph with flame ionization detection (FID) (HP 5890 Series II, Hewlett Packard, Palo Alto, CA). A schematic of the instrument is shown in Figure 2.1. The GC column was an Al_2O_3 PLOT (Porous Layer Open Tubular) column deactivated with KCl (I.D.: 0.53 mm, Length: 30 m, 19095P-K23, Agilent, Wilmington, DE). The sample was drawn through the microtrap by a vacuum reservoir (V ~ 25 l). The sampling flow was controlled using a mass flow controller (FC-280-SAV, Tylan Corp., Carson, CA). The pressure increase during trapping was measured with an electronic pressure gauge (622A12TBE, MKS Instruments, Andover, MA) and used to calculate the sampling volume. A diaphragm pump (N813.5 ANE/AF, Neuberger, Freiburg, Germany) was used to evacuate the reservoir to approximately 5 mbar when the inlet system was idle. The relative standard error of the sampling volume (n = 50) was 0.2% for a 0.6 l sampling volume. Two four-port valves and one six-port valve (A44 UWE and A4C6UWE respectively, Valco Inst., Houston, TX), maintained at 60 ºC with valve heaters (HA1, Valco Inst.) were used for switching gas flows. The microtrap could be isolated from the flow path with two solenoid valves (Y 141010-08, Kip Inc, Farmington, CT and ETO-3, Clippard Inc, Cincinnati, OH). The vacuum reservoir, the pump and the inlet port could be separated

from the system with shut-off valves (SS-BNVCR4-C, Swagelok, Solon, OH). Most fittings were stainless steel VCR (Swagelok) while few stainless steel Swagelok connectors were used (Swagelok).

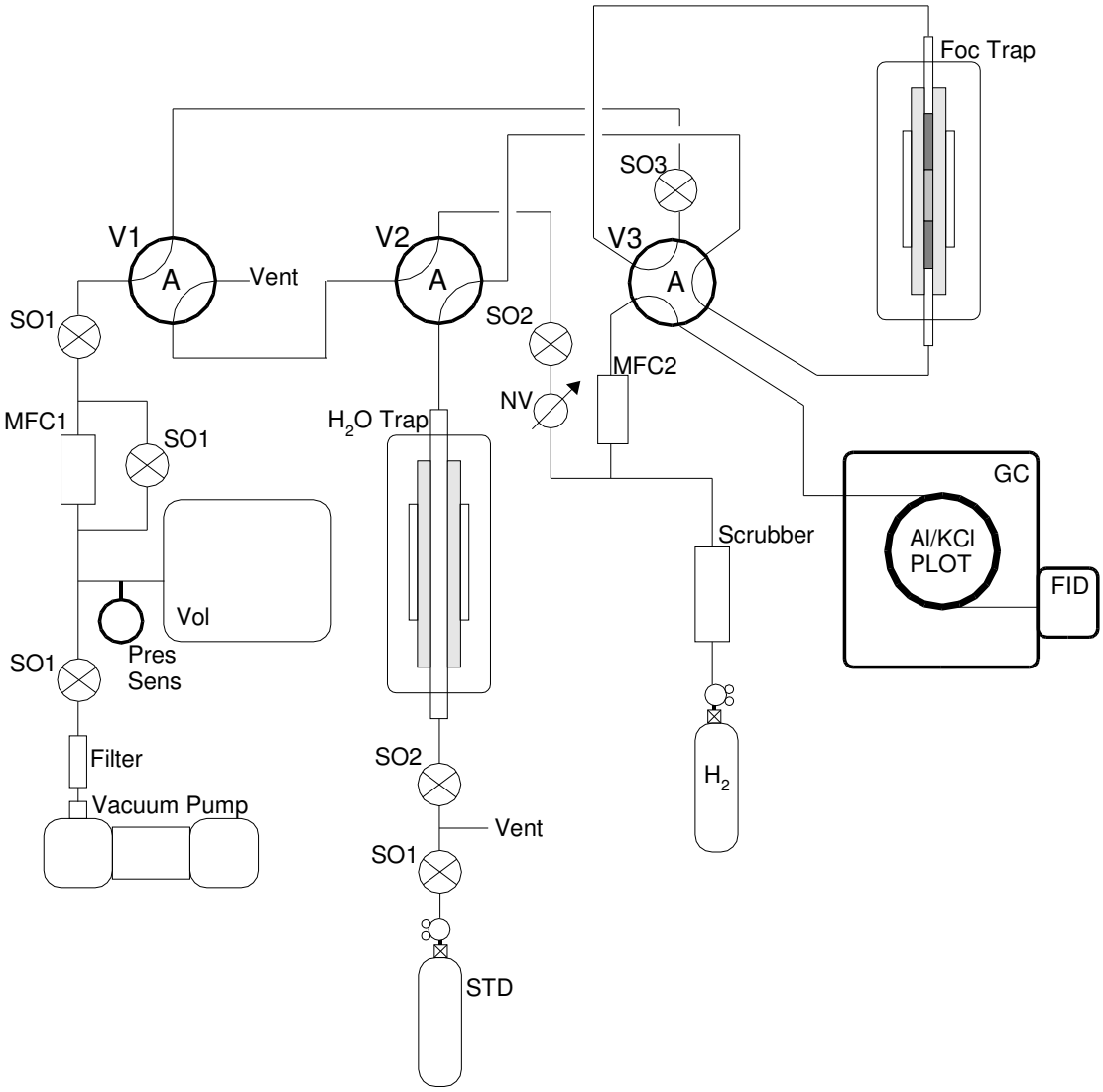

Figure 2.1: Instrument schematic, identification of individual components: Al/KCl PLOT: GC-column, 19095P-K23, Agilent, Wilmington, DE; FID: flame ionization detector; Filter: particle filter; Foc Trap: focusing trap, see text; GC: gas chromatograph, HP 5890 II, Hewlett Packard, Palo Alto, CA; H_2O Trap: water trap, see text; MFC1: mass flow controller FC-280-SAV, Tylan Corp., Carson, CA; MFC2: mass flow controller: UFC 1100A, Unit Instrument Inc, Yorba Linda, CA; NV: needle valve; Pres Sens: pressure sensor, 622A12TBE, MKS Instruments, Andover, MA; Scrubber: oxygen trap, 7213, Alltech, Deerfield, IL, hydrocarbon trap, 7201, Alltech, indicating oxygen trap, 4004, Alltech; SO 1: shut off valves, SS-BNVCR4-C, Swagelok, Solon, OH, SO 2: shut off valve: Y 141010-08, Kip Inc, Farmington, CT, SO 3: shut off valve: ETO-3, Clippard Inc, Cincinnati, OH; V1 and V2: 4-port, 2-position valve, A44UWE, Valco Inst., Houston, TX; V3: 6-port, 2-position valve

A4C6UWE, Valco; Vacuum Pump: diaphragm pump, N813.5 ANE/AF, Neuberger, Freiburg, Germany,
The entire injection system was computer-controlled by a digital I/O board and an analog/digital I/O board (NI PCI-DIO-32 HS and NI-PCI 6014, National Instruments, Austin, TX) using a custom-programmed LabView code (National Instruments). Zero air was generated by flowing compressed air over catalyst pellets, 1% platinum on alumina (20616, Sigma-Aldrich, St. Louis, MO) at 390 ºC.

Calibration: This GC system was calibrated by determining a carbon response factor from sampling a single compound neo-hexane standard (2, 2 - dimethylbutane, Scott Specialty Gases, Longmont, CO) and from direct column injection of a C1 to C6 n-alkane standard (M7018, Alltech, Deerfield, IL). Effective carbon numbers were used to correct for different FID response rates (Jorgensen et al., 1990).

Microtrap Housing: A description of the microtrap housing assembly has been previously published (Tanner et al., 2006). The instrument described here, however, used dual two-stage Peltier cooling elements (two times CP 1.4-127-045L and CP 1.4-127-10L, Melcor, Trenton NJ), which cooled the microtrap to –30 ºC. The heat sinks were cooled with high-flow (1.4 m^3 min^{-1}) fans (FFB0612EHE, Delta Electronics, Fremont, CA). The microtrap housing was encased with aluminum panels and the interior was constantly purged with dehumidified air to prevent water ice built-up from ambient humidity on the cooled parts.

Microtrap design: Stainless steel tubing (extra thin wall, length: 19.0 cm, I.D.: 1.82 mm, O.D.: 2.10 mm, V: 0.5 cm^3) was used as the trap exterior. A type K thermocouple (Diameter: 0.5 mm, length: 15 cm KMQSS-020-6, Omega Engineering, Stamford, CT) was fed through a 1/8” tee (SS-200-3, Swagelok, Solon, OH) into the center of the microtrap. The adsorbents were bordered on both sides by binder-free glass fiber filters (APFD09050, Millipore, Billerica, MA) and 1/16” stainless steel tubing to keep the adsorbent bed in place. The trap was heated resistively to 310 ºC within 3 s during desorption. Further details may be found in Tanner et al., (2006).

Sampling sequence: First a sample was drawn through the cooled microtrap at 60 ml min^{-1} for 10 min. The microtrap was then purged with H_2 at 20 ml min^{-1} for 30 s to remove oxygen

from the trap. Subsequently, the microtrap was heated to 310 ºC within 3 s, and after another 5 s the 6-port valve was switched to the inject position. An 8 s desorption time was empirically determined to result in the fastest and sharpest transfer of all trapped analytes onto the GC column during injection. After an injection time of 20 s the 6 port valve was switched back to its default position and the microtrap was baked out for 2 minutes at 325 ºC under H_2 purge. The GC-oven program was: 4 minutes at 40 ºC, 10 ºC min^{-1} to 200 ºC, 200 ºC for 5 minutes.

Standard: NMHC in compressed air (breathing air grade cylinder, Airgas, Loveland, CO) were quantified by GC-MS/FID. Twenty-three compounds in the C2 to C6 range and methyl chloride were identified at high pptV to low ppbV mixing ratios (Table 2.1).

Table 2.1: NMHC mixing ratios (in ppbV) of the standard used (relative standard deviation ~ 7 %) with GC retention times and boiling points

Compound	Retention Time (min)	Mixing Ratio (pptV)	Boiling Point* (ºC)
ethane	1.90	2980	-89
ethene	2.31	8290	-104
propane	3.19	2650	-42
propene	5.85	9650	-48
i-butane	7.00	1090	-10
acetylene	7.32	512	-85
n-butane	7.46	3310	-0.5
methyl-chloride	8.88	154	-29
t-2-butene	9.68	1150	1
1-butene	9.79	1490	6
2-methyl-propene	10.19	22100	6.9
c-2-butene	10.48	731	0
i-pentane	11.04	3810	28
n-pentane	11.43	1560	36
3-methyl-1-butene	12.11	38	20
t-2-pentene	12.41	133	36
2-methyl-1-butene	12.73	137	31
2-methylbutene[+]	12.91	800	31
c-2-pentene	13.04	147	37
2-2-dimethylbutane	13.98	266	50
2-3-dimethylbutane	14.29	140	58
2-methyl-pentane	14.36	533	61
3-methyl-pentane	14.42	330	63
n-hexane	14.79	258	69

*source: NIST webbook

[+]unidentified 2-methylbutene

The cylinder air had a relative humidity of 5% (dewpoint of –15 ºC) (determined as average of two measurements with thermohygrometers (35612-00, Oakton, Vernon Hills, IL)). Analyte concentrations for the standard were determined on a cryogenic prefocussing GC-FID system that was calibrated against a scale of gravimetrically prepared reference standards.

Adsorbent Materials: Nine commercial adsorbent materials that were previously used in light NMHC sampling studies were investigated. These included three carbon molecular sieves (Carboxen 1000, Carbosieve SIII, Carboxen 563), two inorganic molecular sieves (molecular sieve 5A, molecular sieve 4A), two graphitized carbon blacks (Carbotrap, Carboxen 1016) and two inorganic metal/semi-metal oxides (silica gel, activated alumina) (Table 2.2).

Table 2.2: Evaluated adsorbent materials with their properties: Density: gravimetric density; Surface Area: Surface Area as provided by supplier; net adsorbent mass: mass of individual adsorbent filled into trap for evaluation; Pressure Drop: pressure drop across adsorbent trap filled with adsorbent at a 50 ml min^{-1} sampling flow (air)

Adsorbent	Mesh Size	Density g/cm^3	Surface Area* m^2/g	Net Adsorbent Mass mg	Pressure Drop mbar	Supplier Name, Location, State
Carboxen 1000	60/80	0.52	>1200	56	260	Supelco, Bellefonte, PA
Carbosieve S III	60/80	0.76	820	64	250	Supelco, Bellefonte, PA
Molecular Sieve 5A	40/60	0.89	800	68	120	Alltech, Deerfield, IL
Molecular Sieve 4A	40/60	1.07	800	81	130	Alltech, Deerfield, IL
Silica Gel	20/45	0.56	750	43	80	Supelco, Bellefonte, PA
Carboxen 563	20/45	0.55	510	40	70	Sigma-Aldrich, St. Louis, MO
Activated Alumina	40/60	1.14	350	86	150	Alltech, Deerfield, IL
Carbotrap	20/40	0.32	100	34	§	Supelco, Bellefonte, PA
Carboxen 1016	60/80	0.45	75	44	250	Supelco, Bellefonte, PA

* supplier information

§ No pressure drop is given for Carbotrap as a gradual increase in the flow resistance was observed for this material.

Humidifier: A custom-made humidifier (Karbiwnyk et al., 2002) was used to enrich the dilution air with water vapor. Air could be humidified from 20-95 +/- 2% relative humidity at room temperature.

Water trap: The water trap is similar to that described by (Tanner et al., 2006) except that it had a two-stage Peltier cooling system (similar to the adsorbent microtrap), which allowed

for trapping temperatures of –35 ºC. The trap was heated to 80 ºC under vacuum during the regeneration phase.

2.3 Experiments

2.3.1 Adsorbent material evaluation:

An individual adsorbent was filled into a trap to yield a bed length of 3.7 +/- 0.1 cm in the center of the trap (see Table 2.2 for the respective weights). All traps were first conditioned by baking them out three times under 30 ml min^{-1} hydrogen purge at 325 ºC for 10 minutes. The adsorption and desorption efficiency of each adsorbent was then evaluated by sampling 600 ml of the standard at a trapping temperature of –10 ºC with subsequent desorption and GC analysis. The adsorption capacity for Carbosieve S III and Carboxen 1000 was also tested at –30 ºC. The adsorption efficiency of the developed three-stage adsorbent trap was also evaluated at –10 and –30 ºC. After the first injection the microtrap was sealed and cooled down to –10 ºC (or –30 ºC respectively) and injected again after 45 minutes to evaluate the fraction of analytes that was not desorbed during the first desorption step.

Two types of blank experiments were performed to test for contaminant levels introduced from the adsorbent materials. First, a trap for each adsorbent was baked out at 325 ºC under a 30 ml min^{-1} hydrogen flow for 10 min, sealed and cooled down. After 15 minutes the trap was thermally desorbed and injected onto the GC column. This experiment was used to evaluate the blank and inherent contaminant formation from the adsorbent bed itself. Secondly, 600 ml of zero air was analyzed. This experiment investigated the possible formation of contaminants by the interaction of the adsorbent material with air drawn through the adsorbent bed. Results from the different adsorbents were compared by determining the total integrated peak area (using fixed peak detection parameters) in the ethane to n-hexane elution range. This peak area was then converted into pg carbon using the FID response factor.

Linearity Tests: Increasing volumes of the standard (from 100 to 800 ml in 100 ml increments) were sampled on the three-stage adsorbent trap to evaluate the linearity of the sampling and analysis processes. The sampling flow was 60 ml min^{-1} and the trapping

temperature was –30°C. The smallest integratable peak at a signal to noise ratio of 3.5 in the chromatogram of the 100 ml sample was used to estimate detection limits.

Trapping Temperature: The trapping efficiency for the three-stage adsorbent trap was investigated at increasing trapping temperatures (from –30°C to 25°C in 5°C increments) to evaluate the analyte retention and desorption efficiency. Three 600 ml samples were analyzed at each temperature. The –30°C samples were set to be the 100% reference value.

2.3.2 Interference from water vapor:

The trapping efficiency of the three-stage adsorbent trap was evaluated under varying humidity levels at –30 ºC trapping temperature. The dry standard (dewpoint –15 ºC) was diluted (18:1) with humidified zero air to a dew point of 17.5 ºC (70% R.H. at 25 ºC). The sampling air was then drawn through the water trap at water trap temperatures ranging from –35 ºC to 25 ºC (5 ºC increments). The water trap reduced the air humidity to the dew point corresponding to the water trap temperature.

2.4 Results and Discussion

2.4.1 Adsorbent material evaluation:

The results of the recovery experiments for all adsorbent materials and the three-stage adsorbent trap (sorted for alkanes, alkenes and two additional compounds (acetylene and methyl chloride) in elution order) are displayed in Figures 2.2 through 11. The individual adsorbent materials showed significant differences in their adsorption/desorption efficiency. Results for individual adsorbents, in order of decreasing adsorbent surface area, were as follows:

Carboxen 1000 (Figure 2.2 a, b): Carboxen 1000 was found to be the second strongest adsorbent among the investigated products. At –10 ºC trapping temperature this material exhibited a very broad trapping range, although ethane and ethene were not completely retained. All C2 to C6 compounds, except ethene and acetylene, were trapped quantitatively at –30 ºC. Even though Carboxen 1000 is reported to have the highest

surface area (1200 m^2 g^{-1}) of all investigated compounds this material was found to be a weaker adsorbent than Carbosieve S III (in agreement with previous reports (Betz and Supina, 1989, Sturges and Elkins, 1993). However, heavier compounds that could not be quantitatively desorbed from Carbosieve S III (such as pentane) were completely recovered from Carboxen 1000. Background levels in the blank experiments were low (Table 2.3). These results indicate that Carboxen 1000 is a versatile adsorbent for the C2 to C6 volatility range.

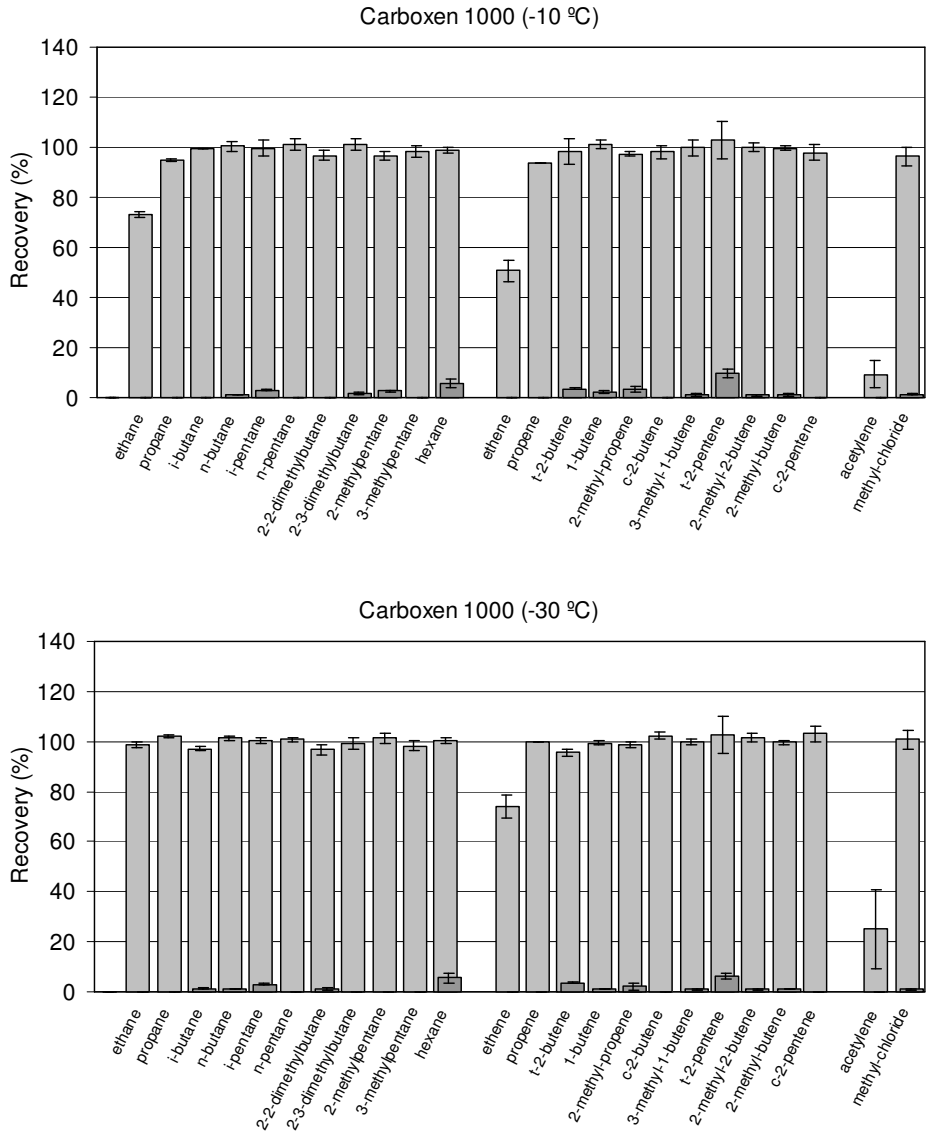

Figures 2.2 a, b: Recovery for target compounds from Carboxen 1000 at –10 and –30 ºC. Dark gray section represents the peak area that was found on the microtrap for the respective compound in a second desorption run. Error bars indicate standard deviation for n = 5 injections.

Carbosieve S III (Figure 2.3 a, b): Carbosieve S III was the strongest adsorbent among the investigated materials. Ethane was trapped quantitatively at –10 ºC but only 75% of ethene was retained. Recovery of acetylene was 10% at –10 ºC. Ethane and ethene were completely retained at – 30 ºC. Acetylene was the only tested compound that was not quantitatively retained at –30 ºC.

Table 2.3: Mass carbon (in pg) in the ethane to hexane range found in the 2nd desorption, zero air and trap blank experiments as average of n = 3

Adsorbent	Trapping Temperature (ºC)	Mass Carbon (pg) in Trap Blank	Zero-Air Blank	2nd Desorption
Carboxen 1000	- 10 ºC	0.34	0.72	1.91
Carboxen 1000	- 30 ºC	0.32	0.78	1.68
Carbosieve S III	- 10 ºC	0.37	0.77	6.64
Carbosieve S III	- 30 ºC	0.36	0.77	5.89
Molecular Sieve 5A	- 10 ºC	0.65	11.02	3.36
Molecular Sieve 4A	- 10 ºC	0.16	1.32	1.11
Silica Gel	- 10 ºC	0.18	0.47	0.56
Carboxen 563	- 10 ºC	0.24	1.00	2.68
Activated Alumina	- 10 ºC	0.22	0.67	0.33
Carbotrap	- 10 ºC	0.13	0.59	0.53
Carboxen 1016	- 10 ºC	0.15	0.54	0.62
3-Stage Adsorbent Trap	- 10 ºC	0.22	0.42	0.41
3-Stage Adsorbent Trap	- 30 ºC	0.34	0.47	0.37

However, only C2 and C3 compounds could be desorbed completely under the applied conditions. The significant amounts found in the 2nd desorption experiments illustrate that this adsorbent was too strong to release these compounds unless more stringent desorption conditions were applied. After proper conditioning, trap and zero air blanks showed low levels of contamination in the C2-C5 elution range. Similar findings for Carbosieve S III were reported in two earlier studies. Badol et al. (2004) showed that 110 mg of Carbosieve S III at –30 ºC were necessary to achieve a breakthrough volume > 700 ml for acetylene. These values are in good agreement with our results, as we used about half of the adsorbent mass. Betz and Supina (1989) found that Carbosieve S III had the highest adsorption capacity for ethane among 10 investigated adsorbents. This study also showed large amounts of the heavier analytes in the 2nd desorption experiments.

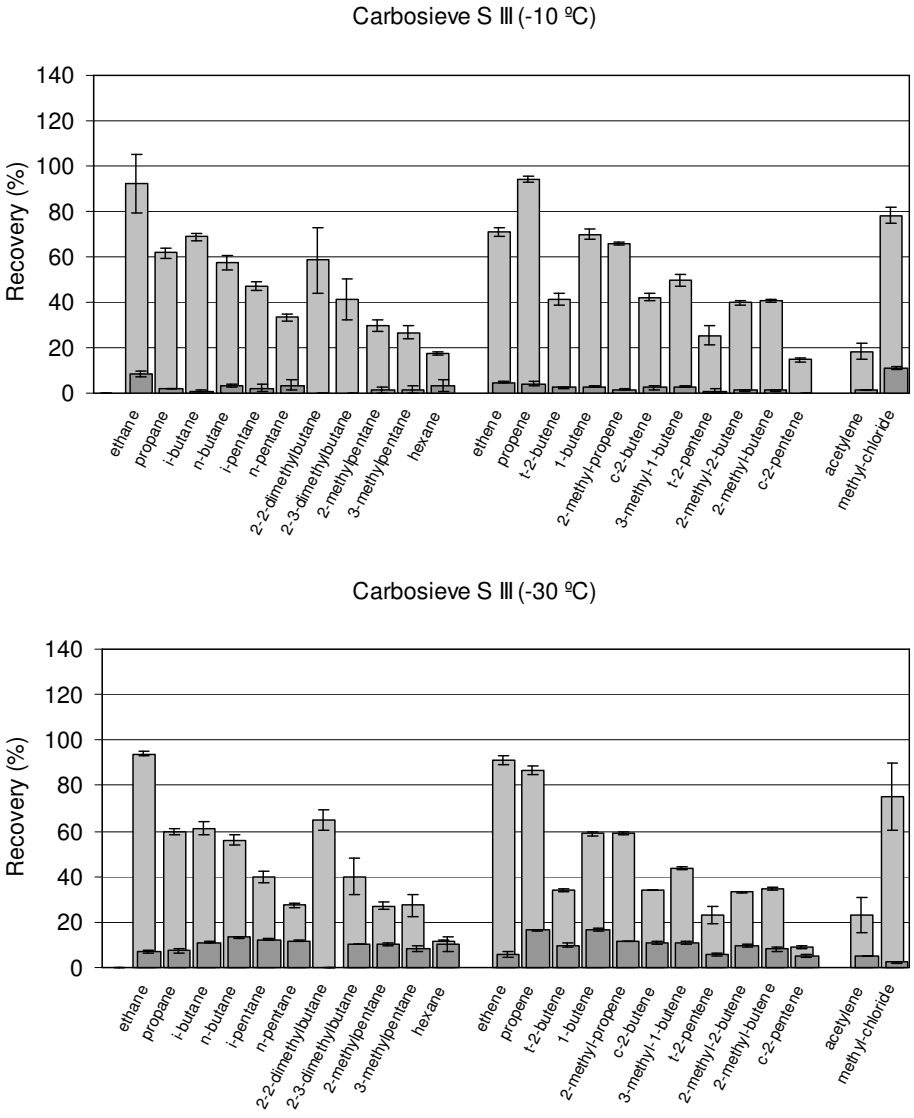

Figures 2.3 a, b: Recovery for target compounds from Carbosieve S III at –10 and –30 ºC. Dark gray section represents the peak area that was found on the microtrap for the respective compound in a second desorption run. Error bars indicate standard deviation for n = 5 injections.

Molecular Sieve 5A (Figure 2.4): The composition of the standard was dramatically altered when samples were collected on Molecular Sieve 5A. Recovery rates of unsaturated compounds were elevated while saturated compounds were reduced. Blank experiments showed no additional peaks (Table 2.1), hence none of the observed analyte increases could be attributed to contamination from Molecular Sieve 5A itself. A second microtrap was filled to evaluate whether these results were reproducible. Both traps showed identical results. The second desorption experiments showed high values of unsaturated VOCs.

The zero air blank for this material showed very high contamination with hydrocarbons (one order of magnitude higher than for the other adsorbents). These findings suggest that contaminants are formed while air is drawn through the adsorbent bed.

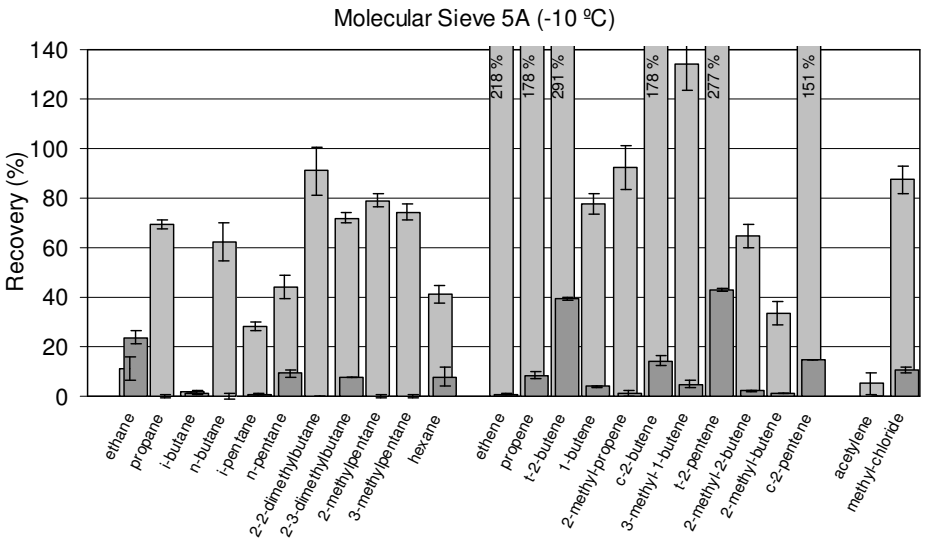

Figure 2.4: Recovery for target compounds from Molecular Sieve 5A at –10 ºC. Dark gray section represents the peak area that was found on the microtrap for the respective compound in a second desorption run. Error bars indicate standard deviation for n = 5 injections.

Molecular Sieve 4A (Figure 2.5): Molecular Sieve 4A was found to be a relatively weak adsorbent. Recovery rates increased from C2 to C6 compounds; ethane was retained by only 10%, hexane recovery was ~ 90%. The results infer that this adsorbent material is best suited for compounds heavier than hexane.

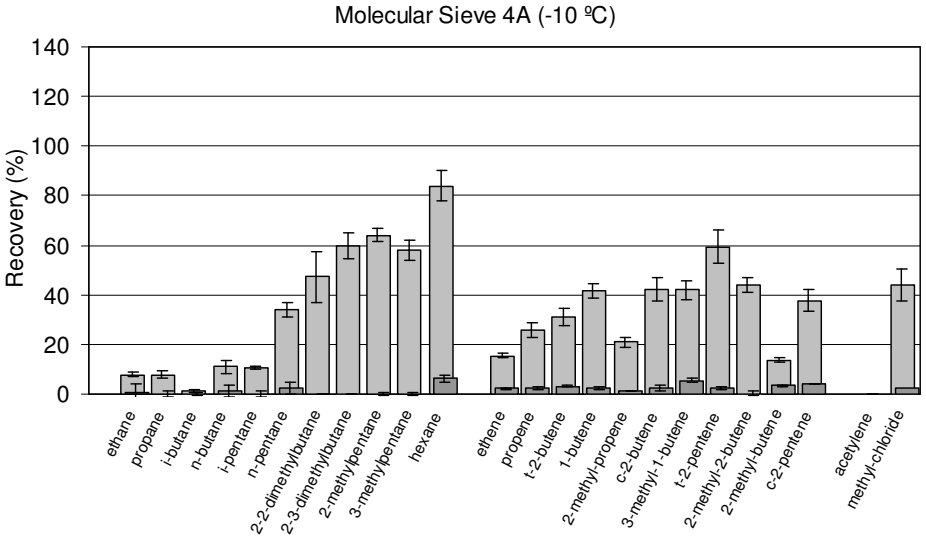

Figure 2.5: Recovery for target compounds from Molecular Sieve 4A at –10 ºC. Dark gray section represents the peak area that was found on the microtrap for the respective compound in a second desorption run. Error bars indicate standard deviation for n = 5 injections.

Silica Gel (Figure 2.6):

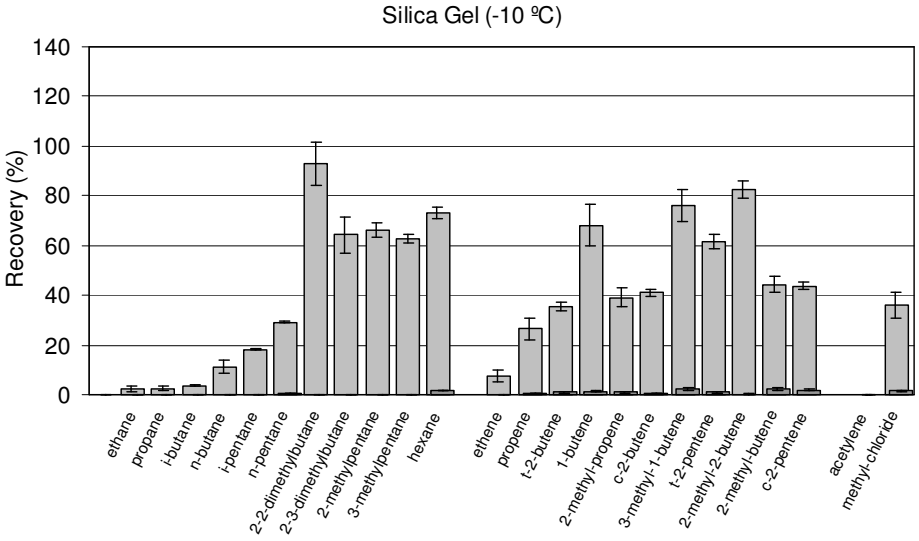

Figure 2.6: Recovery for target compounds from Silica Gel at –10 ºC. Dark gray section represents the peak area that was found on the microtrap for the respective compound in a second desorption run. Error bars indicate standard deviation for n = 5 injections.

Most of the target analytes were not trapped quantitatively on Silica Gel. The best trapping performance was found for the heavier compounds (C5 and up). Silica Gel adsorbent was

difficult to fill into the microtrap tubing as this material easily became electrostatically charged which made it challenging to fill a well-defined amount of adsorbent into the trap.

Carboxen 563 (Figure 2.7): Carboxen 563 performed similar to Carboxen 1000. It exhibited a very broad adsorption/desorption range, however, somewhat shifted to heavier compounds. Five compounds, four of them unsaturated (ethane, ethene, acetylene, propene, 2-methyl-butene) could not be quantitatively recovered at a trapping temperature of – 10 ºC. Carboxen 563 appears to be a versatile material that is well suited for the trapping of most C3 to C6 NMHC.

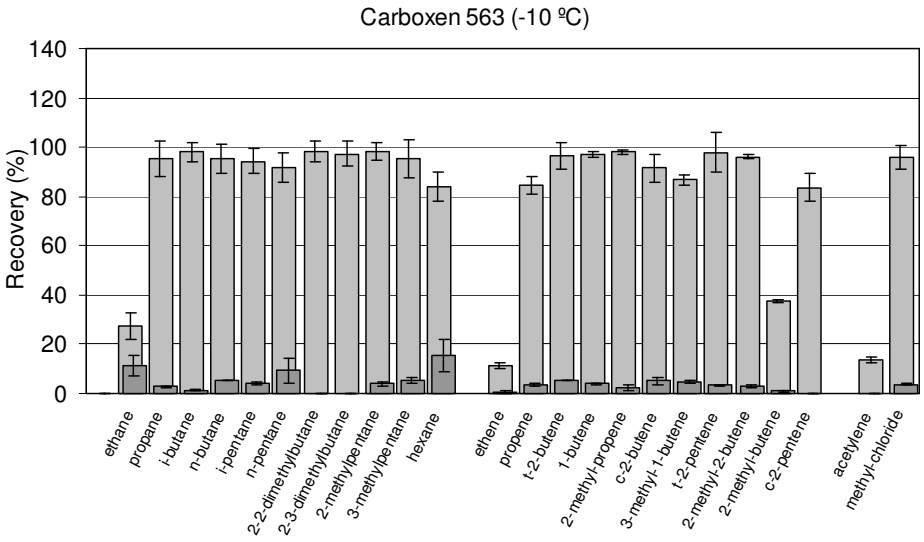

Figure 2.7: Recovery for target compounds from Carboxen 563 at –10 ºC. Dark gray section represents the peak area that was found on the microtrap for the respective compound in a second desorption run. Error bars indicate standard deviation for n = 5 injections.

Activated Alumina (Figure 2.8): Activated Alumina was found to be a medium strength adsorbent. The adsorbent showed similar adsorption characteristics as Molecular Sieve 4A with better recovery for unsaturated compounds. The majority of C2 and C3 NMHC were lost. C4 to C6 compounds were retained at 70 to 80%, several unsaturated compounds were trapped quantitatively.

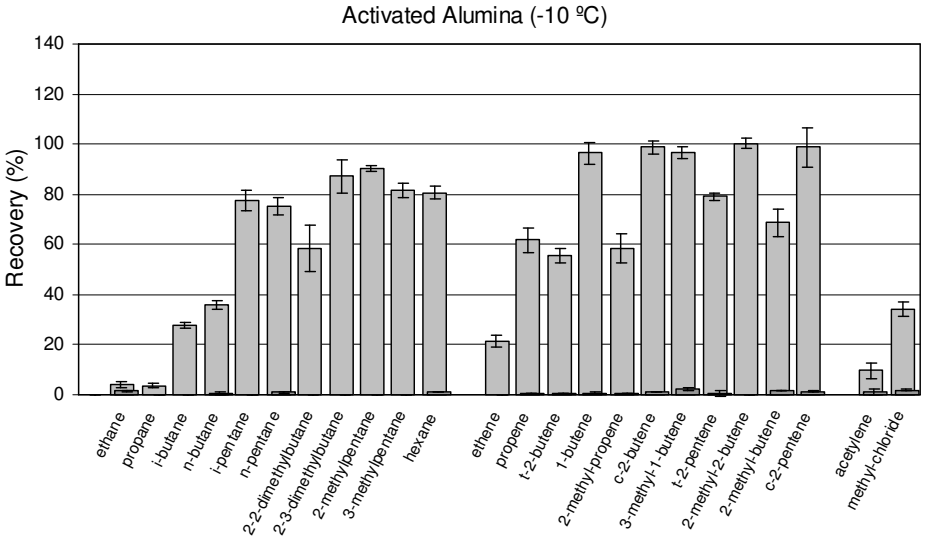

Figure 2.8: Recovery for target compounds from Activated Alumina at –10 ºC. Dark gray section represents the peak area that was found on the microtrap for the respective compound in a second desorption run. Error bars indicate standard deviation for n = 5 injections.

Carbotrap (Figure 2.9):

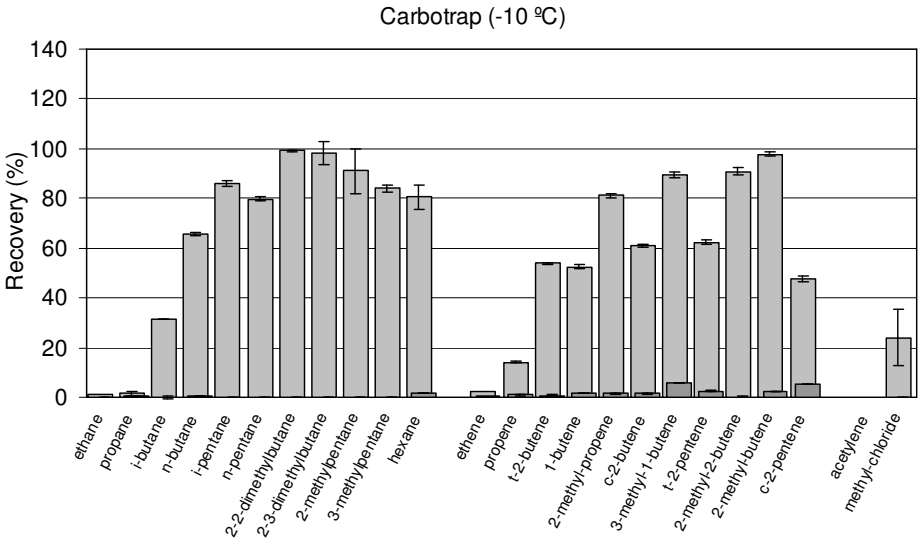

Figure 2.9: Recovery for target compounds from Carbotrap at –10 ºC. Dark gray section represents the peak area that was found on the microtrap for the respective compound in a second desorption run. Error bars indicate standard deviation for n = 5 injections.

Carbotrap was one of the two materials with the lowest surface area (100 m^2 g^{-1}) tested in this study. Carbotrap performed best for C5 and higher compounds, although iso - and n-

pentane as well as hexane were only retained to about 80%. Carbotrap was found to disintegrate into smaller particles inside the microtrap during the trap filling process and after a number of heating cycles. The fine particles that were formed caused a steady increase of trap flow resistance over time. This behavior has previously been noted for other graphitized carbon blacks (Dettmer and Engewald, 2002). Based on these results we discontinued using Carbotrap in microtrap applications.

Carboxen 1016 (Figure 2.10): Carboxen 1016 has physical properties (surface area, temperature limit) similar to Carbotrap. However this material did not exhibit the degradation that was observed for Carbotrap. Carboxen 1016 retained most compounds with boiling points equal or higher of C4, with resulting recovery rates close to 100%. Saturated and non-saturated compounds were retained equally.

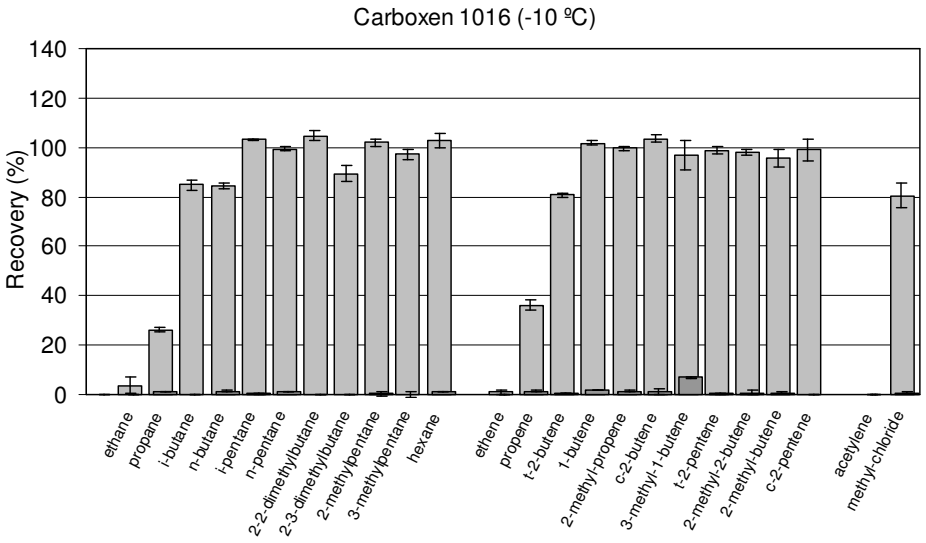

Figure 2.10:
Recovery for target compounds from Carboxen 1016 at –10 ºC. Dark gray section represents the peak area that was found on the microtrap for the respective compound in a second desorption run. Error bars indicate standard deviation for n = 5 (Carboxen 1016) and n = 15 (three-stage adsorbent trap) injections.

Blank Experiments: The results of the two blank experiments and the 2nd desorption experiments are given in Table 2.3. Similar blank signals for both the trap blank and zero air runs were observed for all investigated materials except for Molecular Sieve 5A where the blanks were remarkably high. On several occasions the carbon molecular sieves had

higher trap blanks and zero air backgrounds than the investigated carbon blacks. The second desorption results correlated with the adsorbent strength. Higher residues were found on the stronger adsorbents, indicative of incomplete desorption during the first desorption step. These experiments revealed highly variable contaminant levels for two later eluting compounds, which were tentatively identified as benzene and toluene. Carboxen and Carbosieve materials (with the exception of Carboxen 1000) showed a high background of these two aromatic compounds that prevented their analysis at low pptv levels. More research is in progress to further investigate the suitability of these adsorbent materials for benzene and toluene analysis.

Multi-stage adsorbent trap (Figure 2.11a, b): As none of the individual nine adsorbents proved to retain and release the full range of C2 to C6 target NMHC, a multistage adsorbent microtrap was developed to cover a broader volatility range. Three favorable adsorbents were selected among the tested materials. This trap contained Carboxen 1016 (adsorbent bed length: 1.3 cm; 20 mg), Carboxen 563 (adsorbent bed length: 3.7 cm; 40 mg) and Carbosieve SIII (adsorbent bed length: 3.6 cm; 60 mg), with the strongest adsorbent (Carbosieve S III) at the outlet side and the weakest (Carboxen 1016) at the inlet side. Results for the three-stage trap at -10 and –30 ºC trapping temperature are shown in Figures 2.11 a, b. Most C2 to C6 NMHC compounds were quantitatively trapped and released from this microtrap with very good reproducibility and precision, especially at –30 ºC trapping temperature. Recovery rates for most compounds (with the exception of 3-methyl-1-butene and acetylene) were between 95 and 100%. A trapping temperature of –30 ºC was necessary to trap ethene quantitatively. Somewhat reduced recovery rates (and higher residues in the second desorption analysis) were found for some analytes at –10 ºC. A probable explanation was incomplete fixation and migration of heavier NMHC further into the adsorbent bed. The reproducibility of the analysis was excellent at –30 ºC. The average relative standard deviation for all 24 compounds was 2.5% (n=15).

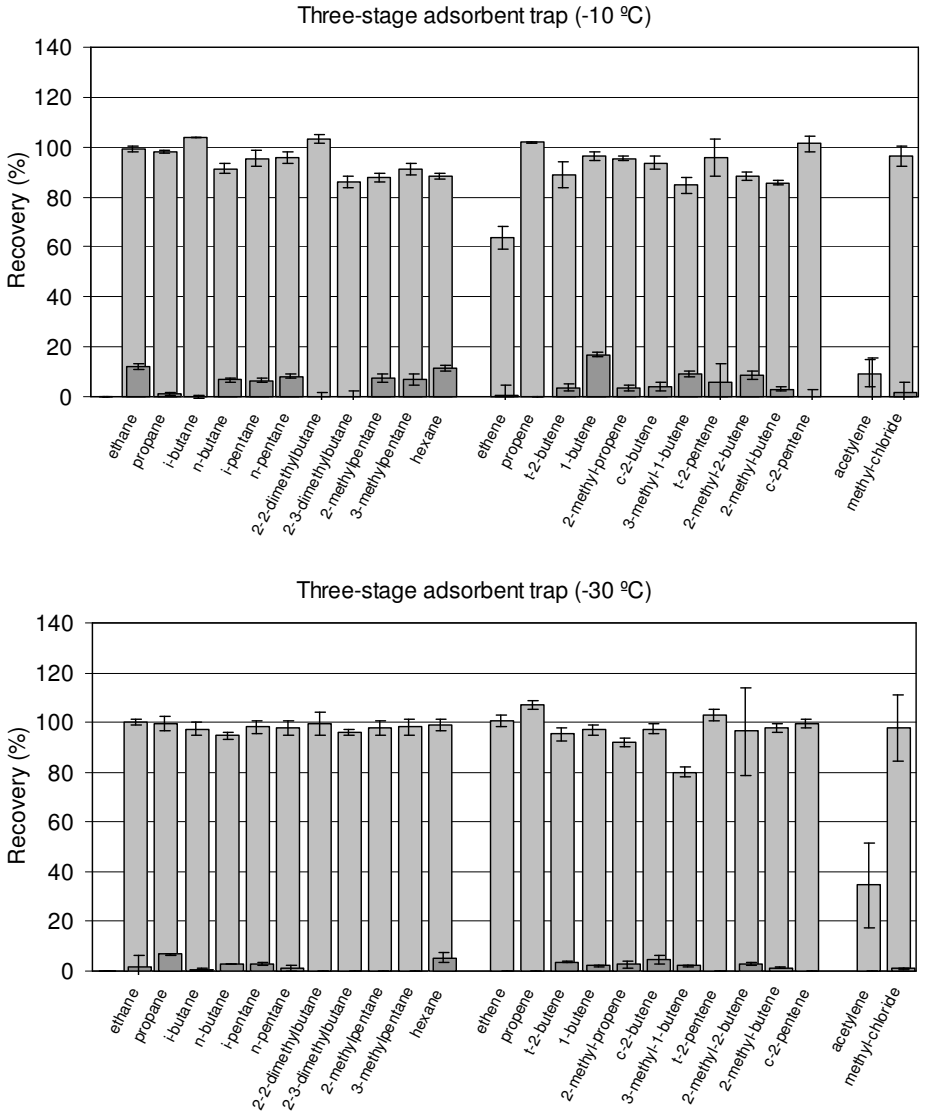

Figures 2.11 a, b: Recovery for target compounds from C 3-stage adsorbent microtrap (Carboxen 1016, Carboxen 563, Carbosieve S III) at – 10 and –30 ºC. Dark gray section represents the peak area that was found on the microtrap for the respective compound in a second desorption run. Error bars indicate standard deviation for n = 15 injections.

Contaminant levels for the three-stage trap were equal or better than for the individual adsorbents. In particular 2nd desorption results were favorable. These findings illustrate an important advantage in using multi-stage adsorbent traps. Heavier compounds are trapped on the first bed and do not migrate onto one of the stronger adsorbents. Consequently, with a properly selected adsorbent combination, it is easier to desorb a wide range of target compounds.

Interestingly, the retention of analytes is not clearly correlated with their boiling points. For instance, boiling points for the C2 compounds are ethane –89 ºC; ethene –104 ºC, acetylene –81 ºC. Acetylene, being the least volatile in this series, was found to have the lowest breakthrough volume. Obviously, the breakthrough volume of individual compounds is not only related to the analyte volatility but furthermore depends on molecular structure and size (Badol et al., 2004). Several measures could be taken to achieve quantitative trapping of acetylene, such as further reducing the trapping temperature; increasing of the mass of Carbosieve S III adsorbent in the microtrap or reducing the sampling volume. None of these measures were further pursued in this study, as they would have compromised other desired applications.

Sampling linearity: The results of this experiment are shown in Figure 2.12 a-c. All compounds, except acetylene, showed a linear response over the 100 – 800 ml sampling range, yielding regression line R^2 values of > 0.98. The breakthrough volume of acetylene was estimated to be approximately 250 ml at –30 ºC trapping temperature, which is in good agreement with the results by Badol et al. (2004).

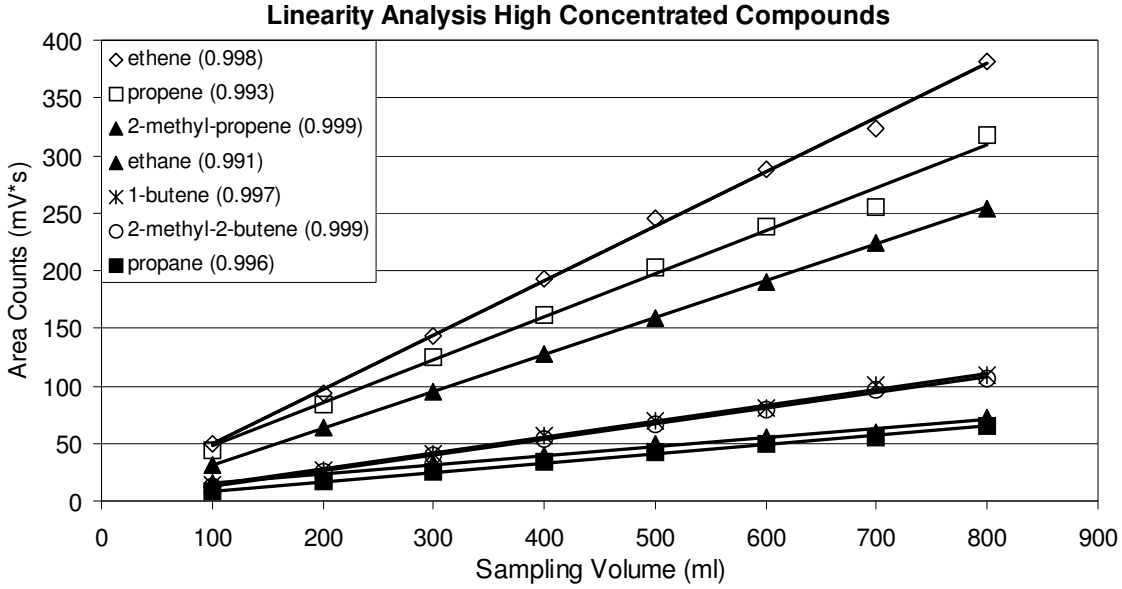

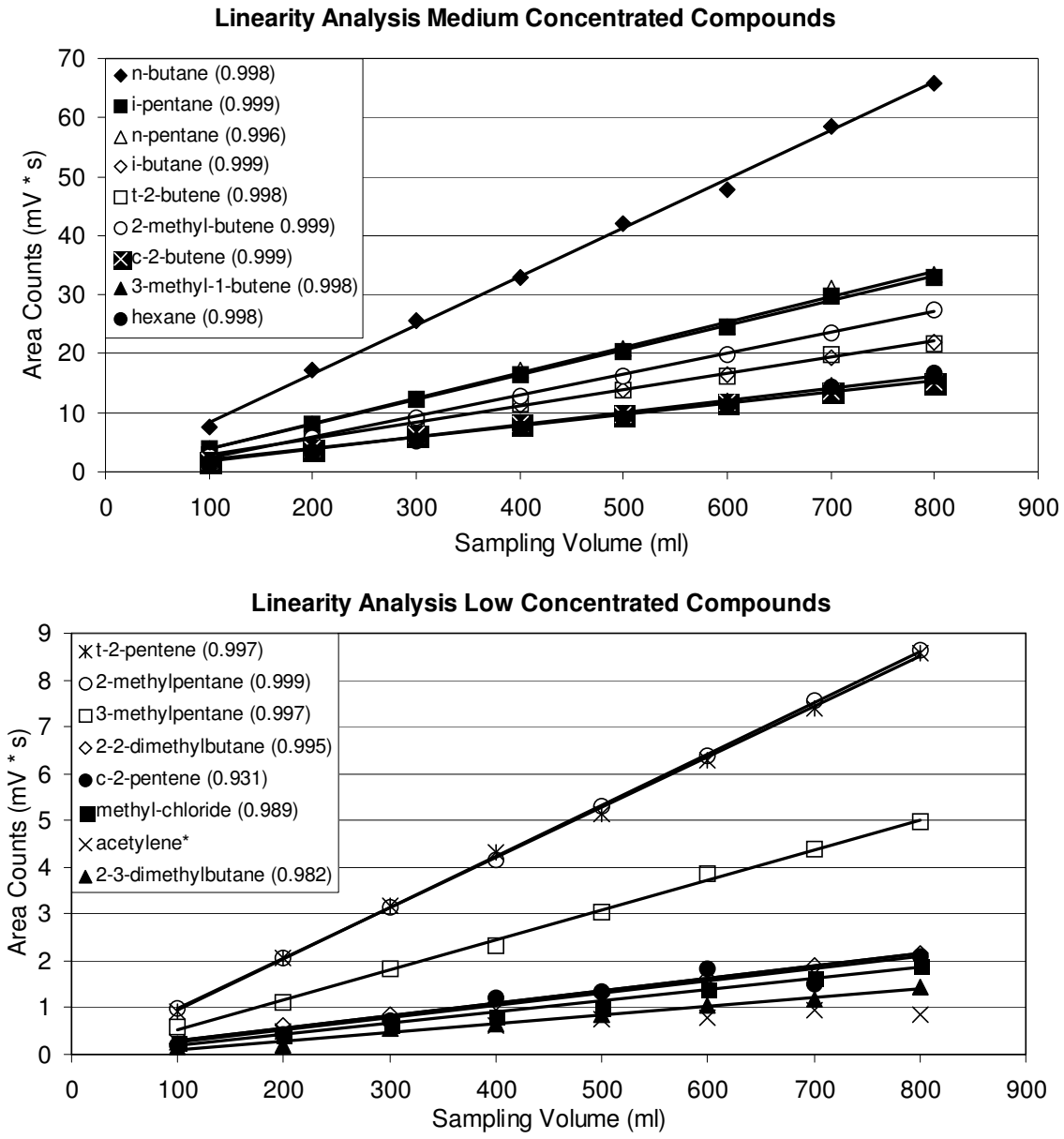

Figure 2.12 a-c: Sampling linearity for target compounds from three-stage adsorbent trap. Saturated compounds are represented by solid and unsaturated by open symbols, respectively. Sampling Volume increased from 100 to 800 ml. R^2 factors for individual compounds are given in the legend behind compound name; no R^2 value is given for acetylene due to exceedance of its breakthrough volume.

Trapping temperature dependency: The results for the experiments at increasing trapping temperatures (three-stage trap) show that trapping efficiency improves with reduced temperature (Fig. 13). The required temperature below which individual compounds were still retained quantitatively with the three-stage trap can be determined from this figure. For better graphical presentation, all data were normalized to the –30 ºC results.

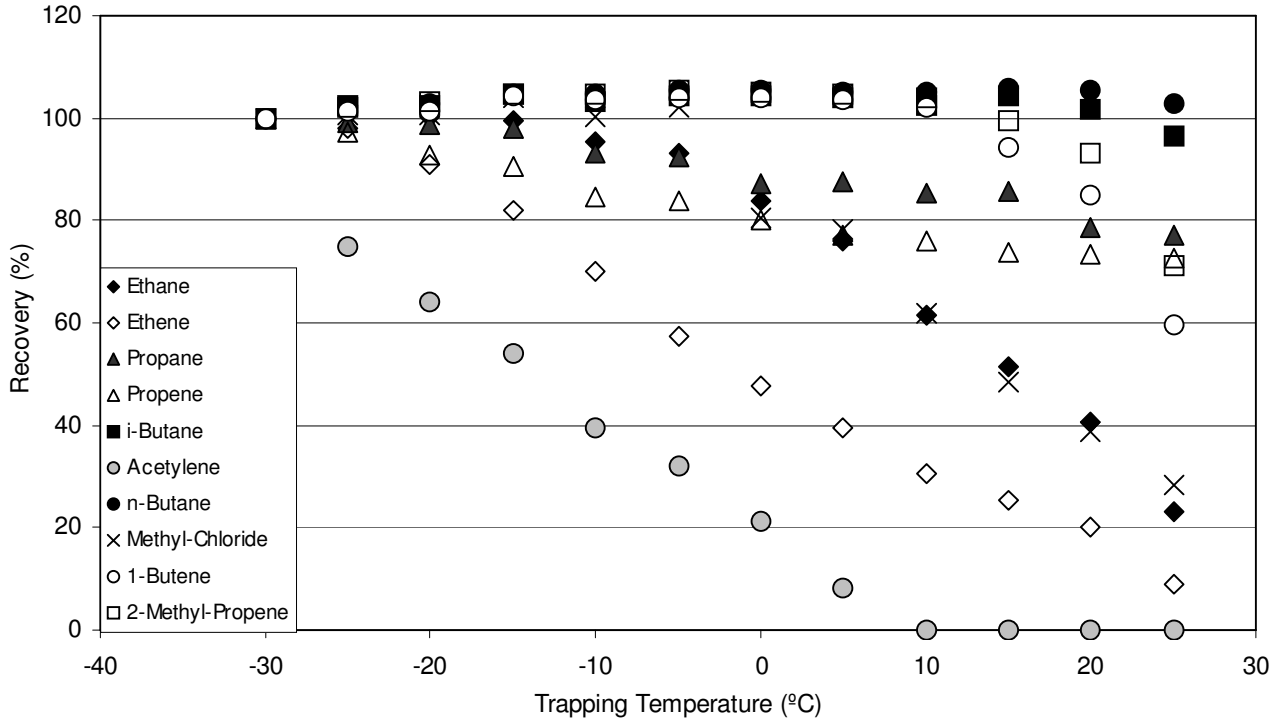

Figure 2.13: Recovery for key target compounds (600 ml sample volume) at different trapping temperatures on the three-stage adsorbent trap. Saturated compounds are represented by solid and unsaturated by open symbols, respectively. Area counts at – 30 ºC were used as the 100% reference value while area counts from other experiments were scaled accordingly except Acetylene which was only recovered by 35% at – 30 ºC trapping temperature. Compounds not displayed in this figure did not show temperature dependency under the investigated conditions.

Recovery rates do asymptotically approach 100% with decreasing temperature. All analytes (besides acetylene) were found close to unity between –25 ºC and –30 ºC trapping temperature. Acetylene was only recovered by ~35% at –30 ºC and was lost completely at +5 ºC. Ethene and propene were not retained quantitatively at temperatures above –20 ºC Ethane and propane were found to diverge from unity at temperatures above –10 ºC, methyl-chloride was quantitatively retained below –10 ºC and unsaturated C4 compounds diverged from unity at temperatures >10 ºC. A slightly reduced recovery rate

was observed for i-butane at a trapping temperature of 25 ºC. All compounds with a higher retention time than n-butane were retained quantitatively at room temperature.

2.4.2 Interference from water vapor

Elevated humidity levels affect the analytical performance two-fold. 1: The effective sampling volume may be reduced due to freeze-out of water in the trap and subsequent increase in flow resistance up to a complete blockage. 2: Water molecules may occupy the micropores which are of the carbon molecular sieves thus reducing the trapping efficiency for light hydrocarbons.

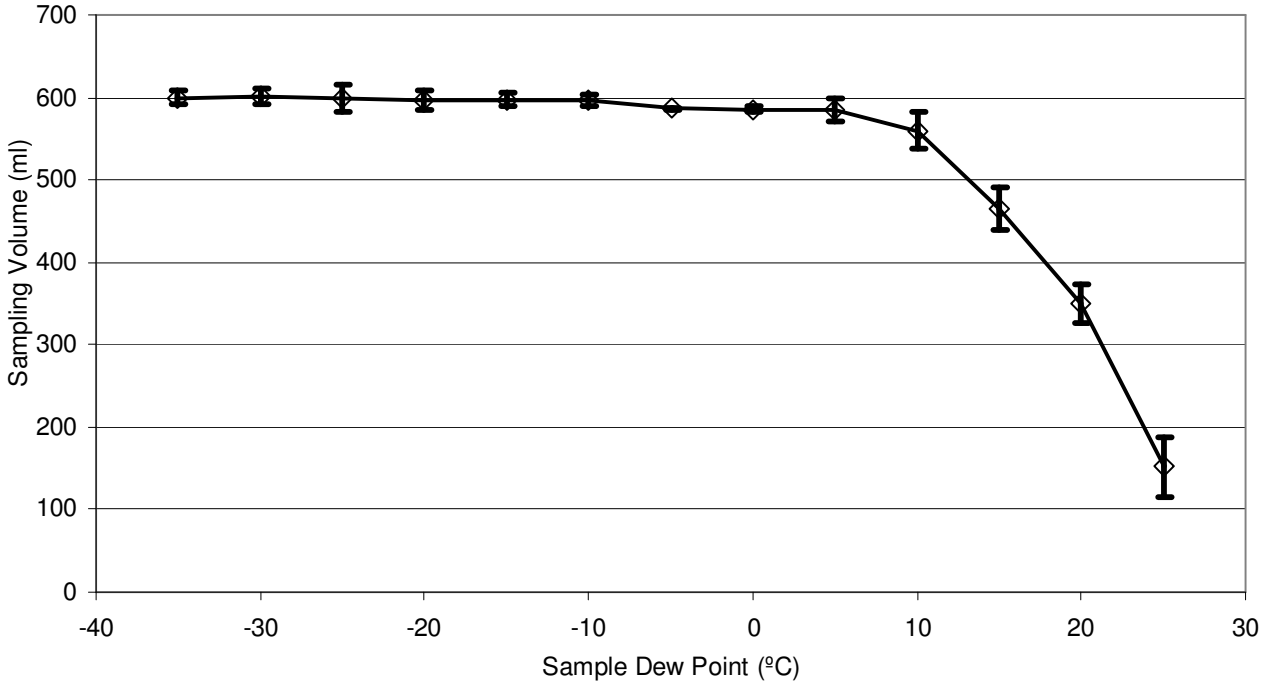

Figure 2.14: Decrease in the effective sampling volume vs. water trap temperature from water freeze-out. Error bars represent standard error of sampling volume for three measurements each. Trapping temperature of three-stage adsorbent trap was – 30 ºC.

The effect of the water vapor on the effective sampling volume is documented in Figure 2.14. At high humidities, water froze out in the microtrap, causing the flow resistance to increase. Ultimately the sampling flow rate would drop to zero as the pressure drop across the microtrap and mass flow controller became too large to maintain sampling flow. The illustrated volumes were calculated using the pressure change in the vacuum reservoir over the 10 min sampling interval. Significant loss of sampling volume started to

occur at a sample dew point >10 ºC (corresponding to a relative humidity > 40% at room temperature). These results are close to the threshold relative humidity of 35% as determined by Gawrys et al. (2001) above which the induced filling of micropores became significant.

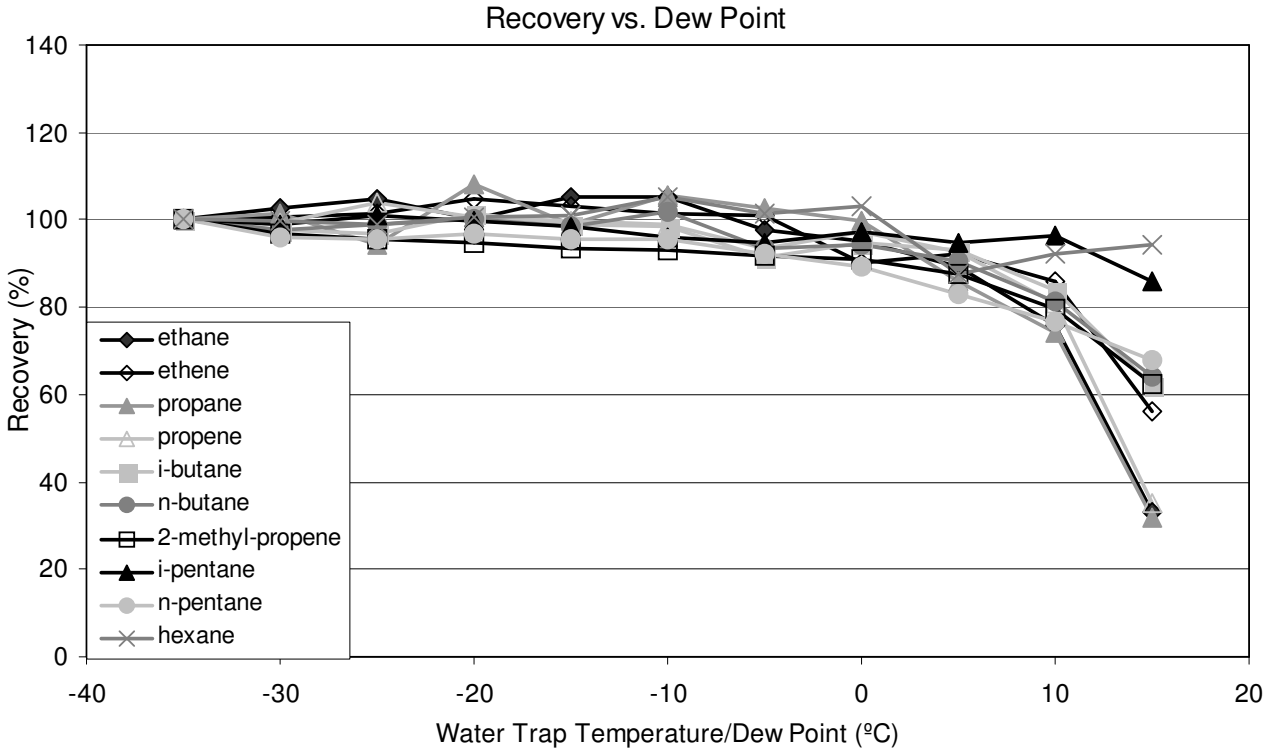

Figure 2.15: Recoveries of selected compounds at increasing water trap temperature (= sample dewpoint). Saturated compounds are represented by solid and unsaturated by open symbols, respectively.

Figure 2.15 shows the effect of elevated humidity on the recovery of individual compounds. In cases where the sampling volume was reduced due to freeze up, analyte concentrations and recovery ratios were calculated under consideration of the actual (reduced) sampling volume. The recovery ratios for all compounds were close to unity at a sampling air dew point < –10 ºC, however between dewpoints of –10 ºC and 15 ºC significant compound losses were observed. The most affected compounds were ethane, propane and propene, which were lost by 65% at 15 ºC. According to Betz, et al. (1989) water occupies the micropores of the carbon molecular sieves, which are also responsible for retaining these light NMHC compounds. In contrast, Carbon Blacks, such as Carboxen 1016 (Fastyn et al., 2003) were not subject to significant water adsorption. Our results

confirm these earlier reports as C2 and C3 hydrocarbons (trapped on the carbon molecular sieves) were most affected by elevated humidity levels whereas C5 and C6 compounds (trapped on the Carboxen 1016 bed) were hardly affected and showed relatively small loss rates. It was necessary to dry the air sample to a dewpoint of <-10 ºC with the peltier-cooled water trap to quantitatively recover all analytes (except acetylene).

2.5 Conclusions and implications for microtrap thermodesorption applications

The critical step in developing a cryogen-free focusing system for GC analysis of NMHC is the choice of the adsorbent material. Of nine commonly used adsorbents that were tested in this study, three materials (Molecular Sieve 5A, Carbotrap and Silica Gel) were found to be unsuitable for trapping C2 to C6 compounds under the chosen analytical conditions. Carbosieve S III, Carboxen 1000, Carboxen 563, Carboxen 1016, Molecular Sieve 4A, and Activated Alumina performed well within a specified volatility range. Carboxen materials were found to be a favorable adsorbent choice for retention and easy thermal release of a wide range of NMHC. Carbosieve SIII was the strongest identified adsorbent and was necessary to retain ethene quantitatively under the chosen experimental conditions.

The range of compounds to be analyzed can be widened by using a multibed adsorbent system with adsorbents of progressively increasing adsorption strength. Subambient temperatures were required to achieve quantitative retention of the most volatile (C2-C3) NMHC. Required cooling can be achieved with a one or two-stage Peltier cooling system, which for many reasons (cost, automation) is advantageous over trapping with liquid cryogens.

Water vapor was found to be a major interference in this application, especially for the sampling of the lightest hydrocarbons (C2 to C4). A drying step that preceded the sample focusing was found to mitigate this interference. Sample drying was achieved by a Peltier-cooled water freezeout trap. Water can easily be removed from this trap between sample focusing periods by heating under air flow or vacuum. This water trap was found to be well suited for this application as it could be regenerated many times and has proven to perform well for long-term operation.

2.6 Acknowledgements

Paul Goldan (NOAA – ESRL, Physical Science Division, Boulder, CO) provided the reference analysis of the VOC standard. This research was funded in part by the NOAA Climate and Global Change Program grant NA03OAR4310072.

3 Sampling of Atmospheric Sesquiterpenes: Sampling Losses and Mitigation of Ozone Interference

Abstract

Atmospheric standards containing parts-per-billion levels of fourteen semi-volatile hydrocarbon compounds, including eight sesquiterpenes (SQT; longipinene, α-copaene, isolongifolene, α -cedrene, *trans*-caryophyllene, aromadendrene, α -humulene, δ -cadinene), two oxidized sesquiterpenoids (*cis*-nerolidol, *trans*-nerolidol), one biogenic ketone (geranylacetone) and three aromatic compounds (1,3,5-tri-isopropylbenzene, diphenylmethane, nonylbenzene) were collected onto four solid adsorbent materials at increasing ozone mixing ratios (0 to 100 ppbV O_3) for analysis by thermodesorption-gas chromatography. Substantial sampling losses of up to > 90 % were found for the most reactive SQT, even at the lowest ozone level investigated of 20 ppbV. Loss rates from the ozone-SQT reaction were used to derive estimates of gas-phase ozone reaction rate constants for longipinene, α-copaene, isolongifolene, geranylacetone, aromadendrene, δ-cadinene, *cis*-nerolidol and *trans*-nerolidol. Three different ozone mitigation techniques were investigated to prevent these sampling losses. These strategies included a) placing glass fibre filters impregnated with sodium thiosulfate ($Na_2S_2O_3$) into the sampling line, b) titration of ozone in the sampling stream with nitric oxide (NO) and c) catalytically removing ozone with a commercially available manganese dioxide (MnO_2) catalyst. All three techniques reduced ozone mixing ratios from 100 ppbV to < 0.6 ppbV at sampling flow rates of 1 l min^{-1}. When the $Na_2S_2O_3$ filters and the NO-titration techniques were applied, SQT loss rates decreased to 0 % to 5 % for most SQT compounds and from > 90 % to ~ 10 - 50 % for the two most reactive compounds at ozone mixing ratios of up to 100 ppbV. The commercial manganese dioxide scrubber, however, caused complete analyte losses (> 98 %) even at 0 ppbV ozone. These results underline the need and present applicable techniques for removal of ozone in air samples for SQT analysis by solid adsorption.

Published in *Environmental Science and Technology* with D. Helmig and J. Ortega as co-authors

3.1 Introduction

Sesquiterpene hydrocarbons ($C_{15}H_{24}$, SQT) as well as their oxygenated derivatives, e.g. alcohols, aldehydes and ketones ($C_{15}H_{22}O$, $C_{15}H_{24}O$, $C_{15}H_{26}O$) have been found in biogenic volatile organic compound (BVOC) emissions from both natural and agricultural vegetation (Buttery et al., 1985, Bicchi et al., 1989, Omata et al., 1990, Winter et al., 1992, König et al., 1995, Rudolph et al., 1997, Schuh et al., 1997, Llusia and Penuelas, 1998, Zhang et al., 1999, Hansen and Seufert, 1999, Ciccioli et al., 1999, Bartelt and Wicklow, 1999, Helmig et al., 1999, Kim et al., 2000, Angelopoulos et al., 2000, Hakola et al., 2001, Köllner et al., 2004, Engelberth et al., 2004, Huang et al., 2003). Some studies estimate that SQT may contribute up to 16% of the overall BVOC landscape flux in some areas (Ciccioli et al., 1999, Helmig et al., 1999). However, quantitative SQT flux data are difficult to obtain and remain highly uncertain due to analytical constraints that stem from the low volatility and high reactivity of SQT compounds (Grosjean et al., 1993, Shu and Atkinson, 1994, Shu and Atkinson, 1995, Hoffmann et al., 1997).

Atmospheric oxidation of SQT occurs both by ozonolysis and by reaction with the OH and NO_3 radical. Reaction rate constants vary widely among different SQT. SQT atmospheric lifetimes from reaction with ambient oxidants are expected to be short. For instance, reported ozone lifetime estimates are ~ 1 min for α-humulene (Hoffmann, 1995), and considering all three oxidation pathways, daytime/nighttime lifetime estimates are ~ 1 - 2 min for *trans*-caryophyllene and α-humulene; ~ 2 min - 2 h for α-copaene, ~ 4 min - 2 h for α-cedrene, and 50 min – 4 hours for longifolene (Shu and Atkinson, 1995). Interestingly, one of the most common and most thoroughly investigated SQT, *trans*-caryophyllene, is also one of the most reactive compounds.

The oxidation products of *trans*-caryophyllene were found to reside almost completely in the aerosol-phase (Hoffmann et al., 1997) and SQT are suspected to play an important role in biogenic aerosol formation. Gas phase oxidation products of *trans*-caryophyllene that have been identified include 3,3-dimethyl-γ-methylene-2-(3-oxobutyl)-cyclobutanebutanal, 3,3-dimethyl-γ-oxo-2-(3-oxobuty)-cyclo-butanebutanal and formaldehyde (Calogirou et al., 1997). Reactions of sesquiterpenoid compounds (nerolidol, farnesol) common in epicuticular waxes of Mediterranean plants (Quercus ilex, Citrus sinensis, Quercus suber, Quercus freinetto, Pinus pinea) at ozone mixing ratios of 50 – 100

ppbV yielded significant emissions of geranylacetone, 6-methyl-5-heptene-2-one, 4-oxopentanal and acetone (Fruekilde et al., 1998). Tobacco plants (Nicotiana tabacum) show strong SQT-emissions after being exposed to elevated ozone levels (120-170 ppbV) (Heiden et al., 1999).

Several studies have addressed the analytical problems arising from interactions between unsaturated terpenoid compounds and ozone during sampling procedures. Calogirou et al. (1996) found that saturated terpenoid compounds (1,8-cineole, camphor and bornyl-acetate) showed no losses due to ozone, while unsaturated compounds with one double bond (e.g.: camphene, α-pinene, sabinene) showed moderate loss rates (5-35 %) and compounds with two or more double bonds (e.g.: β-*trans*-ocimene, α-terpinene, *trans*-caryophyllene) showed very strong depletion (80-100 %) at ozone mixing ratios of 120 ppbV on Tenax TA cartridges. Larsen et al. (1997) compared results from ten European laboratories that analyzed the same monoterpene standard. The sampling was performed at various ozone levels (8, 65 and 125 ppbV). The results were usually accurate and precise at 8 ppbV ozone. However, under elevated ozone conditions (65 and 125 ppbV) significant losses (up to 100 % for some compounds) were found. Laboratories utilizing ozone mitigation techniques reported much higher recovery rates and improved accuracy. SQT loss rates reported by Hoffmann (1995) during solid adsorption sampling without ozone mitigation at 23 ppbV ozone were longicyclene ~ 0 %; γ-muurolene ~ 20 %; α-copaene ~ 40 %; γ-cadinene ~ 55 %; isocaryophyllene ~ 75 %; *cis*-α-bergamotene ~ 85 %; *trans*-caryophyllene, α-humulene and α-cubebene > 95 %.

The effect of ozone on the integrity of the adsorbent material has to be considered as well. Cao and Hewitt (1994) investigated degradation of several adsorbent materials (Tenax TA, Tenax GR, Carbotrap and Chromosorb 106) during passive sampling at 180 ppbV ozone over one week. No artifact formation was found for Carbotrap and Chromosorb 106, whereas for Tenax TA and Tenax GR oxidation products such as benzaldehyde, phenol and acetophenone were identified. Similar observations have been made by others (Helmig and Arey, 1992, Bowyer and Pleil, 1995). In another study on the sampling effects of oxidant-containing air on Tenax TA adsorbent, several degradation products were identified from the reaction with nitrogen dioxide and ozone, but none for reaction with nitric oxide (Klenø et al., 2002).

Conclusively, these studies have shown that many BVOC (especially SQT) are rapidly depleted at elevated ozone concentrations. Consequently, ozone mitigation techniques are required during BVOC sampling. Several techniques for selective ozone removal have previously been applied to reduce these sampling losses. A review of ozone mitigation techniques was presented by Helmig (1997). Further research, with particular focus on how to minimize sampling losses of biogenic compounds, has been published subsequently (Komenda et al., 2001, Fick et al., 2001, Konrad et al., 2003).

Three promising ozone mitigation methods that have been extensively used in the past were further investigated in this research with emphasis on SQT analysis. These include a) the application of sodium thiosulfate impregnated filters, b) titration of ozone with nitric oxide and c) catalytic removal of ozone with manganese dioxide coated screens. In the first method, the sample flow is directed through a glass-fiber filter impregnated with sodium thiosulfate. Details of this method are discussed by Lehmpuhl and Birks (1996). This technique has been applied successfully in some studies on light biogenic hydrocarbons such as isoprene and monoterpenes (Strömvall and Peterson, 1992). Helmig et al. (1997) used $Na_2S_2O_3$ impregnated filters and reported a quantitative ozone removal capacity in 1000 l air at background ozone mixing ratios (< 25 ppbV). Fick et al. (2001) showed that 200 mg of crystalline $Na_2S_2O_3$ have an ozone removal capacity of 10 l of air at 73-78 ppbV ozone.

Nitric Oxide (NO) is oxidized by ozone with the first order rate constant of k (298 K, 101.3 hPa) = 1.8×10^{-14} cm^3 $molecule^{-1}$ s^{-1}. Mochida et al. (2003) analyzed this technique in an extensive modeling study with a Regional Atmospheric Chemistry Model (RACM) developed by Stockwell et al. (1997). According to these calculations ozone mixing ratios will be reduced by a factor of 100 within ~ 1.5 s when the NO concentration is 100 times higher than the ozone concentration. Besides removing ozone, titration with NO can also reduce concentrations of other atmospheric oxidants, such as OH and NO_3. NO titration was utilized by Sirju and Shepson (1995) in the analysis of aldehydes by the DNPH (dinitrophenyl-hydrazine) technique. Kuster et al. (1986) experienced unacceptable chromatographic interferences in non-methane-hydrocarbon analysis while applying this technique. Karst et al. (1993) reported interferences in the determination of aldehyde-DNPH derivatives from nitrogen dioxide, one of the products formed in the NO + ozone reaction. Wedel et al. (1998) applied this technique to remove ozone prior to the

preconcentration step in measurements of volatile organic compounds. The recovery rate for α-cedrene increased from 0 % to 72 % (at 100 ppbV O_3) when 1 ppmV of NO was added. NO did not negatively affect the α-cedrene recovery. Komenda et al. (2003) applied the NO titration technique using a 1 ppmV NO mixing ratio for quantifying isoprene and its oxidation products in ambient air.

MnO_2 destroys ozone catalytically. Hoffmann et al. (1993) and Hoffmann (1995) used MnO_2 coated nets taken from an ozone analyzer to remove ozone prior to monoterpene and SQT trapping on solid adsorbents and found improved recoveries at 23 ppbv ozone. Jüttner (1988) experienced dramatically higher recoveries for monoterpenes (2 to 32 times higher) by applying this type of ozone scrubber. Calogirou et al. (1996) designed and evaluated a scrubber that was made from MnO_2 coated copper screens. Monoterpene losses were prevented for all but the most reactive compounds during sampling at elevated ozone mixing ratios (60 ppbV). Recovery rates for *trans*-caryophyllene under the same conditions improved from 4% to 36%. Janson and Kristenson (1991) reported monoterpene loss of up 30 % to the scrubber during sampling of ambient air. In all these studies the scrubbers were optimised for ozone removal at very specific face velocities.

3.2 Experiments

Analytical techniques: The equipment, procedures and analytical techniques employed have been described in detail previously (Helmig et al., 2003, 2004), and are therefore only summarized here. SQT standards generated with a capillary diffusion system were used for the analytical experiments. The standard contains eight SQT (longipinene, α-copaene, isolongifolene, α-cedrene, *trans*-caryophyllene, aromadendrene, α-humulene and δ-cadinene), 3 aromatic compounds (1, 3, 5, tri-isopropylbenzene, diphenylmethane and nonylbenzene), 1 biogenic ketone (geranylacetone) and four oxygenated SQT (*cis*-nerolidol, *trans*-nerolidol, cedrol and caryophyllene-oxide) in nitrogen. Chemical structures of the biogenic analytes can be found in (Helmig et al., 2003) and in figure 3.1. The aromatic compounds were included because of their low reactivity with ozone. The concurrent analysis of these aromatic compounds was expected to provide ways for

monitoring instrument performance and to yield further insight into analyte versus adsorbent effects.

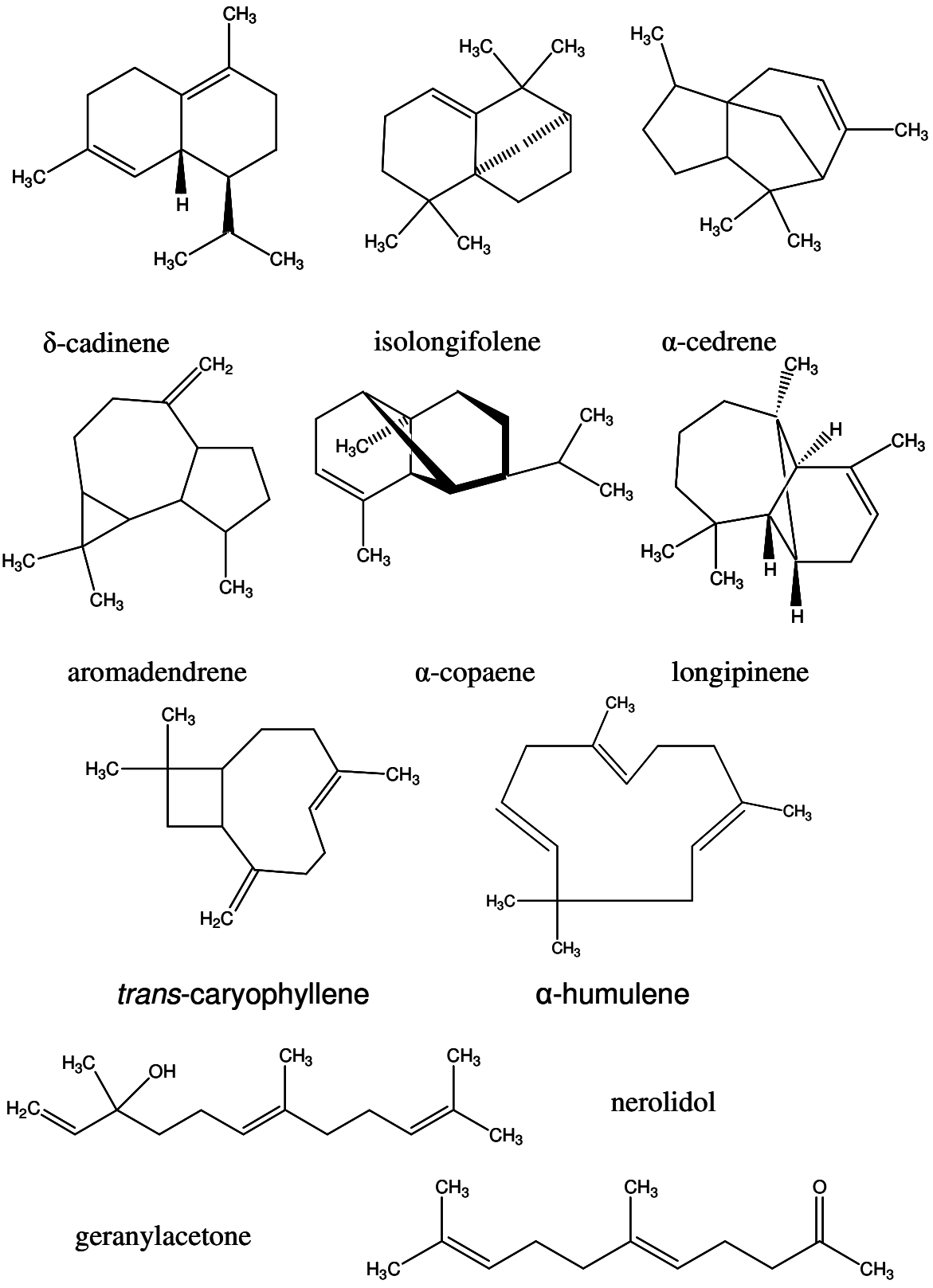

Figure 3.1: Chemical structures of investigated BVOC

The output from the CDS was diluted by adding zero air, which could also be enriched with ozone. The control range for ozone was 5 to 150 ppbV ozone. Samples were collected on solid adsorbent cartridges with a custom-made autosampler (Helmig et al., 2004). The four solid adsorbents used (Tenax TA, Tenax GR, Carbotrap and Carbotrap C; Alltech, Deerfield, IL and Supelco, Bellefonte, PA respectively) have previously been found suitable in SQT analysis and were further investigated in this study to determine sampling interferences from ozone. An extensive review of the physical properties and analytical performances of these adsorbents was given by Dettmer and Engewald (2002). Loaded adsorbent cartridges were thermally desorbed and quantified by GC-FID using a Perkin Elmer-ATD-400 automated thermodesorption system interfaced to a PE Autosystem XL gas chromatograph (PerkinElmer, Boston, MA). The following ATD-400 parameters were used: He purge flow 37 ml min^{-1}, primary desorption temperature 300°C, primary desorption time 10 min, second stage trap temperature during primary desorption – 30 °C, second stage trap desorption temperature 350°C, hold time 5 min. The second stage trap was filled with Unibeads (Alltech, Deerfield, IL). The ATD-400 outlet split flow during the second stage desorption was 7.7 ml min^{-1}. Other GC parameters were: FID hydrogen 45 ml min^{-1}, FID air 350 ml min^{-1}, He carrier gas flow 2.5 ml min^{-1}; GC oven program: 40°C for 5 min, 20°C min^{-1} to 100°C, 2°C min^{-1} to 160°C, 40°C min^{-1} to 250 °C, final time 5 min. The column was a DB-1, 0.32 mm I.D. x 30 m-length with a 0.25 μm film thickness (J. & W. Scientific, Palo Alto, CA).

Ozone generator: The dilution air was enriched with ozone to reach ozone mixing ratios between 5 and 150 ppbV with an UV ozone generator (Model OG-2, UVP, Upland, CA).

Ozone analyzers: Ozone in the sample flow was recorded using two instruments. High ozone mixing ratios were quantified with a Monitor Labs ozone analyzer (Model 8810, Monitor Labs Inc., San Diego, CA). This analyzer has a 1 ppbV precision and a detection limit of approximately 2 ppbV. Ozone mixing ratios below 2 ppbV were measured with an ozone-ethene chemiluminescence instrument (Model 8410, Monitor Labs). The detection limit of this instrument is ~ 0.2 ppbV.

Sodium-thiosulfate-impregnated ozone filters: The ozone filters were prepared by flowing 10 ml of a 10 % aqueous solution of $Na_2S_2O_3$ through 25 mm diameter glass fiber filter disks (1 µm pore size, polypropylene housing, product number 4523, Glass Acrodisk, Gelman Laboratory, Ann Arbor, Mi) and subsequent drying under a nitrogen purge flow of 100 ml min^{-1} at 50°C for 4 hours. These filters were tested at 100 ppbV ozone and 300 ml min^{-1} flow rate. Several filters can be operated in series. One filter reduced the ozone mixing ratio to ~ 0.4 ppbV, while two and three filters in series reduced ozone mixing ratios to ~ 0.2 ppbV under these conditions.

Ozone removal by NO titration: By using NO titration for ozone mitigation, the resulting ozone mixing ratio can be calculated by:

$$[O_3] = [O_3]_0 \times e^{(-kt[NO])} \qquad \text{rct. 3.1}$$

Approximately 2 ml min^{-1} of a ~ 1% mixture of NO (Airgas, Loveland, CO) in nitrogen was added to the diluted standard flow, resulting in an NO mixing ratio of ~ 10 ppmV. The NO flow rate was controlled by the regulator pressure and by a 0.1 mm I.D. deactivated fused silica capillary flow restrictor. After the mixing of the two gas flows, the sample air was flown through Teflon tubing (length: 3 m, I.D.: 0.4 cm) prior to the solid adsorbent trapping. Under these flow conditions, the Reynolds number was calculated to be 4300, which is clearly in the turbulent regime allowing adequate mixing. This resulted in a residence time of ~ 1.5 s in the tubing and ensured enough time for the ozone + NO reaction to take place. According to rct. 3.1, the expected ozone concentration by the time the sample reaches the adsorbent cartridge will be approximately 0.1 % of the initial mixing ratio. At an initial ozone mixing ratio of 100 ppbV, ozone at the outlet was below the 0.2 ppbV detection limit of the chemiluminescence instrument. In another study (Wedel et al., 1998) NO addition resulting in a lower mixing ratio of 1 ppmV destroyed 90 % of ambient ozone. Similar NO mixing ratios were also used by Komenda et al., 2003.

Ozone removal by a manganese dioxide catalyst: In several previous studies custom-made and carefully optimized manganese dioxide catalysts were used as ozone scrubbers (Hoffmann, 1995, Calogirou et al., 1996, 1997). Here, we investigated whether a

commercially available catalyst would be suitable for ozone removal in SQT quantification. The scrubber was a manganese dioxide catalyst canister (Diameter 9.5 cm, Length 4.5 cm) (O.B.E. Corporation, Fredericksberg, TX) which contained 25 MnO_2 – coated copper screens in a steel canister. This catalyst is normally used to provide an ozone-free reference gas in UV ozone analyzers. This scrubber reduced ozone mixing ratios from 100 ppbV to 0.6 ppbV at a flow rate of 300 ml min^{-1}.

3.3 Results and Discussion

3.3.1 SQT Losses in the presence of ozone

SQT sampling losses from reaction with ozone were investigated by loading cartridges of the four adsorbents with 1.6 l of standard sample air. The CDS output was diluted by a factor of 90, resulting in individual mixing ratios for BVOCs of 0.84 ppbV (*cis*-nerolidol), 0.91 ppbV (*trans*-nerolidol), 1.17 ppbV (δ-cadinene), 2.78 ppbV (α-humulene), 3.52 ppbV (α-copaene), 3.70 ppbV (α-cedrene), 3.73 ppbV (aromadendrene), 5.86 ppbV (isolongifolene), 6.25 ppbV (geranylacetone), 6.79 ppbV (longipinene), 11.28 ppbV (*trans*-caryophyllene). These concentrations are somewhat higher (~ 10 -100 x) than typical BVOC concentrations in forest air but within the range of BVOC concentrations in branch or leaf enclosure experiments. Cartridges were loaded at a sampling flow rate of 160 ml min^{-1}. Ozone mixing ratios in the sampling stream were set to 0, 20 40, 60, 80, 100 ppbV (+/- 2 ppbV at all levels). Two replicate cartridges were sampled under each condition. After this series another sample was collected at 0 ppbV ozone to test the reproducibility of the initial conditions.

Analytes were quantified based on their FID area counts and effective carbon numbers (Helmig et al., 2003). The first cartridge of each series was loaded at an ozone mixing ratio of 0 ppbV and was used as the reference (100 % value). Results for the SQT shown in Figure 3.2 reemphasize that ozone indeed severely affects recoveries. Significant SQT losses were observed for almost all compounds on all adsorbents (see also table 3.1 for numeric display of results for all investigated compounds.

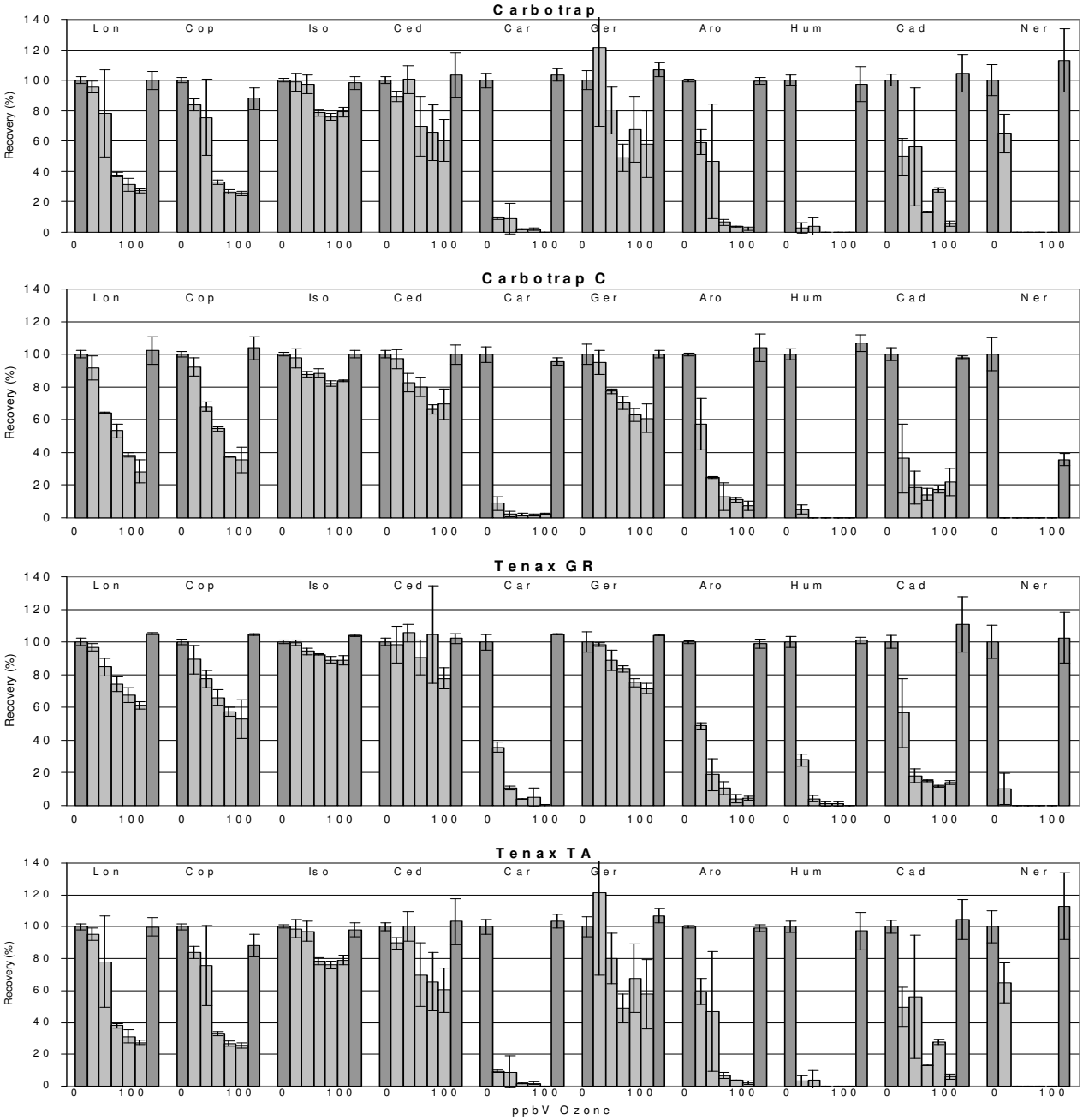

Figure 3.2: SQT recovery vs. ozone concentration (0, 20, 40, 60, 80, 100, 0 ppbV) for ten investigated BVOCs (from left to right in order of GC retention time). Abbreviations are: Lon: longipinene, Cop: α-copaene, Iso: isolongifolene, Ced: α-cedrene, Car: *trans*-caryophyllene, Ger: geranyl-acetone, Aro: aromadendrene, Hum: α-humulene, Cad: δ-cadinene, Ner: nerolidol, average of the *cis* and *trans* isomer). Error bars represent the relative standard deviation over two runs. Dark gray columns indicate runs without the addition of ozone; light gray indicates runs with added ozone.

Table 3.1: Recovery rates (%) for SQT, related compounds and three aromatic compounds at varying ozone mixing ratios on four adsorbents without application of mitigation techniques; error margins represent the relative standard deviation for n = 2.

Compound	Recoveries (%) on Carbotrap at ozone mixing ratio (ppbV)						
	0	20	40	60	80	100	0
1, 3, 5 Tri-isopropylbenzene	100.0 +/- 8.4	102.8 +/- 4.6	100.5 +/- 2.9	88.0 +/- 4.1	90.1 +/- 1.5	93.0 +/- 1.6	103.1 +/- 1.4
Longipinene	100.0 +/- 2.2	95.6 +/- 3.8	78.1 +/- 28.6	37.9 +/- 1.2	31.3 +/- 4.1	27.3 +/- 1.4	99.9 +/- 5.8
α-Copaene	100.0 +/- 0.1	84.0 +/- 3.9	75.6 +/- 25.0	33.0 +/- 1.5	26.7 +/- 1.5	25.6 +/- 1.4	88.1 +/- 7.2
Isolongifolene	100.0 +/- 3.4	98.7 +/- 5.7	97.1 +/- 6.2	78.6 +/- 2.2	76.0 +/- 2.3	79.1 +/- 3.1	98.1 +/- 4.4
Diphenylmethane	100.0 +/- 6.1	88.7 +/- 5.6	96.1 +/- 1.2	78.5 +/- 3.9	66.0 +/- 7.5	75.0 +/- 15.8	102.8 +/- 9.0
α-Cedrene	100.0 +/- 10.1	89.6 +/- 3.4	100.4 +/- 9.3	69.8 +/- 19.8	65.6 +/- 18.2	60.4 +/- 13.9	103.3 +/- 14.5
trans-Caryophyllene	100.0 +/- 8.6	9.5 +/- 0.9	9.0 +/- 10.1	1.9 +/- 0.1	1.8 +/- 0.8	<LOD*	103.7 +/- 4.2
Geranylacetone	100.0 +/- 4.6	121.5 +/- 51.8	80.2 +/- 15.6	48.9 +/- 9.1	67.6 +/- 21.5	57.7 +/- 21.9	107.0 +/- 4.7
Aromadendrene	100.0 +/- 6.5	59.2 +/- 8.1	46.8 +/- 37.7	6.6 +/- 2.0	3.8 +/- 0.2	2.0 +/- 1.1	99.3 +/- 2.2
α-Humulene	100.0 +/- 11.6	<LOD	<LOD	<LOD	<LOD	<LOD	97.4 +/- 11.7
δ-Cadinene	100.0 +/- 15.5	49.8 +/- 12.1	56.0 +/- 38.8	13.1 +/- 0.1	27.8 +/- 1.4	5.8 +/- 1.6	104.7 +/- 12.4
cis-Nerolidol	100.0 +/- 11.6	57.1 +/- 8.3	<LOD	<LOD	<LOD	<LOD	117.1 +/- 11.1
trans-Nerolidol	100.0 +/- 8.0	74.3 +/- 18.5	<LOD	<LOD	<LOD	<LOD	107.8 +/- 29.8
Nonylbenzene	100.0 +/- 14.6	80.5 +/- 13.9	81.0 +/- 4.8	75.4 +/- 0.2	85.4 +/- 10.5	89.2 +/- 23.1	98.5 +/- 9.6

Compound	Recoveries (%) on Carbotrap C at ozone mixing ratio (ppbV)						
	0	20	40	60	80	100	0
1, 3, 5 Tri-isopropylbenzene	100.0 +/- 3.6	97.7 +/- 6.0	89.8 +/- 2.7	93.9 +/- 3.6	88.5 +/- 2.0	89.1 +/- 4.5	97.4 +/- 1.9
Longipinene	100.0 +/- 0.6	91.8 +/- 7.5	64.2 +/- 0.2	53.4 +/- 4.3	38.4 +/- 1.5	28.4 +/- 6.9	102.2 +/- 8.3
α-Copaene	100.0 +/- 2.4	92.2 +/- 5.8	68.2 +/- 2.8	54.3 +/- 1.3	37.3 +/- 0.3	35.5 +/- 7.9	103.8 +/- 6.9
Isolongifolene	100.0 +/- 4.1	97.6 +/- 6.1	87.8 +/- 1.8	88.5 +/- 2.6	82.3 +/- 1.6	83.8 +/- 0.5	100.2 +/- 2.3
Diphenylmethane	100.0 +/- 3.0	95.1 +/- 11.6	83.7 +/- 4.5	88.6 +/- 6.9	85.1 +/- 5.9	92.5 +/- 0.8	110.7 +/- 6.3
α-Cedrene	100.0 +/- 3.6	97.2 +/- 5.8	82.7 +/- 5.5	79.9 +/- 5.9	66.4 +/- 2.9	69.6 +/- 9.2	99.9 +/- 5.9
trans-Caryophyllene	100.0 +/- 4.0	8.8 +/- 4.3	2.1 +/- 1.8	1.7 +/- 0.8	1.7 +/- 0.3	2.5 +/- 0.0	95.6 +/- 2.0
Geranylacetone	100.0 +/- 3.4	94.9 +/- 7.2	77.5 +/- 1.4	70.4 +/- 4.1	63.0 +/- 3.7	60.8 +/- 8.7	100.0 +/- 2.2
Aromadendrene	100.0 +/- 6.8	57.2 +/- 15.8	24.9 +/- 0.6	13.1 +/- 8.4	11.0 +/- 1.2	7.3 +/- 2.7	104.2 +/- 8.5
α-Humulene	100.0 +/- 1.2	5.0 +/- 3.0	<LOD	<LOD	<LOD	<LOD	107.0 +/- 5.2
δ-Cadinene	100.0 +/- 6.7	36.4 +/- 21.2	18.6 +/- 10.2	14.3 +/- 3.7	17.5 +/- 2.2	21.9 +/- 8.3	97.9 +/- 0.9
cis-Nerolidol	100.0 +/- 7.9	<LOD	<LOD	<LOD	<LOD	<LOD	32.6 +/- 2.9
trans-Nerolidol	100.0 +/- 3.3	<LOD	<LOD	<LOD	<LOD	<LOD	42.7 +/- 3.7
Nonylbenzene	100.0 +/- 5.3	89.2 +/- 3.7	82.4 +/- 0.2	83.2 +/- 8.8	99.0 +/- 2.9	84.8 +/- 6.7	113.0 +/- 20.0

* LOD: Limit Of Detection

Table 3.1 (continued)

Compound	Recoveries (%) on Tenax GR at ozone mixing ratio (ppbV)						
	0	20	40	60	80	100	0
1, 3, 5 Tri-isopropylbenzene	100.0 +/- 11.7	100.1 +/- 0.3	98.2 +/- 0.5	96.4 +/- 2.1	97.9 +/- 3.3	95.3 +/- 0.5	105.0 +/- 0.6
Longipinene	100.0 +/- 4.7	96.9 +/- 2.2	84.7 +/- 5.5	74.2 +/- 4.5	67.6 +/- 4.3	61.2 +/- 2.0	105.1 +/- 0.4
α-Copaene	100.0 +/- 0.9	89.2 +/- 8.6	77.5 +/- 5.5	66.0 +/- 4.7	57.1 +/- 2.7	53.0 +/- 11.8	104.6 +/- 0.6
Isolongifolene	100.0 +/- 1.1	99.6 +/- 1.6	94.2 +/- 1.7	92.4 +/- 0.4	89.1 +/- 2.1	88.8 +/- 2.8	103.9 +/- 0.3
Diphenylmethane	100.0 +/- 3.5	90.3 +/- 4.2	91.4 +/- 0.1	98.3 +/- 7.0	96.9 +/- 3.6	92.3 +/- 1.4	97.2 +/- 1.1
α-Cedrene	100.0 +/- 10.1	98.5 +/- 11.4	105.4 +/- 5.1	90.6 +/- 10.6	104.7 +/- 29.8	77.9 +/- 6.6	102.2 +/- 3.0
trans-Caryophyllene	100.0 +/- 15.7	35.6 +/- 3.1	10.9 +/- 1.1	3.9 +/- 0.1	5.1 +/- 5.4	0.2 +/- 0.3	104.6 +/- 0.2
Geranylacetone	100.0 +/- 10.0	98.2 +/- 1.1	88.7 +/- 6.0	83.6 +/- 2.1	75.2 +/- 2.5	71.5 +/- 3.1	104.2 +/- 0.2
Aromadendrene	100.0 +/- 10.9	48.7 +/- 1.9	18.9 +/- 9.8	10.9 +/- 3.9	4.2 +/- 2.4	4.5 +/- 1.0	99.0 +/- 3.0
α-Humulene	100.0 +/- 2.2	27.9 +/- 3.8	4.0 +/- 2.0	<LOD	0.9 +/- 1.2	0.0 +/- 0.0	101.1 +/- 1.9
δ-Cadinene	100.0 +/- 10.8	56.6 +/- 20.9	18.2 +/- 4.2	15.2 +/- 0.4	11.7 +/- 0.5	13.9 +/- 1.2	110.7 +/- 15.4
cis-Nerolidol	100.0 +/- 12.9	<LOD*	<LOD	<LOD	<LOD	<LOD	107.2 +/- 13.5
trans-Nerolidol	100.0 +/- 13.4	17.5 +/- 9.9	<LOD	<LOD	<LOD	<LOD	99.7 +/- 2.6
Nonylbenzene	100.0 +/- 3.1	85.7 +/- 1.2	80.5 +/- 4.8	86.7 +/- 4.0	88.1 +/- 6.4	87.3 +/- 7.7	96.9 +/- 4.8

Compound	Recoveries (%) on Tenax TA at ozone mixing ratio (ppbV)						
	0	20	40	60	80	100	0
1, 3, 5 Tri-isopropylbenzene	100.0 +/- 1.2	99.0 +/- 3.5	95.6 +/- 0.7	97.8 +/- 4.5	98.5 +/- 1.5	94.9 +/- 4.3	98.8 +/- 2.9
Longipinene	100.0 +/- 0.8	89.9 +/- 1.3	65.6 +/- 1.5	57.9 +/- 6.2	53.7 +/- 10.9	39.9 +/- 1.0	99.9 +/- 0.4
α-Copaene	100.0 +/- 2.5	91.2 +/- 2.3	79.6 +/- 3.0	61.8 +/- 2.7	58.3 +/- 11.8	42.2 +/- 4.5	102.1 +/- 5.2
Isolongifolene	100.0 +/- 0.7	97.7 +/- 3.1	93.1 +/- 1.2	95.4 +/- 4.8	95.7 +/- 2.8	94.0 +/- 4.5	98.6 +/- 3.9
Diphenylmethane	100.0 +/- 2.2	93.3 +/- 3.7	105.0 +/- 2.6	92.3 +/- 5.7	92.4 +/- 4.2	93.4 +/- 4.8	98.4 +/- 5.5
α-Cedrene	100.0 +/- 1.1	94.5 +/- 2.6	74.8 +/- 2.7	79.0 +/- 1.0	77.1 +/- 2.5	66.2 +/- 2.5	97.9 +/- 4.1
trans-Caryophyllene	100.0 +/- 3.4	5.6 +/- 0.7	11.7 +/- 0.4	1.1 +/- 0.7	1.0 +/- 0.5	1.0 +/- 0.6	99.5 +/- 6.4
Geranylacetone	100.0 +/- 3.4	95.3 +/- 3.9	64.2 +/- 1.2	81.6 +/- 1.8	75.8 +/- 6.8	61.1 +/- 1.5	98.8 +/- 5.0
Aromadendrene	100.0 +/- 3.7	33.7 +/- 1.8	1.1 +/- 0.1	13.2 +/- 0.3	9.1 +/- 5.2	3.9 +/- 1.5	98.5 +/- 7.2
α-Humulene	100.0 +/- 4.9	3.0 +/- 0.4	<LOD	<LOD	<LOD	<LOD	100.3 +/- 7.6
δ-Cadinene	100.0 +/- 6.3	64.5 +/- 10.0	46.8 +/- 1.3	26.6 +/- 1.3	22.4 +/- 1.1	10.0 +/- 8.0	91.3 +/- 10.4
cis-Nerolidol	100.0 +/- 15.6	<LOD	<LOD	<LOD	<LOD	<LOD	95.2 +/- 13.1
trans-Nerolidol	100.0 +/- 20.2	<LOD	<LOD	<LOD	<LOD	<LOD	97.5 +/- 10.3
Nonylbenzene	100.0 +/- 2.6	101.0 +/- 0.5	81.6 +/- 2.8	93.6 +/- 6.1	89.0 +/- 3.4	87.8 +/- 2.3	97.7 +/- 0.3

* LOD: Limit Of Detection

Loss rates varied widely from approximately 2 % (isolongifolene) to 90 % (*trans*-caryophyllene, α-humulene) even at the lowest ozone level (20 ppbV) tested. At 100 ppbV ozone the range of observed losses was from 10 % (isolongifolene) to 100 % (*trans*-caryophyllene, α-humulene). The aromatic compounds were stable with respect to ozone and had recoveries between 90 and 100% at all ozone mixing ratios. The adsorbent type had only a small impact on the SQT loss rate. The carbon based adsorbents Carbotrap and Carbotrap C displayed qualitatively similar behavior. The loss rates on Tenax TA appeared to be slightly lower than those observed on Carbotrap and Carbotrap C. Tenax GR generally showed 20 % higher recovery rates than the other adsorbents at elevated ozone levels.

SQT losses were related to the chemical structure of the respective compound. Unsaturated compounds with multiple double bonds (δ-cadinene and *trans*-caryophyllene (2 double bonds) as well as α-humulene (3 double bonds)) were the most depleted analytes. The other SQT have only one double bond and were found to be less depleted. The observed loss rates appeared to correlate well with previously published atmospheric ozone reaction rate constants, i.e.: *trans*-caryophyllene ~ α-humulene > α-copaene > α-cedrene (Hoffmann, 1995; Shu and Atkinson, 1995). Oxygenated SQT experienced substantial losses and could only be recovered at the lowest ozone mixing ratios.

As mentioned above, ozone did not affect the aromatic compounds, which demonstrates the stability of these molecules towards reaction with ozone. This observation proves that the SQT losses were due to SQT-ozone reactions and were not related to an ozone-induced degradation of the adsorbent material.

No apparent SQT oxidation reaction products were identified in the chromatograms. However, the current analytical set-up is not optimized for to either detecting possible volatile ozone-SQT reaction products (such as acetone, formaldehyde or organic acids) or oxygenated, heavier molecular weight products. Adsorbent degradation products, as identified previously by others (Klenø et al., 2002) were not found in our measurements either.

Estimates of SQT-ozone reaction rate constants Gas phase reaction rate constants (*k*) for the reaction of five SQT with ozone were taken from the literature (Shu and Atkinson, 1995). Four of these compounds included in our study (with their ozone reaction constants

in 10^{-17} cm ^{3} molecule^{-1} s $^{-1}$) were α-cedrene (2.78), α-copaene (15.8), *trans*-caryophyllene (1160), and α-humulene (1170). A linear correlation was found when ln *k* was plotted vs. the mean of the observed loss rates on the four adsorbents (see previous section). This analysis was performed for the 20, 40, 60, 80 and 100 ppb ozone experiments. These correlations were then used to estimate SQT-ozone reaction rate constants for the remaining SQT compounds. The derived mean rate constants (with standard deviation) are listed in Table 3.2.

These rate constants rely on the data given by Atkinson and Shu (22), who reported relative uncertainties of ~50 %. Furthermore, given the rather indirect approach of our analysis, the derived reaction rate constants should be regarded as rather approximate values, but to the best of our knowledge, these are the first reaction rate estimates provided for these seven compounds with respect to ozone.

Table 3.2: Mean and standard deviation of SQT-ozone reaction rate constants that were estimated from loss rates on four adsorbents at 20, 40, 60, 80 and 100 ppbV, respectively. Literature values (in 10^{-17} cm ^{3} molecule $^{-1}$ s $^{-1}$) for α-cedrene (2.78), α-copaene (15.8), *trans*-caryophyllene (1160), α-humulene (1170) were used to derive a correlation between observed sampling loss rates and reaction rate constants. The reaction rate constants that were obtained for these reference compounds from the correlation analysis are also included (in italic letters) in this table.

Compound	Reaction Rate Constant 10^{-17} cm ^{3} molecule $^{-1}$ s $^{-1}$
Isolongifolene	2.6 +/- 0.7
α-Cedrene	*3.4 +/- 0.2*
Geranylacetone	7.6 +/- 3.9
α-Copaene	*29 +/- 9*
Longipinene	29 +/- 11
γ-Cadinene	320 +/- 67
Aromadendrene	650 +/- 240
trans-caryophyllene	*1100 +/- 51*
α-humulene	*1400 +/- 88*
cis-Nerolidol	3100 +/- 2200
trans-Nerolidol	2300 +/- 1800

Sampling flow rate effects Experiments were performed at different sampling flow rates (keeping sample volume constant) to determine if the SQT losses were happening in the gas phase or on the adsorbent bed. Sample volumes of 1.6 l were collected at 100 ppbV

ozone and at sampling flow rates of 160, 120, 80, and 40 ml min^{-1} over 10 min, 13.3, 20 and 40 min, respectively. The estimated residence times in the sampling apparatus for the different flow rates are ~ 5 s (160 ml min^{-1} sampling), ~ 7 s, ~ 10 s and ~ 20 s respectively. At the highest flow rate (160 ml min^{-1}) and 100 ppbV of ozone a maximum gas-phase depletion of 10 % is calculated for the most reactive compounds (α-humulene and *trans*-caryophyllene) according to their literature reaction rate constants (Shu and Atkinson, 1995). Considering that the SQT mixing ratios for these compounds are approximately 2 and 10 ppbV (α-humulene and *trans*-caryophyllene, respectively) and that a 1:1 (molar/molar) reaction of SQT:ozone occurs, the maximum ozone reduction due to gas phase reaction with SQT is expected to be small (< 2% of total ozone mixing ratio). Since the other compounds are either less concentrated or have significantly lower reaction rate constants, their contribution to a further decrease in the ozone mixing ratio is negligible as well. Consequently, high ozone levels (≥ 98 ppbV) remained in the sampling air during the adsorption step. The time that the analytes were exposed to ozone in the gas phase increased by a factor of four as the sampling flow rates decreased from 160 to 40 ml min^{-1}. If the majority of SQT losses from ozone reaction would occur in the gas-phase, increased loss rates should be observed at the lower flow rates. The recovery rates for the different sample flows were calculated relative to experiments at 0 ppbV ozone and 160 ml min^{-1} sampling flow. Results for longipinene, a SQT that shows a moderate loss at 100 ppbV, were expected to yield a sensitive analysis of this effect. No significant differences (Figure 3.3) were seen for longipinene or any other less reactive SQT in this experiment. The most reactive compounds (α-humulene and *trans*-caryophyllene) were completely removed at all sampling flow rates at 100 ppbV ozone. Although it is impossible to definitively determine the location where the depletion of these reactive compounds occurred, these results imply that the majority of the SQT + ozone loss reaction takes place on the adsorbent bed. This conclusion agrees with previous observations (Calogirou et al., 1996), which showed that monoterpenes similarly were lost due to ozone reactions on the adsorbent bed.

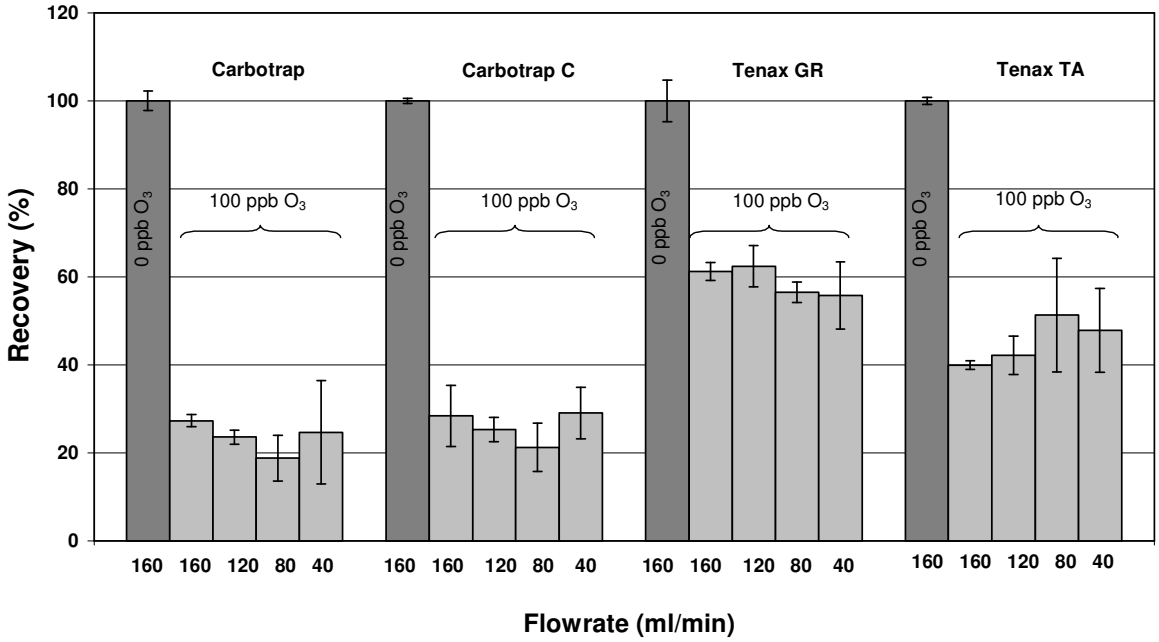

Figure 3.3
Recovery rates for longipinene at different sampling flows (same sampling volume) on four different adsorbents.

3.3.2 Ozone mitigation techniques

Sodium thiosulfate filter technique: Two adsorbent cartridges were loaded initially without an ozone filter in the sampling stream at 0 ppbV ozone. The FID area counts of this analysis were used as a reference for the calculation of recovery rates. Cartridges were then loaded with the filter in the sampling stream at 0, 20, 40, 60, 80 and 100 ppbV ozone mixing ratios. The 0 ppbV ozone/filter sample was collected to investigate possible SQT losses to the filter materials. After these experiments the filter was removed and two cartridges were loaded again without the filter at 0 ppbV ozone, replicating the initial experiment. Figure 3.4 shows the recoveries of the SQTs at the various ozone mixing ratios and table 3.3 the numeric results for all investigated compounds.

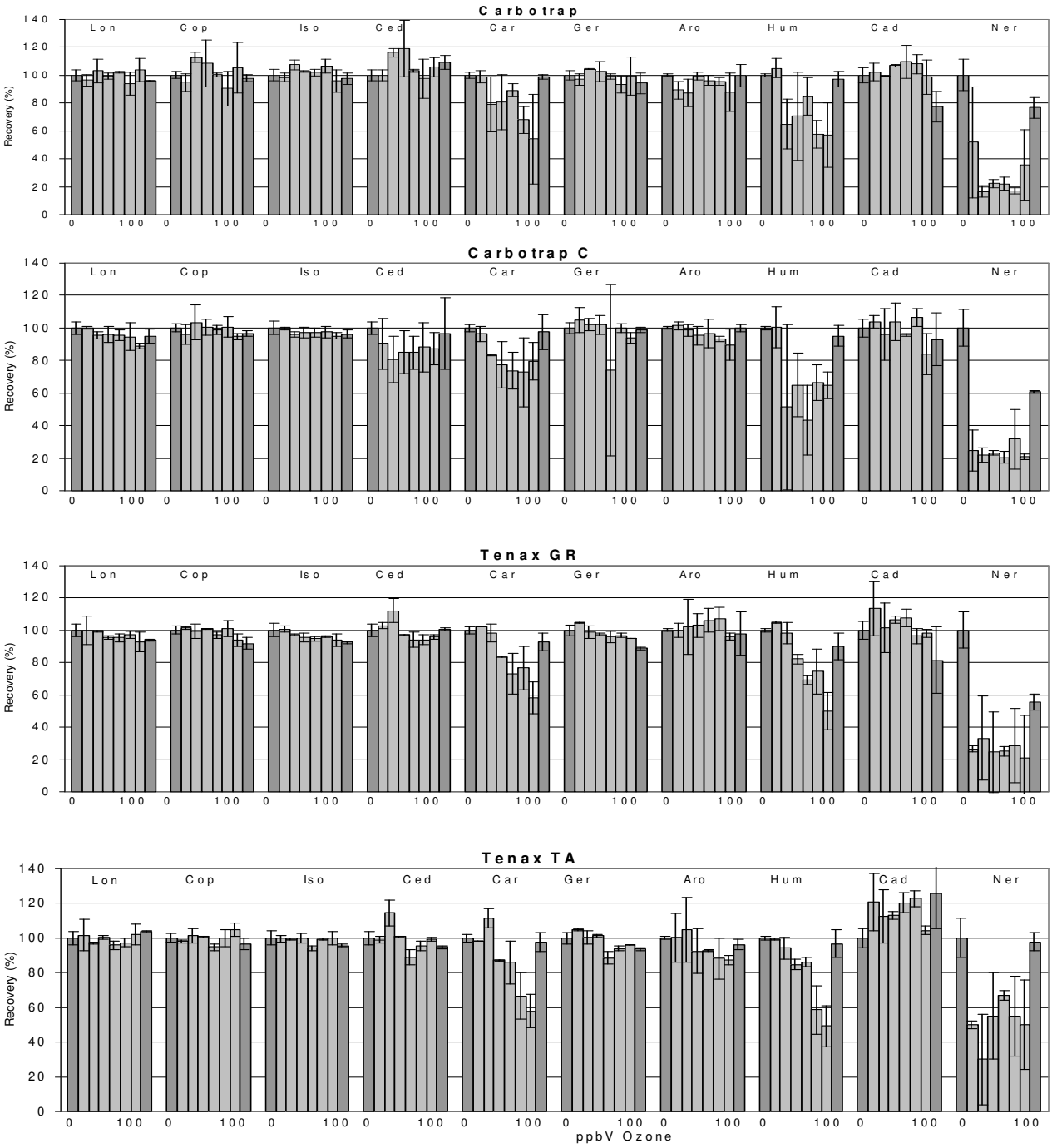

Figure 3.4: Recovery rates with a sodium thiosulfate impregnated filter in the sampling stream for ten investigated BVOCs at 0, 0, 20, 40, 60, 80, 100 and 0 ppbV ozone. Abbreviations are the same as in Fig. 1. Dark gray color bars indicates runs without ozone added and no mitigation techniques applied, light gray color bar indicate experiments at ozone mixing ratios from 0 to 100 ppbV with the filter in the sampling stream.

Table 3.3: Recovery rates (%) at increasing ozone mixing ratios on four adsorbents using the $Na_2S_2O_3$-filter technique; errors represent standard deviation for n = 2.

Compound	Recoveries (%) Carbotrap at ozone mixing ratio (ppbV)							
	0 no filter	0 + filter	20 + filter	40 + filter	60 + filter	80 + filter	100 + filter	0 no filter
1, 3, 5 Tri-isopropylbenzene	100.0 +/- 4.1	101.2 +/- 4.2	101.0 +/- 7.5	105.6 +/- 0.2	101.5 +/- 2.0	102.6 +/- 0.8	103.0 +/- 2.5	99.1 +/- 3.5
Longipinene	100.0 +/- 1.0	96.4 +/- 4.3	103.0 +/- 8.3	99.3 +/- 2.2	101.9 +/- 0.6	93.8 +/- 8.5	103.9 +/- 8.2	96.1 +/- 0.1
α-Copaene	100.0 +/- 1.7	94.7 +/- 6.6	112.8 +/- 3.7	108.4 +/- 16.6	100.2 +/- 1.3	90.4 +/- 12.3	105.4 +/- 18.3	97.9 +/- 2.4
Isolongifolene	100.0 +/- 4.1	98.5 +/- 3.3	107.5 +/- 3.6	102.7 +/- 0.7	102.0 +/- 2.5	106.6 +/- 5.0	95.9 +/- 7.9	97.7 +/- 4.2
Diphenylmethane	100.0 +/- 4.6	103.6 +/- 22.7	106.4 +/- 13.9	101.6 +/- 7.0	100.8 +/- 8.3	95.4 +/- 6.4	111.7 +/- 20.1	94.1 +/- 7.9
α-Cedrene	100.0 +/- 6.6	100.1 +/- 3.9	116.1 +/- 3.0	119.2 +/- 20.2	103.2 +/- 1.2	97.6 +/- 14.0	105.7 +/- 6.9	109.4 +/- 4.9
trans-Caryophyllene	100.0 +/- 4.6	99.0 +/- 4.3	79.1 +/- 19.8	80.8 +/- 19.6	89.1 +/- 4.6	68.0 +/- 9.7	54.2 +/- 32.0	98.8 +/- 1.5
Geranylacetone	100.0 +/- 3.8	97.1 +/- 4.2	104.5 +/- 0.3	102.6 +/- 7.2	99.2 +/- 2.0	93.1 +/- 6.0	99.3 +/- 13.9	94.2 +/- 7.6
Aromadendrene	100.0 +/- 3.1	89.4 +/- 6.3	87.2 +/- 9.9	99.4 +/- 2.8	96.1 +/- 3.6	95.5 +/- 2.9	87.6 +/- 13.7	99.8 +/- 8.0
α-Humulene	100.0 +/- 2.5	105.1 +/- 6.9	65.1 +/- 18.1	70.7 +/- 31.7	84.8 +/- 13.3	57.4 +/- 9.9	44.5 +/- 23.2	97.1 +/- 5.3
δ-Cadinene	100.0 +/- 6.8	102.3 +/- 6.4	99.5 +/- 0.1	106.9 +/- 0.8	109.6 +/- 11.7	108.0 +/- 7.1	98.6 +/- 12.5	77.3 +/- 11.0
cis-Nerolidol	100.0 +/- 8.0	51.9 +/- 39.6	16.6 +/- 4.0	22.2 +/- 3.0	22.2 +/- 4.8	17.0 +/- 2.2	35.5 +/- 25.7	76.8 +/- 7.4
trans-Nerolidol	100.0 +/- 9.3	29.5 +/- 0.2	21.7 +/- 2.4	4.9 +/- 2.8	<LOD*	<LOD	42.2 +/- 49.2	63.5 +/- 27.6
Nonylbenzene	100.0 +/- 12.6	117.4 +/- 28.8	71.9 +/- 6.1	70.2 +/- 13.5	64.9 +/- 8.6	66.4 +/- 11.9	112.2 +/- 70.9	77.2 +/- 9.2

Compound	Recoveries (%) Carbotrap C at ozone mixing ratio (ppbV)							
	0 no filter	0 + filter	20 + filter	40 + filter	60 + filter	80 + filter	100 + filter	0 no filter
1, 3, 5 Tri-isopropylbenzene	100.0 +/- 1.3	99.3 +/- 1.9	95.3 +/- 0.9	96.0 +/- 2.9	96.2 +/- 2.4	96.8 +/- 4.6	94.4 +/- 2.2	96.5 +/- 3.0
Longipinene	100.0 +/- 1.8	100.1 +/- 1.0	95.4 +/- 2.0	96.1 +/- 4.8	95.4 +/- 3.4	94.5 +/- 8.4	89.1 +/- 1.6	94.9 +/- 4.5
α-Copaene	100.0 +/- 0.4	96.2 +/- 6.2	103.3 +/- 10.7	100.5 +/- 5.2	98.9 +/- 2.5	100.7 +/- 6.2	94.8 +/- 1.9	96.5 +/- 1.5
Isolongifolene	100.0 +/- 1.0	99.7 +/- 0.8	95.9 +/- 1.6	97.3 +/- 3.4	97.2 +/- 2.5	97.6 +/- 3.6	95.2 +/- 1.8	96.2 +/- 2.5
Diphenylmethane	100.0 +/- 2.7	93.7 +/- 17.0	87.4 +/- 1.7	90.0 +/- 2.8	91.6 +/- 3.9	88.7 +/- 0.1	85.2 +/- 2.4	89.6 +/- 3.8
α-Cedrene	100.0 +/- 22.4	90.4 +/- 15.5	80.7 +/- 14.3	85.2 +/- 13.2	84.9 +/- 10.1	88.2 +/- 15.0	87.3 +/- 9.9	96.6 +/- 22.1
trans-Caryophyllene	100.0 +/- 6.5	96.4 +/- 4.7	83.5 +/- 0.5	77.5 +/- 14.2	73.8 +/- 11.1	72.9 +/- 21.0	79.5 +/- 11.6	97.5 +/- 10.5
Geranylacetone	100.0 +/- 5.1	104.8 +/- 7.9	102.2 +/- 4.0	101.9 +/- 5.8	84.3 +/- 5.7	99.8 +/- 2.8	93.9 +/- 3.5	98.8 +/- 1.6
Aromadendrene	100.0 +/- 10.8	101.3 +/- 2.7	98.6 +/- 3.6	95.4 +/- 5.8	96.7 +/- 8.9	93.5 +/- 1.6	89.9 +/- 9.7	99.9 +/- 2.2
α-Humulene	100.0 +/- 9.8	100.3 +/- 12.7	91.0 +/- 50.9	64.9 +/- 19.6	43.4 +/- 21.3	66.3 +/- 11.0	65.0 +/- 8.2	95.1 +/- 6.3
δ-Cadinene	100.0 +/- 7.1	103.7 +/- 4.0	96.0 +/- 15.9	103.7 +/- 11.3	95.8 +/- 0.9	106.4 +/- 5.4	84.2 +/- 12.7	92.9 +/- 16.3
cis-Nerolidol	100.0 +/- 19.0	49.5 +/- 39.8	20.5 +/- 4.3	21.8 +/- 1.4	19.4 +/- 3.5	30.5 +/- 18.1	19.7 +/- 1.6	31.5 +/- 0.9
trans-Nerolidol	100.0 +/- 12.6	24.3 +/- 12.5	12.8 +/- 3.9	12.5 +/- 2.6	9.3 +/- 2.2	5.6 +/- 8.7	8.6 +/- 0.7	56.9 +/- 49.3
Nonylbenzene	100.0 +/- 14.8	73.8 +/- 34.3	78.9 +/- 10.7	75.0 +/- 7.8	65.3 +/- 1.4	92.1 +/- 15.2	74.3 +/- 7.6	79.8 +/- 16.9

* LOD: Limit Of Detection

Table 3.3 (continued)

Compound	Recoveries (%) on Tenax GR at ozone mixing ratio (ppbV)							
	0 no filter	0 + filter	20 + filter	40 + filter	60 + filter	80 + filter	100 + filter	0 no filter
1, 3, 5 Tri-isopropylbenzene	100.0 +/- 5.5	105.0 +/- 10.6	102.5 +/- 1.6	97.2 +/- 6.8	98.6 +/- 6.5	98.5 +/- 4.9	96.4 +/- 5.6	94.2 +/- 1.6
Longipinene	100.0 +/- 12.9	99.8 +/- 3.7	99.4 +/- 0.6	95.6 +/- 4.7	95.4 +/- 3.6	97.2 +/- 0.7	92.7 +/- 3.7	94.0 +/- 3.8
α-Copaene	100.0 +/- 5.5	101.4 +/- 5.2	99.3 +/- 2.6	100.8 +/- 10.8	97.1 +/- 4.3	101.2 +/- 2.0	93.7 +/- 4.2	91.9 +/- 0.3
Isolongifolene	100.0 +/- 5.7	100.6 +/- 3.9	97.3 +/- 0.5	95.5 +/- 4.1	94.7 +/- 3.5	96.1 +/- 0.7	93.8 +/- 3.4	92.6 +/- 2.7
Diphenylmethane	100.0 +/- 0.7	107.2 +/- 24.8	108.7 +/- 1.0	98.0 +/- 10.1	100.8 +/- 9.4	102.2 +/- 8.4	96.5 +/- 12.1	86.1 +/- 1.3
α-Cedrene	100.0 +/- 12.0	102.9 +/- 7.2	112.2 +/- 14.4	97.0 +/- 7.5	94.1 +/- 8.6	94.1 +/- 9.0	95.8 +/- 6.8	100.7 +/- 4.4
trans-Caryophyllene	100.0 +/- 7.9	102.0 +/- 9.5	98.2 +/- 2.6	83.6 +/- 12.1	73.1 +/- 19.8	76.7 +/- 6.4	58.2 +/- 21.2	92.9 +/- 2.2
Geranylacetone	100.0 +/- 5.9	104.8 +/- 5.7	98.7 +/- 2.8	97.3 +/- 3.9	95.9 +/- 5.9	96.7 +/- 5.0	95.1 +/- 5.2	88.8 +/- 7.2
Aromadendrene	100.0 +/- 18.7	99.8 +/- 4.3	101.9 +/- 16.9	102.6 +/- 7.4	99.3 +/- 7.3	97.3 +/- 7.1	93.2 +/- 2.1	102.7 +/- 14.0
α-Humulene	100.0 +/- 6.0	104.8 +/- 15.3	98.1 +/- 0.0	82.2 +/- 16.4	69.1 +/- 24.1	74.6 +/- 6.7	50.0 +/- 27.7	90.2 +/- 6.5
δ-Cadinene	100.0 +/- 10.5	113.5 +/- 8.5	101.7 +/- 14.8	106.4 +/- 2.1	107.6 +/- 1.3	96.6 +/- 13.5	98.1 +/- 7.0	81.5 +/- 9.6
cis-Nerolidol	100.0 +/- 13.6	26.5 +/- 17.5	33.0 +/- 2.0	24.5 +/- 13.8	25.1 +/- 17.2	28.6 +/- 8.8	21.0 +/- 19.8	55.5 +/- 4.0
trans-Nerolidol	100.0 +/- 31.3	26.0 +/- 4.3	23.5 +/- 5.7	16.9 +/- 6.6	6.3 +/- 2.5	36.0 +/- 22.7	18.1 +/- 6.5	54.6 +/- 1.9
Nonylbenzene	100.0 +/- 13.7	83.9 +/- 41.1	103.9 +/- 2.4	91.0 +/- 16.4	91.6 +/- 17.6	95.0 +/- 11.9	92.1 +/- 15.9	88.6 +/- 9.0

Compound	Recoveries (%) on Tenax TA at ozone mixing ratio (ppbV)							
	0 no filter	0 + filter	20 + filter	40 + filter	60 + filter	80 + filter	100 + filter	0 no filter
1, 3, 5 Tri-isopropylbenzene	100.0 +/- 1.3	98.8 +/- 1.1	99.8 +/- 1.8	100.9 +/- 2.8	93.2 +/- 2.1	97.8 +/- 1.9	100.0 +/- 0.2	98.2 +/- 0.4
Longipinene	100.0 +/- 0.5	101.7 +/- 1.0	97.1 +/- 2.4	100.4 +/- 2.4	95.9 +/- 6.1	97.4 +/- 0.7	101.9 +/- 8.5	103.9 +/- 8.9
α-Copaene	100.0 +/- 4.2	98.2 +/- 0.3	101.3 +/- 1.9	100.9 +/- 5.0	94.8 +/- 3.8	99.7 +/- 3.4	104.6 +/- 10.6	96.6 +/- 0.7
Isolongifolene	100.0 +/- 0.4	99.8 +/- 2.7	99.5 +/- 1.4	99.8 +/- 0.5	94.3 +/- 3.9	99.4 +/- 1.0	99.9 +/- 1.2	95.7 +/- 1.9
Diphenylmethane	100.0 +/- 1.1	91.2 +/- 0.7	116.8 +/- 3.5	105.3 +/- 16.7	84.1 +/- 8.5	96.9 +/- 1.9	105.8 +/- 10.8	97.8 +/- 2.5
α-Cedrene	100.0 +/- 7.3	99.0 +/- 0.4	114.5 +/- 4.4	100.9 +/- 2.9	89.1 +/- 1.2	95.5 +/- 0.7	99.3 +/- 4.3	94.7 +/- 2.1
trans-Caryophyllene	100.0 +/- 5.5	98.4 +/- 0.1	111.2 +/- 12.5	87.1 +/- 13.3	86.0 +/- 9.7	66.7 +/- 5.3	57.9 +/- 19.6	97.7 +/- 0.1
Geranylacetone	100.0 +/- 3.9	104.8 +/- 0.7	100.5 +/- 3.4	101.4 +/- 1.4	88.7 +/- 0.2	93.9 +/- 0.9	96.0 +/- 7.2	93.8 +/- 0.4
Aromadendrene	100.0 +/- 18.7	100.4 +/- 3.7	105.0 +/- 8.5	92.5 +/- 1.0	92.9 +/- 4.8	88.2 +/- 1.0	87.4 +/- 9.6	102.7 +/- 14.0
α-Humulene	100.0 +/- 6.5	99.4 +/- 3.1	94.3 +/- 2.9	84.8 +/- 14.1	86.1 +/- 11.7	58.7 +/- 8.2	49.2 +/- 23.3	96.9 +/- 0.5
δ-Cadinene	100.0 +/- 15.4	120.9 +/- 2.3	112.4 +/- 5.7	113.2 +/- 4.7	120.4 +/- 2.5	122.9 +/- 20.5	104.5 +/- 4.0	126.0 +/- 16.6
cis-Nerolidol	100.0 +/- 38.1	<LOD*	20.3 +/- 2.9	<LOD	<LOD	<LOD	<LOD	93.1 +/- 9.0
trans-Nerolidol	100.0 +/- 6.6	25.9 +/- 24.6	38.9 +/- 2.7	<LOD	17.7 +/- 5.3	6.5 +/- 0.2	24.7 +/- 2.1	106.1 +/- 1.9
Nonylbenzene	100.0 +/- 6.5	73.3 +/- 0.8	109.1 +/- 11.9	98.2 +/- 36.3	55.3 +/- 10.2	75.1 +/- 3.3	97.7 +/- 31.9	90.6 +/- 4.8

* LOD: Limit Of Detection

One $Na_2S_2O_3$-filter reduced ozone in the sampling air to approximately 0.4 % of the initial value. The filter did not cause any significant SQT loss for the non-oxidized analytes and did not introduce any contamination peaks. Heavier, oxidized compounds (such as *cis*- and *trans*-Nerolidol) were lost to the filter by approximately 50 to 65 %. SQT losses due to ozone reaction were significantly reduced compared to the experiments without any ozone mitigation. SQT with one double bond (e.g.: isolongifolene or longipinene) were quantitatively retrieved up to the highest ozone mixing ratio tested (100 ppbV). However, *trans*-caryophyllene and α-humulene still showed loss rates of 40 to 50 % at 100 ppbV ozone on the different adsorbents. Results for the four studied adsorbents were quite similar.

These observations agree with earlier reports, where $Na_2S_2O_3$–impregnated filters were successfully used in monoterpene and light hydrocarbon analysis (Fick et al., 2001, Strömvall and Peterson, 1992, Helmig et al., 1997). Our results now expand on these results and demonstrate that $Na_2S_2O_3$–impregnated filters can also be utilized for sampling heavier molecular weight compounds such as SQT. However, compounds with higher polarity and lower vapor pressure than SQT (such as the oxygenated SQT) do suffer significant losses to this type of filter.

Experiments with increasing number of $Na_2S_2O_3$–impregnated filters: A significant reduction in SQT losses, though not a complete prevention of all analyte losses, was found for the most reactive SQT with one $Na_2S_2O_3$–impregnated filter in the sampling stream. Therefore, we investigated if several filters in series would yield a further improvement. A single $Na_2S_2O_3$–filter reduces the ozone mixing ratio from an initial value of 100 ppbV to ~ 0.4 ppbV. Several filters in series result in a further scrubbing of ozone (remaining ozone levels were < 0.2 ppbV). However, this improvement may possibly be offset, especially for the heavier compounds, by higher absorption losses to the filter material. One, two and three sodium thiosulfate-impregnated filters were placed into the sampling stream at 100 ppbV ozone. The recovery rates for each experiment were compared to conditions at 0 ppbV ozone without any filters added. The average recovery rates for one selected SQT with high losses from ozone, i.e. α-humulene on four adsorbents are displayed in Figure 3.5.

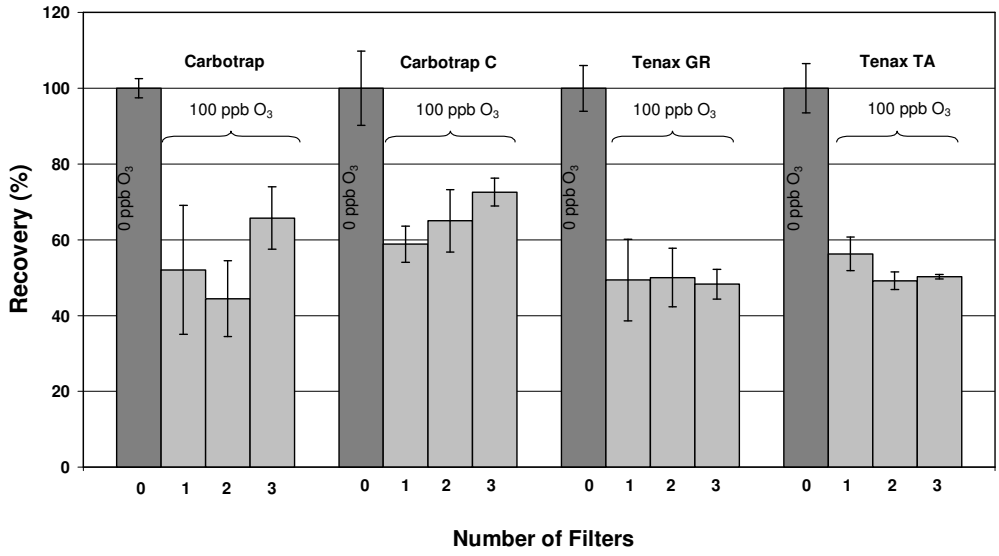

Figure 3.5: Recovery rates for α-humulene using an increasing number of sodium thiosulfate filters at 100 ppbV ozone.

No additional absorption losses were observed for the non-oxygenated SQT in the 2– and 3-filter experiments. SQT loss rates from ozone reactions decreased slightly, but not substantially (~ 10 % for α-humulene). However, oxygenated compounds were almost completely lost due to absorption on the additional filters. Similar to the findings reported above, no significant differences for the individual adsorbent materials were seen.

NO-titration technique: Two initial samples were taken (without NO added) at 0 ppbV ozone. The results of this analysis were used as a reference for the calculation of recovery rates. Cartridges were then loaded with 2 ml min^{-1} of 1 % NO in N_2 added to the sampling stream at 0, 20, 40, 60, 80 and 100 ppbV ozone. After these experiments the NO flow was turned off and two cartridges were loaded again without NO added at 0 ppbV O_3. Bargraph results for SQT are displayed in Fig

ure 3.6 and numeric data for all investigated compounds is shown in table 3.4.

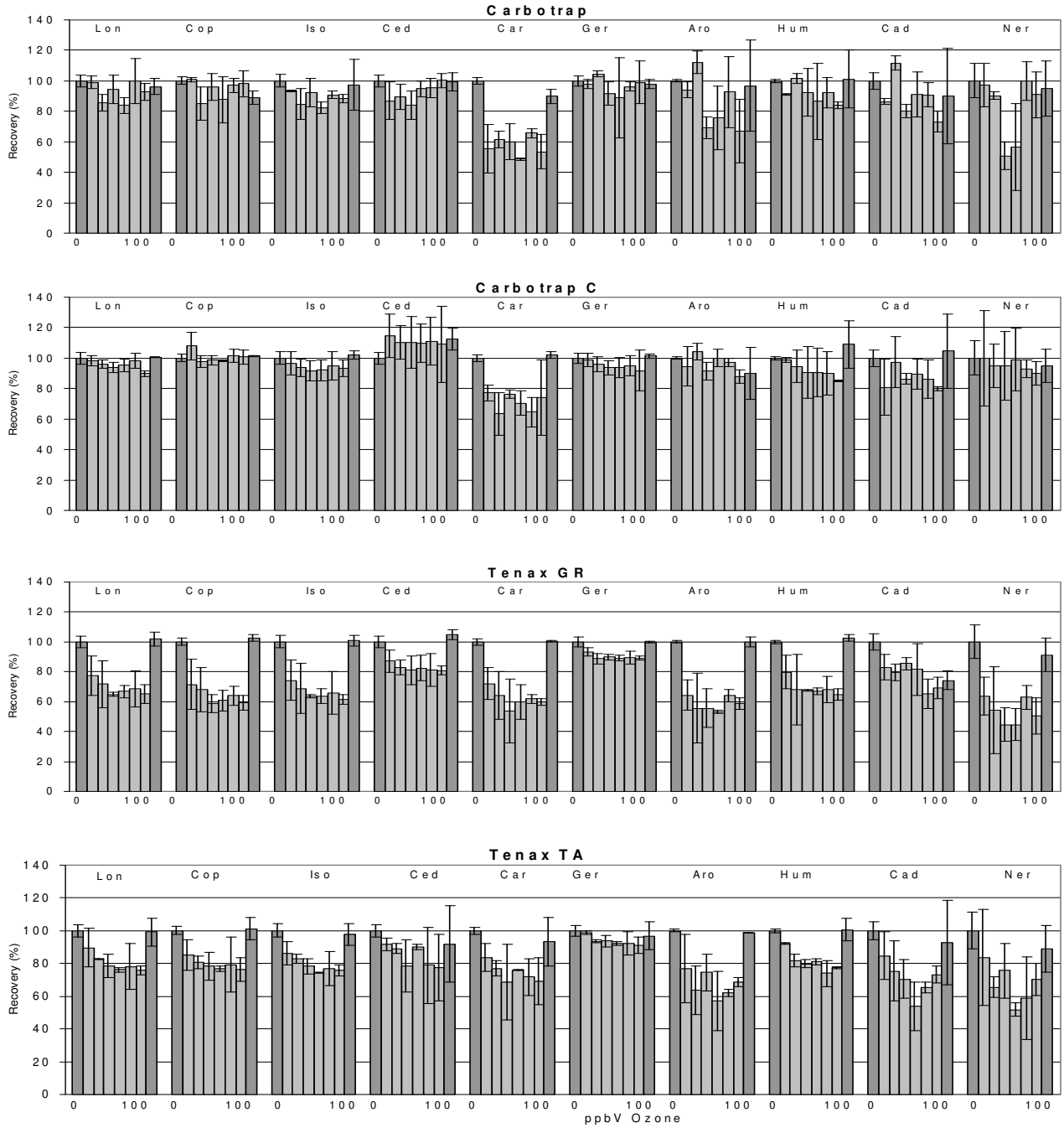

Figure 3.6: Recovery rates in NO experiments for ten investigated BVOCs at 0, 0, 20, 40, 60, 80, 100, 0 ppbV ozone. Abbreviations are the same as in Fig. 1. Dark gray color bars indicate runs without ozone added and no mitigation techniques applied, light gray color bar indicate experiments at ozone mixing ratios from 0 to 100 ppbV with 2 ml min^{-1} of 1 % NO in nitrogen added to the sampling stream.

Table 3.4: Recovery rates (%)at increasing ozone mixing ratios on four adsorbents materials using the NO-titration technique. Errors represent relative standard deviation for n = 2.

Compound	Recoveries (%) on Carbotrap at ozone mixing ratio (ppbV)							
	0 no NO	0 + NO	20 + NO	40 + NO	60 + NO	80 + NO	100 + NO	0 no NO
1, 3, 5 Tri-isopropylbenzene	100.0 +/- 2.6	101.1 +/- 1.2	77.4 +/- 5.4	97.0 +/- 8.6	81.8 +/- 1.9	92.6 +/- 4.1	87.2 +/- 0.6	99.6 +/- 5.8
Longipinene	100.0 +/- 3.7	99.0 +/- 4.2	85.8 +/- 5.5	94.4 +/- 9.1	83.7 +/- 5.4	100.0 +/- 14.8	92.8 +/- 5.3	96.3 +/- 5.2
α-Copaene	100.0 +/- 3.3	100.8 +/- 1.6	85.0 +/- 10.9	96.1 +/- 8.8	87.8 +/- 15.1	97.0 +/- 4.6	98.1 +/- 8.4	88.9 +/- 4.3
Isolongifolene	100.0 +/- 6.4	93.4 +/- 0.7	84.8 +/- 10.3	92.1 +/- 9.3	82.5 +/- 3.9	90.7 +/- 2.3	88.5 +/- 2.8	97.3 +/- 16.7
Diphenylmethane	100.0 +/- 0.5	98.7 +/- 6.9	69.4 +/- 1.3	68.3 +/- 16.9	65.2 +/- 9.8	90.3 +/- 20.0	73.3 +/- 14.3	102.7 +/- 15.9
α-Cedrene	100.0 +/- 5.3	86.9 +/- 12.3	89.5 +/- 8.2	84.2 +/- 9.2	95.0 +/- 5.2	95.3 +/- 6.4	100.3 +/- 4.7	99.4 +/- 6.1
trans-Caryophyllene	100.0 +/- 1.2	55.2 +/- 15.9	61.5 +/- 5.4	60.1 +/- 11.9	48.6 +/- 0.7	65.6 +/- 3.2	53.5 +/- 11.3	90.0 +/- 4.6
Geranylacetone	100.0 +/- 2.4	97.9 +/- 3.0	104.6 +/- 2.0	91.8 +/- 7.6	88.8 +/- 26.4	96.3 +/- 3.1	99.1 +/- 13.9	97.8 +/- 3.0
Aromadendrene	100.0 +/- 1.6	94.1 +/- 5.4	112.1 +/- 7.4	69.3 +/- 7.1	75.8 +/- 21.0	92.7 +/- 23.4	67.0 +/- 20.6	96.8 +/- 29.9
α-Humulene	100.0 +/- 2.5	91.2 +/- 0.7	101.6 +/- 3.2	92.5 +/- 15.9	86.7 +/- 25.0	92.2 +/- 10.1	84.0 +/- 2.1	101.1 +/- 18.9
δ-Cadinene	100.0 +/- 19.0	86.3 +/- 1.9	111.6 +/- 4.5	80.1 +/- 4.3	91.1 +/- 45.7	90.8 +/- 7.9	73.1 +/- 6.9	89.9 +/- 31.3
cis-Nerolidol	100.0 +/- 8.1	97.1 +/- 14.1	63.5 +/- 2.6	42.9 +/- 9.0	56.5 +/- 28.5	100.5 +/- 12.7	81.3 +/- 35.0	63.7 +/- 18.0
trans-Nerolidol	100.0 +/- 20.7	106.6 +/- 4.0	115.5 +/- 6.1	56.7 +/- 15.7	101.3 +/- 17.3	98.4 +/- 7.4	96.9 +/- 3.6	96.7 +/- 17.9
Nonylbenzene	100.0 +/- 24.0	95.0 +/- 7.7	114.5 +/- 52.0	81.5 +/- 10.3	99.5 +/- 36.7	91.0 +/- 8.4	84.6 +/- 14.1	86.9 +/- 13.1

Compound	Recoveries (%) on Carbotrap C at ozone mixing ratio (ppbV)							
	0 no NO	0 + NO	20 + NO	40 + NO	60 + NO	80+ NO	100 + NO	0 no NO
1, 3, 5 Tri-isopropylbenzene	100.0 +/- 3.9	98.3 +/- 4.8	97.7 +/- 1.9	93.7 +/- 3.1	94.9 +/- 3.8	95.7 +/- 5.8	98.0 +/- 2.4	104.0 +/- 1.9
Longipinene	100.0 +/- 2.2	98.2 +/- 3.4	96.0 +/- 2.7	93.9 +/- 3.3	95.3 +/- 4.0	98.3 +/- 5.1	89.8 +/- 2.0	100.6 +/- 0.3
α-Copaene	100.0 +/- 3.7	107.9 +/- 9.0	97.7 +/- 4.1	98.8 +/- 3.0	98.4 +/- 0.7	101.5 +/- 4.4	100.8 +/- 4.8	101.3 +/- 0.1
Isolongifolene	100.0 +/- 6.2	96.7 +/- 7.5	93.8 +/- 5.8	91.5 +/- 6.5	92.1 +/- 6.9	95.1 +/- 9.3	93.3 +/- 5.4	102.1 +/- 2.6
Diphenylmethane	100.0 +/- 8.8	104.1 +/- 15.2	95.2 +/- 13.0	71.3 +/- 11.0	96.8 +/- 15.8	95.4 +/- 7.4	71.1 +/- 33.5	56.5 +/- 17.2
α-Cedrene	100.0 +/- 13.4	114.7 +/- 14.0	110.4 +/- 10.8	110.4 +/- 16.9	109.8 +/- 12.4	111.1 +/- 15.7	109.2 +/- 24.9	112.5 +/- 7.0
trans-Caryophyllene	100.0 +/- 7.3	77.2 +/- 5.2	63.6 +/- 14.1	76.5 +/- 2.8	70.5 +/- 7.9	64.5 +/- 9.4	74.2 +/- 24.6	102.2 +/- 2.2
Geranylacetone	100.0 +/- 7.4	98.6 +/- 4.4	96.1 +/- 4.8	93.6 +/- 4.7	93.9 +/- 6.4	95.0 +/- 6.5	91.9 +/- 13.5	101.4 +/- 1.4
Aromadendrene	100.0 +/- 4.2	94.6 +/- 12.9	104.3 +/- 5.7	91.5 +/- 5.8	100.0 +/- 5.8	97.1 +/- 2.8	87.7 +/- 4.5	90.2 +/- 17.1
α-Humulene	100.0 +/- 0.1	98.9 +/- 1.5	94.7 +/- 10.9	90.7 +/- 17.0	90.4 +/- 15.9	90.1 +/- 14.3	85.0 +/- 0.7	109.0 +/- 15.9
δ-Cadinene	100.0 +/- 7.0	81.0 +/- 18.5	97.3 +/- 16.6	86.3 +/- 3.5	89.5 +/- 9.8	86.2 +/- 12.6	80.0 +/- 1.3	104.8 +/- 24.5
cis-Nerolidol	100.0 +/- 12.5	121.1 +/- 31.3	99.3 +/- 14.2	109.2 +/- 22.3	116.4 +/- 20.4	99.0 +/- 5.8	94.8 +/- 7.9	128.2 +/- 10.9
trans-Nerolidol	100.0 +/- 15.5	78.0 +/- 43.7	78.4 +/- 61.7	90.5 +/- 25.3	91.9 +/- 52.7	54.4 +/- 6.5	78.7 +/- 68.6	56.5 +/- 7.9
Nonylbenzene	100.0 +/- 26.4	99.3 +/- 16.7	87.2 +/- 11.3	90.0 +/- 7.6	83.8 +/- 16.7	90.2 +/- 4.0	82.8 +/- 16.1	92.4 +/- 35.2

Table 3.4 (continued)

Compound	Recoveries (%) on Tenax GR at ozone mixing ratio (ppbV)							
	0 no NO	0 + NO	20 + NO	40 + NO	60 + NO	80 + NO	100 + NO	0 no NO
1, 3, 5 Tri-isopropylbenzene	100.0 +/- 2.5	92.0 +/- 3.7	87.7 +/- 3.9	87.2 +/- 2.0	87.5 +/- 2.6	88.0 +/- 5.1	89.4 +/- 5.6	102.5 +/- 4.7
Longipinene	100.0 +/- 3.0	77.5 +/- 10.3	71.7 +/- 11.4	65.0 +/- 0.9	66.7 +/- 2.9	68.6 +/- 8.2	65.2 +/- 4.2	102.0 +/- 4.9
α-Copaene	100.0 +/- 1.5	71.6 +/- 12.1	68.2 +/- 10.1	58.8 +/- 3.6	60.9 +/- 4.2	64.0 +/- 3.9	59.3 +/- 3.1	102.5 +/- 2.1
Isolongifolene	100.0 +/- 2.0	74.4 +/- 10.0	68.7 +/- 11.5	63.8 +/- 0.7	63.8 +/- 3.2	65.7 +/- 9.3	61.4 +/- 2.0	100.9 +/- 3.6
Diphenylmethane	100.0 +/- 3.1	116.0 +/- 0.5	117.8 +/- 9.1	128.2 +/- 20.9	114.1 +/- 16.1	116.1 +/- 15.5	115.6 +/- 5.2	100.4 +/- 10.0
α-Cedrene	100.0 +/- 5.6	87.1 +/- 6.6	82.8 +/- 4.1	81.1 +/- 7.8	82.6 +/- 7.1	81.3 +/- 9.0	81.0 +/- 2.3	104.8 +/- 3.4
trans-Caryophyllene	100.0 +/- 4.7	72.2 +/- 7.7	64.3 +/- 10.2	53.5 +/- 11.5	59.9 +/- 7.0	61.9 +/- 1.8	60.0 +/- 1.2	100.4 +/- 0.5
Geranylacetone	100.0 +/- 2.5	93.4 +/- 2.5	88.7 +/- 3.2	89.9 +/- 1.8	89.2 +/- 1.8	89.5 +/- 4.1	89.1 +/- 1.2	99.7 +/- 0.5
Aromadendrene	100.0 +/- 3.0	64.4 +/- 6.5	55.7 +/- 13.0	55.7 +/- 7.1	53.2 +/- 0.5	64.0 +/- 2.6	58.6 +/- 2.3	99.8 +/- 3.1
α-Humulene	100.0 +/- 1.4	79.8 +/- 9.1	68.2 +/- 16.1	67.5 +/- 0.5	67.0 +/- 1.4	68.1 +/- 5.9	64.8 +/- 2.6	102.6 +/- 2.1
δ-Cadinene	100.0 +/- 4.4	83.1 +/- 8.7	79.5 +/- 5.6	85.4 +/- 3.9	81.6 +/- 17.2	65.3 +/- 9.9	69.1 +/- 7.3	74.3 +/- 4.6
cis-Nerolidol	100.0 +/- 1.1	63.6 +/- 8.0	54.2 +/- 15.7	44.7 +/- 5.0	44.6 +/- 4.8	62.9 +/- 4.9	50.3 +/- 6.1	91.3 +/- 10.4
trans-Nerolidol	100.0 +/- 4.2	72.4 +/- 3.5	62.4 +/- 12.1	48.6 +/- 2.3	44.6 +/- 4.3	64.4 +/- 4.0	57.7 +/- 8.6	76.6 +/- 7.5
Nonylbenzene	100.0 +/- 5.8	93.4 +/- 0.2	92.2 +/- 1.7	98.7 +/- 5.2	96.2 +/- 4.9	96.7 +/- 8.8	97.5 +/- 6.1	99.0 +/- 3.8

Compound	Recoveries (%) on Tenax TA at ozone mixing ratio (ppbV)							
	0 no NO	0 + NO	20 + NO	40 + NO	60 + NO	80 + NO	100 + NO	0 no NO
1, 3, 5 Tri-isopropylbenzene	100.0 +/- 6.0	101.7 +/- 0.6	95.5 +/- 4.1	95.5 +/- 2.8	93.4 +/- 0.6	100.5 +/- 5.3	93.9 +/- 5.4	101.8 +/- 4.2
Longipinene	100.0 +/- 13.3	89.7 +/- 10.5	82.8 +/- 0.2	78.6 +/- 5.7	76.2 +/- 1.0	78.1 +/- 10.9	75.6 +/- 2.1	99.1 +/- 8.2
α-Copaene	100.0 +/- 6.9	85.1 +/- 8.0	80.7 +/- 2.9	78.3 +/- 6.8	76.8 +/- 1.4	79.3 +/- 13.1	76.5 +/- 5.5	101.1 +/- 6.9
Isolongifolene	100.0 +/- 6.8	86.2 +/- 6.1	82.7 +/- 2.2	78.3 +/- 3.5	74.2 +/- 0.2	76.9 +/- 8.0	75.8 +/- 2.3	97.8 +/- 6.3
Diphenylmethane	100.0 +/- 9.0	126.7 +/- 2.8	114.5 +/- 16.8	118.9 +/- 20.7	100.9 +/- 5.3	113.1 +/- 1.7	114.3 +/- 8.8	95.3 +/- 2.7
α-Cedrene	100.0 +/- 14.9	91.5 +/- 3.5	89.2 +/- 2.9	78.7 +/- 12.5	90.0 +/- 1.4	79.0 +/- 18.4	77.5 +/- 15.8	91.9 +/- 21.5
trans-Caryophyllene	100.0 +/- 9.9	83.6 +/- 7.1	77.1 +/- 3.5	68.6 +/- 15.7	76.0 +/- 0.1	71.7 +/- 8.0	69.3 +/- 9.8	93.5 +/- 13.8
Geranylacetone	100.0 +/- 6.1	98.9 +/- 1.2	93.6 +/- 0.6	93.6 +/- 3.4	92.2 +/- 1.0	92.2 +/- 6.6	91.1 +/- 4.7	96.9 +/- 8.4
Aromadendrene	100.0 +/- 9.1	77.0 +/- 16.1	63.5 +/- 9.5	74.4 +/- 8.3	57.2 +/- 10.3	62.1 +/- 1.5	68.4 +/- 1.9	98.8 +/- 0.0
α-Humulene	100.0 +/- 6.3	92.2 +/- 0.7	81.7 +/- 3.1	79.8 +/- 2.0	81.1 +/- 1.5	73.9 +/- 5.8	77.4 +/- 0.4	100.7 +/- 7.1
δ-Cadinene	100.0 +/- 1.3	84.6 +/- 12.3	75.4 +/- 13.9	70.5 +/- 8.5	53.8 +/- 8.0	65.2 +/- 2.1	73.2 +/- 3.8	92.7 +/- 23.9
cis-Nerolidol	100.0 +/- 21.3	83.6 +/- 24.6	65.5 +/- 4.2	75.5 +/- 12.7	51.7 +/- 2.2	58.6 +/- 14.9	70.4 +/- 7.0	89.0 +/- 12.7
trans-Nerolidol	100.0 +/- 5.3	84.0 +/- 42.7	58.4 +/- 25.9	59.9 +/- 6.6	54.7 +/- 10.2	76.8 +/- 9.6	62.7 +/- 10.8	88.1 +/- 11.3
Nonylbenzene	100.0 +/- 5.0	92.2 +/- 16.1	98.5 +/- 16.6	95.5 +/- 26.4	80.4 +/- 4.9	88.0 +/- 5.2	92.2 +/- 20.3	81.2 +/- 12.2

Titration of ozone with NO did prevent some, but not all of the SQT ozone sampling losses. However, it is apparent, that NO itself did cause analyte losses for some of the SQT. On all four adsorbents loss rates of 25 to 45 % were observed for *trans*-caryophyllene and α-humulene with NO added in the absence of ozone. Therefore, these losses have to be attributed to reaction of these SQT with NO. Recovery rates remained widely constant with increasing ozone concentrations. Results on the carbon based adsorbents (Carbotrap and Carbotrap C) were somewhat better than for the Tenax-type adsorbents. No physical changes/degradation of the adsorbent materials or chromatographic interferences were observed in these experiments.

Manganese dioxide–scrubber: The scrubber was placed into the sampling stream in the same location as the sodium-thiosulfate filters. Almost complete removal of all analytes resulted from this scrubber. A second, identical scrubber was tested to study if this result was reproducible. Results for the second scrubber agreed with the first observation. Since previous studies (Helmig et al., 2003) have shown that SQT losses to walls of tubing and other internal surfaces can be overcome by heating these components, another experiment was performed with one of the scrubbers placed in a GC oven at 100˚C during sampling. Again, all analytes were lost under this condition. Higher temperatures than 100°C were not investigated because of the temperature limit of the scrubber housing. Because all analytes were lost in these experiments, no numerical data for this experiment is given. However, example chromatograms with and without the scrubber in the sampling stream are shown in figure 3.7 a, b. Our findings agree with some earlier reports, where high loss rates for *trans*-caryophyllene (64 %) were observed on a custom made MnO_2 – scrubber (Calogirou et al., 1996). The low cost and long lifetimes of commercially available manganese dioxide scrubbers make their use attractive. However, under our experimental conditions, they do not appear suitable for this application. These findings infer that, if manganese dioxide scrubbers are to be used as an ozone mitigation technique for VOC sampling, the total surface area that the analytes are exposed to, the sampling flow rate, and the residence time of analytes in the scrubber container need to be carefully investigated and optimized.

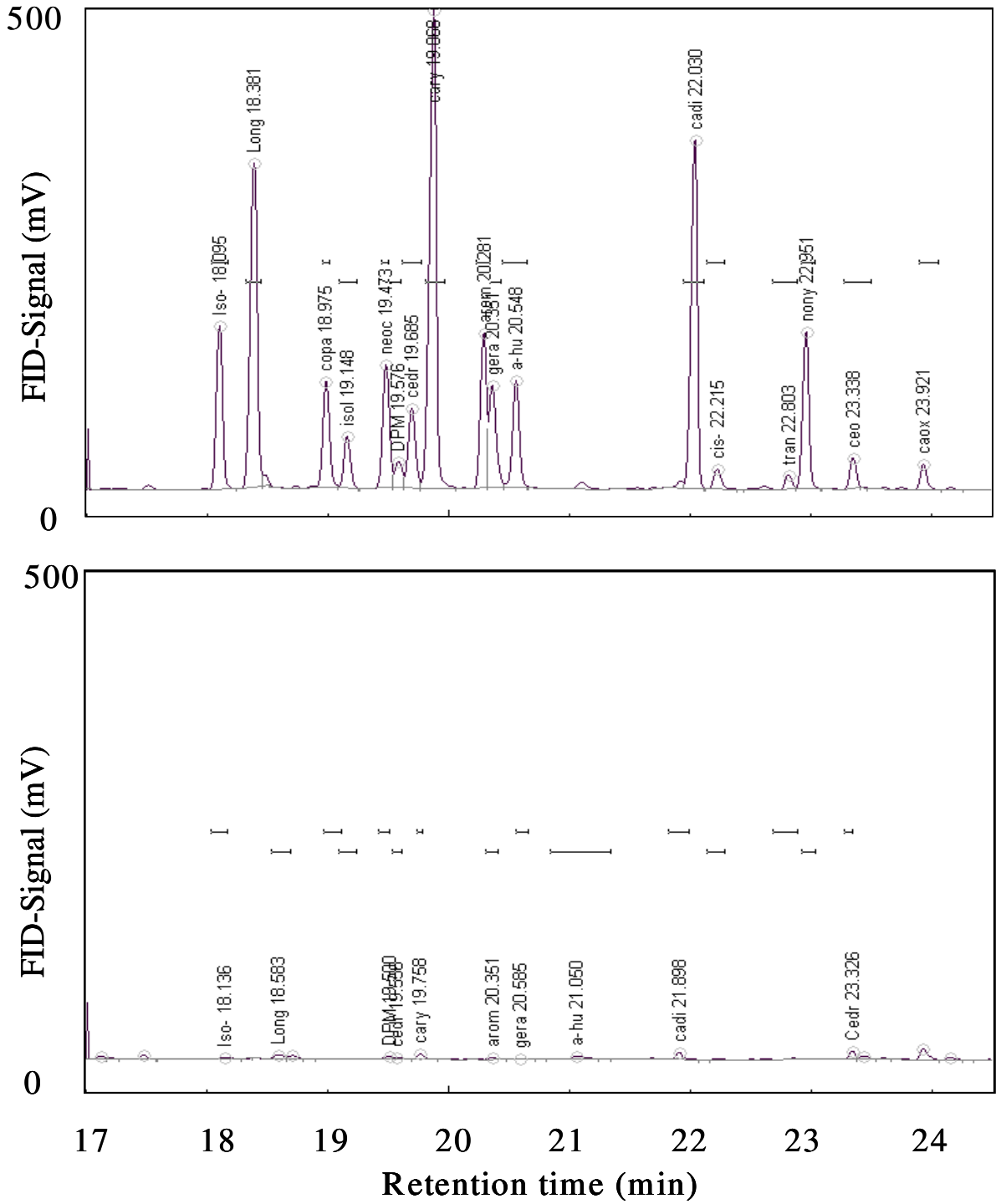

Figure 3.7 a, b: Chromatogram of the SQT-standard without (a) and with (b) the MnO_2 – catalyst in the sampling flow path at 0 ppbV ozone. Abbreviations: Iso: 1- 3- 5-triisopropylbenzene, Long: longipinene, copa: α-copaene, isol: isolongifolene, neoc: neoclovene, DPM: diphenylmethane, cedr: α-cedrene, cary: β-caryophyllene, gera: geranylacetone, α-humulene, cadi: δ-cadinene, cis: *cis*-nerolidol, *trans*: *trans*-nerolidol, nony: nonylbenzene, ceo: cedrol, caox: caryophyllene-oxide.

3.4 Implications for research on sesquiterpene flux studies

These experiments reemphasize the need of ozone management during the sampling of SQT in air that contains even low ppbV levels of ozone. The degree of SQT analyte loss correlates with the number of double bonds in the SQT molecule. Highly unsaturated compounds (2-3 double bonds) suffer the highest depletion rates. In contrast, aromatic compounds, that were included in these experiments, were inert towards ozone and did not experience sampling losses.

Substantial losses of SQT were observed at even the lowest ozone levels tested (20 ppb ozone), which is well within the range of expected ambient ozone concentrations. It is striking that *trans*-caryophyllene and α-humulene, two of the most common and most thoroughly investigated SQT, were the two analytes that experienced the highest sampling losses among the compounds investigated and hence can be considered as two analytes that are the most difficult to analyze in ambient air.

Two out of three investigated ozone mitigation techniques were found to successfully remove ozone and to yield substantial improvements on all four of the adsorbents tested. The $Na_2S_2O_3$ filter and the NO titration techniques were equally effective in reducing ozone levels to concentrations required to quantify most SQT reliably. However, for the NO titration technique, it is necessary to correct for eventual losses of SQT compounds due to reaction with NO. The commercial MnO_2 ozone scrubbers tested in these experiments were unsuitable for the sampling of SQTs and other organic compounds in the same volatility range.

We found that sodium thiosulfate filters are the preferred method for field work due to their small size, ease of preparation and low cost. Since these filters have a limited capacity for removing ozone, it is important to either replace them regularly or to monitor their effectiveness with an ozone monitor.

Nitric oxide titration is a more elaborate ozone mitigation technique. Nitric oxide is extremely toxic and stringent safety procedures have to be followed for transport and storage of pressurized gas cylinders containing NO. Pure NO is difficult to acquire and this method is significantly more expensive than using sodium thiosulfate filters. However, a small NO gas cylinder, e.g. 10 l of 1% NO at 100 psi, in continuous application will last

much longer than a single sodium thiosulfate filter. With this gas volume it is possible to remove ozone from more than 60,000 l of ambient air in a 1 l min^{-1} air sampling flow. For long term, automated SQT sampling NO titration may therefore be a preferred technique.

Substantial residual losses of *trans*-caryophyllene and α-humulene occurred even though it appeared that ozone levels were reduced well below the 1 ppbv level with these two techniques. These losses were significant enough to prohibit an accurate quantification of these compounds in the presence of ozone. These experiments re-emphasize that an accurate quantification of reactive SQT, such as *trans*-caryophyllene and α-humulene in ambient air may not be feasible with adsorbent sampling techniques. These limitations particularly apply to flux measurements of these compounds by gradient or eddy accumulation techniques (with solid adsorbent sampling) where highly precise concentration measurements are needed to determine the difference in concentrations between updraft and downdraft samples or at different levels above the surface. Laboratory SQT studies have shown that certain materials in the sampling stream require temperatures on the order of 150°C to prevent adsorption losses and that long equilibration times are necessary for these components to reach steady state (Helmig et al., 2003). These effects constitute another limitation for ambient eddy accumulation flux measurement applications where a fast separation of updraft and downdraft air samples is needed.

These observations further imply that atmospheric SQT probably will have high deposition losses from uptake to environmental substrates. Many SQT have short (minutes) atmospheric lifetimes, which will result in low ambient mixing ratios, even close to their biogenic sources. Above-canopy flux measurements will likely underestimate flux estimates derived from leaf or branch level emission rate measurements because of losses occurring within the canopy. Conclusively, these effects pose severe limitations on ambient scale SQT flux measurements with currently available technology.

Vegetation enclosure experiments appear to be the best approach to estimate SQT fluxes. The experiments presented here emphasize the need to conduct enclosure experiments in an ozone-free environment. For these experiments we recommend the following procedures when sampling on solid adsorbents:

a) Use of either synthetic air or scrubbed air for the enclosure purge air so that BVOC emissions from the foliage are not exposed to ozone.

b) Maintaining short residence times (~ 2-4 minutes) within the enclosure so that overheating is minimized, BVOC concentrations are high enough (1-10 ppbV) to obtain an adequate signal, and possible photochemical reactions are minimized.

c) Monitoring of ozone in the enclosure system to address the concerns listed above.

d) Use of either NO titration or sodium thiosulfate impregnated glass fiber filters in the sampling flow prior to trapping analytes on the adsorbent materials.

By adhering to these procedures, analyte losses due to ozone reaction are minimized and the ability to quantitatively estimate emission rates and to infer SQT landscape fluxes is greatly improved.

3.5 Acknowledgements

This research was supported through the National Science Foundation, Atmospheric Chemistry Program, ATM-9911186 and 0304704. Christine Dolliver helped preparing adsorbent cartridges.

4 Sampling, Storage, and Analysis of C2-C7 Non – Methane Hydrocarbons from Whole Air Glass Sampling Flasks

Abstract

An analytical technique for analyzing the light non-methane hydrocarbons (NMHC) ethane, propane, isobutane, butane, isopentane, pentane, hexane, isoprene, benzene and toluene from whole air samples collected in 2.5 l-glass flasks used in the NOAA-ESRL-GMD (National Oceanic and Atmospheric Administration, Earth Systems Research Laboratory, Global Monitoring Division, Boulder, CO, USA) cooperative air sampling network was developed. This method relies on utilizing the remaining, below-ambient pressure sample fraction after the completion of all routine greenhouse gas measurements. A sample extraction method with a cryogen-free custom-made inlet system coupled to a gas chromatograph (GC) with flame ionization detection (FID) was developed for withdrawing a sample aliquot from the flask. We demonstrate that C2 to C7 NMHCs, depending on mixing ratios, can be measured with an accuracy and repeatability of 10-20% or better. Hexane was systematically overestimated due to a chromatographic coelution problem. Saturated NMHCs were stable, showing less than 5% mixing ratio changes in the glass flasks for up to one year. Ethene and propene showed approximately 30% yr^{-1} increases. A series of blank experiments showed negligible contamination from the sampling process and/or storage (< 10 pptv yr^{-1}) of samples in these glass flasks. Results from flask sampling and subsequent NMHC analysis were compared to in-situ NMHC measurements at the the Global Atmospheric Watch site in Hohenpeissenberg, Germany. This 9-months comparison showed good agreement between both methods with 87% of all data comparisons falling within the accuracy objectives of the World Meteorological Organization Global Volatile Organic Compound monitoring network.

This section is in preparation for submission to *Analytical Chemistry* with D.Helmig, J. Hueber, C. Plass-Dülmer as co-authors

4.1 Introduction

Recent reports have called for light non-methane hydrocarbon (NMHC) measurements with high regional and temporal resolution to further assess atmospheric composition and processes such as the global distribution of the hydroxyl radical (·OH) (WMO-Report, 1995; Krol and Lelieveld, 2003). Since then several automated background stations to continuously monitor NMHCs have gone on-line (e.g.: Plass Dülmer et al., 2002, Tanner et al., 2006). Besides these local in-situ measurements, a global NMHC sampling network is highly desirable for investigations on the global distribution of NMHC and their atmospheric oxidation chemistry. Several whole air flask sampling networks are operational (e.g. the National Oceanic and Atmospheric Administration (ESRL), USA, cooperative air sampling network (Conway et al., 1994 and Hoffmann et al., 2006), the Australian Commonwealth Scientific and Industrial Research Organization (CSIRO) sampling network: (Langenfelds et al., 2002) or the European Monitoring and Evaluation Program (EMEP) network (Hakola et al., 2006). The ESRL and CSIRO networks are configured for greenhouse gas monitoring, in particular of the stable gases CO_2, methane and N_2O. The EMEP program focuses on the quantification of nitrogen and sulfur containing volatile compounds. Analyses of light NMHCs in flask samples from the extensive ESRL greenhouse gas sampling network would potentially provide a critical step towards the desired global measurements of atmospheric NMHC.

Flask Types: Sampling flasks and protocols for NMHC whole air sampling have been investigated carefully by previous researchers. As a result, a host of information has become available on how to achieve precise and accurate measurements for NMHC with whole air canister sampling methods. Most studies describe whole air sampling with various types of electropolished stainless steel canisters. These have been used in many atmospheric research applications for surface and aircraft collection of NMHC samples, e.g. during the CARIBIC campaign (Brenninkmeijer, et al. 1999); the PEM-Tropics A and B campaigns (Colman, et al. 2001); Safari 2000 (Jost et al., 2003) and the Trace-P campaign (Blake et al., 2003). Other groups have used fused-silica-lined stainless-steel sampling canisters (Saito et al., 2000). Stainless steel canisters routinely were used in the above

mentioned C2-C6 NMHC at two Finnish background stations. The precision of these measurements calculated as the standard deviation of pairs of flasks sampled in parallel was better than 20% for most compounds.

Flask Treatment and Conditioning: Pretreatment of sampling canisters is of high importance to avoid contamination or decomposition of the air samples (Plass-Dülmer et al., 2006). Most groups follow pre-sampling conditioning protocols with multiple steps of evacuating and pressurizing of the canisters with either humidified zero air (Bottenheim et al., 2002) or a humidified inert gas such as liquid nitrogen boil-off (Milne et al. 2000). Electropolished stainless-steel canisters were evacuated 5 times and pressurized with humidified air in the work described by Bottenheim et al. (2002). Sample containers received a similar treatment during the Trace-P campaign (Blake et al., 2003). The stainless steel canisters used during the CARIBIC campaign were steam-cleaned prior to their deployment (Brenninkmeijer et al., 1999). Flask conditioning methods for the glass flask in the ESRL network are detailed by Conway et al. (1994) and Dlugokencky et al. (1994).

Sample storage: It is generally preferable to keep shipment and storage times of sampling canisters to a minimum in order to reduce possible contamination or sample decomposition. Blake et al. (2003) analyzed their cylinders within 10 days of sampling. CARIBIC samples are only taken on the return leg of the flight to reduce storage times (Brenninkmeijer et al., 1999). However, given logistical constraints, sample storage and transport times of up to one year are not uncommon during network operations at very remote sites, e.g. in the Antarctic. Few reports are available for the behavior of NMHC in whole air samples for storage times in excess of a few months. Light NMHC (C2 to C6) were stable for up to 4 months in fused silica-lined stainless steel canisters used by Saito et al., (2000). Kuster et al. (1996) and Milne et al. (2000) recommended pressurizing sampling cylinders with zero gas or sampling air to avoid inward contamination during storage and shipment to the sampling site whereas Apel et al. (2003) recommended shipping canisters evacuated to the field locations.

Chemical reactions: Ozone is inevitably co-sampled during whole air sample collection unless a selective ozone scrubbing technique is used. As a strong oxidant, ozone can react with unsaturated hydrocarbons such as ethene, propene or isoprene (Pinho et al., 2006) and has to be regarded as a potential source of analytical bias (Helmig, 1997). Reaction rate constants for the reaction with ozone at ambient temperature are for instance 1.45×10^{-18} cm^3 $molec^{-1}$ s^{-1} for ethene, 1.41×10^{-17} cm^3 $molec^{-1}$ s^{-1} for propene and 1.28×10^{-17} cm^3 $molec^{-1}$ s^{-1} for isoprene (Atkinson, 1994), which will lead to a significant loss of these analytes in the sampling containers within several hours unless ozone is selectively removed in the sampling procedure or container. Bottenheim et al. (2002) compared flask measurements with data from an in-situ GC at Alert, Canada It was found that ethene in the electropolished stainless steel canisters canisters was not affected by co-sampling of ozone over a storage time of 2 to 3 months. These observations suggest destruction of ozone in the sampler or in these canisters at much faster rates than the reactions occurring with unsaturated NMHC.

Contrary to the suspicion that unsaturated NMHCs may be lost during canister sampling due to reaction with ozone, unsaturated light alkenes (ethene, propene) were most often reported as showing increased concentration, implying significant analytical artifact formation during whole air canister sampling (Donahue and Prinn, 1993; Ramacher et al., 1997; Rudolph, 1999; Volz-Thomas et al., 2002, Plass-Dülmer et al., 2006). An evaluation of potential causes for these analytical problems was attempted during the AMOHA part 4 campaign (Plass-Dülmer et al., 2006) as part of a canister sampling intercomparison effort. It was identified that overheating of sampling canister during conditioning was one potential source of artificially enhanced propene concentrations.

Sample analysis techniques: Two methods are generally used for quantifying NMHC from sampling canisters. 1: cryogenic focusing using a coolant such as liquid nitrogen (e.g.: Bottenheim et al., 2002, Blake et al., 2003, Hakola et al., 2006) and 2: sample preconcentration using solid adsorbents at near-ambient or subambient temperatures (e.g.: Helmig, 1999). Both of these sample focusing techniques are then followed by thermodesorption with subsequent compound separation and detection by gas chromatography techniques. International laboratory intercomparison studies showed that

both these sampling methods are accurate and precise ways to quantify NMHCs (Apel et al., 2003, Plass-Dülmer et al., 2006). Laboratories reporting the highest accuracy and precision were often characterized by usage of high quality standards (e.g.: national laboratory standards from e.g. the National Institute of Standards and Technoloy (NIST), USA; National Physical Laboratory (NPL), UK; Norsk Institutt for Luftforskning, NILU, Norway), extensive testing of solid adsorbent trapping systems (if applicable) and regular participation in intercomparison studies. Minimum data quality guidelines for the GAW-VOC intercomparison were defined by Rappenglück et al. (2006), and were such that saturated NMHC measurements should have an accuracy of better than 10% with a repeatability of better than 5% above 100 pptv mixing ratio, and an accuracy and repeatability of ≤ 50% each below 100 pptv.

This brief review re-emphasizes that most whole-air sampling of NMHC has been done using steel flasks. Unfortunately no published studies are available on the characterization of NMHC analysis from glass flasks as employed by most CO_2 flask sampling networks. However, the findings from related studies suggest that it should be feasible to analyze C2-C7 NMHCs from glass flasks such as those used in regional and global air monitoring networks. This approach would possibly allow studies of the global NMHC distribution by taking advantage of existing sampling protocols and infrastructure within one or several of the operating greenhouse gas monitoring networks.

Our research intent therefore was to develop and characterize an analytical method for the quantification of C2-C7 NMHC from the ESRL Global Monitoring Devision (GMD), Boulder, Colorado, cooperative air sampling network. This network currently consists of 59 active surface sampling stations, where usually one pair of flask samples is collected every week. This network is currently the most extensive global flask sampling network in operation, both in terms of sites and total numbers of samples. Typical turnaround time of sampling flasks is on the order of weeks (continental North American sites) to one year (Antarctic sites). After return to Boulder, these samples are analyzed by two different laboratories (ESRL GMD and at the Institute of Arctic and Alpine Research (INSTAAR), University of Colorado. Gases and methods of the individual analyses steps are: automated trace gas analyzer (ESRL GMD) for CH_4 (GC-FID); CO and H_2, (GC-reduction gas detector); SF_6 + N_2O (GC-ECD) and CO_2 by near infrared spectrometery (Conway, et

al., 1994); at INSTAAR's Stable Isotope Laboratory (SIL) $^{13}CO_2$, $^{13}CH_4$ and $CO^{18}O$ are analyzed by mass spectrometric techniques (Trollier et al., 1996). After completion of these measurements the flasks are at subambient pressure when they reach our laboratory for NMHC analysis (Table 4.1).

Table 4.1: Analyses steps, gases analyzed, and remaining sampling volumes after completion of analyses by different instruments within the ESRL cooperate gas sampling network analytical sequence.

Instrument	location	gases	remaining sample volume (ml)	remaining flask Pres. (mbar)
before analysis			2500	1270
trace gas analyzer	NOAA	CO_2, CH_4, CO, N_2O, SF_6	2000	1045
CO2 stable isotopes MS	INSTAAR/SIL*	$^{13}CO_2$	1400	775
GC-MS	INSTAAR/SIL	$^{13}CH_4$	1200	685
GC-MS	INSTAAR/SIL	CH_3D	1100	595
GC-FID	INSTAAR/ARL+	C2-C6 NMHC	500	325
		total volume analyzed	2000	

source: NOAA GMD website
* Institute for Arctic and Alpine Research / Stable Isotope Laboratory
+Institute for Arctic and Alpine Research / Atmospheric Research Laboratory (this study)

A number of analytical challenges had to be addressed: hitherto the sampling procedures had not been developed, optimized or characterized for NMHC sampling; samples are collected by different personnel at the network sites; samples are below ambient pressure and remaining for NMHC analysis are in the sub-liter range. Given the high number of samples targeted to be analyzed each week, a system with a high throughput and low cost per analysis was desirable. NMHC had to investigated for the long storage times that occur during transport and storage for samples from remote stations.

4.2 Instrumental

A custom-made sample extraction and inlet system interfaced to a GC-flame ionization detection (FID) instrument was specifically tailored towards the requirements of this project. The instrument is fully automated and is currently capable of analyzing 12 sampling flasks bracketed by 4 calibration runs (2 0-air, 2 standards) unattended and in series.

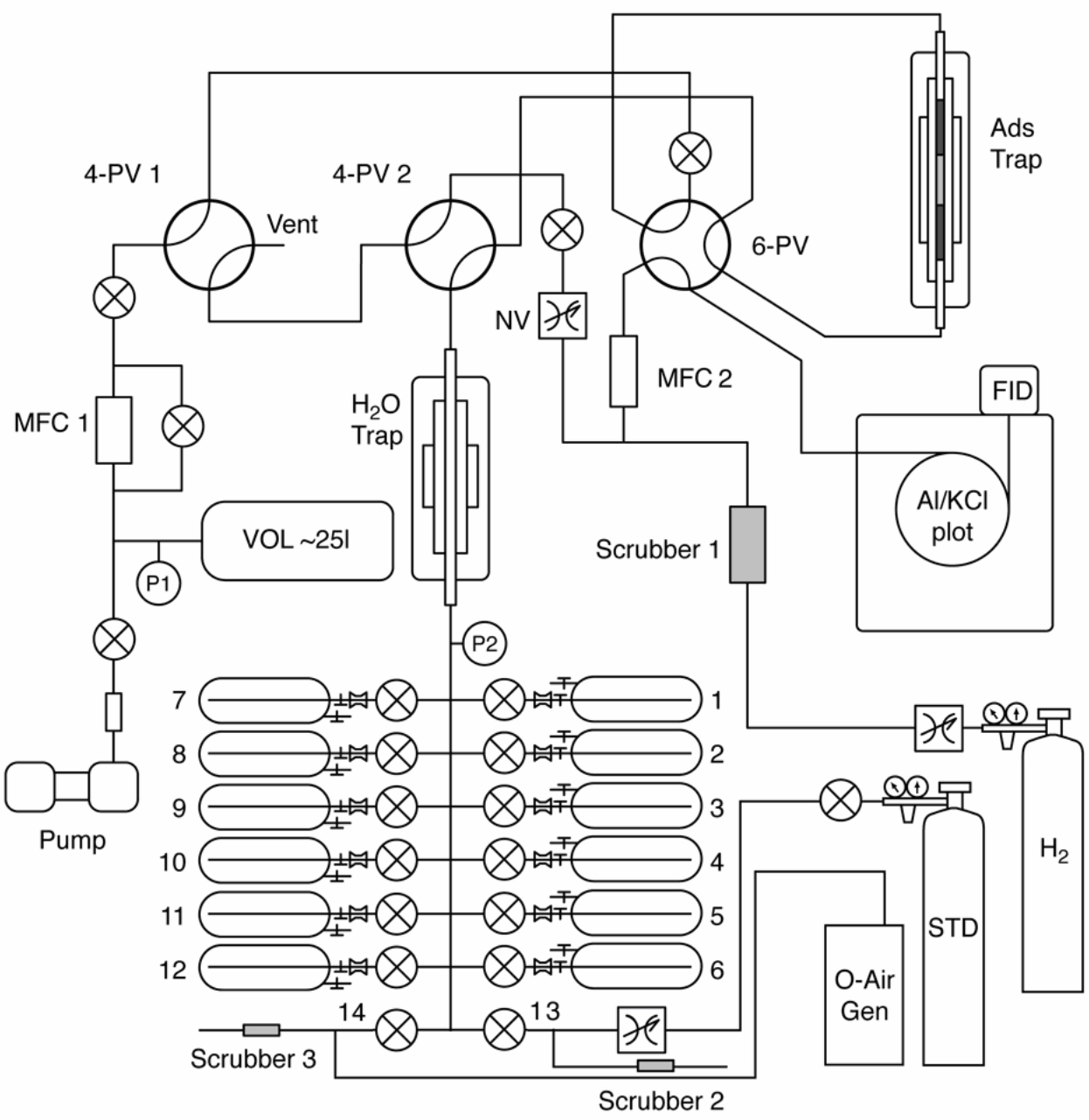

Figure 4.1: Instrument schematic. 4-PV-1 and 2, 4-port, 2-position valve, A44 UWE, Valco, Houston, TX, USA; 6-PV, 6-port, 2-position valve, A4C6UWE; Al/KCl Plot, GC column; FID, flame ionization detector; Filter, particle filter; Ads Trap, adsorbent trap; GC, gas chromatograph (5890 series II, HP, Santa Clara, CA); H_2O trap, water trap; MFC1, mass flow controller (FC-280-SAV, Tylan, Carson, CA, USA); MFC2, mass flow controller (UFC 1100a, Unit Instrument Inc, Yorba Linda, CA); NV, needle valve; P1, pressure gauge (622A12TBE, MKS Instruments, Andover, MA, USA); P2: pressure gauge (C-68848-26, Cole Parmer, Vernon Hills, IL, USA); Scrubber, oxygen trap, (7213, Alltech, Deerfield, IL, USA), hydrocarbon trap (7201, Alltech), indicating oxygen trap (4004, Alltech); Shut-off valve (SS-BNVCR4-C, Swagelok); Vacuum pump (N813.5 ANE/AF, Neuberger, Freiburg, Germany); Vol, vacuum reservoir V ~ 25 l

The single-stage solid adsorption thermodesorption system was designed in order to avoid the usage and expense of a cryogenic coolant. A cryogen-free analysis system was also deemed to reduce the susceptibility to interruptions during automated processing of large sample sets.

Detailed descriptions of technical aspect of the focusing system have been provided previously (Tanner et al., 2006; Pollmann et al., 2006) and only a brief overview is given here. The instrument (Figure 4.1) relies on a solid adsorption/thermodesorption technique, using a custom-built microtrap filled with 10 mg Carboxen 1016 and 100 mg Carboxen 1000 that is cooled to –30 ºC. A vacuum reservoir is used to extract an airsample from the flasks through the focusing trap and the pressure change within this reservoir iss utilized to determine the extracted sample volume. After sample preconcentration the trap is first purged with carrier gas (H_2) to remove residual air, and then heated resistively to 310 ºC within 3 s. Desorbed analytes are injected onto an Al_2O_3 - KCl deactivated porous layer open tubular (PLOT) column (length: 50 m, I.D: 0.53 mm, 19095P-K23, Agilent, Wilmigton, DE, USA). Analytes are identified by retention times and quantified by FID. Peak identification was confirmed by splitting the column flow and analyzing a portion of the GC eluent by mass spectrometry. Zero air for the operation of FID and for blank measurements was generated on-site by flowing compressed air over a heated (375 ºC) catalyst (PtO (1%) on Al_2O_3; 23,211-4, Sigma Aldrich, Deerfield, IL, USA).

An automated inlet manifold with 12 flask and 2 standard ports was designed to connect the sampling flasks to this GC-system. The manifold was custom-welded (MKS, Boulder, CO, USA) using 6 mm stainless steel tubing and Swagelok (Solon, OH, USA) welding components (6 union crosses, 316L-4-ATW-4, and 1 union tee, 316L-4-ATW3). The connection between the valve manifold and the sampling flasks was established with VCR to 12 mm tube bulkhead fittings (316L-4-VCR-61-4TB7, Swagelok) and flask adapters (SS-8-UT-6-4, Swagelok). Each flask can be individually accessed from the manifold using pneumatically controlled shut-off valves (6LV-BNBW4-C, Swagelok). The entire system (manifold and preconcentration system) is computer-controlled and automated using LabView software (National Instruments, Austin, TX, USA).

NMHC standards and calibration procedures: A reference gas (Pollmann et al., 2006, referenced as P 2006 from here on out) calibrated by an outside laboratory using gravimetrically prepared standards was used to establish a calibration scale. This reference gas and in-house generated 0-air were analyzed regularly, during most times twice daily for over a period of more than one year. Compound response factors were calculated from integrated peak areas and the reference analyte mixing ratios. These response factors were used in all described experiments and later for the network sample analysis. The instrument background was monitored by the daily 0-air runs prior and after a set of sample flasks was analyzed. A change in the response by more than 5% was used as an indication for instrumental problems.

Additionally, a series of comparison experiments with two reference gases and three standards were conducted to confirm and validate the calibration scale.

Table 4.2: NMHC mixing ratios in reference gases and standards used in this study.

Compound	Breathing Air reference mixing ratio (ppbv)$^{+}$	Niwot Ridge reference mixing ratio (ppbv)$^{+}$	Synthetic Air reference mixing ratio (ppbv)*
Ethane	4.15	1.38	10.62
Ethene	2.28	0.38	4.93
Propane	2.23	0.39	9.90
Propene	1.60	0.315	2.03
Isobutane	0.71	0.056	4.44
Butane	1.59	0.093	8.47
trans-2-Butene			1.01
1-Butene			2.17
2-Methylpropene			3.01
cis-2-Butene			2.12
Isopentane	2.19	0.052	6.48
Pentane	1.36	0.037	7.64
2-2-Dimethylbutane			2.02
2-3-Dimethylbutane			1.57
2-Methylpentane			0.86
3-Methylpentane			1.07
Hexane	0.20	0.011	2.70
Isoprene			4.18
Benzene			1.72
Toluene			2.41

$^{+}$mixing ratio determind by cryogenic enrichment GC-FID/MS; precision 7%
NOAA, CSD, Bulder, CO, USA
*mixing ratio determind by cryogenic enrichment GC-FID/MS; precision 6%
NCAR, ACD, Boulder, CO, USA

Compounds and their mixing ratios for the two reference gases and for two of the quantitative standards are listed in Table 4.2: 1. A gas cylinder containing compressed air (BA) (breathing-air grade, Airgas, Boulder, CO) was calibrated for C2-C6 NMHC by an outside laboratory using GC-FID, GC-MS in reference to a gravimetrically prepared scale of NMHC standards (ESRL - Chemical Science Division (CSD), Boulder, CO, USA). 2. Ambient air was filled into an acu-life treated aluminum cylinder at Niwot Ridge (NR), Colorado, a high altitude, background air sampling site (40º 3' N, 105º 36' W, 3345 m asl) following the ESRL Tech Memorandum (Kitzis and Zhao, 1999). C2-C6 NMHC were quantified in the same manner as for the BA reference gas. The measurement accuracy of the NMHC mixing ratios in these two reference gases is estimated to be ≤ 10%. 3. A NIST-traceable 2-component (2,2-dimethyl-butane, n-decane) standard from Scott Specialty Gases (Longmont, CO) was used. 4. A 54 synthetic air standard, containing 54 NMHC ranging from C2 to C8 at mixing ratios between 0.9-10 ppbv was obtained from the National Center for Atmospheric Research, Boulder, CO. 5. A 38 compounds halogenated/partially halogenated hydrocarbon standard (41900-U, Scott Specialty Gases) was used for peak identification experiments.

Flask Sampler: Personal Sampling Units (PSU) are used by ESRL at all their surface sampling sites (Conway et al., 1994; Dlugokencky et al., 1994). These samplers are custom-manufactured by ESRL (see also figure 4.2). The air sample is usually taken from ~ 5 m above ground through 1/4" Teflon tubing attached to the telescope pole. Air is drawn through the tubing at a flow rate of 5-7 l min^{-1} by a one-stage Teflon-membrane pump and is then pushed through a pair of flasks for 7 minutes. Samplers used in humid environments are equipped with a thermoelectric water condenser to reduce the sample dewpoint and to prevent water condensation in the flasks at lower temperatures. After the initial purge time the outlet valve (SS-OGS-2, Swagelok) is closed and the flasks are pressurized to approximately 1200 hPa. A pressure release valve (Y334350, Airgas, Boulder, CO) opens when the desired pressure is reached and the flasks are purged for another 3-5 minutes at this elevated pressure. Subsequently, the pump is turned off which seals the flasks for leak checking. The flasks valves are then closed and the air sample is shipped to Boulder, CO, USA for analysis.

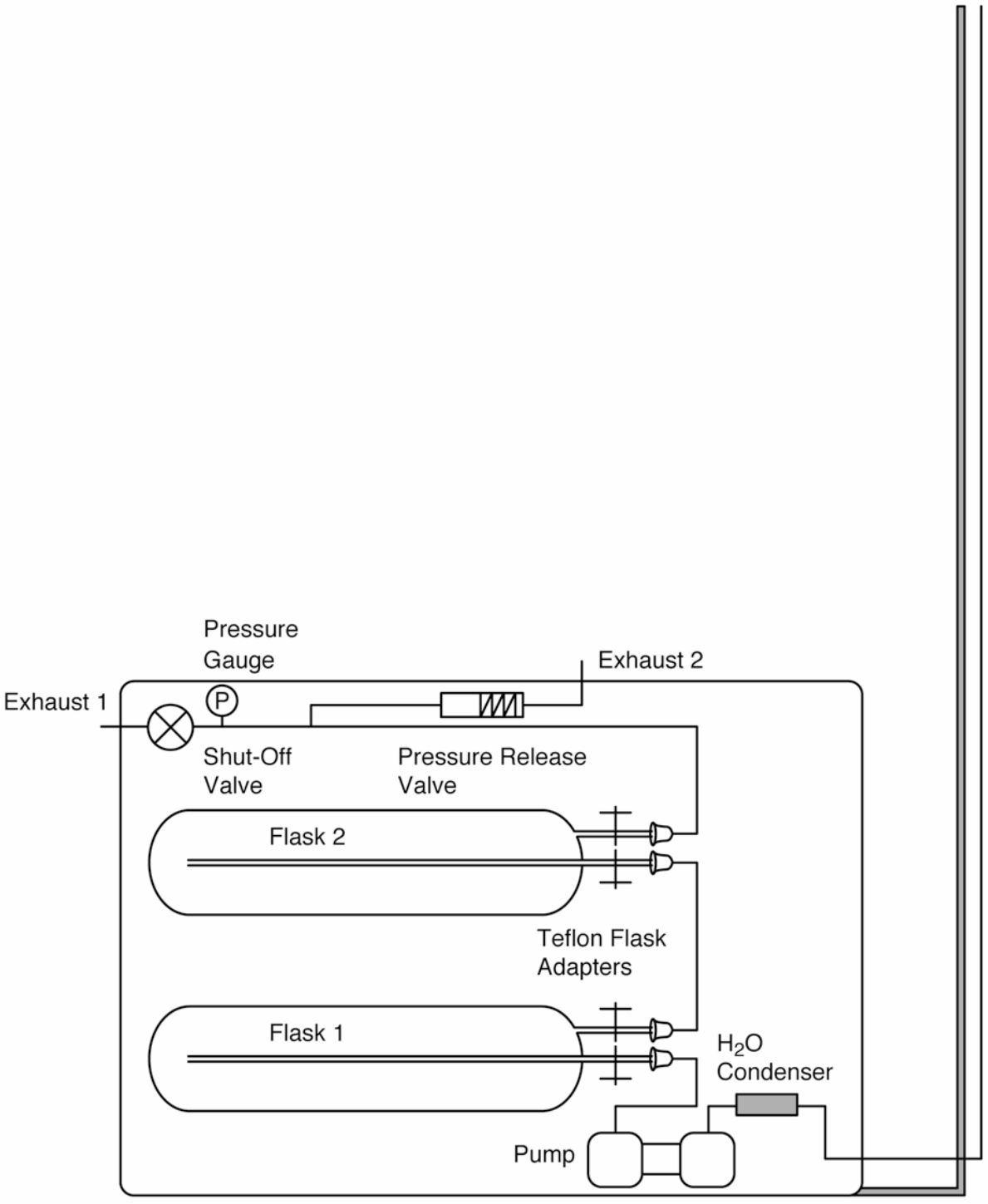

Figure 4.2: Schematic drawing of ESRL GMD personal sampling unit (PSU). Individual components are identified in the text.

Flasks: The ESRL network flasks are custom-made from borosilicate glass by Allen Scientific Glass (Boulder, CO, USA). The flasks have two stopcocks equipped with Teflon

O-rings (Glass Expansion, Pocasset, MA, USA) (Figure 4.2). One of the valves connects to a glass extending almost to the bottom of the flask. The second valve is located on one of the outside corners at the top end of the flask. This design facilitates complete replacement of the fill-gas with sample air during the filling process. The outside of the flasks is coated with a light-proof polymer to minimize potential photochemical degradation reactions and to avoid shattering in case of accidental breakage.

Flask conditioning procedures have been detailed by Dlugokencky et al. (1994). Flasks are evacuated to 0.8 Pa at room temperature and sealed. After 24 h the flasks are leakchecked and filled with synthetic air (< 1 ppm H_2O) to 1013 hPa. Flasks are then shipped to the sampling stations. This fill gas has a mixing ratio of 330 ppm CO_2, which allows detecting accidental incomplete filling of flasks after return from the network stations.

4.3 Experiments

In this section we first describe experiments that test and demonstrate the feasibility of NMHC measurements from the NOOA cooperate network flasks. Later we demonstrate the accuracy and precision achievable for NMHC measurements from the network flasks.

4.3.1 Sampling method validation

Humidity in flasks: Previous studies have shown that atmospheric water vapor can strongly interfere with solid adsorption NMHC focusing and subsequent GC analysis (e.g. Helmig and Vierling, 1995; Karbiwnyk et al., 2002; Pollmann et al., 2006). It has also been found that reducing the sample air dew point to below –10 ºC was necessary to facilitate interference-free analysis of humid samples (Pollmann et al., 2006). It was unknown to what extent atmospheric water vapor is extracted from the flasks and how much of the sampled water vapor was possibly lost by uptake to the internal surfaces of the glass flasks. As mentioned earlier, the gas pressure in the sample flasks decreases over the course of the sequential analysis steps, with our NMHC quantification being at the end of the measurement sequence (Table 4.1). Therefore, we also investigated whether water retrieval potentially increases with declining sample pressure (e.g. by releasing proportionally more water from the walls at reduced pressure). The flask conditioning

resembled ESRL's standard procedures as much as possible. Five network flasks were connected to a Teflon membrane pump (N813.5ANE/AF, Neuberger, Freiburg, Germany) and evacuated to 50 Pa. The flasks were stored for 24h and then purged with humidified zero air (80% relative humidity, dewpoint 17 ºC) at 1 l min^{-1} for 30 minutes. The relative humidity level was confirmed by measurements with two thermohygrometers (WD-35612-00, Oakton, Vernon Hills, IL). Flasks were stored in the dark and individual flasks were analyzed after 1.5, 2.5, 3.5, 4.5 and 5.5 days of storage. Seven 250 ml-sample aliquots (up to 1.75 l of total) were sequentially extracted at 50 ml min^{-1} through a drierite (calcium sulfate, $CaSO_4$) cartridge. The drierite cartridges were weighed after each extraction step and the weight increase was used to calculate the water extraction rate from the flasks. The water recovery was evaluated in comparison to the theoretically expected (at 100 % recovery) amount of water in each sample aliquot.

Sampler testing: A field PSU-sampler that was brought back to the ESRL laboratory for routine inspection and maintenance was randomly chosen for evaluating the suitability of a network sampler for NMHC collection. The BA reference gas was filled into 6 network flasks (3 pairs) to 1200 hPA pressure using the sampler while strictly following the sampling guidelines established by ESRL. The 6 test flasks filled with the standard were then analyzed using the flask manifold. For reference, the same standard was also analyzed (n = 4) directly from the compressed gas cylinder. The ratios of NMHCs from the flasks vs. the direct cylinder measurements were used to evaluate recovery rates from the flask filling procedure. Particular attention was also placed on eventual contamination stemming from the PSU.

Sample extraction: The internal pressure of the sampling flasks shows a notable variation upon arrival at our laboratory depending on the amount of sample withdrawn during the previous analyses (Table 4.1), where, on occasion, selected samples are also analyzed multiple times to investigate potential analytical inconsistencies. It was therefore necessary to evaluate the influence of the internal flask pressure on the recovery of individual compounds and to determine the minimum pressure at which a full sample could be extracted. The NR reference gas (Table 4.2) was purged through a pair of network flasks

at 1 l min^{-1} for 20 minutes before valves were closed to yield a sample pressure of ~860 hPa (ambient pressure at Boulder's altitude of 1600 m asl). The air from the flask was then extracted and analyzed in 600 ml, and later 300 ml and 200 ml aliquots to achieve good coverage over the reduced pressure range. These extractions were bracketed by direct measurements of 600 ml, 300 ml and 200 ml of the reference gas from the cylinder. This experiment was continued until no further sample extraction from the flasks was possible.

Sample stability: Aliquots of the NR reference gas were used for testing the stability of low-concentration NMHC during storage in the network flasks. A total of 24 flasks were filled using the same protocol as described for the sampler testing above and stored in the dark at room temperature. A pair of these samples was analyzed approximately every month to study the potential degradation/changes of analytes and during storage. A similar experiment was conducted by filling a series of 24 flasks with house 0-air in order to evaluate the eventual buildup of contaminations, e.g. by inward diffusion through the Teflon-sealed flask valves.

4.3.2 Calibration, accuracy, and precision

Evaluation of calibration scale: The calibration scale was based on the P 2006 reference gas and the 2, 2-dimethybutane standard. This calibration scale gas was evaluated by comparing the quantitative results from the measurement of the breathing air reference gas, the Niwot Ridge reference gas and the synthetic air standard with the stated reference NMHC mixing ratios in these different gas mixtures.

Intercomparison with Hohenpeissenberg: During April 2006, collection of flask samples at the Deutscher Wetterdienst Hohenpeissenberg WMO-GAW station was initiated. Flasks filling times overlap with the sample collection of two independent cryogenic-GC systems (Plass-Dülmer et al., 2002) at this site. Sampling inlets for the flask sampling and the in-situ measurements are located at the same height (10 m above ground) and approximately 2 m apart on top of the laboratory building at Hohenpeissenberg. Flask samples are only collected when wind speeds are >2m/s and when CO concentrations are stable, in order to minimize sampling under highly variable conditions of air composition. The in-situ GC

method collects an air sample over a 15-minute integration time. The flask purging and filling is timed such that it occurs during this same period, however the sample collected in the pair of flasks represents a ~1 min snapshot of the air composition that is purged through the PSU during the last minute before the flask valves are closed The Hohenpeissenberg samples were subjected to the same handling and analytical practices as flasks from all other ESRL network sites including the prior analyses for greenhouse gases and stable isotopes before NMHC measurements.

This test cannot be seen as a classic intercomparison experiment as the samples analyzed by both laboratories are not strictly identical (see above). A systematic uncertainty of not more than 10% was estimated due to these differences in sampling time. Additionally, the average analytical uncertainty (accuracy and precision) for C2-C7 NMHC for the Hohenpeissenberg in-situ measurements was determined at 7% (Plass Dülmer et al., 2002). This results in an estimated systematic comparison uncertainty of 13%.

The GAW data quality objective was subsequently adjusted by propagation of error to account for this additional uncertainty. Flask and in-situ NMHC measurements had to agree within 17% to meet the GAW data quality objective above 100 pptv and within 52% below 100 pptv.

Analytical precision: The repeatability of this analysis was determined from several experiments where multiple analyses of the same air sample filled in different flasks was performed. Furthermore, we used the deviation in NMHC data in pair of flask samples that were collected concurrently at network sites. A total of 1300 available measurements in flask pairs were available for this evaluation.

4.4 Results and discussion

4.3.1 Sampling method validation

Water Tests: Figure 4.3 shows the amounts of water extracted from the flasks that were filled with humidified 0-air. These data show a linear increase of the amount of water with increasing sampling. Also, the relative amount of water extracted with each sample aliquot remained constant and did not increase at reduced pressures. This analysis shows that, within the uncertainty of the humidity measurements (~ 7%), all water vapor that was introduced into the flasks was reversibly retrieved during the sample extraction from the flasks. Furthermore, no changes in the water extraction rate over the 7-day test period were noticed. This finding indicates that water vapor remains completely in the gas phase and is not lost to the flask walls for at least the length of time and the sample filling and storage conditions that were investigated in this experiment.

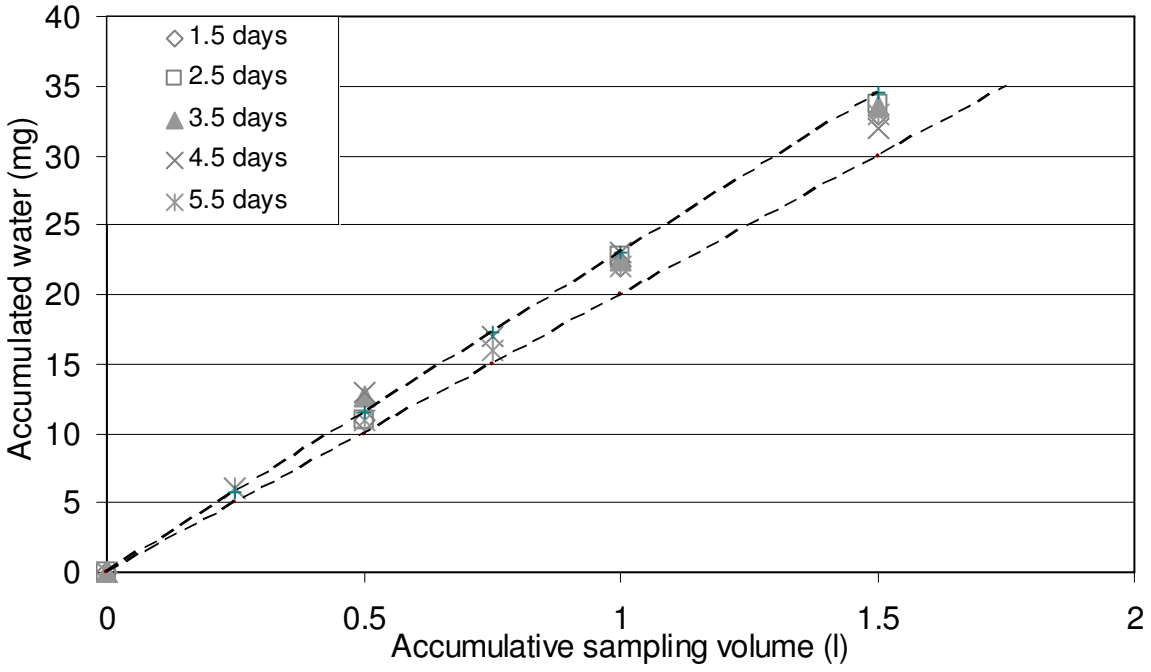

Figure 4.3: Mass of extracted water in five flasks that were extracted after 1.5-5.5 days of storage. Dashed lines represent the expected bounds (lower to higher estimate) of from the humidity measurements.

Sampler Testing: Figure 4.4 shows the ratio between the direct analysis of the NR reference gas and results obtained after filling and extraction of the standard from flasks. The agreement between both measurements is within 10% for all considered NMHC with no systematic bias towards compound losses or gains using this flask filling technique. This experiment proved that the tested PSU did not cause any significant changes to the NMHC composition and concentrations.

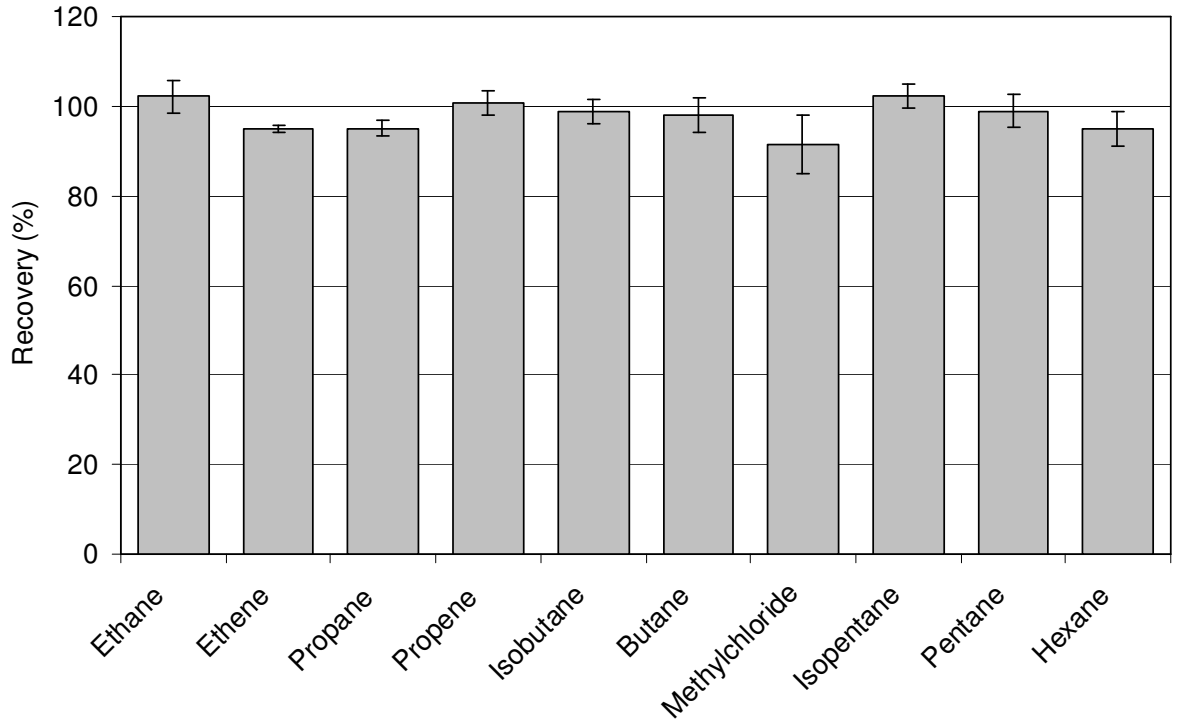

Figure 4.4: Recovery ratios of target compounds in the BA reference gas when sampled with the PSU and analyzed from the flask referenced to direct sampling from the standard cylinder. Bar graphs show average recovery ratios from the analysis of 6 individual flasks. Error bars represent the overall uncertainty calculated from 6 flask and three standard measurements by propagation of error.

Sample extraction: Table 4.3 displays the ratio of NMHC area counts from flask analysis at different internal pressures relative to direct cylinder analysis. The measured NMHC mixing ratios were found to be not depending on the internal flask pressure. NMHC recovery declined proportionally to the reduced sample volume once the flask pressure

was too low to extract a full sample at approximately 200 hPa. This pressure is usually not reached during routine flask analysis or not even in case of previous multiple quantifications (table 4.1). It can be concluded that internal flask pressure fluctuations do not influence the quantification of NMHC mixing ratios.

Table 4.3: NMHC recovery (percentage of expected mixing ratio, mean of two flask experiments) as a function of declining flask pressure.

		Ratio (flask/cylinder)							
cumulative extraction (ml)	0[+]	200	400	600	800	1000	1200	1400	1600*
internal pressure (hPa)	860[+]	804	710	612	517	420	326	235	157*
ethane		104	103	100	103	100	102	107	109
ethene		95	94	93	93	91	93	95	97
propane		93	93	90	97	91	90	94	94
propene		99	97	96	96	94	96	99	101
isobutane		107	105	106	105	103	106	108	112
butane		107	107	106	106	104	106	108	110
isopentane		110	109	108	107	105	107	110	112
pentane		108	107	106	106	103	105	109	111
hexane		98	98	97	99	100	100	103	104

[+]starting conditions
*incomplete extraction

Sample stability: Figure 4.5a summarizes results from the storage test of the NR reference gas. The low molecular weight analytes ethane and propane did not show any significant changes during this one-year test period and their determined mixing ratios from the flasks in general agreed to within 3% of the direct measurement from the cylinder. Similarly, heavier molecular weights (butanes and pentanes) did not show any significant changes; their mixing ratios from the flask samples agreed within 6% with the reference measurements. The unsaturated compounds ethene and propene showed a much higher variability. For these analytes the average repeatability in flaks pairs was much poorer, on the order of 30% for ethene and 28% for propene. Furthermore, both analytes showed increases during storage, on the order of 20% yr^{-1} for ethene and 35% yr^{-1} for propene.

The storage experiment of the 0-air samples (Figure 4.5b) in the flasks showed consistently lower blank readings in the flask samples than in the daily blank experiments during the beginning of this experiment (for the reasons discussed above). Average blank levels were below the detection limit (5 pptv carbon) for most of the saturated NMHCs.

Unsaturated compounds (ethene and propene) showed both higher background levels and an overall higher variability. These results are in line with the above-discussed problems for unsaturated compounds in the storage experiment of the ambient air standard.

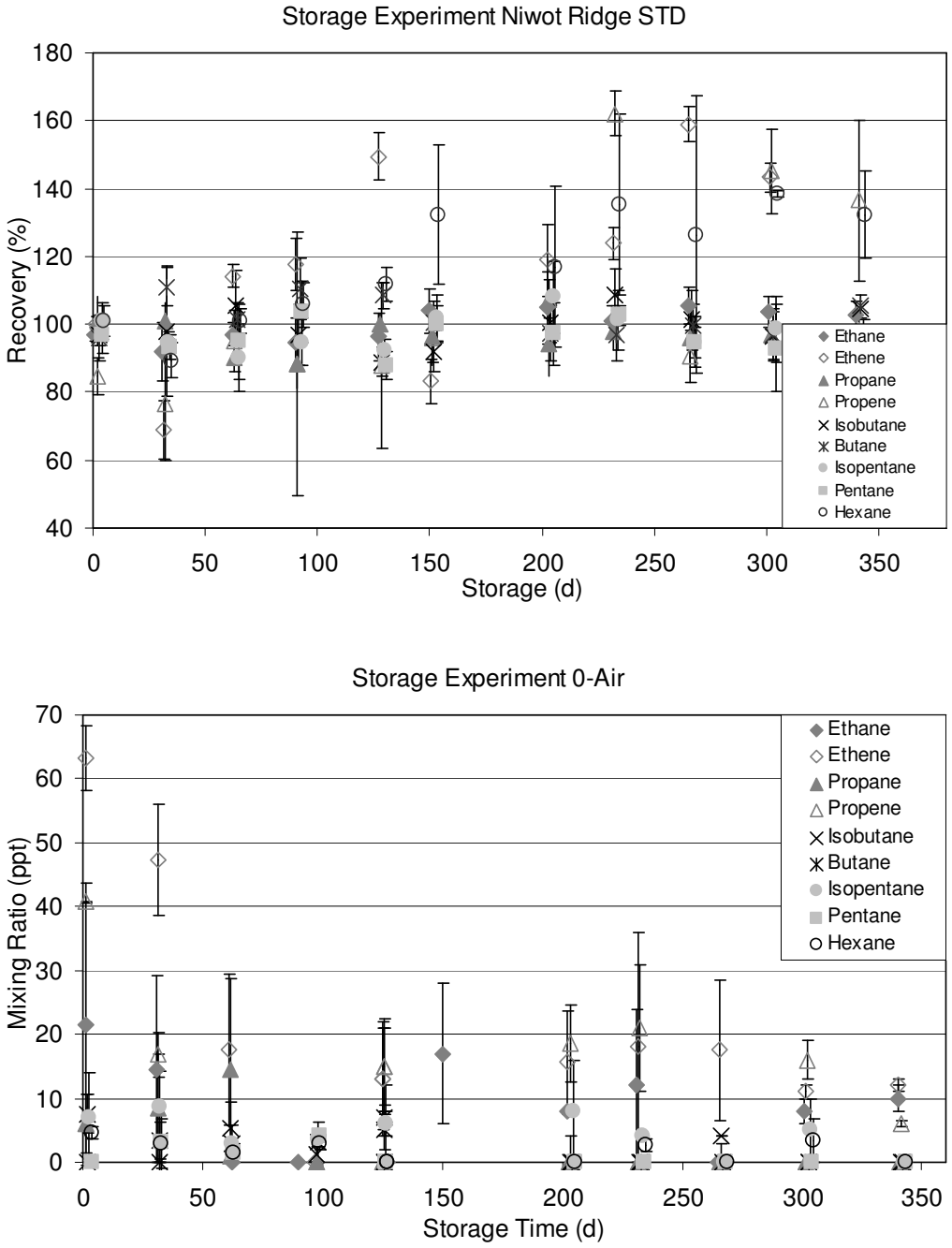

Figure: 4.5 a, b: Recovery (average of quantification of two flasks) for target compounds after storing the standard in network flasks for up to one year. Figure b shows the results for the storage of 0-air under the same conditions. Error bars represent the standard deviation from the analysis of two flasks (with one sample analysis from each flask).

4.3.2 Calibration, accuracy, and precision

Blanks, detection limit, response factors, stability of calibration: The analysis of the laboratory-generated 0-Air showed contamination peaks of up to 50 pptv over the first several months of this experiment (Figure 4.6b). We identified that the cause of this contamination was first the suction into and then diffusive sampling of a small fraction of room air into the manifold when the instrument was collecting 0-air samples. The zero air sampling valve 14 (Figure 4.1) is opened at the beginning of the sampling stage. At this point, the manifold (internal volume ~ 60 ml) is still under vacuum. Room air together with 0-air was drawn through the tee, which was connected to a vent outlet in order to bleed off excess flow during zero air collection. This systematic error occurred only when standard samples were loaded as the system is sealed during flask analysis. Subsequent changes to the manifold set-up and sampling sequence were implemented to correct for this error. A 90 s manifold purge step was added prior to the preconcentration step; during this time 0-air is flown through the manifold at a flow rate of 60 ml min^{-1} but bypasses the adsorbent trap. Secondly, the manifold outlet was equipped with a Carbosieve SIII cartridge to scrub NMHC from room air. After the implementation of these changes the 0-air blanks were significantly lower, with average blank readings well below 10 pptv.

The instrumental detection limit is thus limited by the minimum integratable peak and not by significant blank mixing ratios. The detection limit was determined from the smallest peaks that could be reliably integrated and where on the order of 5 pptC (Pollmann et al., 2006).

The response factors for 11 compounds were calculated from the close to daily analysis of the P 2006 reference gas between April 2005 – November 2006. Representative results for five saturated C2-C5 NMHC are plotted in Figure 4.4a. Modifications to the instrument configuration during this time typically caused notable changes in the response factor (see legend of Figure 4.6a, b). Response factors for individual compounds deviate from the overall mean carbon response factor by up to 15 %, similar to findings reported previously by other investigators (e.g. Plass Dülmer et al., 2002) and it has been recommended to use multi-component standards for determining individual compound responses rather than using a uniform per carbon response factor (Apel et al.,

2003). The calibration scale was evaluated by quantifying NMHC in the Niwot Ridge and breathing air reference gases as well as in the synthetic air standard in comparison to the reference values. The response factors determined from these regular calibration measurements were also used to quantify NMHC in the daily flask measurements.

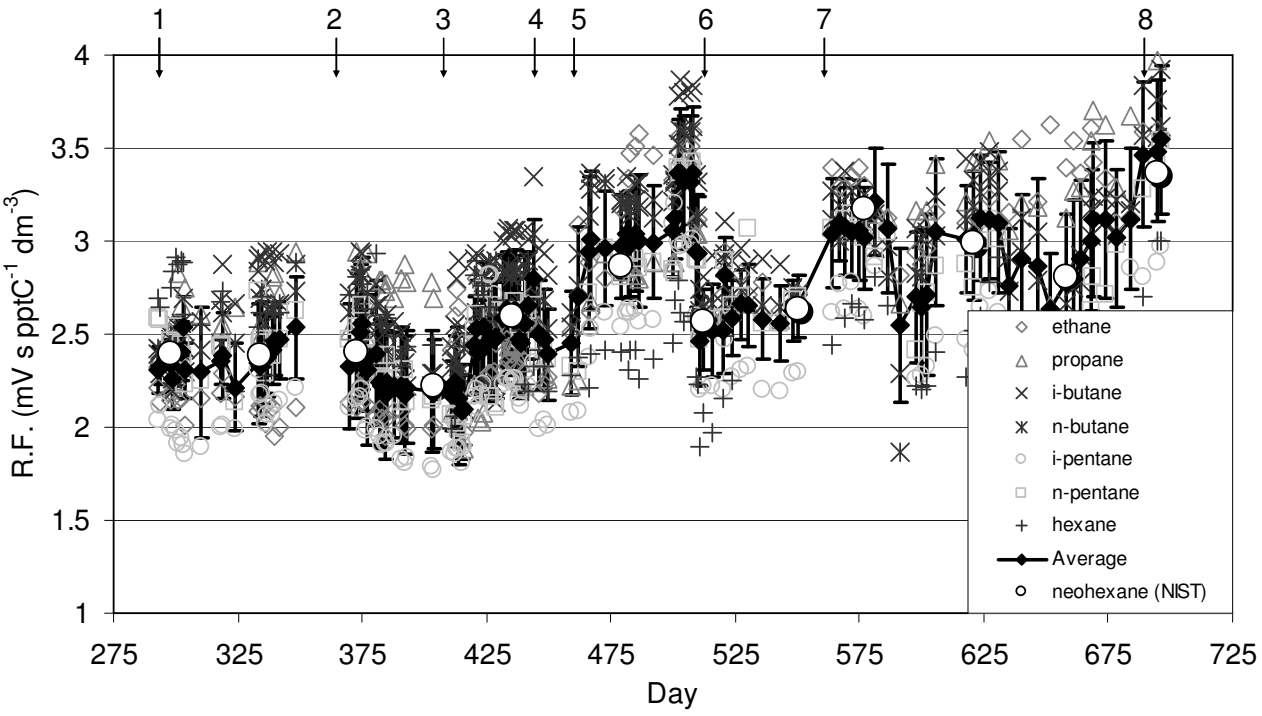

Figure 4.6 a: Temporal evolution (running day starting January 1, 2005) of individual detector response factors (R.F.) from direct cylinder analysis of the BA reference gas and the NH standard. The adsorbent trap was changes were made at times indicated by arrows numbered 1, 2, 4, 7, 8; the adsorbents trap filling was changed from Carboxen 1016 (20 mg), Carboxen 516 (60 mg), Carbosieve S III (40 mg) to a combination of Carboxen 1016 (5 mg) and Carboxen 1000 (100 mg) on day 313 (arrow #3), as tests showed that this adsorbent combination resulted in a significant reduction of instrumental blanks for aromatic compounds (Pollmann et al., 2006); the technique for introduction of the 0-air sample was changed at event #5; the FID was cleaned and FID flows were adjusted at event #6.

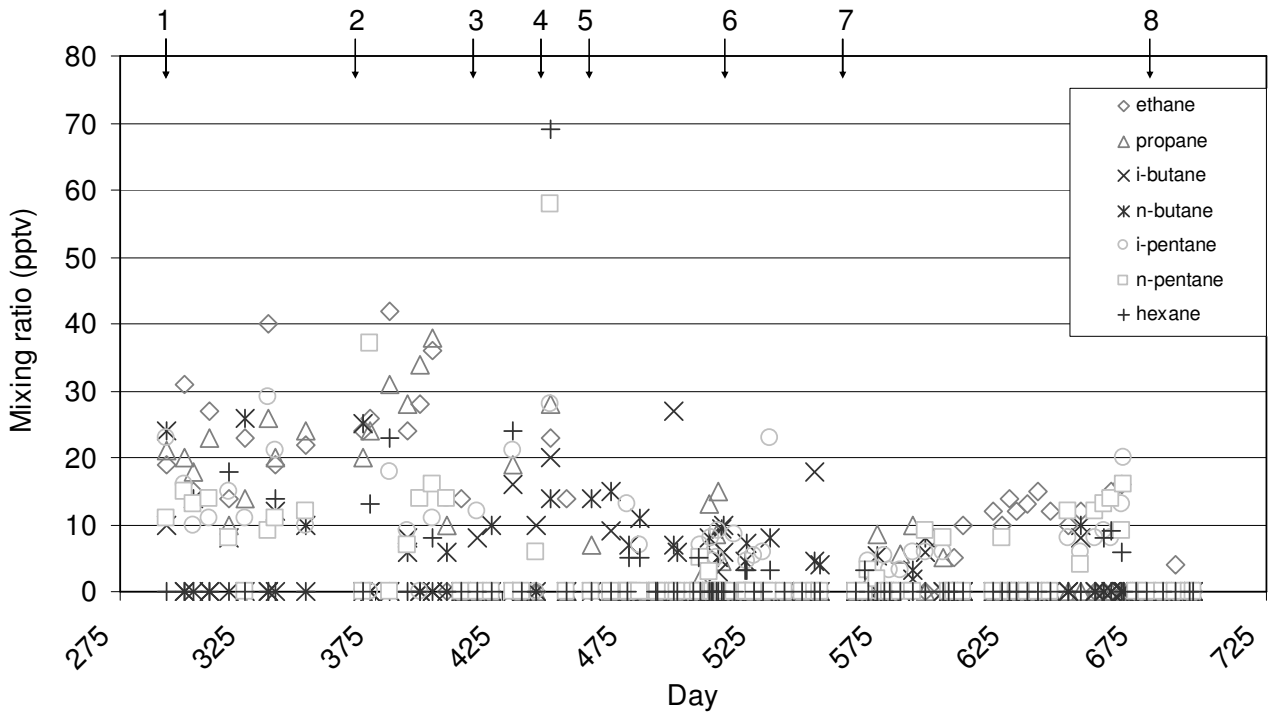

Figure 4.6 b: Instrument blanks (plotted against running day starting January 1 2005. Numbered errors depict same events as detailed in Figure 4.6a.

Results from the quantification of the Niwot Ridge (Figure 4.7) and breathing air reference gases (Figure 4.8), as well as the synthetic air standard (Figure 4.9) for C2-C5 compounds are within 3 - 10% of the reference values from other laboratories and standard suppliers. These agreements fell well within the GAW data quality objective. However, results for hexane were 25% to 65% higher than the reference values.

The synthetic, multicomponent standard (see Table 4.2) contains a higher number of calibrated compounds than P 2006. An average response factor was used to determine the mixing ratios of isoprene, the branched hexane isomers and the aromatic compounds as no calibration gas was available. NMHC measurements of the synthetic air standard with the flask instrument were found on average within 4% agreement to the provided reference values from NCAR-ACD. A slightly higher deviation from unity was found for compounds without an available reference gas. Results for 2-2-dimethylbutane were more than 45% above the certified value. The mass spectral analysis of this peak showed that this compound coelutes with methylcyclopentane. Using the sum of the 2, 2-dimethylbutane and methylcyclopentane as a reference this peak resulted in a 105% recovery rate for the

combined compounds. Hexane was quantified with acceptable accuracy from this standard, much in contrast to the results from the ambient air reference gases.

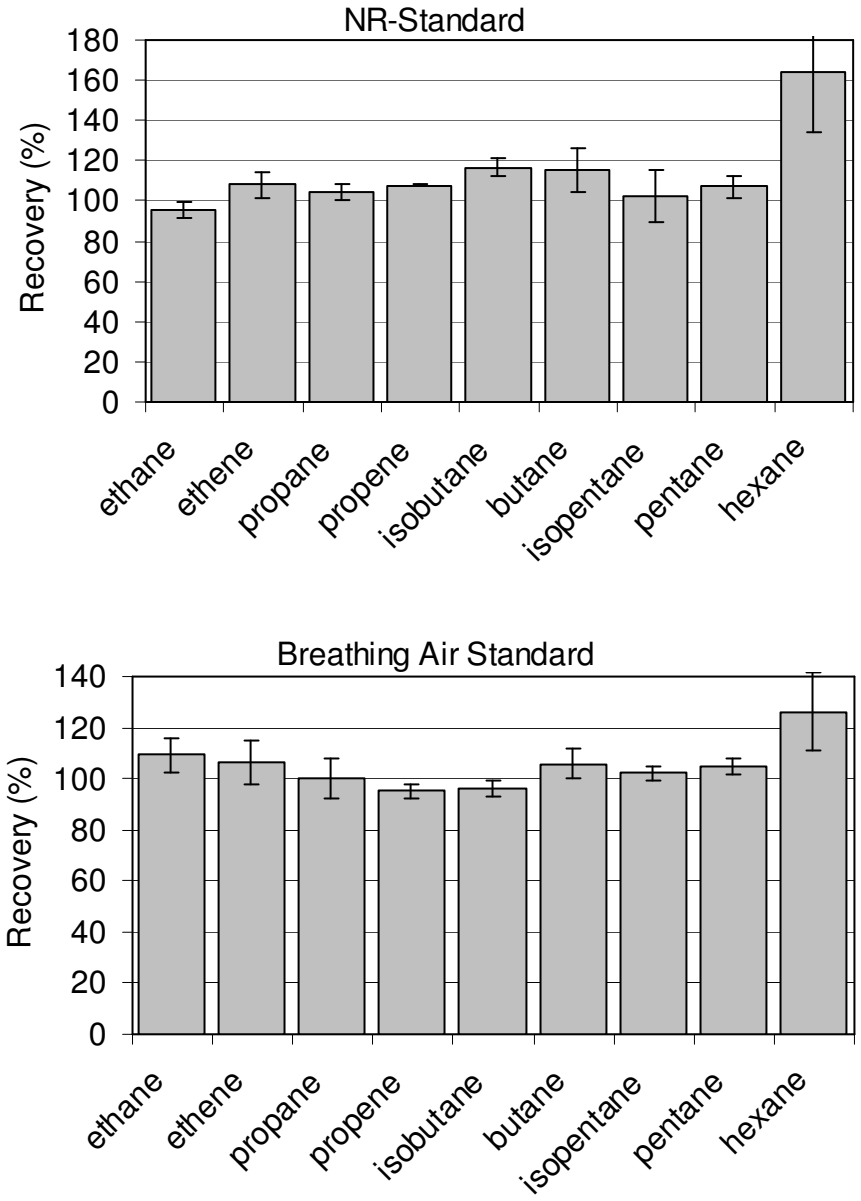

Figures 4.7, 4.8: Standard measurements ratios relative to reference values by ESRL CSD. Each bar represents the average of 5 consecutive standard measurements by direct cylinder quantification. Error bars for the recovery ratios were calculated from the cylinder repeatability and the precision of the reference measurements (table 4.2) using propagation of error.

Initially, isoprene, benzene and toluene were not included in the set of compounds measured from the flasks due to the lack of a reliable standard. However, the accuracy in

the quantification of these analytes met the stated data quality guidelines. These findings infer that these three NMHC could potentially be analyzed from network flasks. Since these compounds were not included in the extensive sampler and storage tests, some questions related to their behavior in the flasks remain open at this time. However, findings from the intercomparison measurements (see below) provide confidence for the reliable analysis of all of these three compounds from flask samples.

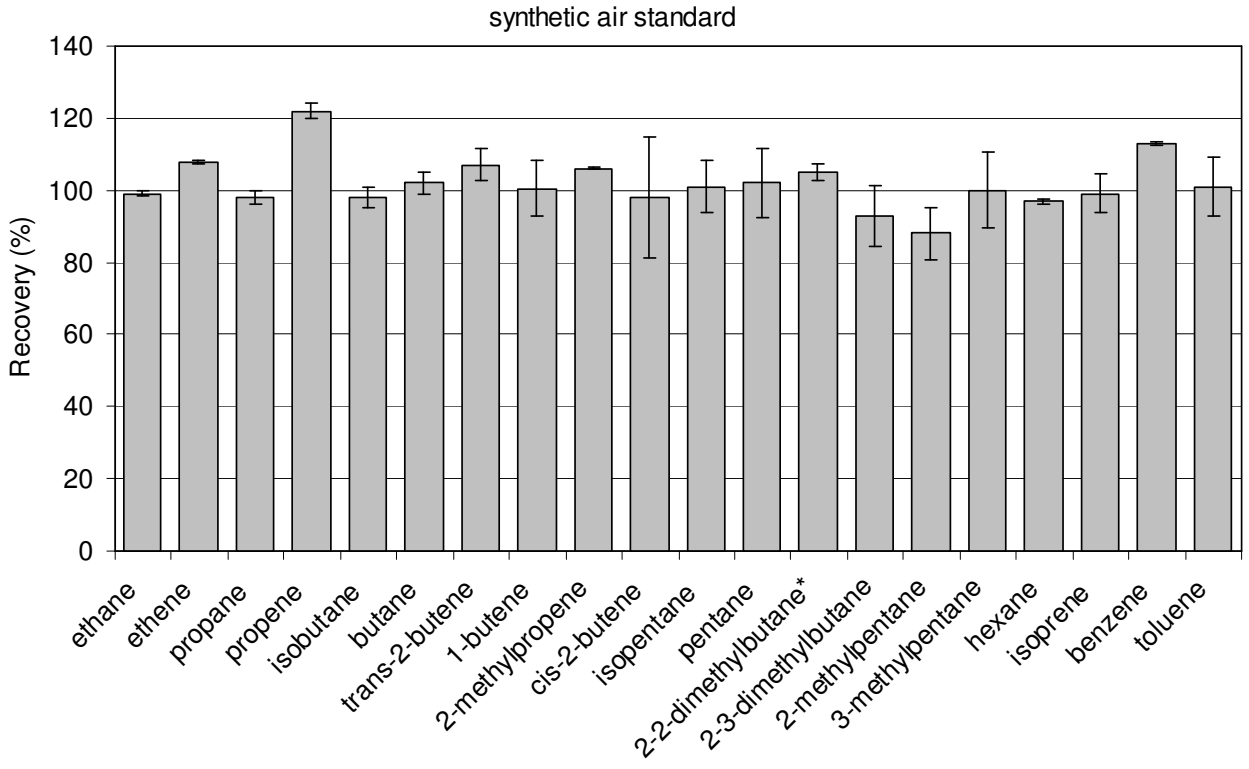

Figure 4.9: Recovery ratios of target compounds in the synthetic air standard when sampled with the PSU and analyzed from the flask referenced to direct sampling from the standard cylinder. Bar graphs show average recovery ratios from the analysis of 6 individual flasks. Error bars represent the overall uncertainty calculated from 6 flask and three standard measurements by propagation of error.

It was striking that the accuracy for hexane was unacceptable in both of the ambient reference gases but better than 5% for the synthetic standard. The mass-spectrometric analyses of the synthetic standard as well as of the 38 halogenated/partially halogenated hydrocarbons standard showed that under our chromatographic conditions hexane was coeluting with dichloromethane (CH_2Cl_2). CH_2Cl_2 has mostly industrial sources. Ambient air

background levels in the northern and southern hemispheric air are approximately 50 pptv and 10 pptv respectively (Simmonds et al., 2006). Background mixing ratios for hexane are expected to be of similar magnitude or lower than CH_2Cl_2. The FID response for CH_2Cl_2 can be estimated to be approximately 70% that of an un-substituted hydrocarbon (Scanion, 1985). Consequently, under typical northern hemispheric background mixing ratios of 10 pptv of hexane and 50 pptv of dichloromethane, co-elution of these peaks will cause a ~60% error (higher concentrations) in the hexane quantification. Given these constraints hexane can not be reliably quantified in air samples from background sites using our instrumental conditions. Separation of the hexane peak could likely be achieved by switching to a different GC column, or alternatively, quantification might be possible by GC-MS detection in single ion mode.

Intercomparison with Hohenpeissenberg: The comparisons of flask data with the in-situ results from Hohenpeissenberg are shown in Figure 4.10 a-j.

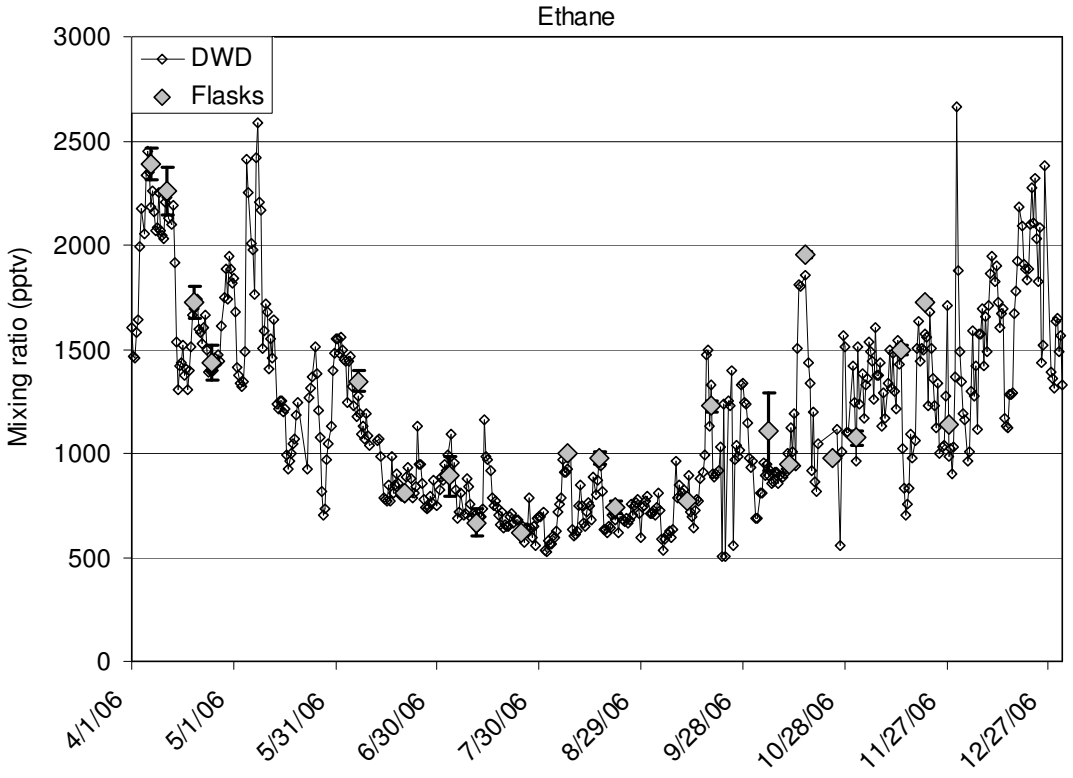

Figure 4.10 a: Legend see Figure 4.10 j

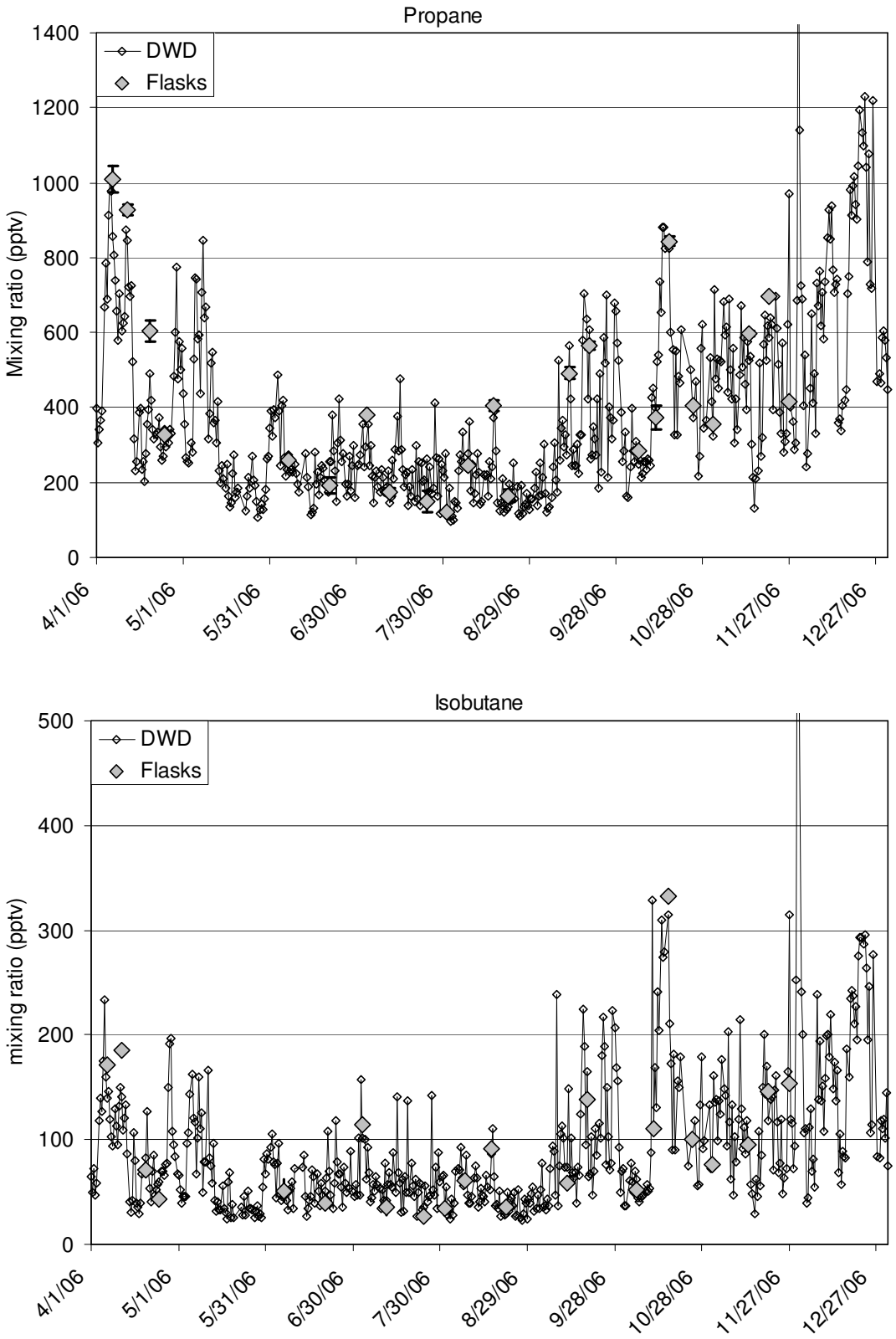

Figures 4.10 b, c: Legend see Figure 4.10 j

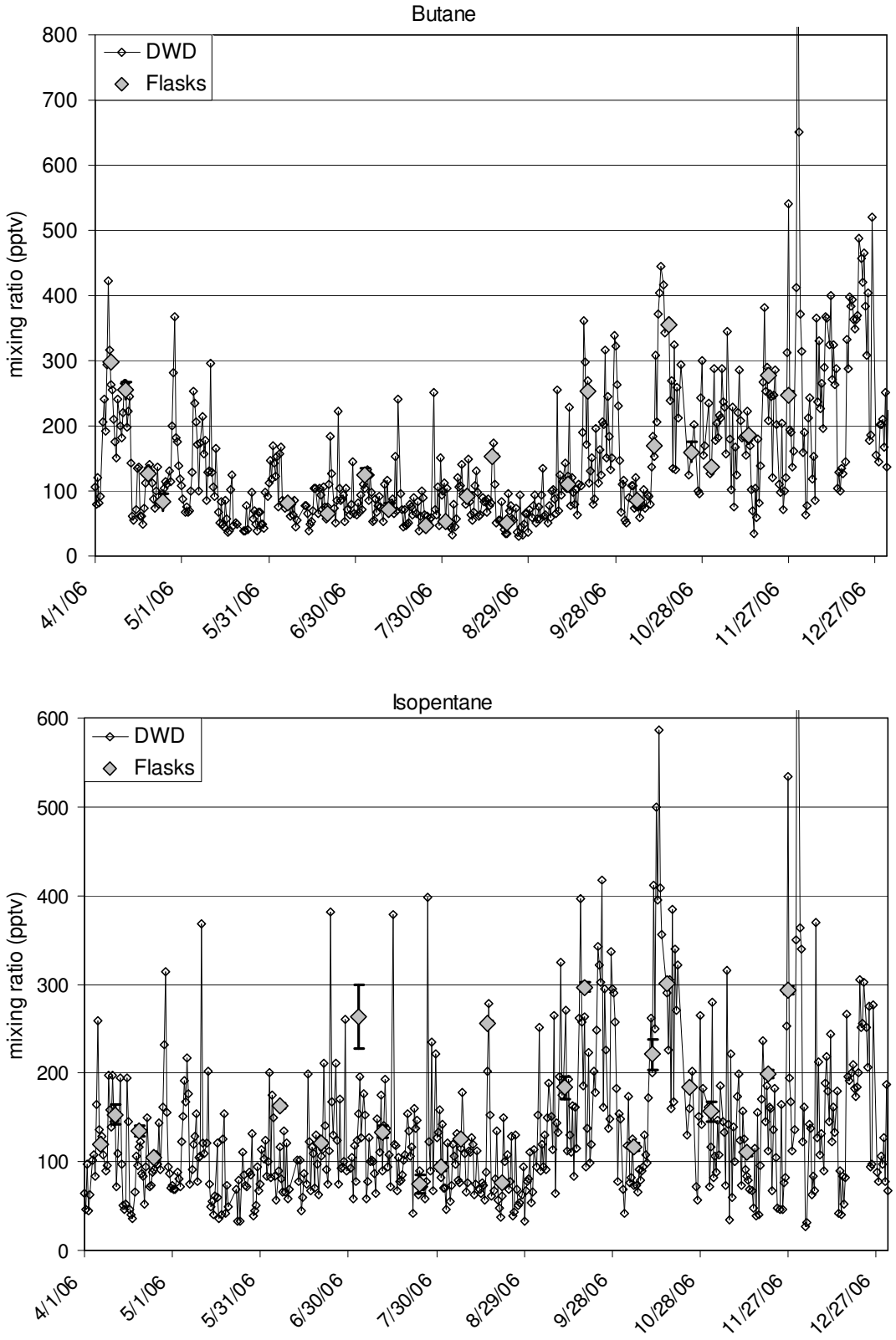

Figures 4.10 d, e: Legend see Figure 4.10 j

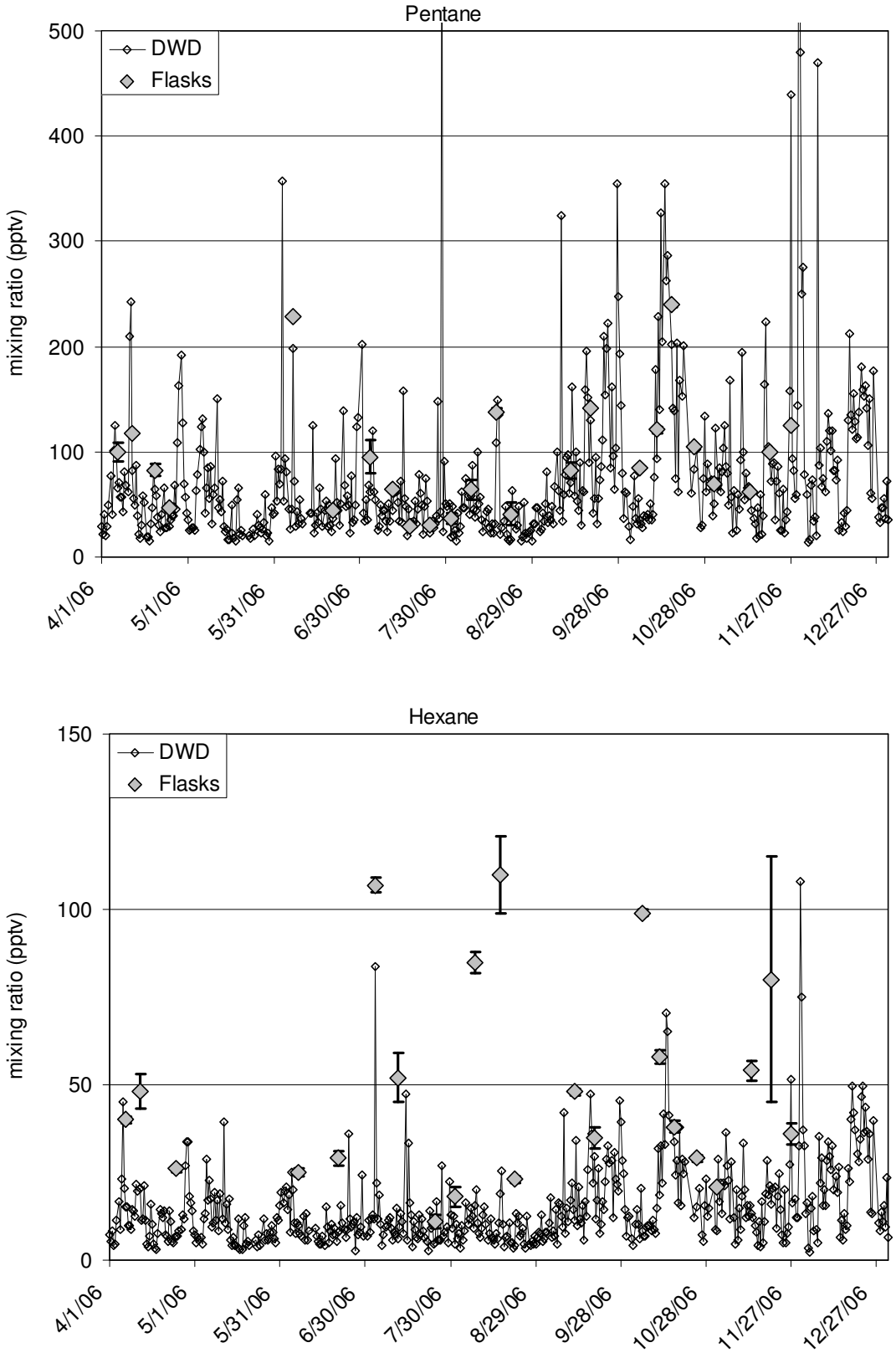

Figure 4.10 f, g: Legend see Figure 4.10 j

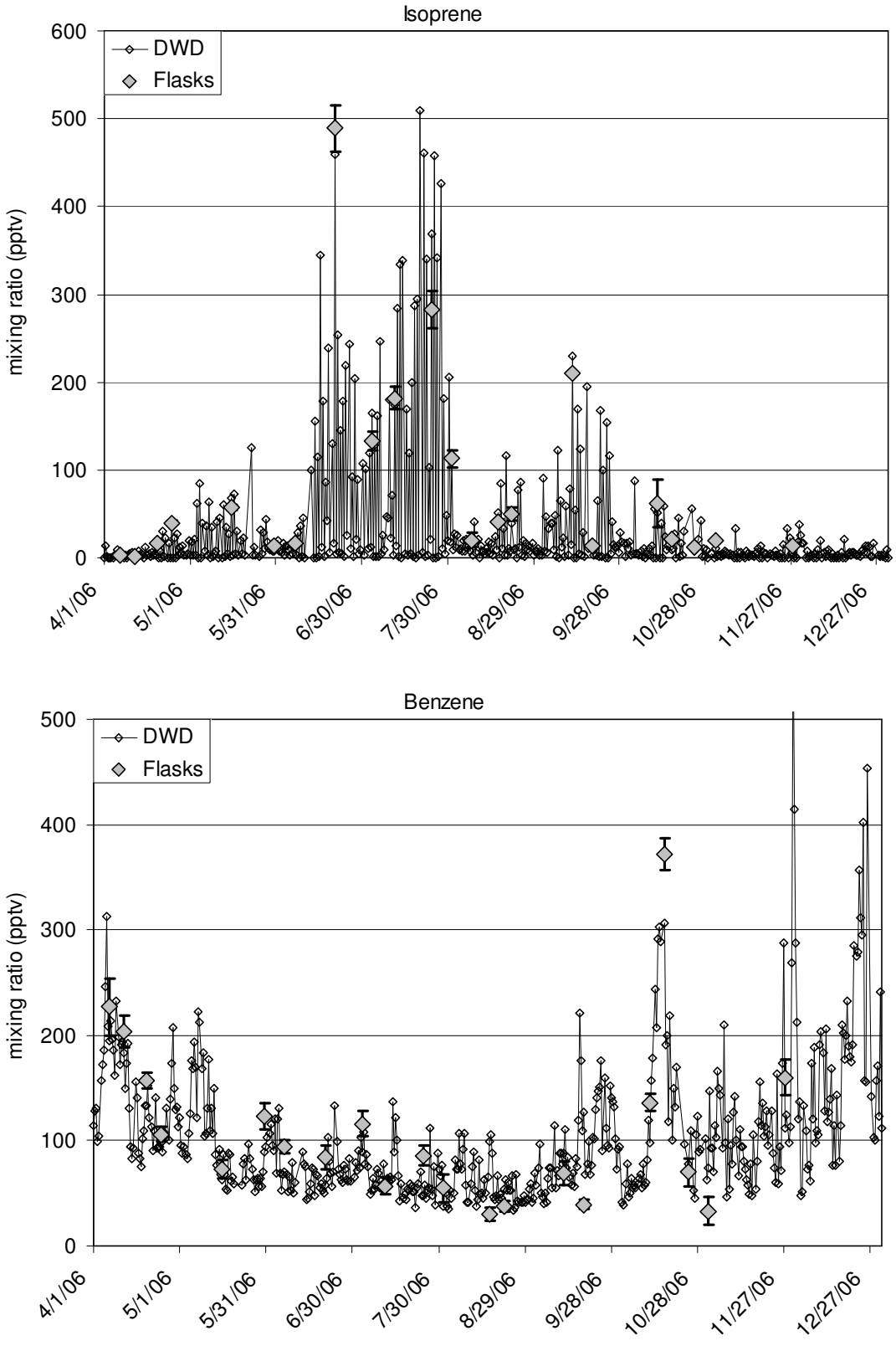

Figure 4.10 h, i: Legend see Figure 4.10 j

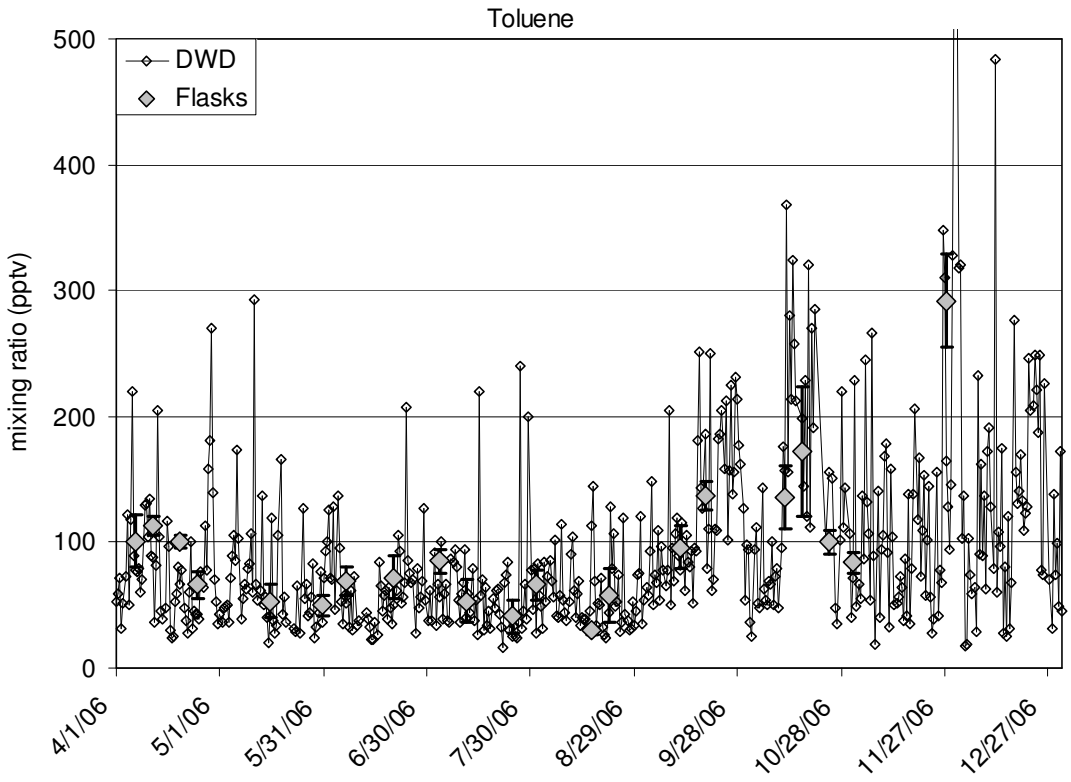

Figures 4.10 j: Comparison of results for ethane (a), propane (b), isobutane (c), butane (d), isopentane (e), pentane (f), hexane (g), isoprene (h), benzene (i) and toluene (j) from the network flasks with the stationary in-situ measurements at the GAW station Hohenpeissenberg during 2006. Flask measurements are shown as large solid symbols and DWD measurements as open, small symbols.

Mixing ratios derived from both methods for saturated C2 to C5 NMHC at levels above 100 pptv typically agree within 5 +/- 2% for ethane, propane and butanes. Pentane differs from the DWD reference measurements on average by 20 +/- 5%.

The agreement below 100 ppt is 10% or better for the remaining butane and isopentane comparison. At these lower levels, pentane values from the flasks are 20 - 30% higher than the in-situ measurements. Flask results for hexane are systematically higher, likely again due to coelution with dichloromethane. Benzene, toluene and isoprene were detected in the flask samples. Their mixing ratios were calculated using an adjusted, average carbon response factor, as mentioned above. A comparison with the reference values shows that the available flask and Hohenpeissenberg data for these compounds deviate by 8 +/- 5% for isoprene, 28 + 13% for benzene, and 39 +/- 19% for toluene.

The overwhelming numbers of available in-situ-flask data comparisons meet the GAW data quality objective (figure 4.11). 96% of the ethane data, 85% of propane data, 96% of iso – and n - butane data as well as 73% of iso and n - pentane data are in agreement with the reference data within the modified data quality objective boundaries of 17% (at levels > 100 pptv) and of 52% (< 100 pptv), respectively. Similarly, 95% of all measurements for isoprene, benzene and toluene are within the quality objective boundaries for accuracy.

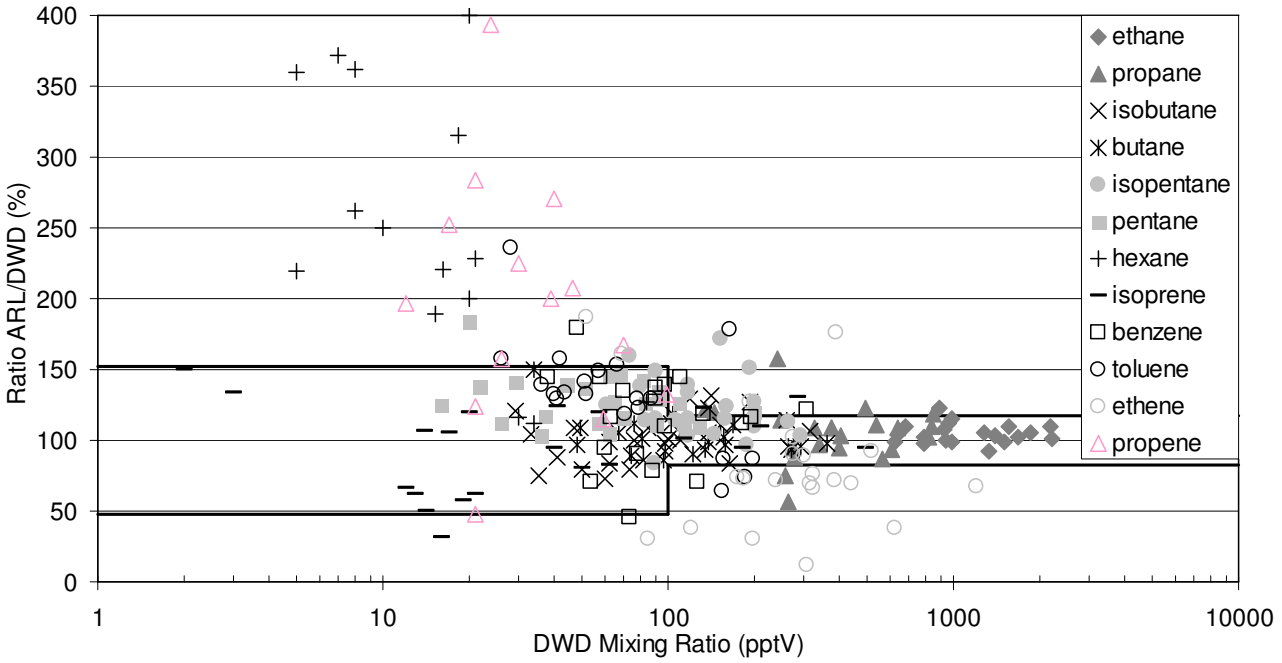

Figure 4.11: Ratio of the results for flask measurements vs. the mixing ratios determined by the in-situ measurements at HP during April-July 2006. Thick black line indicates the boundaries set by the GAW data accuracy quality objective.

Lower agreements were found for ethene and propene measurements, where only 54% and 23% of the comparisons met these requirements. The consistently poorer results for ethene and propene are similar to reported findings in previous studies (Donahue and Prinn, 1993; Ramacher et al., 1997; Rudolph, 1999; Volz-Thomas et al., 2002, Plass-Dülmer et al., 2006).

One possible source of uncertainty and analytical bias in the alkene analysis is due to reaction of these compounds with ozone during the sampling process or during storage.

This effect was investigated by calculating the ratio of the flask results for ethene, propene and isoprene over the in-situ measurement at Hohenpeissenberg and plotting it against the ozone mixing ratio that was recorded at the station during the time of the sample collection (Fig. 11). Expected lifetimes from reaction with ozone at 50 ppbv for these compounds are 10 d for ethene, 0.7 d for propene, and 1 d for isoprene. Since ozone mixing ratios in ambient air typically are much higher than mixing ratios of these unsaturated compounds, complete loss of these analytes would be expected if ozone was not lost during sampling or storage due to other processes. The results in Fig. 11 show no systematic change (decrease) of the isoprene or ethene mixing ratio as a function of increasing ozone; obviously these compounds can be analyzed without any interference from ozone. In contrast, the ratio of propene appears to increase with increasing ozone, indicating a potential generation of propene with increasing ozone. The fact that isoprene does not appear to show a sensitivity towards ozone levels implies that most ozone is rapidly removed during the sampling process or inside the flasks. However, no conclusive cause was found for the increase in propene found in the flask analysis.

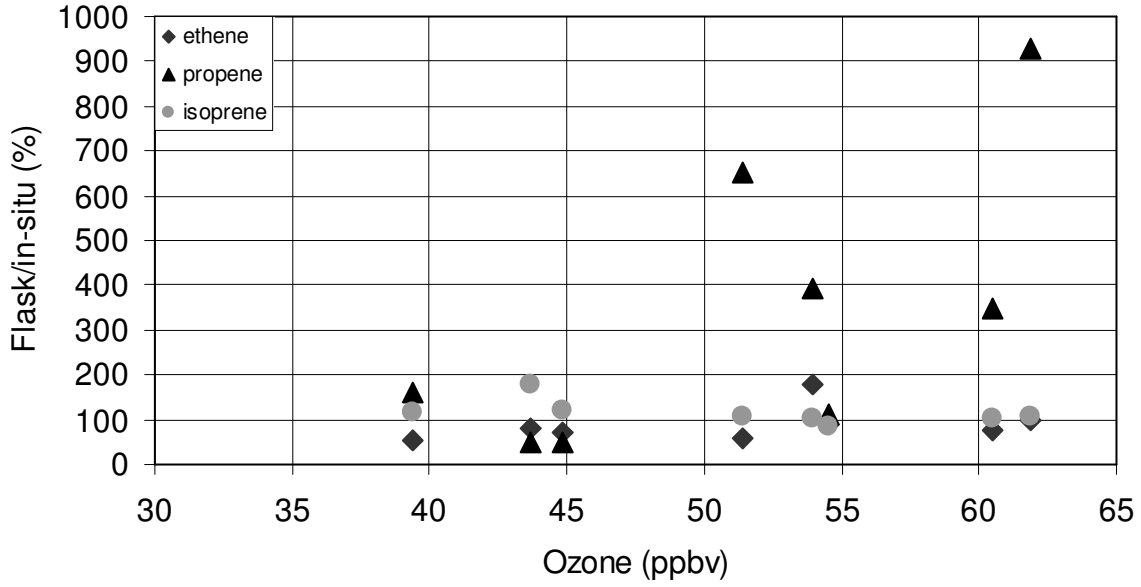

Figure 4.12: Ratios (ARL/DWD) of mixing ratios determined in a pair of flask samples (shown data are the means of n=2 flask/in-situ (n=1) versus the on-line results for quantified unsaturated NMHC as a function of the ambient air ozone mixing ratio during the sample collection period.

Measurement precision: The results for the repeatability analysis are shown in Figure 4.13 a-g which includes all available data from dual flask sampling and the data from laboratory experiments detailed above. As expected, results for repeatability from the direct measurements of reference gases and standards from the gas cylinders generally exhibited the best precision. Here, a median repeatability for NMHC measurements of less than 3% was found. This precision deteriorates from variability and errors introduced in the sampling process, storing and shipping of samples, analyses steps prior to the NMHC quantification. The data for the laboratory experiments that included the filling of and sample retrieval from flasks resulted in median relative precision results of better than 3%.

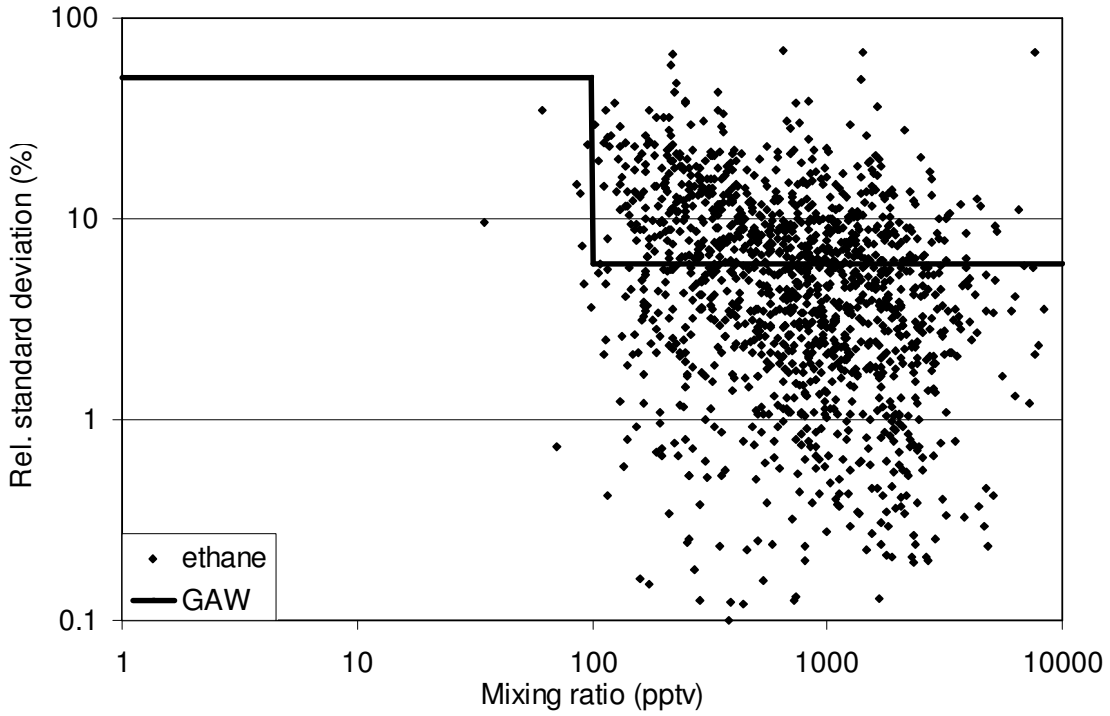

Figure 4.13 a: Legend see Figure 4.13 g

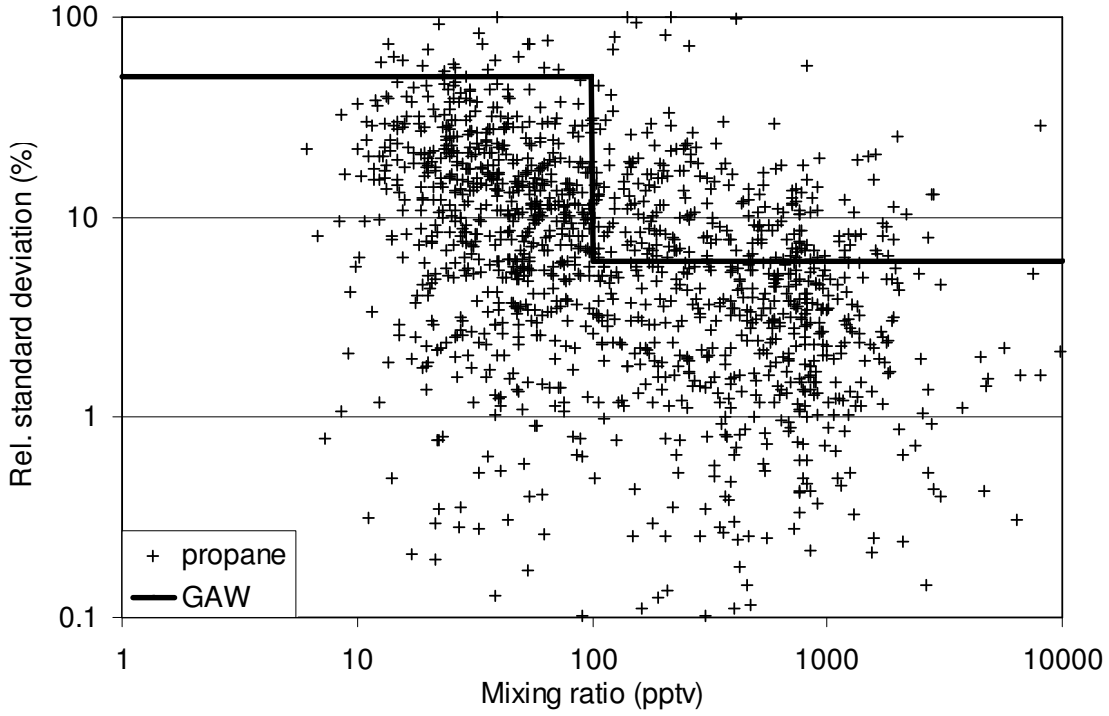

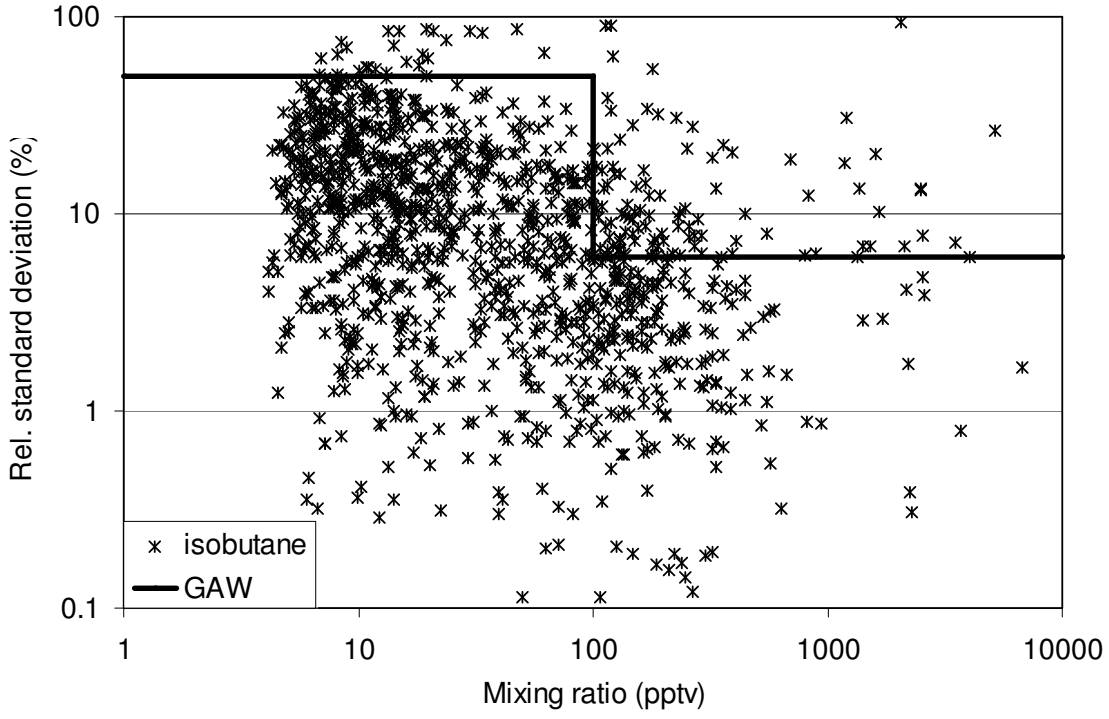

Figure 4.13 c, d: Legend see Figure 4.13 g

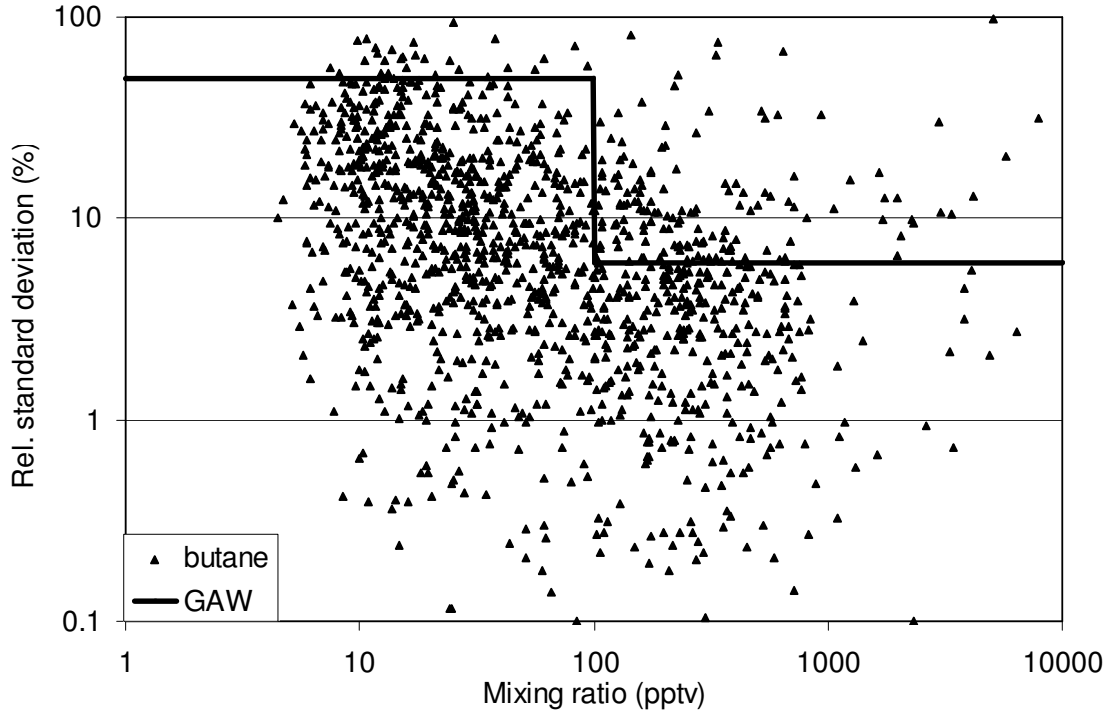

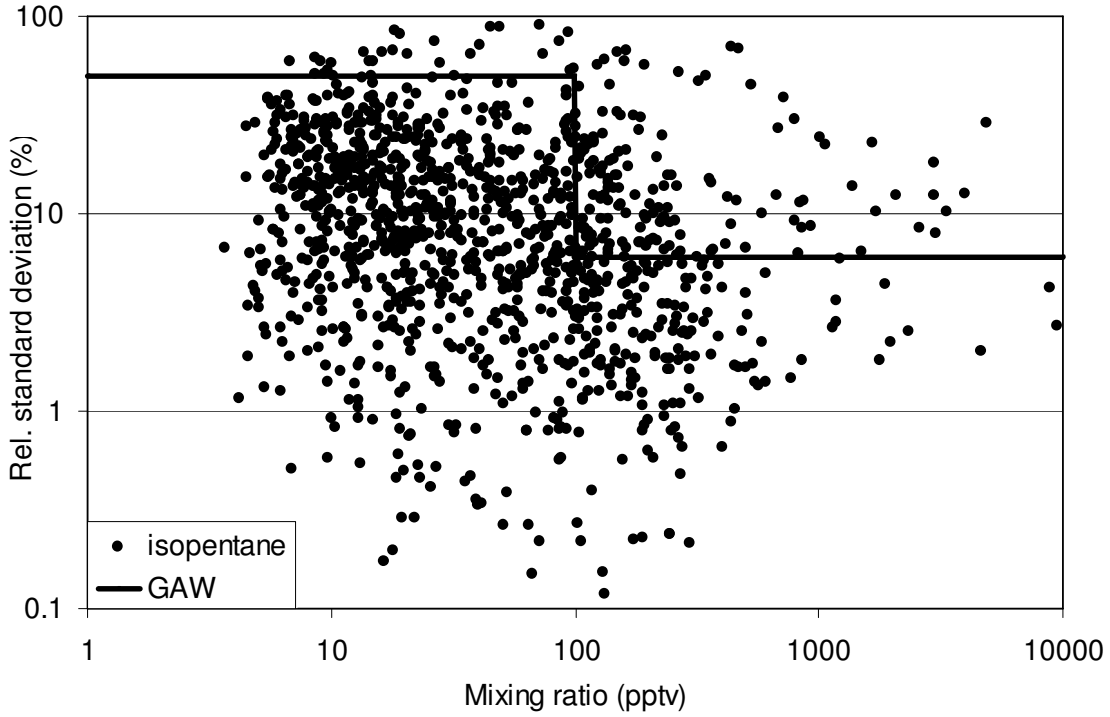

Figure 4.13 e, f: Legend see Figure 4.13 g

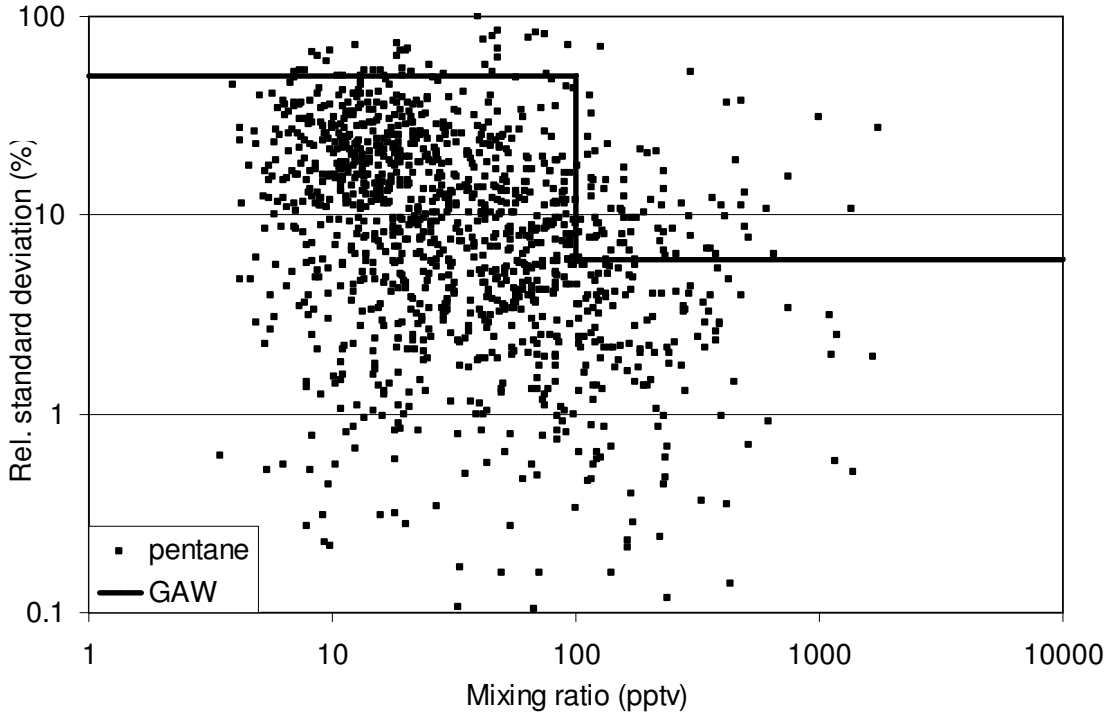

Figure 4.13 g: Measurement precision as function of mixing ratio for ethane (a), propane (b), isobutane (c), butane (d), isopentane (e), pentane (f) from analysis of pairs of flasks from network sites. Solid black line indicated GAW data quality objective for precision (5%, > 100 pptv; 50%, < 100 pptv).

Much wider mixing ratio range and much more variable sampling and handling conditions are expected for the network flask samples. The data from these analyses shown in Figure 4.13 a-f illustrates how the relative precision of the analyses improves with increasing mixing ratio, indicating a larger contribution of analytical errors at lower concentrations. Most of these data show a repeatability of 0-5% above 100 pptv, and approximately 0-10% below 100 pptv. These graphs also include the GAW quality criteria for repeatability. Most results for C3-C5 NMHC measurements meet the GAW data quality guideline for precision (5% above 100 pptv, 50% below 100 pptv): 85 % (propane), 93 % (isobutane), 91 % (butane), 96% (isopentane), 97% (pentane).

Results for ethane are somewhat worse, as only 71% of the flask measurements meet the data quality guideline. However the median precision for ethane measurements was 5%. It can be seen in figure 12a that the relative standard deviation rarely exceeded 10%. A contributing factor to the loss of some precision in the ethane analysis is probably

the more difficult peak integration, as ethane is the earliest eluting peak on the GC-column, in close proximity to the injection peak.

4.5 Conclusions

These experiments define conditions and possibilities for NMHC monitoring using glass flasks, which are the primary sample collection vessels in some of the most extensive regional and global air monitoring networks, such as the ESRL cooperative air sampling network. Saturated NMHC are stable in glass flasks for at least one year. Atmospheric water vapor remains in the gas phase, can consequently be completely extracted from the sampling flasks and therefore needs to be removed prior to the focussing of NMHC by solid adsorption preconcentration. NMHC recoveries from the flasks are not very sensitive towards the sample pressure, which allows quality analysis of NMHC in the remaining sample after completion of several other analytical steps with sample extraction prior to the NMHC quantification.

Extensive tests on the accuracy and precision of this analysis demonstrated that overall more than 90% of results for saturated C2-C5 NMHC, isoprene, benzene and toluene (standard cylinders and flasks) meet the WMO VOC data quality guideline. Hexane was found to coelude with dichloromethane and could not be quantified at the required accuracy. Co-sampling of ozone was found to have a negligible effect on the recovery of ethene and isoprene, which hints towards to fast removal of ozone during the sampling process or during storage in the flasks. Ethene and propene exhibited a series of analytical problems which could not be fully explained and resolved within this study. Our data suggests that these compounds can not be quantified using the tested procedures and materials at background levels with the desired precision and accuracy.

The findings of these experiments demonstrate the feasibility to study regional and global distributions of most C2-C7 NMHC and their atmospheric chemistry using infrastructure and sampling protocols within existing and operational glass flask sampling programs.

4.6 Acknowledgements

D. Tanner (INSTAAR, University of Colorado, Boulder) helped with the instrumental design and construction. P. Goldan (ESRL, Chemical Science Division, Boulder, CO, USA) provided reference analysis of NMHC standards and E. Apel (NCAR, Boulder, CO, USA) made available the synthetic air standard.

5 Global NMHC Measurements from the NOAA – ESRL Cooperative Air Sampling Network: Observations and Assessment of OH Concentrations by Variability Analysis

Abstract

Non-methane hydrocarbons were measured from whole air flask samples provided by the ESRL cooperative air sampling network. Between March 2005 and December 2006 more than 1700 samples (3400 flasks) were analyzed from 37 sites spanning from 82 °N to 90 °S. Global distributions of the NMHCs (non-methane hydrocarbons): ethane, propane, butane and isobutane over these 1.5 years yield insights in the atmospheric budgets of these species. Maximum background mixing ratios in the northern (and southern) troposphere were 2500 pptv ethane, (500 pptv), 1000 pptv propane, (50 pptv) and 350 pptv butane (15 pptv) respectively. Northern hemispheric winter mixing ratios were higher than summer mixing ratios by a factor of 2.5 (ethane), 10 (propane) and 20 (butanes) resulting in sharp concentration changes during spring and fall. The NMHC data were combined with measurements of other atmospheric trace gases made from the flasks (carbon monoxide, methane, hydrogen and sulfurhexafluoride) to analyze the atmospheric variability - lifetime relationship. All stations exhibited a strong variability lifetime dependence confirming that the sites are not significantly influenced by local pollution. Furthermore this variability-lifetime relationship was used to estimate an effective OH concentration for each site. The derived hemispheric winter and summer average OH was: NH (20°N to 90°N) summer: 11.4 10^5 molec cm^{-3}, winter: 6.8 10^5 molec cm^{-3}; SH (20°S-90°S) summer: 4.5 molec cm^{-3}, winter 3.2 10^5 molec cm^{-3} respectively. The tropical (20°N-20°S) OH mixing ratio was not found to be subject to seasonal changes and the 24h average was calculated to be: 40 10^5 molec cm^{-3}. The derived OH values are in good agreement with the available direct measurements and generally agree with the global OH distribution of Spivakovsky et al., 2000. However, OH mixing ratios derived from variability analysis seem to be systematically higher in the tropics than found in Spivakovsky et al., 2000.

The results presented in this chapter are in preparation for submission to Journal of Geophysical Research (NMHC distribution) with D. Helmig, J. Hueber, P. Tans as co-authors and Atmospheric Chemistry and Physics Discussions (variability analysis, OH Distribution) with J. Williams, D. Helmig, J. Hueber, P. Tans and J. Lelieveld as co-authors.

5.1 Introduction

General motivation: Knowledge of the global distribution of non-methane hydrocarbons is essential to the understanding of atmospheric processes such as transport, radical chemistry and photooxidation (Williams, 2004 and references therein). Recent studies have indicated that a global NMHC measurement network with high spatial and temporal resolution (WMO Report, 1995, Krol and Lelieveld, 2003) is necessary to assess these processes. In-situ instruments are now routinely operated at several sites providing NMHC data with high temporal resolution (e.g.: Plass-Dülmer et al., 2002, Tanner et al., 2006), however, measurements with high spatial resolution are currently lacking, in particular on a global scale.

In this study we present results from a GC-FID (gas chromatography – flame ionization detection) instrument for the analysis of NMHC from whole air sampling flasks supplied by the ESRL – GMD cooperative air sampling network (Tanner et al., 2006, Pollmann et al., 2006, 2007). The observations shown here are from the first 20 months of this project. We show that these measurements can provide global distributions of NMHC as a function of time and latitude. The data was further exploited to derive insights into the distribution of OH, the primary sink for NMHC in the atmosphere.

NMHC and OH: Detailed knowledge of the NMHC mixing ratios in an air sample can provide information on the type of sources and the photochemistry impacting the site where the sample was taken. The characteristics of anthropogenic NMHC emission sources to the atmosphere from traffic or fossil fuel production have been identified previously (e.g.: Blake et al., 1992, Goldan et al., 1997, Parrish et al., 1998, Cardenas et al., 1998, Christensen et al., 1999, Derwent et al., 2000, Borbon et al., 2003, 2004). Distinct NMHC emissions from biomass burning episodes have also been identified and characterized, e.g. acetylene, ethane and methylchloride (Blake et al., 1996, Singh et al., 2000). In contrast, biogenic NMHCs are commonly emitted in an unsaturated form for example as ethene, isoprene or monoterpenes from the terrestrial biosphere and the oceans (e.g. Plass et al., 1993, Guenther et al., 1999, Velasco, 2003, Sinha et al., 2007). A detailed analysis of

NMHCs can therefore reveal the source structure and the atmospheric history of an air sample.

The global distribution of NMHC has been reported previously to exhibit a large north - south gradient with a distinct seasonal cycle (e.g. Rudolph, 1995, Bonsang and Boissard, 1999, Blake et al., 2003, Gautrois et al., 2003). The highest NMHC mixing ratios were found in the mid northern latitudes (30 – 60 °N) reflecting the global energy consumption and population density. Maximum NMHC concentrations in the remote northern troposphere were up to 2500 pptv (ethane) and 1000 pptv (propane) during February and minimum mixing ratios were 1000 pptv and 70 pptv respectively during late summer (August) (e.g. Blake et al., 2003, Hakola et al., 2006). NMHC mixing ratio trends in the southern hemisphere were seasonally inversed in comparison to the northern hemisphere and at much lower levels: ethane: 142 pptv, propane: 9 pptv, isobutane: 6 pptv, butane: 10 pptv (Cape Grim, Tasmania, Australia, Lewis et al., 2001).

Gautrois et al., 2003 reported a declining trend in NMHC mixing ratios from 1989 to 1997 for most NMHCs in the high northern troposphere (Alert, Canada, 82.45°N, 62.52°W). In contrast, Hakola et al., 2006 did not observe significant trends during 10 years of continuous NMHC measurements in Finland. However, European emissions were shown to have declined since the 1980s and this should eventually be reflected by reduced NMHC concentrations in the high northern troposphere (Solberg et al., 2005).

The main sink for atmospheric NMHC is the reaction with the hydroxyl radical (OH) (Levy, 1972, Logan, 1981) and significant seasonal changes to the emission strengths of the NMHC sources were not expected on the global scale (Goldstein et al., 1995, Swanson et al., 2003). Therefore the NMHC seasonality at background stations is dominated by the seasonal cycle of OH (Goldstein et al., 1995). The atmospheric concentration of OH in remote regions is directly correlated to solar ultraviolet radiation, ozone and water vapor concentration (Rohrer and Berresheim, 2006). The estimated global average OH mixing ratio of 10^6 molec cm^{-3} has been mostly determined from model calculations using the measured removal of methylchloroform (CH_3CCl_3) from the atmosphere (Prinn et al., 1995, Prinn, 2003, Krol et al., 1998, 2003, Spivakovsky, 2000). Direct measurement methods for the hydroxyl radical are very elaborate (e.g. Eisele et al., 2001, Heard and Pilling, 2003, Mauldin et al., 2004) due to its high reactivity (atmospheric lifetime ~ 1 s). Consequently

these direct OH measurements are only available for short periods of time during intensive field campaigns, except for a single long term study conducted by Rohrer and Berresheim, 2006. A summary of OH mixing ratios obtained from direct measurements during various field campaigns at remote surface stations can be found in Table 5.1.

Table 5.1: Summary of previous direct OH measurements sorted from north to south

Site (latitude, longitude, elevation)	date	analytical technique	24 h average OH mixing ratio (10^5 molec cm^{-3})	Reference
Pennewitt, Germany (53.8°N, 11.7°E, 54 m asl)	Aug 1994	DOAS/LIF	8.7	Plass-Dülmer et al., 1998
Mace Head Ireland (53.33°N, 9.90°W, 25 m asl)	Summer 2002	FAGE	9.1	Smith et al., 2006
Weybourne, UK (53.57°N, 1.07°E, 25 m asl)	Jun 1995	MOAS	n/a	Forberich et al., 1999
Hohenpeissenberg, Germany (47.80°N, 11.01°E, 985 m asl)	June 18-21 2000	CIMS	20	Handisides et al., 2003
Hohenpeissenberg, Germany (47.80°N, 11.01°E, 985 m asl)	1999-2003	CIMS	12.3	Rohrer et al., 2006
Michigan (45.6°N, 84.7°W 230 m asl)	Summer 1998	FAGE	18	Tan et al., 2001b
Whiteface Mountain, NY, USA (44.23°N, 73.51°W, 1483 m asl)	Summer 2002	FAGE	8	Ren et al., 2006
Rock Springs, PA. USA (40.5°N, 77.5°W, 365 m asl)	May - June 2002	FAGE	26	Ren et al., 2005
Fritz Peak, CO, USA (40°N, 105°W, 2680 m asl)	Aug - Oct 1993	long-path spectroscopy	8	Mount et al., 1997
Agrafe Mountains, Greece (39.54°N, 21.44°E, 1180 m asl)	Jul 26 - Aug 2 1997	FAGE	13	Creasey et al., 2001
Finokalia, Crete (35.20°N, 25.40°S, 150 m asl)	Aug 6 - Aug 18 2001	SICIMS	45	Berresheim et al., 2003
Claremont, CA, USA (34.06°N, 117.43°W, m asl)	Sep - 1993	FAGE	20	George et al., 1999
Izaña, Tenerife(28.18°N, 16.30°W, 2370 m asl)	May - 1995	MOAS	20	Armerding et al., 1997
Okinawa Island (26.88°N, 128.25°E, 60 m asl)	Aug - 1999	LIF	<25	Kanaya et al., 2001
Atlantic ship campaign (15°N to 15°S)	Oct 23 - Nov 2 1996	DOAS	50	Brauers et al., 2001
Tropical Pacific (PEM Tropics B)	Mar - Apr 1999	FAGE	30	Tan et al., 2001a
Cape Grim, Australia (40.68°S, 144.68°E, 94 m asl)	Feb - 1999	FAGE	10	Creasey et al., 2003
Palmer Station, Antartica (64.92°S, 64.00°E, 10 m asl)	Feb 16 - 23 1994	SICIMS	1.1	Jefferson et al., 1998
South Pole (90° S, n/a, 2810 m asl)	Nov 15 - Dec 31 2000	SICIMS	25	Mauldin et al., 2004

Variability Analysis: Junge, 1974 first described the correlation between atmospheric variability and the lifetime of trace gases. This approach was later refined by Jobson et al., 1998, 1999 and extended to shorter lived species. Atmospheric trace gases were correlated to atmospheric lifetime according to:

$$\sigma (\ln x) = A \tau^{-b} \qquad \text{eq. 1.5}$$

Only a brief explanation of the variables is given here since this equation was evaluated and applied multiple times in previous publications (Jobson et al., 1998, 1999, Ehhalt et al., 1998, Williams et al., 2000, 2001, 2002, Karl et al., 2001) with *A*, proportionality factor; *b*, usually interpreted as an indicator of the relative strength of the chemical sink with values between 0 and 1, σ (lnx): standard deviation over the natural logarithms of all measurements; τ: atmospheric lifetime.

A low *b* factor (i.e. no correlation between atmospheric variability and lifetime) indicates a nearby anthropogenic source and a negligible influence of chemistry on the

sample set. b = 0.5 has been found for samples from remote tropospheric surface stations while b = 1 is only found for stratospheric samples (Ehhalt et al., 1998, Jobson et al., 1999, Williams et al., 2001). Recently this method was used to estimate the average OH mixing ratio that a sample was exposed to before reaching the measurement station. These studies were within 50% or better of model calculations and direct measurements of OH mixing ratio (Williams et al., 2001, Karl et al., 2001, Bartenbach et al., 2007).

In contrast to the relatively well understood meaning of the b factor, no satisfactory definition of the A factor has been found (Jobson et al., 1998). Previous studies interpreted this factor as an indicator for the age range of the sampled airmass (Williams et al., 2001). High values indicate a large age range (i.e. both fresh emissions and aged air were sampled) whereas smaller values are a sign for a more homogeneous age range of the sampled airmasses. Consequently, high A factors are expected for stations that are occasionally affected by additional sources, or highly variable OH mixing ratios during transport as found in the high northern and southern latitudes. Tropic samples would exhibit low A factors representing more homogenous source distribution as well as rather constant OH mixing ratios and meteorology conditions.

The ESRL canister sampling network: The previous paragraphs describe the amount of information that can be gained by knowing the global distribution of NMHC e.g.: for the evaluation of OH oxidation chemistry. We concluded that an economical and efficient way to access this information was to measure NMHC mixing ratios from flask samples collected by an existing air sampling network (here: the ESRL cooperative air sampling network, Pollmann et al., 2006, 2007). Additional benefits arise from the application of one single instrument over multiple in-situ instruments. The measurements can be readily compared without accounting for instrumental differences.

The ESRL cooperative air sampling network was designed to analyze the global distribution of the greenhouse gases: carbon dioxide (CO_2), methane (CH_4), nitrous oxide (N_2O) and sulfurhexafluoride (SF_6) as well as the distribution of other important atmospheric trace gases such as carbon monoxide (CO), and hydrogen (H_2) (Conway et al., 1994 and Dlugokencky et al., 1994). The network consists currently of 69 surface sampling stations, and several aircraft and tower measurement sites from where canisters

or flasks are filled with air (http://www.esrl.ESRL.gov/gmd/ccgg/index.html). The isotopic composition of carbon dioxide and methane are measured from these flasks by mass spectrometric techniques in order to examine the global carbon cycle (Trolier et al., 1996). Distribution data for gases with atmospheric lifetimes ranging from several thousand years (SF_6, Maiss, 1998) to one day (ethene (C_2H_4), Atkinson, 1994) are now available from the same whole air sample with the implementation of the NMHC measurements. This data can provide unique insight into global atmospheric transport and chemistry processes. Moreover, the NMHC data may be used as a data quality check for individual samples, and to ensure the sample is not influenced by local sources. Parrish et al., 1992 presented a method to evaluate an air sample with respect to atmospheric age, photochemistry and transport kinetics based on the quantification of ethane, propane and butane. This was applied to the dataset.

Summary: These previous studies show that a good knowledge of the atmospheric distribution of NMHC is necessary to evaluate and understand important atmospheric processes such as transport and photooxidation (Krol and Lelieveld, 2003). The global distribution of the hydroxyl radical is still rather uncertain and our understanding of the atmospheric oxidative capacity is limited. The trace gas measurements from the ESRL cooperative flask sampling network provide a, to date, unique tool to evaluate the photooxidation chemistry and trace gas sources on a global scale In this paper we present our observations from 20 months of ethane, propane, isobutane and butane measurements from the cooperative flask network and their application together with isopentane, pentane and stable greenhouse gas measurements in the variability analysis to deduce the global OH distribution.

5.2 Experimental

Instrument: Detailed descriptions of all technical aspects and calibration procedures have been provided elsewhere (Tanner et al., 2006 and Pollmann et al., 2006, 2007 see also chapters 2, 4). Only a brief overview is given here. The system relies on a solid adsorption/ thermodesorption technique for sample pre-concentration. An air sample is extracted from

the flasks, dried with thermoelectric coolers and preconcentrated on a custom-built microtrap filled with 100 mg Carboxen 1000 and 5 mg Carboxen 1016 which is thermoelectrically cooled to –30 ºC. The trap is then purged with carrier gas (H_2) to remove residual oxygen, and heated resistively to 310 ºC within 3 s. Desorbed analytes are injected onto an Al_2O_3 - KCl deactivated PLOT-column (porous layer open tubular, length: 50 m, I.D: 0.53 mm, 19095P-K23, Agilent, Wilmigton, DE, USA). Analytes are identified by retention indexes and quantified by FID (flame ionization detection). Peak identification was confirmed by splitting the column flow and analyzing a portion of the GC eluent by mass spectrometry.

An automated inlet manifold with 12 flask and 2 standard ports was designed to connect the sampling flasks to this GC-system. The manifold was custom-welded (MKS, Boulder, CO, USA) using 1/8“ stainless steel tubing and Swagelok (Solon, OH, USA) welding components (6 union crosses: 316L-4-ATW-4 and 1 union tee: 316L-4-ATW3). The connection between the valve manifold and the sampling flasks was established with VCR to 1/4” tube bulkhead fittings (316L-4-VCR-61-4TB7, Swagelok) and flask adapters (SS-8-UT-6-4, Swagelok). Each flask can be individually accessed from the manifold using pneumatically controlled shut-off valves (6LV-BNBW4-C, Swagelok). The entire system is completely automated and computer-controlled using LabView software (National Instruments, Austin, TX, USA). Analysis of a series of up to 12 flasks is always bracketed by one standard and one zero air run each to maintain high confidence in blanks and calibration stability (Pollmann et al., 2007). Intercomparison with a stationary in-situ instrument (Hohenpeissenberg, Plass Dülmer et al., 2002) proved that this instrument meets the GAW data quality guidelines (Rappenglück et al., 2006, WMO-Report 171, Pollmann et al., 2007).

Evaluation of individual stations: Figures 5.1 a, b and 5.2 a, b show example time series for C2 to C4 NMHC compounds from flask measurements taken at two remote sites 1) Cold Bay, Alaska, USA 55.12°N, 162.42°W and 2) Crozet Island, French Territory, 46.45°S, 51.85°W. Time series with similar data density as these example stations are available for 33 of the 37 NMHC sampling stations (see Table 5.2). Measurements from 4 stations were considered too intermittent and were not regarded (AZR, OXK, TDF, SYO).

Table 5.2: NMHC flask sampling stations in alphabetic order by station code; station, station name; code, site code for network operation; latitude, north: positive, south: negative; longitude: east positive, west negative; altitude, elevation above sea level; NMHC sampling since, first flask sample analyzed for NMHC from the respective site

station	code	latitude	longitude	altitude (m)	NMHC sampling since
Alert, Canada	ALT	82.45	-62.52	210	09/2005
Argyle, MI, USA	AMT	45.03	-68.88	157	11/2005
Ascension Island	ASC	-7.92	-14.42	54	04/2005
Assekrem, Algeria	ASK	23.18	5.42	2728	02/2006
Azores	ARZ	38.77	-27.38	40	02/2005
Baltic Sea, Poland	BAL	55.35	17.22	28	02/2005
Bukit Kototabang, Indonesia	BKT	-0.20	100.32	864	01/2006
Barrow, AK, USA	BRW	71.32	-156.60	11	05/2005
Black Sea, Romania	BSC	44.17	28.68	3	10/2005
Cold Bay, AK, USA	CBA	55.12	162.42	25	05/2005
Cape Grim, Australia	CGO	-40.68	144.68	94	12/2004
Crozet Island	CRZ	-46.45	51.85	120	03/2005
Guam Island	GMI	13.43	144.78	6	06/2005
Halley Station, Antarctica	HBA	-75.58	-26.50	33	02/2005
Hohenpeissenberg, Germany	HPB^{+}	47.80	11.01	990	04/2006
Vestmannaeyjar, Iceland	ICE	63.34	-20.29	127	10/2005
Izana, Tennerife	IZO	28.30	-16.48	2360	12/2005
Cape Kumukahi, HI, USA	KUM	19.52	-154.82	3	05/2005
Park Falls, WI, USA	LEF	45.93	-90.27	868	09/2005
Mace Head, Ireland	MHD	53.33	-9.90	25	03/2005
Midway Island	MID	28.21	-177.38	8	02/2006
Mount Kenya, Kenya	MKN	-0.05	37.30	3897	02/2006
Mauna Loa, HI, USA	MLO^{+}	19.54	-155.58	3397	05/2005
Ochsenkopf, Germany	OXK^{+}	50.06	11.80	1356	07/2006
Pallas, Finland	PAL	67.97	24.12	560	01/2006
Palmer Station, Antarctica	PSA	-64.92	64.00	10	09/2005
Seychelles Island	SEY	-4.67	55.17	7	02/2005
Southern Great Plains, OK, USA	SGP	36.80	-97.50	374	11/2005
Shemya, AK, USA	SHM^{+}	52.72	174.10	40	04/2005
America Samoa	SMO	-14.24	-170.57	42	05/2005
Amundsen Scott Station, Antarctica	SPO	-89.98	24.80	2810	01/2005
Summit, Greenland	SUM	72.58	-38.48	3238	10/2004
Syowa Station, Antarctica	SYO*	-69.00	39.58	14	02/2005
Tierra del Fuego, Argentina	TDF*	-54.87	-68.48	20	10/2004
Trinidad Head, CA, USA	THD	41.05	-124.15	107	05/2005
Wendover, UT, USA	UTA	39.90	-113.72	1628	11/2005
Ny Alesund, Norway	ZEP	78.90	11.88	1320	10/2005

One of the purposes of this study was to determine the global background distribution of light NMHC. Stations that were significantly influenced by local emissions thus had to be removed. Sampling stations were considered to be systematically influenced by local sources when 20% of the ethane data exceeded the seasonal average for this latitudinal region by a factor of 2, or if 20% were outside the photochemically expected range as detailed by Parrish et al., 1992 and Tanner et al., 2006, similarly figure 5.3.

Five northern hemispheric continental measurement stations were excluded on this basis (AMT, BAL, BSC, LEF, and SGP). The NMHC time series from 28 of the remaining 33 stations were available to generate 3-D global background distribution plots for C2 to C4 NMHC. Nonetheless, occasional local pollution may still affect individual sampling stations and could bias this analysis. Similar plots as presented for the example stations in Figure 5.3 a, b were used to filter for individual data points that were subject to stochastic local influence i.e. outside the kinetic and photochemical boundaries. Any data points outside the boundaries were not regarded for this analysis. In total not more than 5% of the measurements for each individual station were subject to such local pollution events and hence disregarded. Measurements not meeting the GAW data quality objective for precision (Rappenglück et al., 2006, WMO report, 2006) based on the dual flask analysis were also removed from the raw data for the 3D plots.

The remaining NMHC data (~ 93%) was processed with IDL 6.2 software (ITT Visual Information Solutions, Boulder, CO, USA). The measurement results were fitted linearly in a 3D grid from Julian day 70 (March 10, 2005) to Julian day 600 (August 25, 2006) and modified with the standard IDL smoothing algorithm.

Variability Analysis: Mixing ratios for eleven species (7 NMHC: ethane, propane, isobutane, butane, isopentane, and pentane and 4 further trace gases (measured by ESRL GMD): methane, carbon monoxide, hydrogen and sulfurhexafluoride) were available from the flask measurements presented here. Atmospheric lifetimes for the NMHCs, carbon monoxide and methane predominately depend on the OH mixing ratio (Atkinson, 1994). In contrast, hydrogen and sulfurhexafluoride have largely independent sinks: soils for H_2 (Rhee et al., 2006) and stratospheric removal above 50 km for SF_6 (Maiss and Brenninkmeijer, 1998). It is thus possible to estimate the average OH mixing ratio that air sampled at an individual

station was exposed to during transport to the station, following the method proposed by Williams et al., (2001). This was considered a viable approach to estimating global OH distributions following the previous work by Jobson et al., 1998, 1999 and Karl et al., 2001). In brief: the variability for each compound was calculated as the standard deviation of the natural logarithms of the individual measurements. The data was then plotted versus the atmospheric lifetime. The lifetimes for hydrogen and sulfurhexafluoride are fairly well known and generally independent of atmospheric photochemistry: 1.4 +/- 0.2 years for H_2 (Rhee et al., 2006) and 3200 years for SF_6 (Maiss and Brenninkmeijer, 1998). The atmospheric lifetimes of the remaining 8 compounds depend on the OH mixing ratio alone (Atkinson, 1994). By varying the OH assumed in the lifetime calculation, a best fit regression or optimum (least square method) to all data can be obtained. The derived OH mixing ratios were expected to correspond to average OH to which airmasses arriving at the site have been exposed since the last influence of anthropogenic sources.

The NMHC variability outside the tropics is greatly enhanced during spring and fall when the changes in OH production generate steep NMHC gradients over these months (Goldstein et al., 1995, Rohrer and Berresheim, 2006). However, sulfurhexafluoride is not subject to this seasonal variation and information on hydrogen seasonality is rather scarce. Consequently, we have chosen to perform this variability analysis over distinct time periods when the OH concentration is less variable, namely for the summer (NH: Jun to Aug, SH: Dec to Feb) and winter (NH: Dec to Feb, SH: Jun to Aug) periods only. However, this limitation does not apply to tropical stations as they are not subject to significant photochemical seasonality.

Average OH concentrations for the individual stations were calculated according to the above described methods. This data was compared to the global OH distribution profile by Spivakovsky et al., 2000. The *A* and *b* factors were evaluated for their meridional distribution.

5.3 Results and Discussion

5.3.1 Individual Stations

Evaluation of example stations: Figures 5.1 a, b show the ethane, propane, isobutane and butane timeseries from the second quarter of 2005 to the end of 2006 for Cold Bay, AK, USA (CBA). A pronounced seasonal cycle for these 4 NMHCs is clearly visible. The minimum NMHC mixing ratios were found during late summer (August): ethane: 700 pptv, propane: 30 pptv, butanes: <10 pptv. NMHC mixing ratios were at a maximum during late winter (February): ethane: 2500 pptv, propane: 800 pptv, isobutane: 150 pptv, butane: 300 pptv. Similar patterns for the seasonal NMHC cycle have been found by other researchers at comparable stations (e.g.: Gautrois et al., 2003, Swanson et al., 2003, Hakola et al., 2006). The seasonal cycles presented here indicate that this station is generally not subject to local anthropogenic pollution. However, several samples during summer of 2006 did show anomalously high butane mixing ratios (days: 526, 529, 537, 561 and 565) possibly indicating local contamination due to fossil fuel evaporation or use.

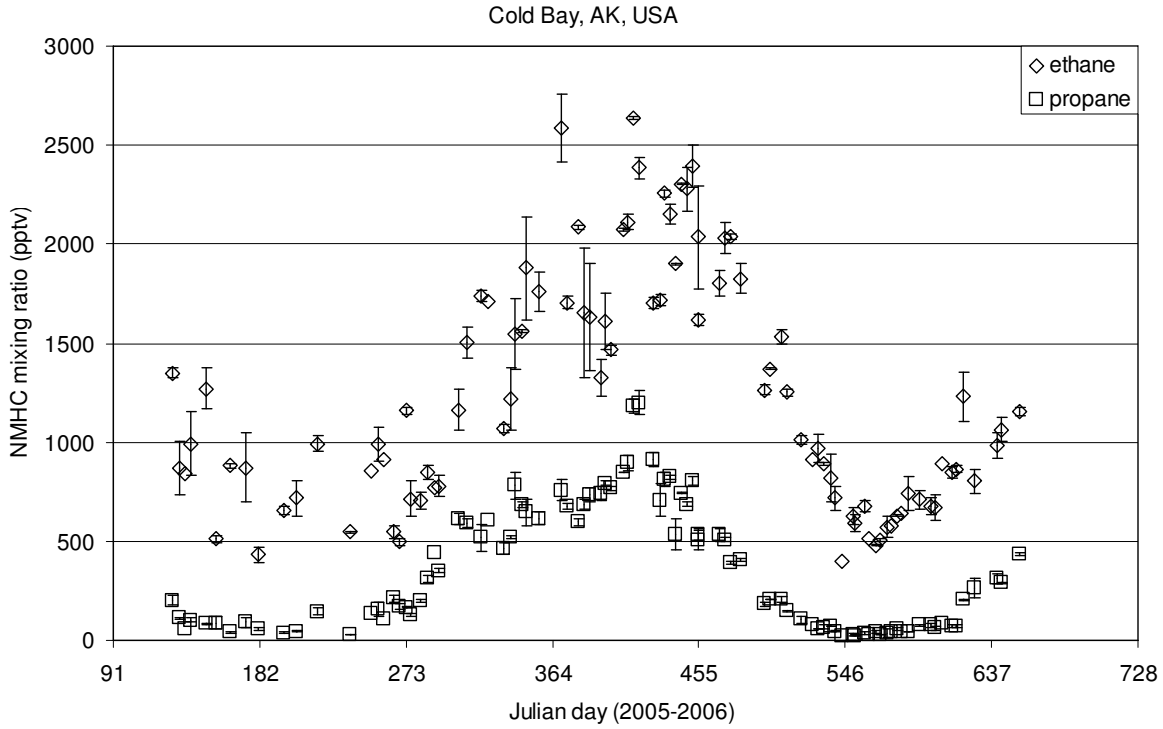

Figure 5.1 a: Seasonal cycle of ethane and propane from Cold Bay, AK, USA in continuous Julian days (1 = Jan 1st 2005). Data points are calculated as average of one pair measurement; error bars represent the standard deviation of the pair.

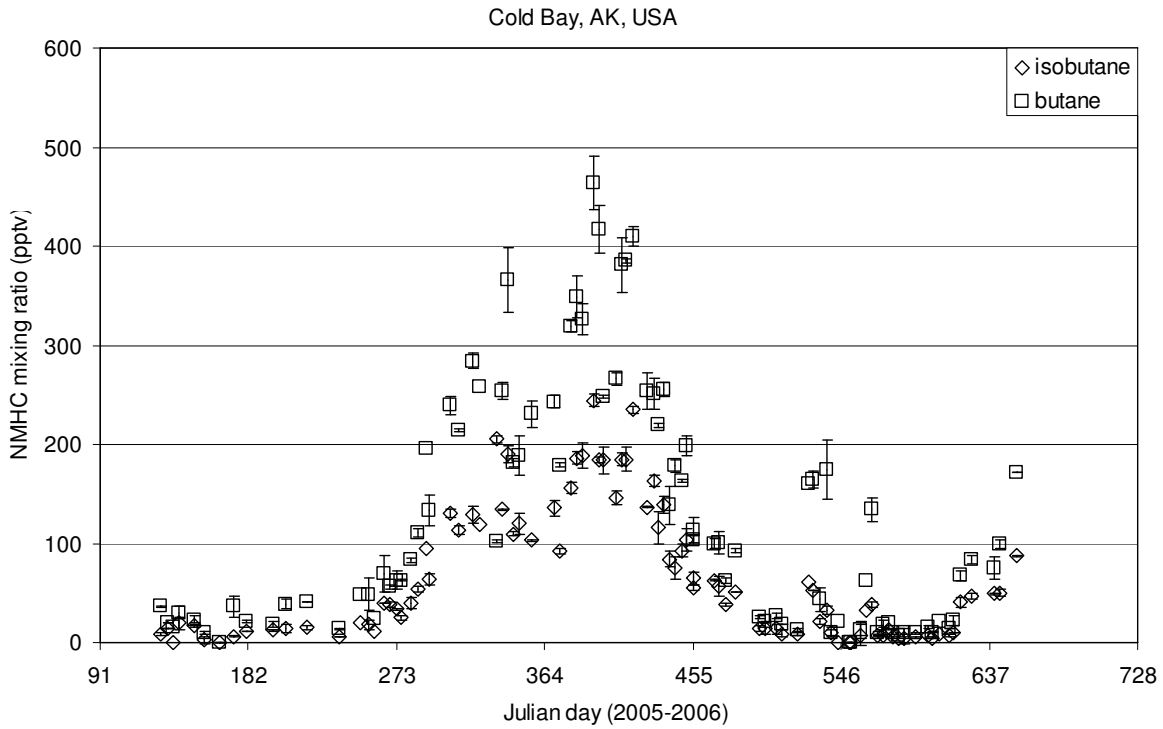

Figure 5.1 b: Seasonal cycle of butane and isobutane from Cold Bay, AK, USA in continuous Julian days (1 = Jan 1st 2005). Data points are calculated as average of one pair measurement; error bars represent the standard deviation of the pair.

Ethane, propane, isobutane and butane mixing ratios from Crozet Island, France, South Atlantic are displayed in Figure 5.2 a, b. As expected for a southern hemisphere site, the seasonality for NMHC was inverse to Cold Bay. Ethane mixing ratios were found at 300 to 500 pptv during winter (June to August) with minimum mixing ratios of 170 pptv during the summer months (December to February). Propane mixing ratios were at a maximum of 60 pptv during winter and less than 20 pptv in summer. Isobutane and butane mixing ratios were often found close to the detection limit of 3 pptv so that the data accuracy and precision is somewhat reduced. Nevertheless, a pronounced seasonal cycle is still discernable with butane mixing ratios of 30 (winter) and <10 (summer). Similar NMHC mixing ratios were also found during the austral summer by Lewis et al., 2001 at Cape Grim, Tasmania, Australia.

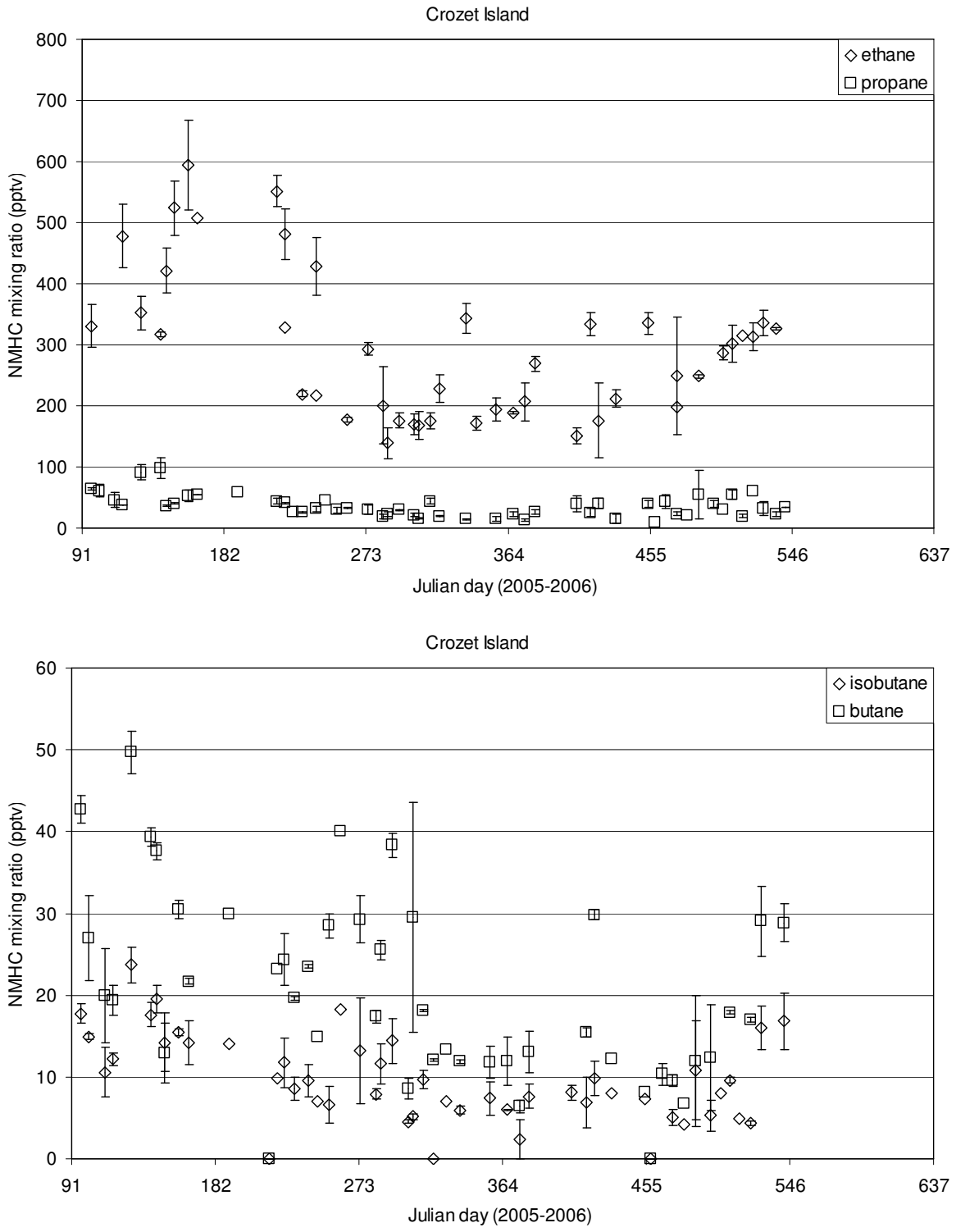

Figure 5.2 a, b: Seasonal cycle of ethane and propane (isobutane and butane) from Cold Bay, AK, USA in continuous Julian days (1 = Jan 1st 2005). Data points are calculated as average of one pair measurement; error bars represent the standard deviation of the pair.

A comparison of these two sites of similar remoteness highlights the large interhemispheric gradient of NMHC mixing ratios and by inference, emissions. Additionally, the seasonal cycle for light NMHC in the southern hemisphere is less pronounced than in the northern hemisphere, possibly indicating longer transport times to these stations and air masses that are significantly depleted of shorter lived compounds.

An analysis of ln (butane/ethane) vs. ln (propane/ethane), as displayed in Figure 5.3 a, b, shows the influence of kinetic and photochemical effects on the NMHC ratios (similar to Parrish et al., 1992, Swanson et al., 2003, Tanner et al., 2006).

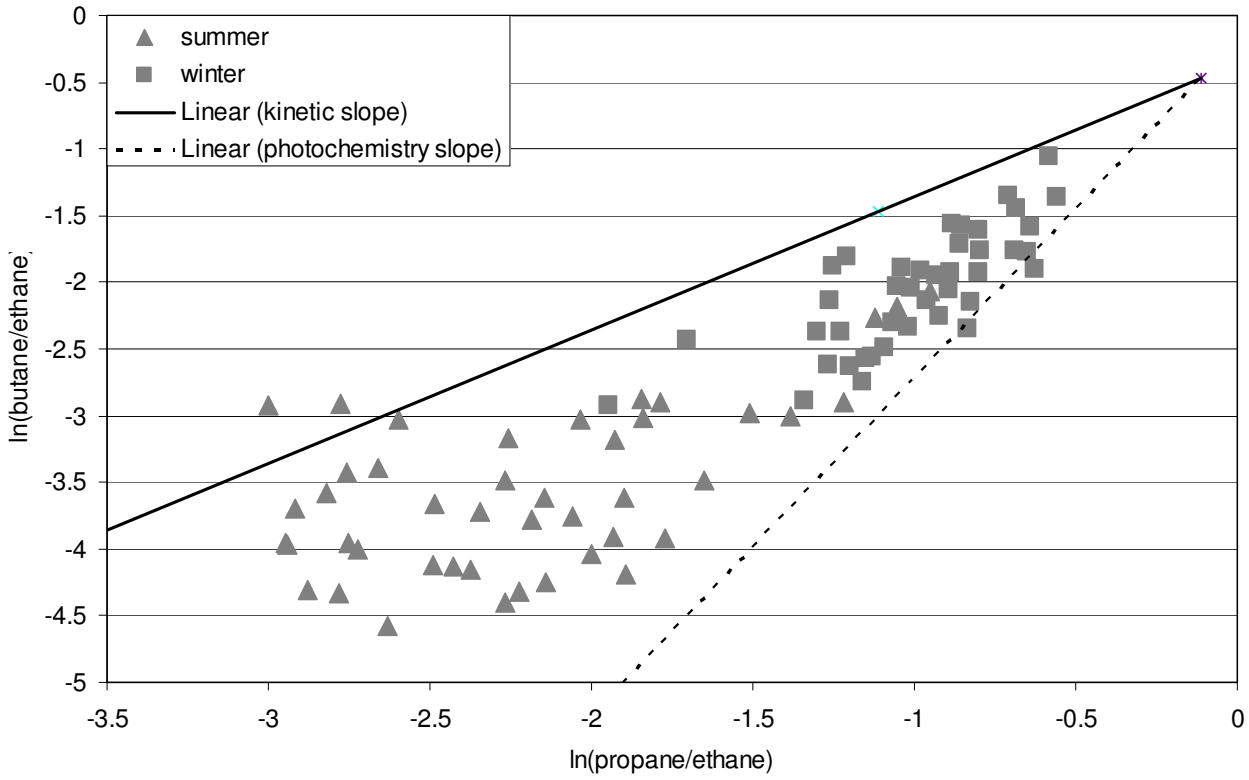

Figure 5.3 a: Evaluation of photochemistry and kinetic transport for Cold Bay, AK, USA according to Parrish et al., 1992. Photochemistry and kinetic slope originate from typical northern hemispheric urban source mixing ratio (Barletta et al., 2005 and references therein).

Figure 5.3 a shows this relationship after the removal of the high butane data for Cold Bay, AK, together with the average northern hemispheric source ratios (Barletta et al., 2005 and references therein) and the calculated kinetic mixing and photochemistry slopes expected from typical northern hemispheric source values. The homogeneity of the air samples from this station is clearly visible. Winter samples were found to the upper right corner of the graph indicating less processed (younger) air masses whereas summer samples were found to be more processed (lower left corner).

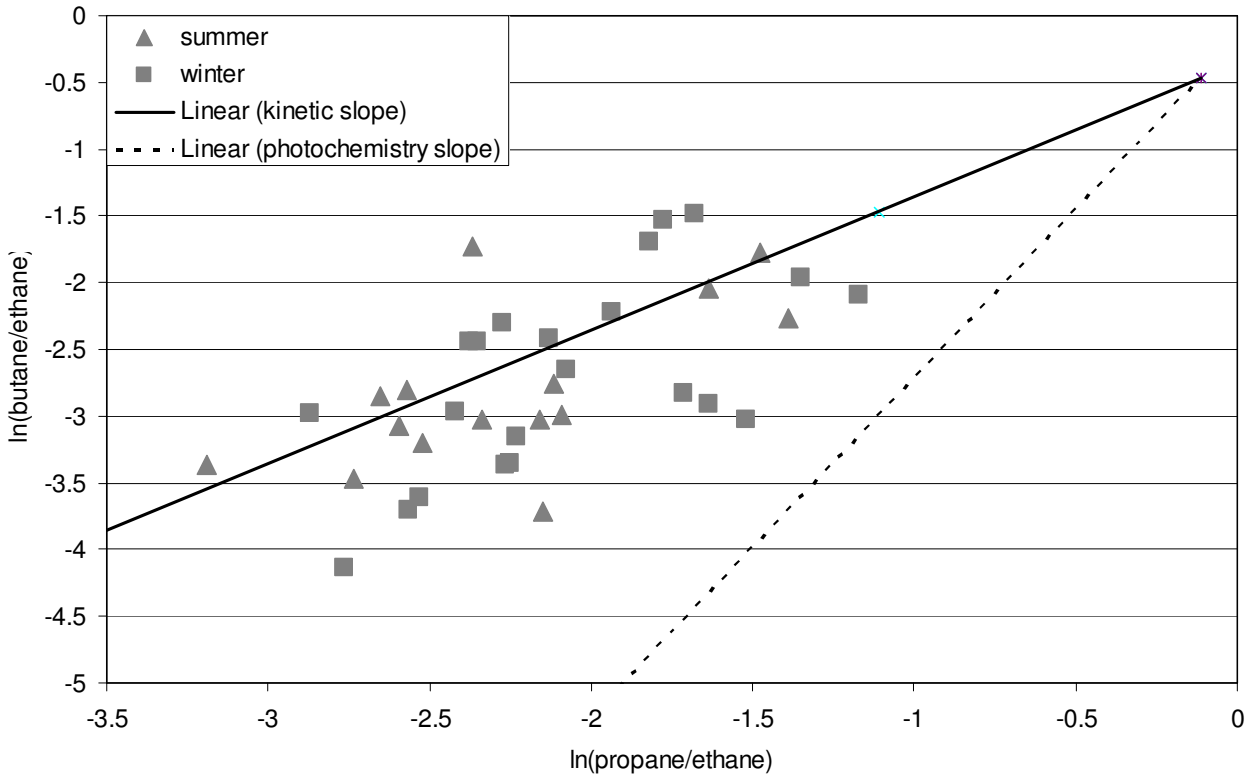

Figure 5.3 b: Evaluation of photochemistry and kinetic transport for Crozet Island, French Territories, South Atlantic according to Parrish et al., 1992. Photochemistry and kinetic slope originate from typical northern hemispheric urban source mixing ratio (Barletta et al., 2005 and references therein).

Figure 5.3 b shows the same analysis for the samples taken from Crozet Island. A clear relationship of these ratios is still visible, indicating the homogeneity of these air samples. However, the characteristics of this plot are significantly different to Cold Bay and the data points do not fall as clearly into the area bordered by the photochemical and kinetic slopes. The typical source mixing ratios for NMHC thus appear to be different than found in the northern hemisphere. Additionally, summer and winter samples are not as distinctively separated as found for Cold Bay. The slope of the regression line is also not as steep indicating a larger ratio of mixing over photochemistry. A comparison with previously presented results (Lewis et al., 2001) showed similar results.

This analysis of two individual stations shows the data quality and information typically available for each sampling station. A similar detailed analysis of all sampling stations would exceed the scope of this thesis and will be presented in later publications. However, the averaged monthly mixing ratios for ethane, propane and butane are displayed for all stations in Figure 5. 4a – l. The respective seasonal cycles are clearly visible. It can also be seen that certain stations regularly exceed typical background mixing ratios by up to a factor of five. These stations were identified as AMT, BAL, BSC, LEF and SGP. In addition, more than 20% of the ln(butane/ethane)/ ln(propane/ethane) data was found outside the kinetic mixing or photochemistry slopes. Conclusively, these stations were not regarded in the following sections.

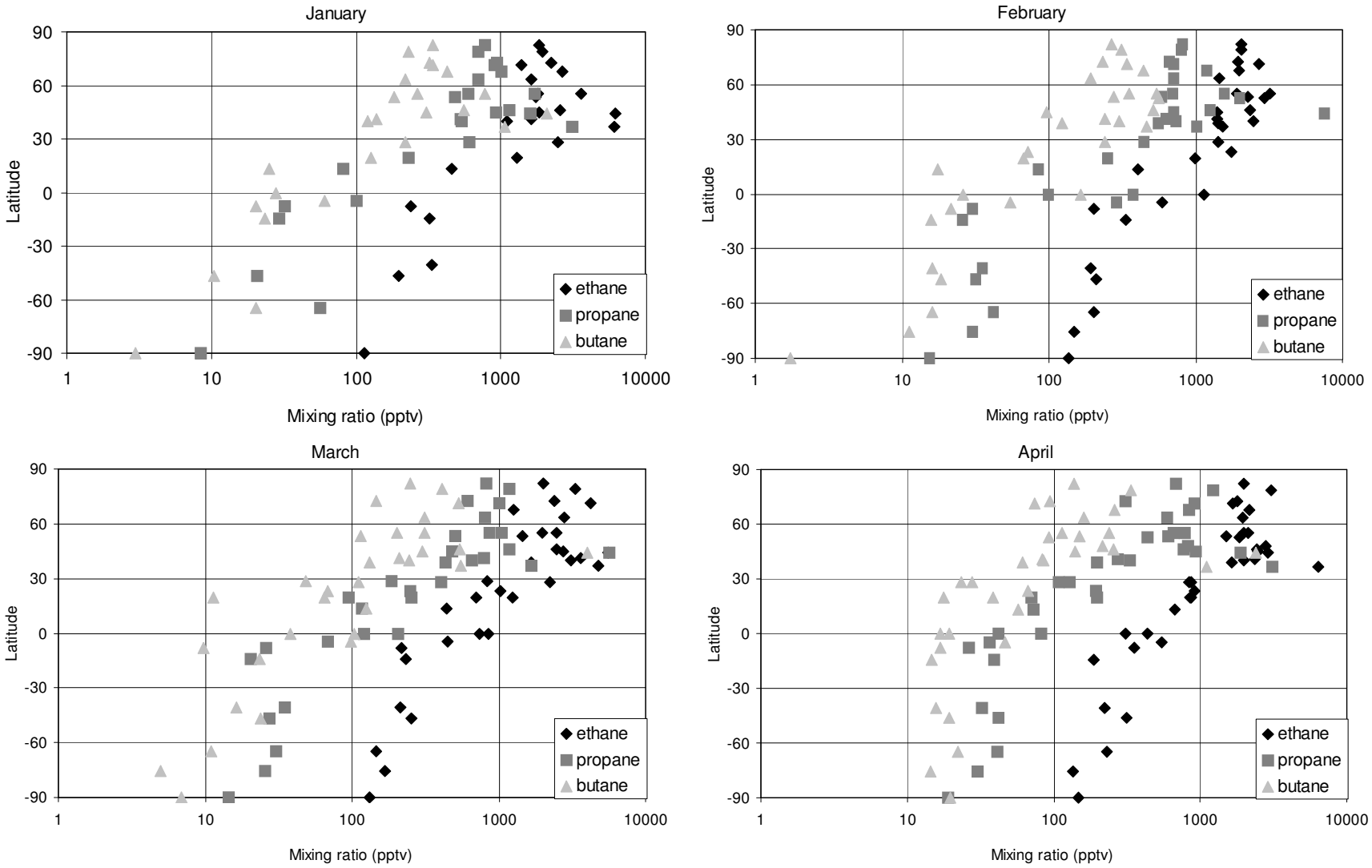

Figure 5.4 a – d: monthly distribution of ethane, propane and butane determined from flask samples provided by the ESRL cooperative air sampling network.

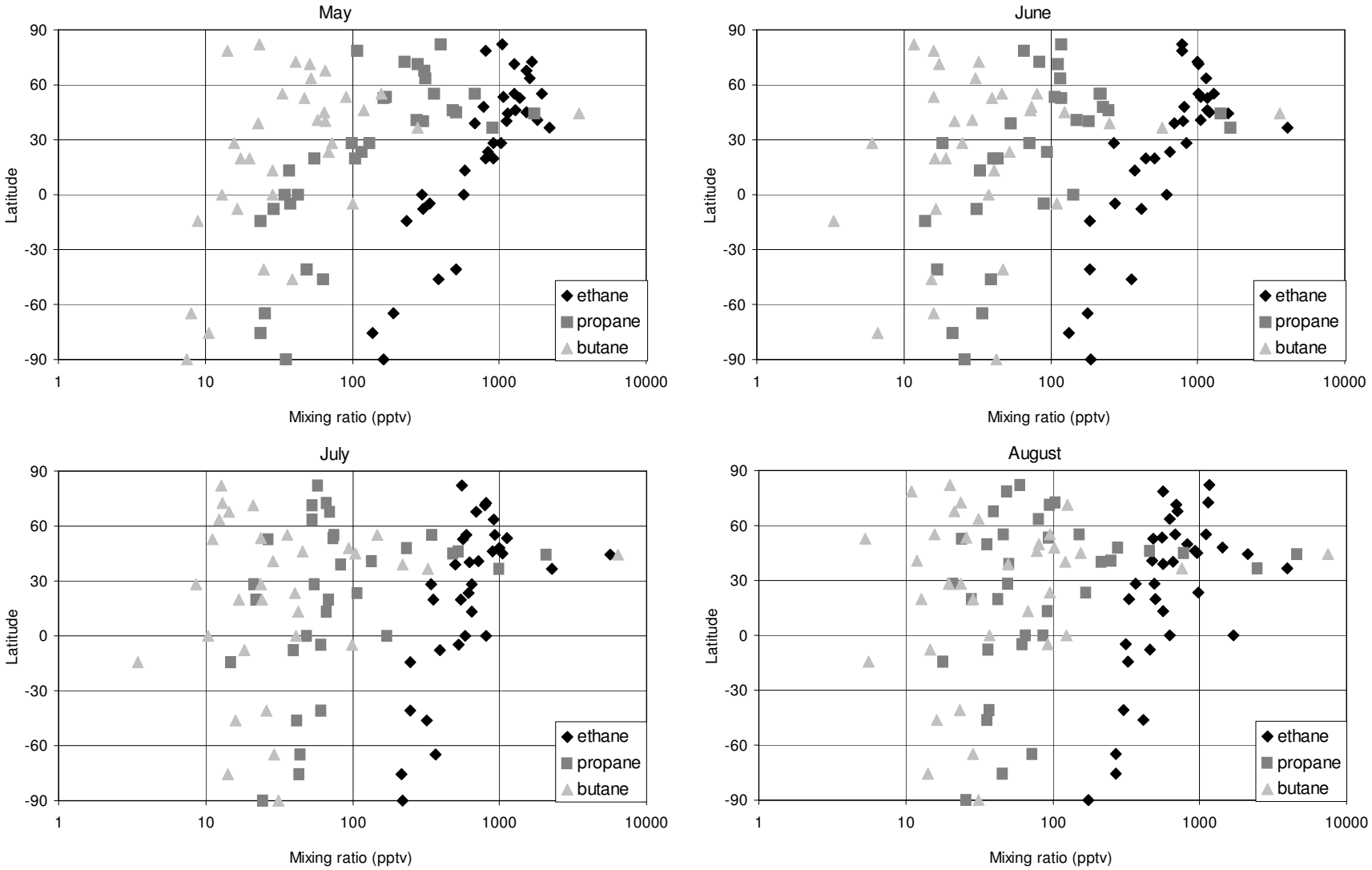

Figure 5.4 e – f: monthly distribution of ethane, propane and butane determined from flask samples provided by the ESRL cooperative air sampling network.

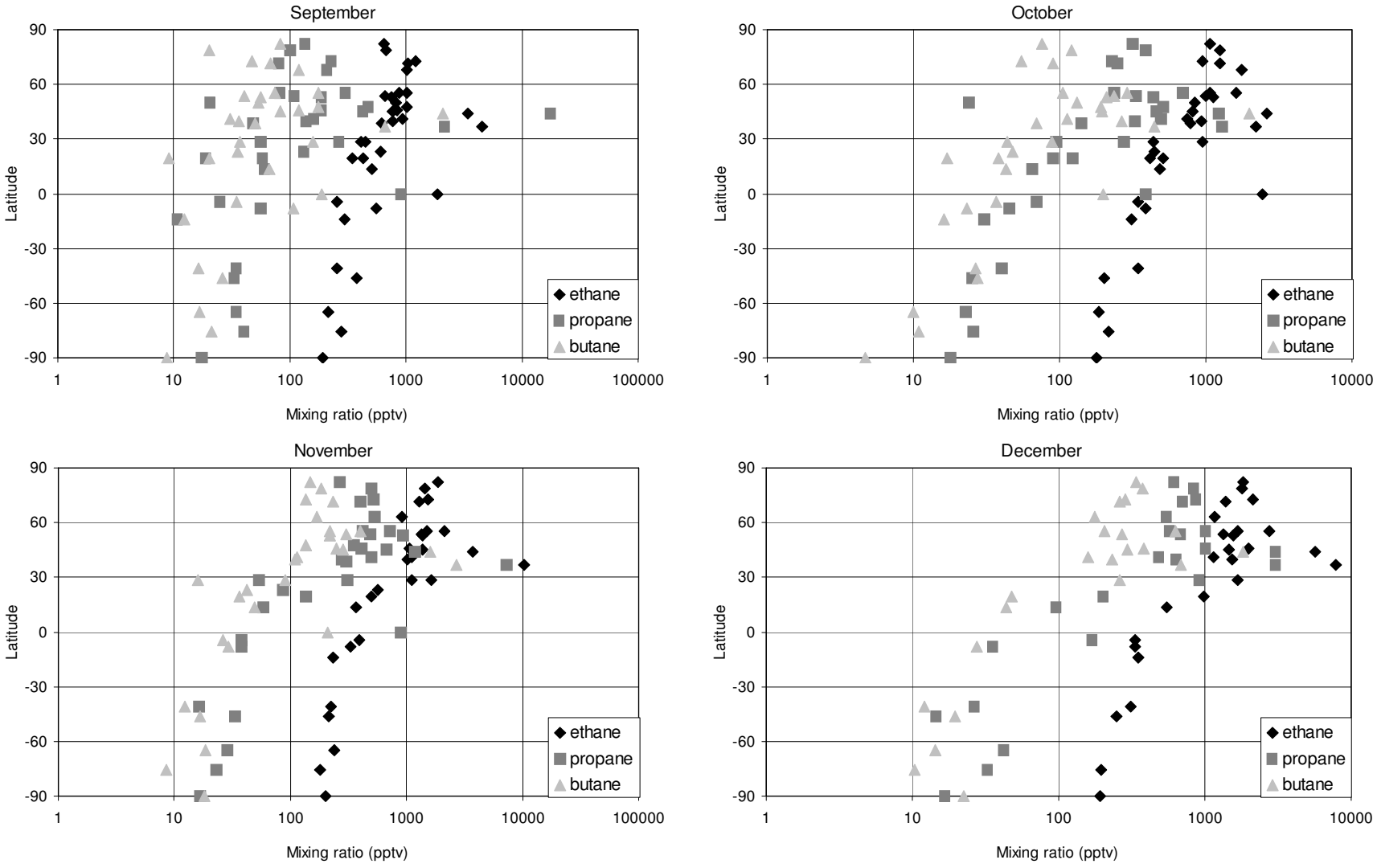

Figure 5.4 i – l: monthly distribution of ethane, propane and butane determined from flask samples provided by the ESRL cooperative air sampling network.

5.3.2 Global Distribution

Ethane: The global seasonal cycle for ethane can be found in Figure 5.5. The seasonality of ethane in the northern hemisphere with low values in August and high in February is clearly visible. The seasonality is inversed in the southern hemisphere. Winter maximum background mixing ratios of 2500 pptv and 500 pptv for the northern and southern hemisphere were found. Minimum mixing ratios were found during summer at 1000 pptv and 150 pptv in the northern and southern hemisphere, respectively. Ethane mixing ratios from tropical sampling stations were found at 800 to 1200 pptv but without a clearly defined seasonal cycle.

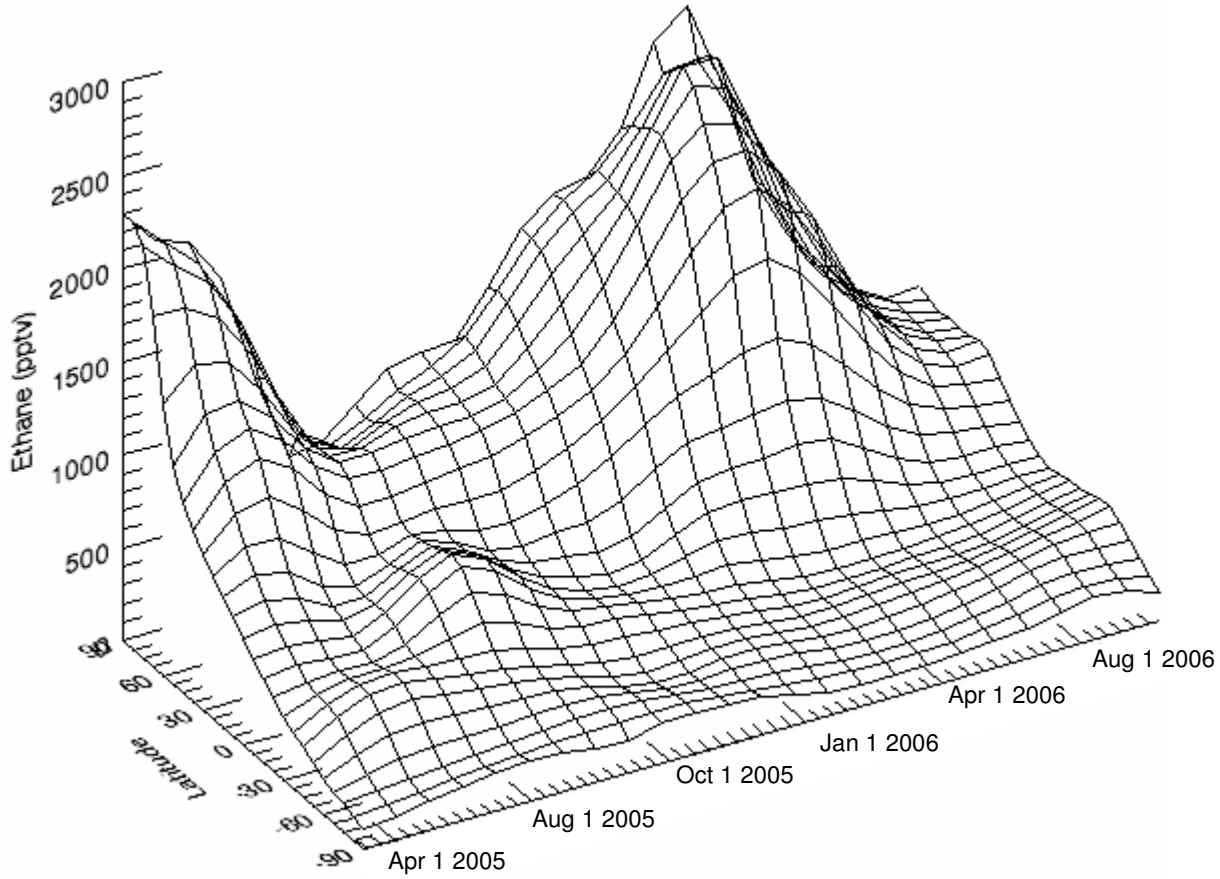

Figure 5.5: Global distribution of ethane derived from NMHC measurements from the NOAA cooperative air sampling network.

The latitudinal distribution of ethane is similar to that of long-lived greenhouse gases such as methane and reflects the global energy consumption. The general shape of the

3-D ethane global distribution plot is similar to previously published data (Rudolph, 1995). However, the 1995 publication shows significantly higher mixing ratios for the northern hemisphere with ethane mixing ratio of up to 3500 pptv in winter and 1500 pptv in spring. A quantitative comparison of these two data sets suggests that the global ethane burden in the remote northern hemisphere has declined by circa 30% (approximately 2.5% yr^{-1}) since the early 1990s. A similar reduction of the ethane mixing ratio on the order of 3% yr^{-1} was described previously for a single arctic site: Alert, Canada (Gautrois et al., 2003). This decrease is most likely caused by a reduction of NMHC emissions from industrialized northern hemispheric countries, perhaps in part to the introduction of catalytic converters or the modernization of the economies of the former Warsaw pact countries (Solberg et al., 2005). In contrast to these observations no reduction of the southern hemispheric ethane was observed compared to Rudolph, 1995 or Lewis et al., 2001.

Propane: The global seasonal distribution for propane can be found in Figure 5.6. The trend in the propane mixing ratio generally follows the ethane trend although absolute numbers are on average a factor of 2.5 (winter) to 10 (summer) lower. Northern hemispheric maximum and minimum mixing ratios were 1000 pptv and 100 pptv respectively. The equivalent Southern hemispheric mixing ratios were 70 pptv and 15 pptv respectively. Equatorial samples showed no clear seasonality with an average mixing ratio of 50 pptv. The ratio between summer and winter mixing ratios for propane (10) is significantly higher than the respective ratio for ethane (2.5). The difference can be explained by the higher reactivity of propane towards OH, and hence faster photochemical removal under high OH conditions during summer.

The interhemispheric gradient between the northern and southern hemisphere is significantly larger as well. It was previously shown that a significant source for ethane in the southern hemisphere is interhemispheric transport from the north (Rudolph, 1995). Propane has a much shorter atmospheric lifetime (~25% of ethane, Atkinson, 1994) and interhemispheric transport can be considered negligible.

A previously published global distribution analysis for propane compiled by the integration of multiple measurement campaigns showed a similar latitudinal distribution of propane (Bonsang and Boissard, 1999). However their analysis included polluted samples

from industrialized regions between 45 °N and 65 °N so that no statements can be made on a potential decline of the tropospheric propane burden.

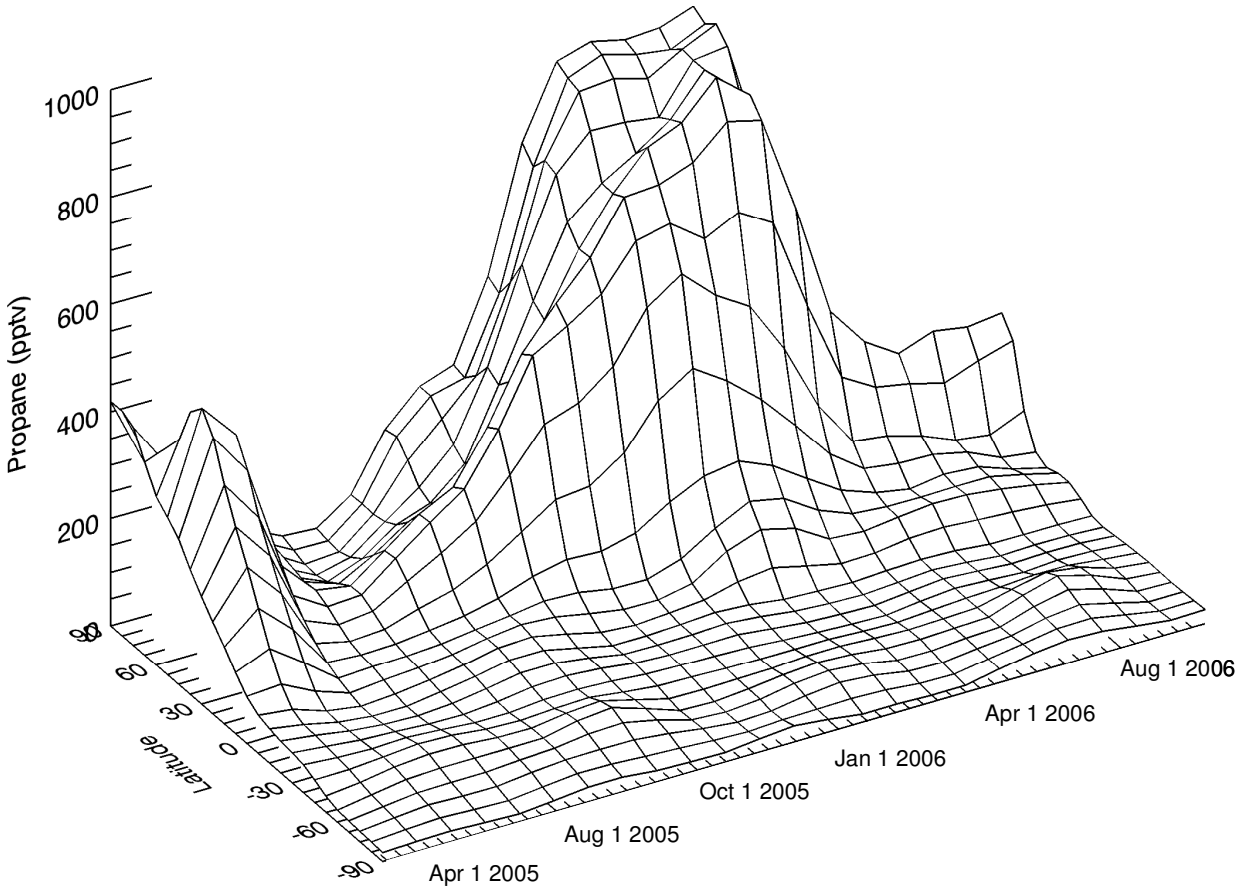

Figure 5.6: Global distribution of propane derived from NMHC measurements from the NOAA cooperative air sampling network.

Isobutane and Butane: The 3-D global distribution plots for isobutane and butane can be found in Figures 5.7 and 5.8. The summer/winter ratio for the butane isomers is significantly higher in the northern troposphere in comparison to the longer lived alkanes ethane and propane (up to 20). The seasonal changes for butane and isobutane show steep slopes between summer and winter. Butane mixing ratios north of 40 °N were found to increase from 40 to 300 pptv within 70 days at the onset of winter (Julian days 270 – 340). Southern hemispheric butane mixing ratios were found to be 10 and 20 pptv for isobutane and butane respectively during the winter and at or below the detection limit of 3

pptv during the summer. However, a distinct seasonal cycle inverse to the northern hemisphere was still observed.

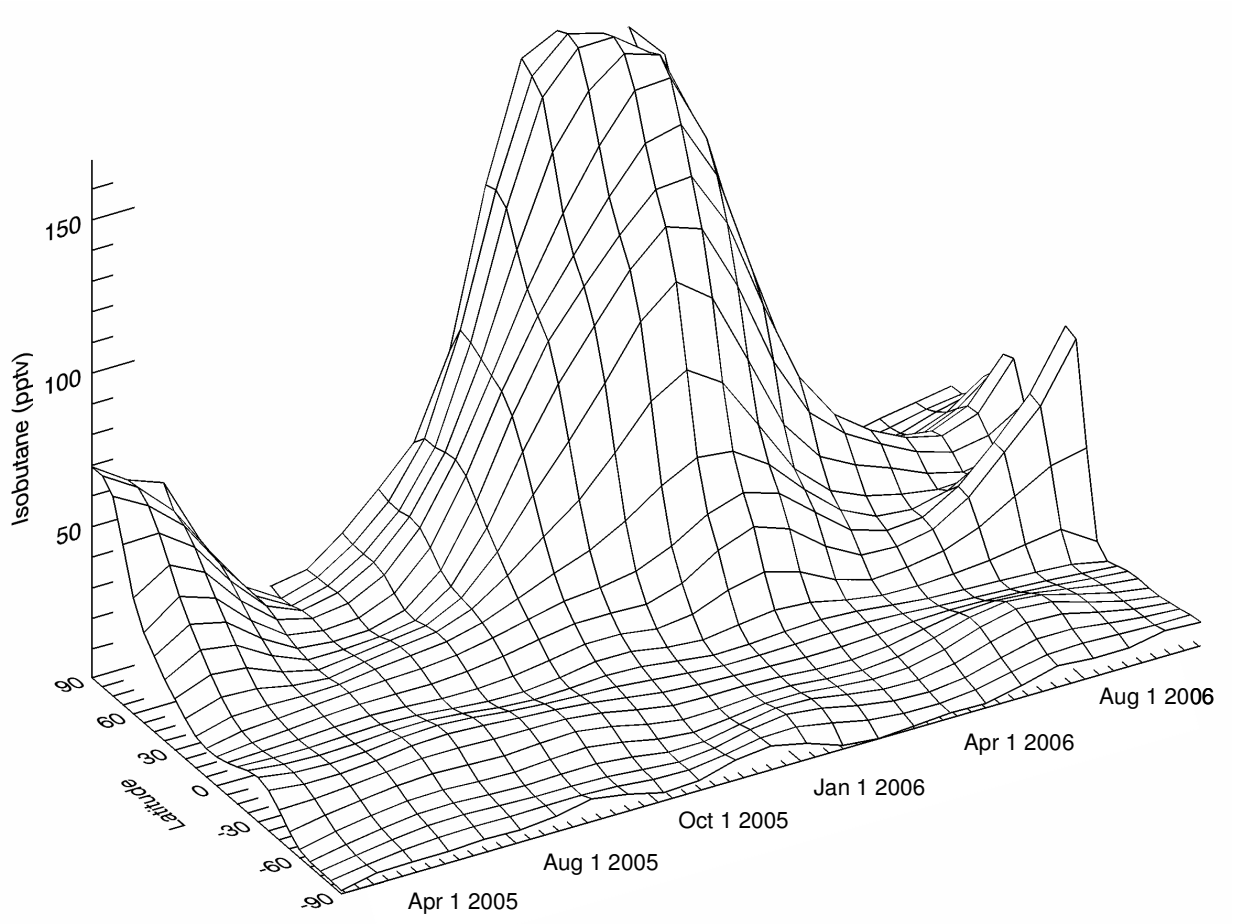

Figure 5.7: Global distribution of isobutane derived from NMHC measurements from the NOAA cooperative air sampling network.

These results (especially for the northern hemisphere) show the distinct anti-correlation between butane and hydroxyl radical abundance as the butane isomers are much more reactive towards OH than ethane or propane. No global distribution profiles of either isobutane or butane have been previously published and thus no statement can be made regarding a global longterm atmospheric trend. A comparison with Gautrois et al., 2003 suggests a decline in the high latitude northern troposphere.

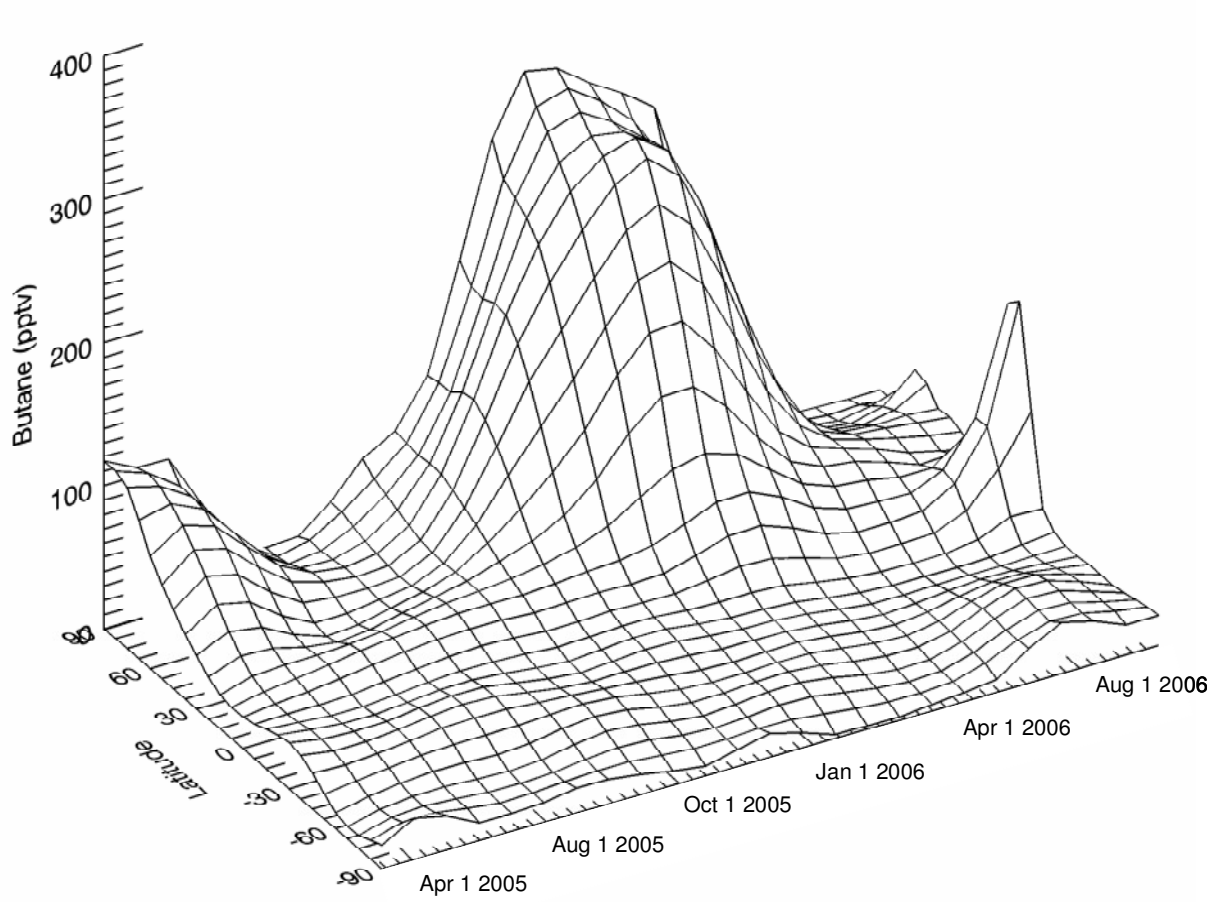

Figure 5.8: Global distribution of butane derived from NMHC measurements from the NOAA cooperative air sampling network.

Previous research has shown that the isobutane/butane ratio is rather stable at approximately 0.5 ± 0.05 (e.g.: Parrish et al., 1998 and Swanson et al., 2003). The global seasonal distribution for the butane isomeric ratio is presented in Figure 5.9. It can be seen that the butane ratio is indeed very planar (i.e. generally featureless) over wide temporal and regional scales. The average ratio was calculated at 0.55 +/- 0.14 in excellent agreement to literature data (Swanson et al., 2003).

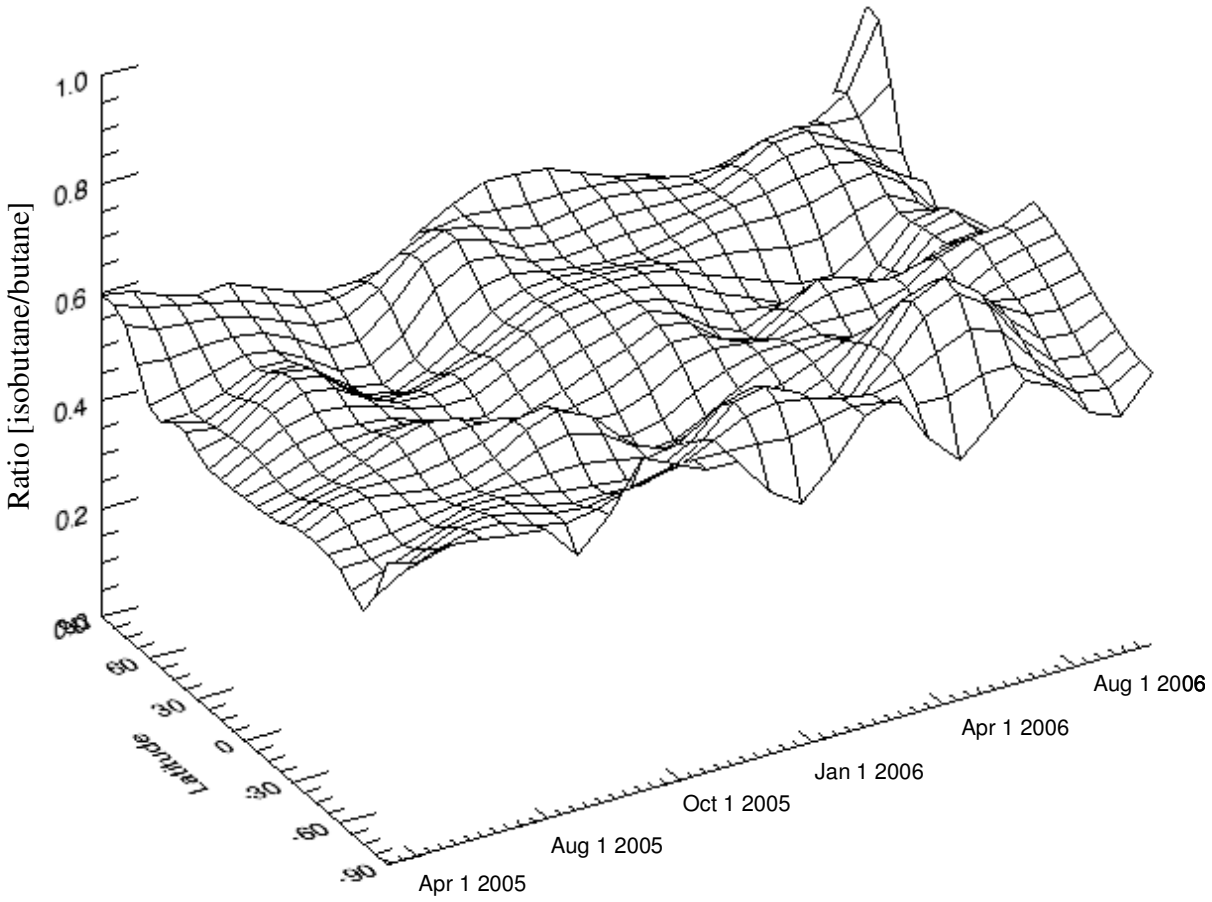

Figure 5.9: Global distribution of the isobutane/butane ratio derived from NMHC measurements from the NOAA cooperative air sampling network.

The roles of Cl radical chemistry in the marine troposphere as well as nighttime nitrate radical chemistry have been repeatedly discussed in the literature (e.g.: Ariya et al., 1998). Laboratory studies have shown that Cl radicals react more readily with n-butane than with isobutane: reaction rate constants: 1.94 * 10^{-10} cm^3 $molec^{-1}$ s^{-1} (butane) and 1.30 * 10^{-10} cm^3 $molec^{-1}$ s^{-1} (isobutane), (Hooshiyar and Niki, 1995). The nitrate radical reacts faster with isobutane (4.5 10^{-16} molec cm^{-3} s^{-1}) than with butane (1.44 10-^{16} molec cm^{-3} s^{-1}) (Atkinson, 1992). Consequently the isobutane over butane ratio should increase during times of significant chlorine radical chemistry and decline in case of nitrate radical reactions. Figure 5.9 shows no evidence of large scale chlorine or nitrate radical chemistry as the isomeric butane ratio remains generally at 0.55. Some scatter was found especially

for measurements in the southern hemisphere which can explained by higher uncertainties for measurements at the detection limit. OH radical chemistry is most likely the main removal pathway of NMHCs in the troposphere, see also next section. Similar results for Summit, Greenland were previously shown by Swanson et al., 2003.

5.3.3 OH Quantification by variability analysis

Variability Analysis: A typical example of the variability analysis for a remote northern hemispheric background site (Cold Bay, AK, USA) from winter and summer is displayed in Figures 5.10 and 5.11 respectively. The variability-lifetime dependence is clearly visible and indicated by both an R^2-factor of > 0.9 and a "b" factor of > 0.5. All C2 to C5 NMHC were found to follow the regression curve, again indicating that OH chemistry is driving the variability and that the station is remote and free of local sources.

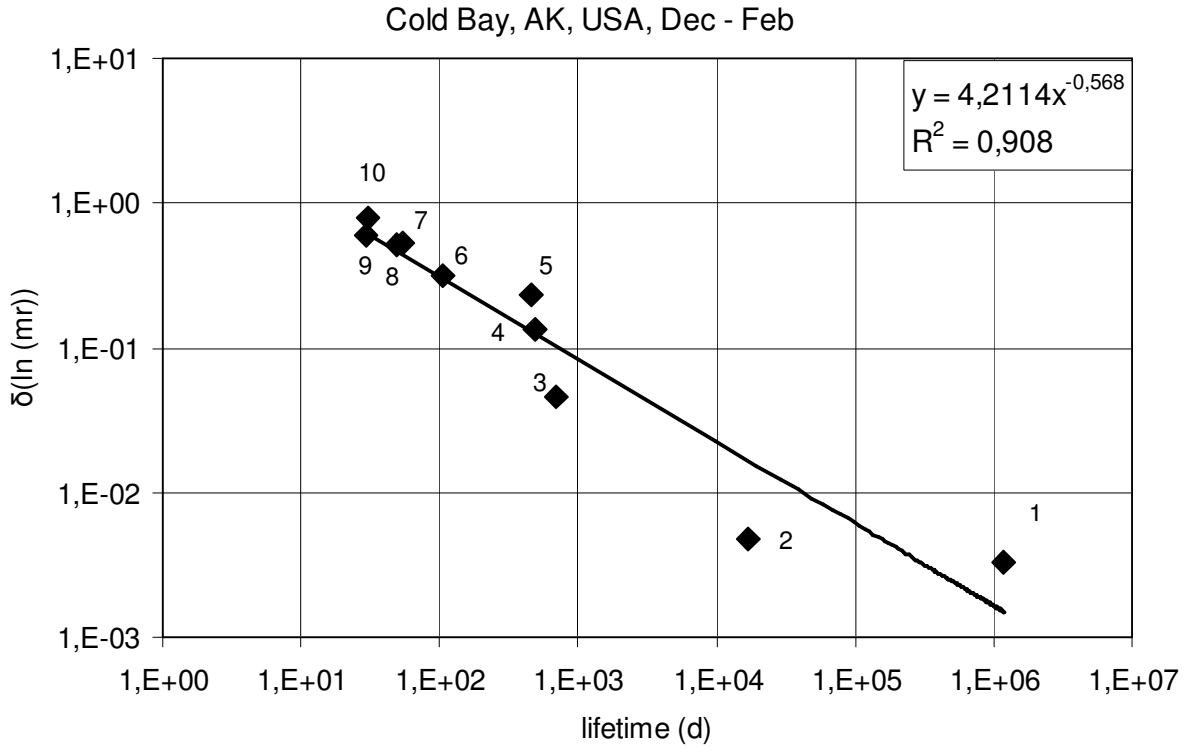

Figure 5.10: Variability analysis for Cold Bay, AK, USA, from December to February (winter); numbers indicate compounds; 1, sulfurhexafluoride; 2, methane; 3, hydrogen; 4, carbon monoxide; 5, ethane; 6, propane; 7, isobutane; 8, butane; 9, isopentane, 10, pentane

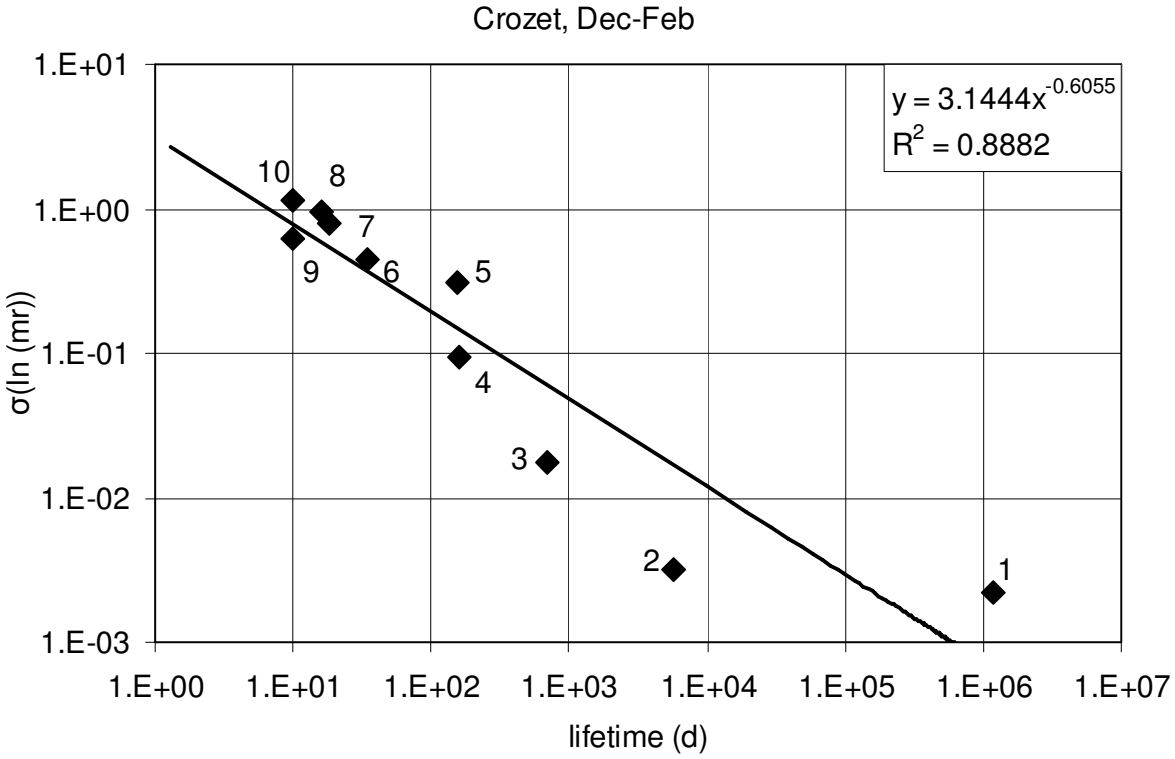

Figure 5.11: Variability analysis for Crozet Island from December to February; numbers indicate compounds; 1, sulfurhexafluoride; 2, methane; 3, hydrogen; 4, carbon monoxide; 5, ethane; 6, propane; 7, isobutane; 8, butane; 9, isopentane, 10, pentane

The variability – lifetime relationship was applied to estimate the seasonal OH mixing ratio as described above (see also: Williams et al., 2000, 2001, Karl et al., 2001, Bartenbach et al., 2007). The derived average effective OH mixing ratios for Cold Bay were determined as 10^5 molec cm^{-3} during winter (Dec – Feb) and 11 * 10^5 molec cm^{-3} during summer (Jun – Aug). These OH values for the Cold Bay station are in close agreement (within 20%) with the most comprehensive distribution study for OH to date (Spivakovsky et al., 2000). However, the two datasets cannot be compared directly as the OH mixing ratios derived by the variability analysis represent the average 24h OH mixing ratio a certain air sample was exposed to during its transport to the sampling station rather than the local OH mixing ratio.

The data from Crozet Island was evaluated similar to the measurements from the Cold Bay station described above. The variability – lifetime relationship is again clearly visible (R^2 ~ 0.9). The "b" factors of ~ 0.6 indicate the pronounced remoteness of this station. The estimated average OH mixing ratio for Crozet Island was 6 molec cm^{-3} (Dec – Feb) and 3 molec cm^{-3} (Jun - Aug). Good agreement compared to Spivakovsky et al., 2000 was found during both seasons (within 20%).

Interestingly, the figures for both stations show that the measured variability of both methane and hydrogen is less than predicted by the variability lifetime fit. This could indicate atmospheric lifetimes longer than stated in the literature or possibly to widespread sources in these regions which act to suppress variability generated by chemistry (as similarly described by Jobson et al., 1998). This effect was found more pronounced during winter and more significantly at Crozet than at Cold Bay.

It was previously shown that the major source for hydrogen in the troposphere is photochemical production by methane oxidation (Novelli et al., 1999, Rhee et al., 2006). This process is dispersed across the troposphere and a reduced variability for hydrogen must be expected. Additionally, the dominant sink is thought to be soils and the predominant sink must then be expected in the northern hemisphere (Rhee et al., 2006). This sink is probably subject to some seasonal changes (melting and thawing of soil) but currently no details are available. It can be expected that hydrogen lifetime during winter would be slightly longer than during summer possibly explaining the observed differences.

Methane sources can affect even remote stations due to the long lifetime. This and the large source strength would reduce methane variability. Similarly, a significant biogenic methane source was recently discovered (Keppler et al., 2006, Ferretti et al., 2007) which possibly also acts to reduce atmospheric variability.

The variability analysis as exemplified in the previous section was conducted on a global scale for all sampling stations with enough temporally continuous data (at least 10 measurements per season) including the locally influenced sites. A summary for the derived parameters including the average 24h OH mixing ratio from the best fit analysis can be found in Table 5.3. The latitudinal distribution of the *A* and *b* factors can be found in Figure 5.12. A clear relationship between the *A* factor and latitude was observed. Minimum values of the *A* factor were found at approximately 1 in tropical regions. Highest values of

the *A* factor were found in the high latitudes at 3 – 4. *A* factors in the northern troposphere exhibit significant differences between summer and winter with lower *A* values during the summer. Similar behavior was not found for the southern hemispheric stations. The latitudinal distribution of the *A* factor follows the behavior predicted in the introduction, representing the age range of an airmass. However, to date the physical meaning of this parameter is rather uncertain and further research is needed.

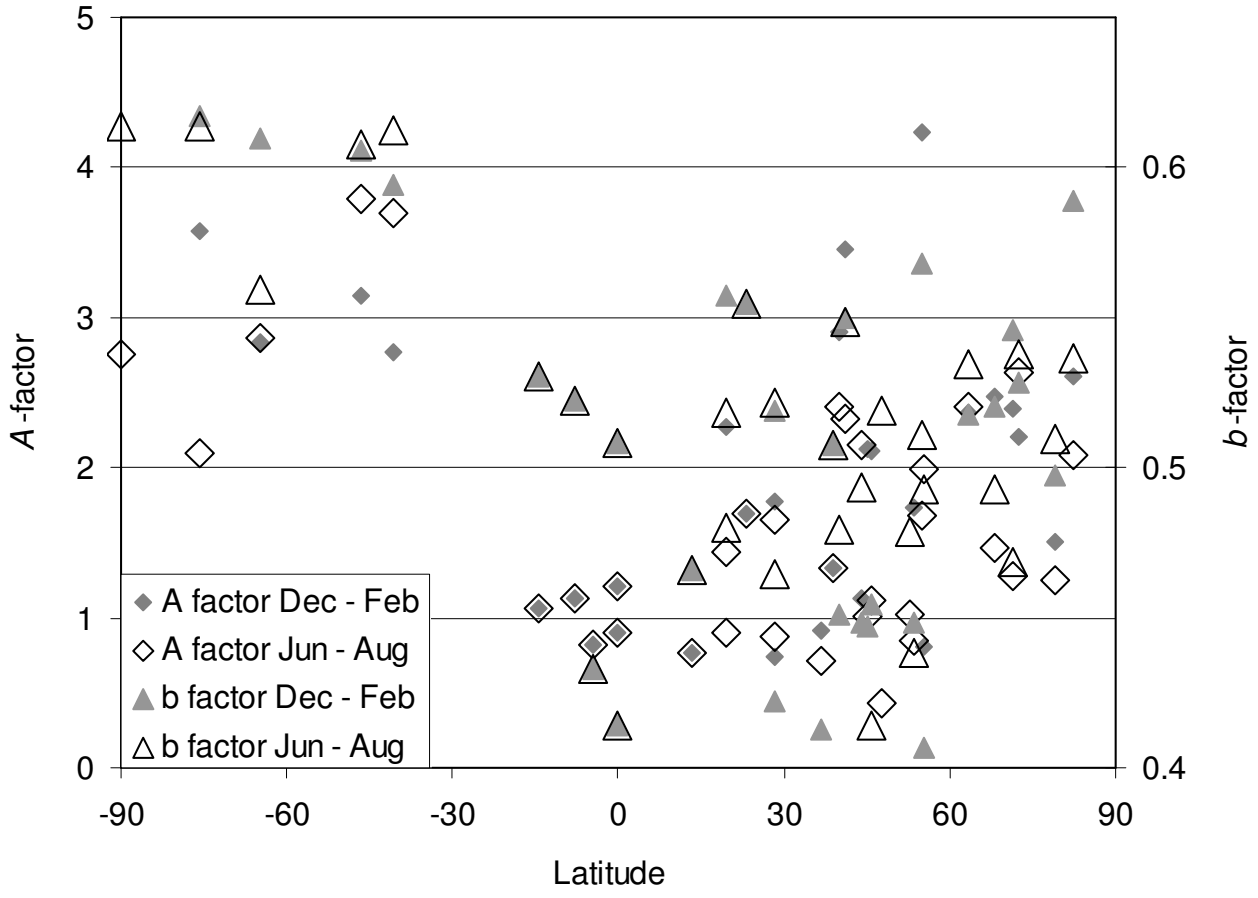

Figure 5.12: latitudinal evolution of analytical factors for the variability lifetime relationship

The airmass transport in the tropics is dominated by the relative constant trade winds. Thus a small band of ages would be expected. In the temperate zone large scale synoptic events such as high pressure fronts etc. exhibit a wider range of wind speeds and directions resulting in a mixing of air masses of a wider age range.

The *b* factor for most stations exceeds 0.5 as would be expected for remote sites where OH chemistry is driving the measured variability, see figure 5.12. Reduced *b* factors of approximately 0.4, indicating some locally influenced airmasses, can be found in the mid northern latitudes from 30 to 60 °N. These stations are within relatively close proximity to pollution sources. Far southern stations (south of 40°S) show *b* factors higher than 0.6 representing extremely remote atmospheric conditions.

Hydroxyl Radical: All stations examined show a clear relationship between atmospheric lifetime and variability as documented by *b* factors > 0.4 and R^2 factor > 0.9 (Table 5.3). We concluded that it is thus possible to determine the average OH mixing ratio an air mass was exposed during transport for all individual stations with sufficient sampling frequency. This latitudinal distribution of OH mixing ratios derived from the variability analysis can be found plotted in Figures 5.13, 5.14 and the numeric values in Table 5.3. The maximum of the OH distribution was found near the equator at approximately 40 * 10^5 molec cm^{-3} and the derived OH concentration decreased towards the high northern and southern latitudes. OH mixing ratios during summer (NH: Jun - Aug; SH: Dec - Feb) in the mid to high latitudes were found to be approximately 10 * 10^5 molec cm^{-3}. Similarly winter (NH: December to February; SH: June to August) hydroxyl radical mixing ratios were found to be 2 * 10^5 molec cm^{-3}.

Tropical mixing ratios determined in this paper by variability analysis were found to be two to three times higher than those calculated by Spivakovsky et al., 2000. Interestingly, the available direct OH measurements agree well with our observations in the tropics (made over the ocean) (Brauers et al., 2001). One tropic station shows rather low OH mixing ratio (Mount Kenya 0.05°S, [OH] = 17 10^5 molec cm^{-3}). This deviation from the observed average tropical mixing ratios can be attributed to the high altitude of this station and hence reduced water vapor availability for the formation of OH.

Table 5.3: Summary, variability analysis; site, station code; b-factor, exponent from equation by Jobson et al., (1998); R^2 factor, best fit factor for regression curve; best fit OH, resulting average OH mixing ratio for summer and winter; average annual values for tropical stations.

site	latitude	longitude	altitude (m)	b-factor		A factor		regression (R^2) factor		best fit OH [10^5 molec cm^3 s^{-1}]	
				December to February	June to August	December to February	June to August	December to February	June to August	December to February	June to August
ALT	82.45	-62.52	210	0.5887	0.5362	2.6074	2.0814	0.9193	0.8972	2	5
AMT	45.03	-68.88	157	0.447	0.3575	2.1284	1.0074	0.93	0.955	3	15
ASC	-7.92	-14.42	54	0.5222		1.1242		0.9049		18	
ASK	23.18	5.42	2728	0.5546		1.6872		0.9354		16	
ARZ	38.77	-27.38	40	0.5077	n/a	1.3264	n/a	0.9089	n/a	11	n/a
BAL	55.35	17.22	28	0.4067	0.4927	0.8017	1.9945	0.9434	0.9412	16	5
BKT	-0.20	100.32	864	0.4142		0.9047		0.9548		40	
BRW	71.32	-156.60	11	0.5458	0.4688	2.39	1.2797	0.9599	0.9193	4	15
BSC	44.17	28.68	3	0.4485	0.4931	1.1316	2.1502	0.9067	0.9377	14	9
CBA	55.12	162.42	25	0.5677	0.5108	4.2325	1.6791	0.9248	0.9406	1	11
CGO	-40.68	144.68	94	0.5945	0.6126	2.7678	3.697	0.8744	0.8748	3	2
CRZ	-46.45	51.85	120	0.6055	0.6078	3.1444	3.7849	0.8882	0.8742	6	3
GMI	13.43	144.78	6	0.4656		0.7616		0.8922		35	
HBA	-75.58	-26.50	33	0.6168	0.6139	3.5774	2.0988	0.8906	0.8614	4	4
HPB[+]	47.80	11.01	990	n/a	0.5189	n/a	0.4326	n/a	0.974	n/a	28
ICE	63.34	-20.29	127	0.5175	0.5342	2.3597	2.406	0.8936	0.9144	1	4
IZO	28.30	-16.48	2360	0.5191	0.4647	1.779	0.8715	0.9193	0.8805	5	15
KUM	19.52	-154.82	3	0.5572	0.4797	2.2759	0.8975	0.9614	0.9598	5	20
LEF	45.93	-90.27	868	0.4547	0.4144	2.1063	1.1118	0.9091	0.8983	3	8
MHD	53.33	-9.90	25	0.4486	0.4383	1.7278	0.8444	0.9534	0.9139	2	9
MID	28.21	-177.38	8	0.4222	0.5215	0.7374	1.6527	0.8505	0.9162	10	8
MKN	-0.05	37.30	3897	0.5083		1.2074		0.9285		17	
MLO[+]	19.54	-155.58	3397	n/a	0.518	n/a	1.4395	n/a	0.9385	n/a	9
OXK[+]	50.06	11.80	1356	n/a	n/a	n/a	n/a	n/a	n/a	n/a	n/a
PAL	67.97	24.12	560	0.5206	0.4925	2.467	1.4667	0.9642	0.9386	4	7
PSA	-64.92	64.00	10	0.6097	0.5591	2.8347	2.8575	0.8845	0.8901	5	4
SEY	-4.67	55.17	7	0.4327		0.8157		0.9398		25	
SGP	36.80	-97.50	374	0.4125	0.3806	0.9139	0.7066	0.9352	0.9181	25	20
SHM[+]	52.72	174.10	40	n/a	0.4788	n/a	1.0172	n/a	0.8978	n/a	16
SMO	-14.24	-170.57	42	0.5305		1.058		0.8846		21	
SPO	-89.98	24.80	2810	n/a	0.6139	n/a	2.7596	n/a	0.865	n/a	7
SUM	72.58	-38.48	3238	0.5283	0.5378	2.2099	2.631	0.9139	0.9069	2	3
SYO*	-69.00	39.58	14	n/a	n/a	n/a	n/a	n/a	n/a	n/a	n/a
TDF*	-54.87	-68.48	20	n/a	n/a	n/a	n/a	n/a	n/a	n/a	n/a
THD	41.05	-124.15	107	0.5499	0.5488	3.4574	2.3284	0.9475	0.9499	3	8
UTA	39.90	-113.72	1628	0.4514	0.4793	2.9043	2.4046	0.9412	0.9386	1	5
ZEP	78.90	11.88	1320	0.4976	0.5098	1.5022	1.2538	0.945	0.9025	4	6

* not enough data

+ only selected seasons available

Calculated OH mixing ratios in the northern hemisphere (Figure 5.13, 5.14) agree better with direct OH measurements from published intensive field campaign data (table 5.1) than with the calculated OH distribution by Spivakovsky et al., 2000. Similarly, more locally influenced continental sites especially in the northern hemisphere were often found to have elevated OH mixing ratios of up to two times larger than the unpolluted background sites. This can be attributed to the conversion of HO_2 into OH by NO (George et al., 1999). The direct OH measurement sites as well as the cooperative flask network stations are usually fairly remote. In contrast, the Spivakovsky model data was produced by integrating over large geographical regions with high NO emissions potentially leading to higher OH mixing ratios than found at remote sampling stations.

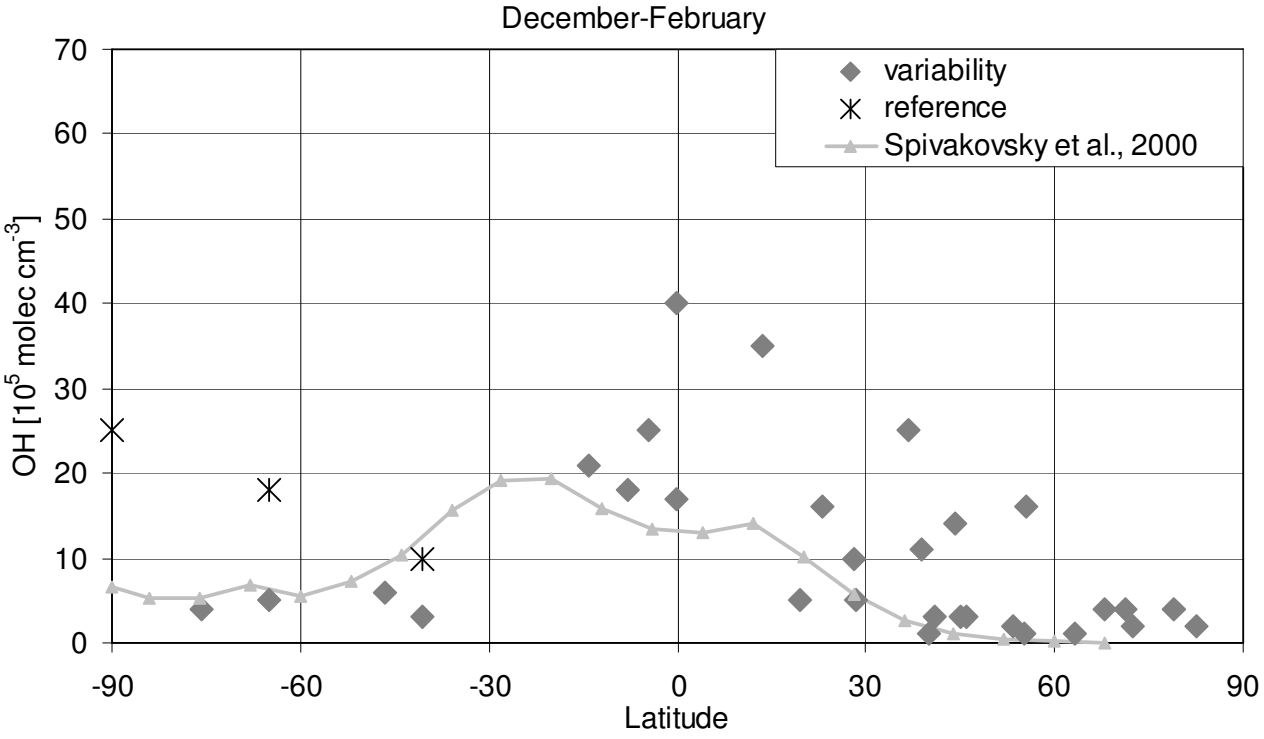

Figure 5.13: Estimated latitudinal OH mixing ratio from December to February derived by variability analysis (diamonds). Crosses indicate OH mixing ratios determined by direct OH measurements (references, see table 5.1); Solid line represents OH distribution calculated by Spivakovsky et al., 2000.

Southern hemispheric OH mixing ratios especially for the Antarctic continent (Jefferson et al., 1998, Mauldin et al., 2003) appear to be underestimated by variability

lifetime analysis compared to summertime direct measurements but agree well with the OH mixing ratio estimated by Spivakovsky et al., 2000. Direct measurements were up to a factor of 3 higher than the derived OH mixing ratios from variability analysis and the Spivakovsky model study. No explanation could be found. Only 2 direct measurement campaigns of OH were made on the Antarctic continent and are available for comparison. More research would be necessary to evaluate the photochemical mechanisms for a remote region such as the Antarctic.

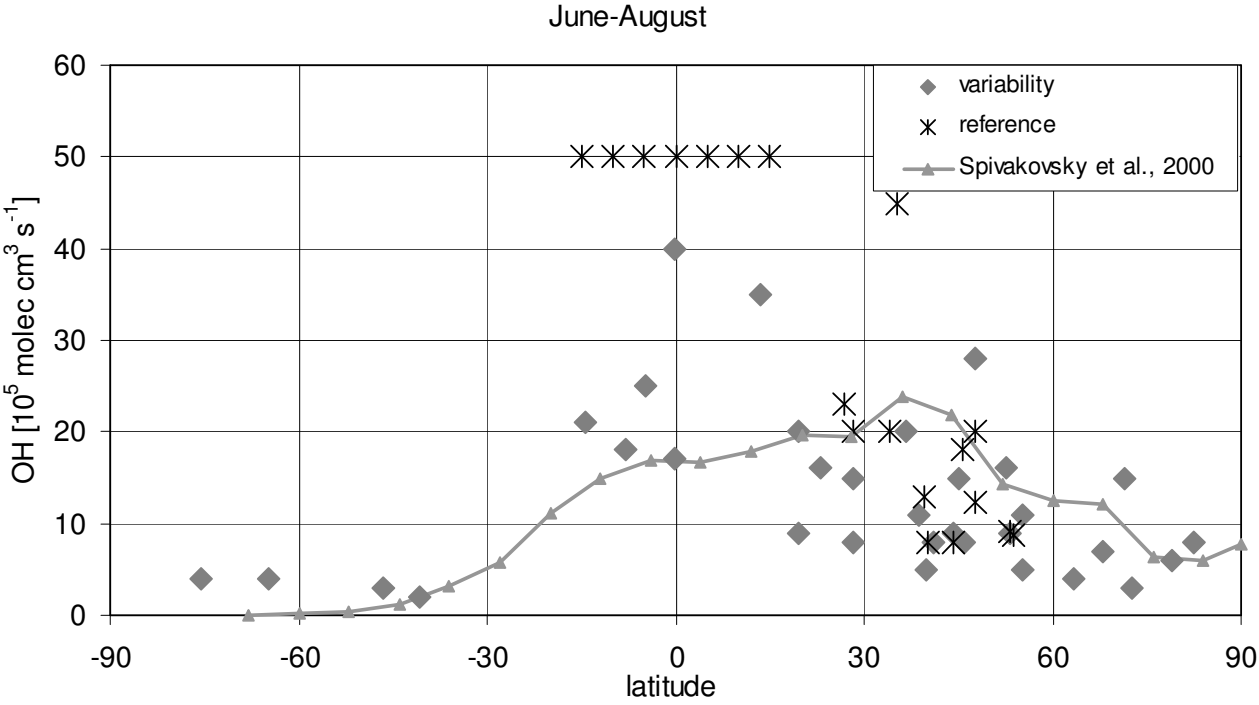

Figure 5.14: Estimated latitudinal OH mixing ratio from June to August derived by variability analysis (diamonds). Crosses indicate OH mixing ratios determined by direct OH measurements (references, see table 5.1); Solid line represents OH distribution calculated by Spivakovsky et al., 2000.

Unfortunately, most intensive field campaigns were conducted during the hemispheric summers so that no winter OH measurements are available for comparison. However, the comparisons on hand generally support the validity of the variability analysis in the estimation of the average OH mixing ratio and indicate that the OH distribution derived by this method is a reasonable representation of the atmospheric OH distribution.

Cl Radical:

Table 5.4: Evaluation of the impact of OH and Cl radical chemistry on atmospheric NMHC variability

Station	marine	Cl only Jun-Aug		OH only Jun-Aug	
		R squared	slope	R squared	slope
ALT	X	0.0926	-0.4276	0.6625	-0.4938
AMT		0.7443	-0.7037	0.4106	-0.2257
ASC	X	0.1708	-0.3659	0.9124	-0.3651
ASK		0.1254	-0.3628	0.914	-0.4228
AZR	X	0.1771	-0.2973	0.6446	-0.2449
BAL	X	0.0558	-0.2719	0.6575	-0.4029
BKT		0.0295	-0.12	0.8186	-0.2731
BRW	X	0.0006	-0.0166	0.526	-0.2067
BSC		0.1343	-0.2801	0.2449	-0.1633
CBA	X	0.3112	-0.5443	0.9347	-0.4072
CGO	X	0.2028	-0.6066	0.9039	-0.553
CRZ	X	0.516	-1.0728	0.8989	-0.6114
GMI	X	0.2243	-0.4823	0.9365	-0.4254
HBA	X	0.7312	-1.0744	0.8782	-0.5861
HPB		0.1003	-0.2886	0.7791	-0.3474
ICE	X	0.2545	-0.5638	0.8234	-0.4379
IZO	X	0.2363	-0.3319	0.9028	-0.2801
KUM	X	0.2233	-0.5696	0.8686	-0.485
LEF		0.5581	-0.5189	0.5391	-0.2202
MHD	X	0.0474	-0.2364	0.6563	-0.3798
MID	X	0.4256	-1.1351	0.805	-0.674
MKN		0.2727	-0.6898	0.957	-0.5579
MLO		0.0727	-0.2353	0.86	-0.3494
OXK		0.0255	-0.1606	0.6059	-0.3377
PAL		0.2776	-0.8501	0.7985	-0.6225
PSA	X	0.022	-0.1989	0.7534	-0.5023
SEY	X	0.2806	-0.4048	0.9056	-0.3242
SGP		0.1677	+0.3047	0.2145	-0.1488
SHM	X	0.1829	-0.4183	0.8305	-0.3849
SMO	X	0.2793	-0.707	0.8936	-0.546
SPO		0.6926	-0.7263	0.7296	-0.4711
SUM		0.2776	-0.6568	0.9566	-0.5265
THD	X	0.205	-0.5432	0.8577	-0.4797
UTA		0.0785	-0.3714	0.7177	-0.485
ZEP	X	0.068	-0.3029	0.7245	-0.4268
mean (marine)		0.2140	-0.4805	0.7717	-0.4190
mean (terrestrial)		0.2541	-0.4588	0.6819	-0.3680
mean (total)		0.2361	-0.4864	0.7578	-0.4105

The relationship between atmospheric variability of C2 to C5 NMHC and the respective atmospheric lifetimes with exclusive regard to either OH or Cl was investigated due to

recent results indicating wide spread Cl radical chemistry (Pszenny et al., 2007, Arsene et al., 2007). The analytical parameters for the regression slope with respect to both atmospheric oxidants are presented in Table 5.4.

The good correlation between C2 – C5 NMHC and OH is obvious (R^2>0.8) as seen above. However, only poor correlation was found between NMHC variability and lifetime with respect to Cl. Cl chemistry as a sink for NMHC might only be of importance within the marine planetary boundary layer while the majority of air mass transport is found in the free troposphere. Similarly the major source for atmospheric Cl radicals was found to be photolytic release of Cl radicals from sea salt aerosol. Conclusively, Cl radical chemistry represents only a minor sink for NMHC on a global scale but may be the dominant sink in selected isolated environments. Further evidence for this assessment is provided in figure 5.8. The isobutane/butane ratio was found to be generally flat and featureless again indicating that no wide spread Cl oxidative chemistry exists.

5.4 Conclusions

In this research article we have presented the global atmospheric distribution of four NMHC (ethane, propane, isobutane and butane) over a 1.7 year timespan. The presented profiles are the first to be compiled with one single method and, to our knowledge, the first global distribution profiles for both butane and isobutane. A comparison with previously published timeseries indicates a declining trend of the ethane mixing ratio of about 2.5% yr^{-1} in the northern troposphere over the past two decades (Rudolph et al., 1995, Gautrois et al., 2003).

Variability analysis was used to assess the available data in terms of local influence. Southern hemispheric stations showed strong remoteness from sources. Mid latitude northern hemispheric stations were found more influenced by local pollution sources. A clear latitudinal distribution of the “A” factor was found and linked to convective events. The average seasonal OH mixing ratios for both hemispheres and the tropics were calculated: NH (20°N to 90°N) summer: 11.4 10^5 molec cm^{-3}, winter: 6.8 10^5 molec cm^{-3}; SH (20°S-90°S) summer: 4.5 molec cm^{-3}, winter 3.2 10^5 molec cm^{-3}, tropical regions 40 10^5 molec cm^{-3} (yearly average). These estimates agree well (within 20 to 50%) with previously

published measurement data and the global OH distribution presented by Spivakovsky et al., 2000. This comparison shows that the variability analysis is a viable tool to estimate the average OH mixing ratio an airsample was exposed to during transport to a measuring station.

5.5 Acknowledgements

This project was funded by ESRL GMD. David Tanner and Jacques Hueber (INSTAAR) assisted with the instrumental development. Ken Masarie (ESRL) helped with the database management. E. Dlugokencky, P. Novelli, P. Lang (all ESRL) provided trace gas data. The authors wish to thank the sampling personnel across the globe and the NOAA flask team; without their efforts this work would not have been possible.

6 Conclusion and future perspectives

The main objective of this work was to improve the understanding of the global distribution of non-methane hydrocarbons (NMHC) and to provide constrains on the global hydroxyl radical cycle based on these measurements. For this task we were given access to whole air flask samples from the NOAA cooperative air sampling network. In total flasks from 37 measurement stations were available for this study. The sampling locations span from 82 °N (Alert, Canada) to 90 °S (Amundsen Scott Station, Antarctica).

After the development of an automated and computer controlled GC system, 3402 flasks (~1500 pairs and 400 individual flasks) were analyzed over the period of 18 months. The sampling air was analyzed for C2-C6 saturated NMHC. Other important atmospheric trace gases as well as their isotopic composition were measured from the same atmospheric airsample by different laboratories namely: CO_2, CO, CH_4, N_2O, H_2, SF_6 and $^{13}CO_2$, $^{13}CH_4$, CH_3D. These concurrent measurements were used in combination with the NMHC measurements to constrain the global hydroxyl radical cycle. Here we summarize the conclusions from chapter 2 – 5 based on the research objectives defined in chapter 1.

Development of a gas chromatographic flame – ionization (GC-FID) system for the analysis of sum-ambient pressure low volume flask samples: In chapter 2 we focus on the instrumental development of a cryogen – free GC FID system for the flask analysis. A detailed investigation of potential solid adsorbents for the development of a cryogen free micro trap for the gas – chromatographic system is presented. Two adsorbent choices (Carboxen 1000 and a three – stage combination of Carbosieve S III, Carboxen 563 and Carboxen 1016) for the quantification of the widest range of analytes were presented. A wide linear response for most compounds was determined. The trapping temperature had to be below -25 °C to ensure 100% recovery for C2 compounds. However, the breakthrough volume for acetylene was exceeded early, below the typical flask sampling volumes.

In chapter 4 the suitability of glass network flasks in NMHC analysis is investigated. NMHC were stable in the network flasks (< 5% deviation from the reference) over a storing

time of at least one year. Inward contamination could not be found. Internal flask pressure fluctuations were found to not affect the recovery of NMHC.

Evaluation of analytical interferences: The effect of water vapor on NMHC measurements by solid adsorption GC – FID were investigated in chapter 2. Atmospheric water vapor was found to significantly interfere with the analysis of NMHC. Elevated water vapor affect the quantification in two ways: 1, The effective sampling volume may be reduced due to freeze-out of water inside the trap leading to increased sampling flow resistance up to complete blockage and 2, Water may occupy the micropores of the carbon molecular sieves thus reducing the trapping efficiency. It was found that the sampling air had to be cooled to a dewpoint of less than -10 °C to avoid this interference. A self – regenerating automated water trap was successfully developed for this instrument.

Several carbon molecular sieves proved to be an internal contamination source for benzene and toluene. Carboxen 1000 was found to have low aromatic contamination and was therefore chosen as primary adsorbent in the further applications.

The effect of ozone during the solid adsorption of biogenic NMHC was investigated in chapter 3. Substantial sampling losses of up to 95% were found even at ozone levels of 20 ppb. These loss rates were found to be proportional to the number of double bonds in the individual molecules. Consequently, it was concluded that co-sampling of ozone will not interfere with the quantification of saturated C2-C6 NMHC. We found in chapter 4 that hexane cannot be determined accurately due to coelution of this compound with dichloromethane (CH_2Cl_2). Additionally, it was found that propene could not be quantified as significant growth of this compound was found in the flasks. Therefore only saturated C2-C5 compounds and ethene were regarded for this thesis.

Analytical accuracy and precision: The analytical parameters reproducibility and repeatability were evaluated in section 4. The NMHC flask measurements were found to follow the WMO – GAW data quality directive as detailed in the GAW report, 2007. Intercomparison and standard comparison exercises were conducted with two local and one international laboratory. Summarized, 87% of the datapoints were found to adhere to the directive. Smaller problems still persist with the ethane precision as only 70% of the

datapoints are in agreement with the directive. Three further compounds (isoprene, benzene, and toluene) that were not regarded in the previous sections were found to follow the GAW standards and will be included in future flask measurements.

Flask Measurements of C2 – C5 NMHC: The global distributions of four NMHC (ethane, propane, isobutane and butane) as measured from the cooperative flask network are shown in chapter 5. These results on the global distribution of OH are to our knowledge the first to be compiled by a single instrument and method (ethane, propane) and the first ever to be presented for butane isomers. A comparison of the derived ethane distribution with earlier work (Rudolph, 1995) showed a significant reduction in the atmospheric ethane by approximately 2.5% yr^{-1} or 30% in total since the late 1980s early 1990s in agreement with Gautrois et al., 2003 and Plass-Dülmer et al., 2007). These and future NMHC measurements from the NOAA cooperative network will be made available to the general research community shortly. The analysis of the butane isomer ratio on a global scale revealed a rather feature less plain at a ratio of isobutane/ butane = 0.5. This suggests that chlorine radical oxidative reactions are not of significance on a global scale.

Evaluation of the OH distribution by variability analysis: The variability analysis was used to estimate the 24h average OH mixing ratio an airsample was exposed to during transport following the method of Williams et al., 2001. Good agreement between our estimations and model calculations by Spivakovsky et al., 2000 were found. Similarly good agreement was found between our OH mixing ratios and local direct OH measurements. Large discrepancy was found in the tropics where our estimations and direct OH measurements suggest significantly higher OH mixing ratios than predicted by model calculations.
The main achievements can be summarized as follows:

- We have developed an analytical method to reliably and reproducibly quantify NMHC from the NOAA cooperative air sampling network.
- We have presented a unique dataset representing the global background mixing ratios of NMHC.

- It was confirmed that trends seen at local stations in the atmospheric burden of ethane (Gautrois et al., 2003, Plass Dülmer, personal conversation, 2007) persist on a global scale.
- We have estimated the local OH mixing ratios at individual stations, improving our understanding of atmospheric oxidation chemistry

Recommendations for future research: Based on the results presented in this work we suggest directions for future research on this topic.

In chapter 2 of this thesis we show the low breakthrough volume of the biomass burning tracer acetylene making its quantification currently not possible. Similarly, hexane cannot be analyzed due to coelution problems (chapter 4). Three additional compounds (isoprene, benzene and toluene, chapter 4) were proven to be quantifiable with acceptable accuracy. We suggest to perform instrumental changes to reliably quantify specifically acetylene and if possible hexane. Aromatic compounds as tracers for anthropogenic pollutions should be included into the routine measurements. Isoprene should be included in the regular data analysis as a tracer for photosynthetic activity. A detailed knowledge of isoprene could help to further constrain the global carbon cycle with respect to photosynthetic activity.

The benefits of intercomparison campaigns as detailed in chapter 4 were clearly visible. The documentation of data quality guide lines by Rappenglück et al., 2006 and GAW report, 2007 were helpful to characterize the analytical parameters. Further international intercomparison efforts should be conducted and the efforts of the GAW community towards a world calibration center (WMO report, 1995) should be pursuit with highest priority.

In parallel to the NMHC measurements several other trace gases as well as the isotopic composition of selected trace gases is measured. It can be expected that further research with respect to these measurements from the same air sample will yield important results to further improve our understanding of atmospheric chemistry.

Most importantly we think that high priority should be placed on the continuation of this project as we expect to gain further knowledge on atmospheric processes if multi-year dataseries would be available. The presented data set (chapter 5) contains a large amount

of information both on a global scale and regional scale (individual stations) that could not be addressed within the limits of this thesis. We suggest making this data available to the atmospheric research community for their respective needs and applications. We propose that individual stations could be analyzed with the tools presented by Parrish et al., 1994, 1996. The results of the global distribution of NMHC can be used in detailed comparison with global scale climate models to further validate these important scientific tools. Additionally these measurements can be used to further investigate the global hydroxyl radical cycle and potentially estimate the robustness of its atmospheric budget.

7 Summary

This thesis focuses on global scale measurements of light reactive non-methane hydrocarbon (NMHC), in the volatility range from ethane to toluene with a special focus on ethane, propane, isobutane, butane, isopentane and pentane. Even though they only occur at the ppt level in the remote troposphere these species can yield insight into key atmospheric processes. 1. Selected hydrocarbons and hydrocarbon ratios were identified as tracers for anthropogenic pollution. 2. Elevated NMHC mixing ratios are necessary to enable ground layer ozone formation. 3. Due to their high reactivity towards atmospheric tracers such as the nitrate ($\bullet NO_3$), chlorine ($\bullet Cl$) and hydroxyl radical ($\bullet OH$) NMHC can serve as ideal tracers to assess the oxidation capacity of the atmosphere. However at the beginning of this work no long term global scale NMHC measurements derived from a single analytical method were available. The global distribution of these atmospheric key species remained largely unknown or was associated with large errors because an integrative approach over multiple large scale field campaigns was necessary.

The overall aim of this thesis was to enhace our knowledge of the global background distribution of light NMHC. This data then was to be applied to derive constraints for the global atmospheric oxidation chemistry. To meet this aim we were given access to whole air flask samples taken from the NOAA – ESRL cooperative air sampling network. In total we had access to samples from 40 stations spanning from 90° South (Amundsen Scott Station, Antarctica) to 82° North (Alert Station, Canada). Most stations were located within the (marine) boundary layer.

Trace gas measurements from the regular network operations (CO, CH_4, H_2, SF_6) were made available by ESRL and provided important reference point to assess the age, transport and oxidation chemistry and airmass was exposed to during transport to the sampling stations.

The specific scientific objectives can be summarized as follows

1. The development of a gas-chromatographic flame – ionization (GC – FID) system capable to meet the above challenges, especially focusing on designing a highly automated system with high sample throughput at low operational costs.

2. Evaluate potential analytical interferences by other trace gases particularly ozone and atmospheric water vapor

3. The establishment of a reproducible calibration for this instrument and the evaluation of analytical parameters (accuracy and precision) with particular emphasis on intercomparisons with other laboratories

4. Obtaining a full year of NMHC measurements from the network flasks with extensive meridional coverage to assess the global distribution of the most important NMHC

5. Evaluate the measurements with respect to atmospheric oxidation chemistry applying analytical techniques such as the variability analysis

The first research objective is addressed by describing the instrumental set-up and the method development in chapter 2. The investigation of multiple adsorbent materials for the design of a microtrap is investigated. This microtrap had to be optimized to be operational in a highly automated system with a large sample throughput and useable without the application of an expensive coolant such as liquid nitrogen. Two set-ups were found suitable under these conditions a: a three stage trap (Carboxen 1016, Carboxen 563, Carbosieve SIII) and a single stage trap (Carboxen 1000) both traps had to be cooled to -30 °C.

Analytical interferences by other atmospheric trace gases were investigated in chapters 2 and 3. Atmospheric water vapor was found to be a major interference for light NMHC (chapter 2). The recovery ratios for light NMHC such as ethane and propane were

significantly reduced. However, heavier NMHC (pentane isomers or hexane) were recovered at much higher ratios. Atmospheric water vapor was found to occupy micropores in the molecular sieves. A sampling volume decrease was observed for air samples with a dew point of 10 °C or higher. Water was found to freeze out inside the microtrap, increasing the flow resistance to a complete flow stoppage. A fully automated regenerating watertrap was developed to control water vapor interference. It was determined that an atmospheric whole air sample needs to be at a dewpoint of less than -25 °C to avoid any analyte losses during whole air solid adsorption sampling.

Ozone was found to be a major interference when sampling unsaturated biogenic volatile organic compounds (BVOC) with a solid adsorption, thermal desorption technique. Analyte losses due to reaction with ozone were found proportional to the available number of doublebonds. Significant interferences during light saturated NMHC analysis as presented in this thesis were not expected.

The analytical parameters accuracy and precision were determined in chapter 4. Several standard and reference gas comparisons with local partner laboratories showed that the described method follows the WMO GAW data quality objective for 90% of the measurements for C2 to C5 NMHC. Hexane was systematically overestimated because of coelution with dichloromethane. This chapter yielded evidence that the previously disregarded compounds isoprene, benzene and toluene may be quantified with acceptable accuracy and precision.

The glass flasks, the whole air sampling methods and the analytical path were investigated extensively for sources of systematical sample contamination. An intercomparison with the GAW station at Hohenpeissenberg was organized. Air samples were subject to the standardized treatment through ESRL before the quantification of NMHC. It was shown that the NMHC quantification for C2 to C5 NMHC and for isoprene, benzene and toluene meets the GAW data quality guideline by 90% or better. The whole air flask NMHC measurements are an accurate representation of local NMHC mixing ratios during the sampling period.

The global distribution of ethane, propane, isobutane and butane over 15 months is documented in chapter 5. A clear seasonal cycle and a strong interhemispheric gradient were identified. Highest mixing ratios were found in the late hemispheric winter months.

NMHC minima were documented for the late hemispheric winter. Maximum background mixing ratios of 2500 pptv (ethane), 1000 pptv (propane), 150 pptv (isobutane) and 300 pptv (butane) were found during late winter in the high northern latitudes. A comparison with previous results suggested a large decline (~30%) in the atmospheric ethane burden since the late 1980s. The results represent to my knowledge the first ever global background distribution data for ethane and propane acquired with one single analytical instrument and method. For the first time ever the global distribution data for the butane isomers is documented.

This dataset combined with other trace gas measurements made available by ESRL were utilized to determine the 24h average OH radical mixing ratio an airsample was exposed to during transport to the individual sampling stations. This analysis was conducted by a further developed variability analysis method based. Sulfurhexafluoride was used as a reference point since it is non-reactive towards OH. The derived OH mixing ratios were compared to direct OH measurements from intensive field campaigns and from model calculations. Generally good agreement was found between measured and variability derived OH mixing ratios. However, the comparison with the model showed a discrepancy in the tropical regions. The measured as well as the here presented OH data were significantly higher than derived by the model calculations.

In summary this thesis yielded a unique and continuously growing dataset to describe the global distribution of light NMHC. A novel method to estimate OH mixing ratios was successfully applied. The main advantage of this method was the independence of source strength estimates. I hope that this measurement program will continue for years to come. I expect that a multitude of new insights into atmospheric chemistry will be presented with the help of these measurements.

8 Bibliography

van Aardenne J.A., Dentener F.J., Olivier J.G.J., Goldewijk C.G.M.K., Lelieveld J., 2001. A 1 degrees x 1 degrees resolution data set of historical anthropogenic trace gas emissions for the period 1890-1990. Global Biogeochemical Cycles, 15, 909-928.

Angelopoulos N.G., Chamberlain K., Pickett J.A., 2000. Factors affecting volatile emissions of intact potato plants, Solanum tuberosum: variability of quantities and stability of ratios. Journal of Chemical Ecology 26, 497-511.

Apel E.C., Calvert J.G., Gilpin T.M., Fehsenfeld F., Lonneman W.A., 2001. Nonmethane Hydrocarbon Intercomparison Experiment (NOMHICE): Task 4, ambient air. Journal of Geophysical Research, 108, Art. No. 4359.

Ariya P.A., Jobson B.T., Sander R., Niki H., Hopper J.F., Anlauf K.G., 1998. Measurements of C-2-C7 hydrocarbons during the Polar Sunrise Experiment 1994: Further evidence for halogen chemistry in the troposphere. Journal of Geophysical Research, 103, 13169-13180.

Armerding W., Comes F.J., Crawack H.J., Forberich O., Gold G., Ruger C., Spiekermann M., Walter J., Cuevas E., Redondas A., Schmitt R., Matuska P., 1997. Testing the daytime oxidizing capacity of the troposphere: 1994 OH field campaign at the Izana Observatory, Tenerife. Journal of Geophysical Research, 102, 10603-10611.

Arsene C., Bougiatioti A., Kankidou M., Bonsang B., Mihalopoulos N., 2007. Tropospheric OH and Cl levels deduced from non-methane hydrocarbon measurements in a marine site. Atmospheric Chemistry and Physics Discussions, 7, 6329-6356.

Atkinson R., Baulch D.L., Cox R.A., Hampson R.F., Kerr J.A., Troe J., 1989. Evaluated kinetic and photochemical data for atmospheric chemistry .3. IUPAC subcommittee on gas kinetic data evaluation for atmospheric chemistry. Journal of Physical and Chemical Reference Data, 18, 881-1097.

Atkinson R., 1990. Gas-phase tropospheric chemistry of organic compounds: a review. Atmospheric Environment, 24, 1-41.

Atkinson R., 1991. Kinetics and mechanisms of the gas-phase reactions of the NO3 radical with organic compounds. Journal of physical and chemical reference data, 20, 459-507.

Atkinson R., Aschmann S.M., 1993. Atmospheric chemistry of the monoterpene reaction-products nopinone, camphenilone, and 4-acety-1-methylcyclohexene. Journal of Atmospheric Chemistry, 16, 337-348.

Atkinson R., 1994. Gas-phase tropospheric chemistry of organic compounds. Journal of Physical and Chemical Reference Data, 2, 1-216.

Atkinson R., Arey J., Aschmann S.M., Corchnoy S.B., Shu Y.H., 1995. Rate constants for the gas-phase reactions of cis-3-hexen-1-ol, cis-3-hexenylacetate, trans-2-hexenal, and linalool with OH and NO3 radicals and O-3 at 296 +/- 2K, and OH radical formation yields from the O-3 reactions. International Journal of Chemical Kinetics, 27, 941-955.

Badol C., Borbon A., Locoge N., Léonardis T., Galloo J.C., 2004. An automated monitoring system for VOC ozone precursors in ambient air: development, implementation and data analysis. Anal. Bioanal. Chem. 378, 1815-1827.

Barletta B., Mainardi S., Rowland F.S., Chan C.Y., Wang X.M., Zou S.C., Chan L.Y., Blake D.R., 2005. Volatile organic compounds in 43 Chinese cities. Atmospheric Environment, 39, 5979-5990.

Bartelt R.J., Wicklow D.T., 1999. Volatiles from *Fusarium verticillioides* (Sacc.) Nirenb. and their attractiveness to nitidukid beetles. Journal of Agricultural and Food Chemistry 47, 2447-2454.

Bartenbach S., Williams J., Plass-Dülmer C., Berresheim H., Lelieveld J., 2007. In-situ measurement of reactive hydrocarbons at Hohenpeissenberg with comprehensive two-dimensional gas chromatography (GC x GC-FID): use in estimating HO and NO3. Atmospheric Chemistry and Physics, 7, 1-14.

Batterdam S.A., Peng C., Braun J., 2002. Levels and compositions of volatile organic compounds on commuting routes in Detroit, Michigan. Atmospheric Environment, 36, 6015-6030.

Berresheim H., Plass Dülmer C., Elste T., Mihapoulos N., Rohrer F., 2003. OH in the coastal boundary layer of Crete during MINOS: Measurements and relationship with ozone photolysis. Atmospheric Chemistry and Physics, 3, 639-649.

Bertschi I.T., Yokelson R.J., Ward D.E., Christian T.J., Hao W.M., 2003a. Trace gas emissions from the production and use of domestic biofuels in Zambia measured by open-path Fourier transform infrared spectroscopy. Journal of Geophysical Research, 108, Art. No. 8469.

Bertschi I.T., Yokelson R.J., Ward D.E., Babbitt R.E., Susott R.A., Goode J.G., Hao W.M., 2003. Trace gas and particle emissions from fires in large diameter and belowground biomass fuels. Journal of Geophysical Research, 108, Art. No. 8472.

Betz W.R., Supina W.R., 1989. Determination of the gas- chromatographic performance-characteristics of several graphitized carbon-blacks. Journal of Chromatography, 471, 105-112.

Blake D.R., Hurst D.F., Smith T.W., Whipple W.J., Chen T.Y., Blake N.J., Rowland F.S., 1992. Summertime measurements of selected nonmethane hydrocarbons in the Arctic and sub-Arctic during the 1988 Arctic Boundary Layer Expedition (ABLE-3A). Journal of Geophysical Research, 97, 16559-16588.

Blake D.R., Chen T.Y., Smith T.Y., Wang C.J.L., Wingenter O.W., Blake N.J., Rowland F.S., Mayer E.W., 1996. Three-dimensional distribution of nonmethane hydrocarbons and halocarbons over the northwestern Pacific during the 1991 Pacific Exploratory Mission (PEM-West A). Journal of Geophysical Research, 101, 1763-1778.

Blake N.J., Blake D.R., Sive B.C., Chen T.Y., Rowland F.S., Collins J.E., Sachse G.W., Anderson B.E., 1996. Biomass burning emissions and vertical distribution of atmospheric methyl halides and other reduced carbon gases in the South Atlantic region. Journal of Geophysical Research-Atmospheres 101, 24151-24164.

Blake N.J., Blake D.R., Sive B.C., Katzenstein A.S., Meinardi, S., Wingenter O.W., Atlas E.L., Flocke F., Ridley B.A., Rowland F.S., 2003. The seasonal evolution of NMHCs and light alkyl nitrates at middle to high northern latitudes during TOPSE. Journal of Geophysical Research, 108, Art. No. 8359.

Bicchi C., D'Amato A., David F., Sandra P., 1989. Capturing of volatiles emitted by living plants by means of thick film open tubular traps. Journal of High Resolution Chromatography Communications 12, 316-321.

Boissard C., Bonsang B., Kanakidou M., Lambert G., 1996. TROPOZ II: global distribution and budgets of methane and light hydrocarbons. Journal of Atmospheric Chemistry, 25, 115-148.

Bonsang and Boissard, 1999. Global distribution of reactive hydrocarbons in the atmosphere. in N. Hewitt (editor) Reactive hydrocarbons in the atmosphere, Academic Press, San Diego.

Borbon A., Fontaine H., Locoge N., Veillerot M., Galloo J.C., 2003. Developing receptor-oriented methods for non-methane hydrocarbon characterization in urban air – Part 1: source identification. Atmospheric Environment, 37, 4051-4064.

Borbon A., Coddeville P., Locoge N., Galloo J.C., 2004. Characterising sources and sinks of rural VOC in eastern France. Chemosphere, 57, 931-942.

Boudries H., Bottenheim J.W., 2000. Cl and Br atom concentration during a surface boundary layer ozone depletion event in the Canadian high Arctic. Geophysical Research Letters, 27, 517-520.

Bousquet P., Hauglustaine D.A., Peylin P., Carouge C., Ciais P., 2005. Two decades of OH variability as inferred by an inversion of atmospheric transport and chemistry of methyl chloroform. Atmospheric Chemistry and Physics, 5, 2635-2656.

Bowyer J.R., Pleil J.D., 1995. Supercritical Fluid Extraction as a means of as a means of cleaning and desorbing common air sampling sorbents. Chemosphere 31, 2905-2918.

Brauers T., Hausmann M., Bister A., Kraus A., Dorn H.P., 2001. OH radicals in the boundary layer of the Atlantic Ocean 1. Measurements by long-path laser adsorption spectroscopy. Journal of Geophysical Research, 106, 7399-7414.

Buttery R.G., Xu C., Ling L.C., 1985. Volatile components of wheat leaves (and stems): possible insect attractants. Journal of Agricultural and Food Chemistry 33, 115-117.

Calogirou A., Larsen B.L., Brussol C., Duane M., Kotzias D., 1996. Decomposition of terpenes by ozone during sampling on tenax. Analytical Chemistry 68, 1499-1506.

Calogirou A., Kotzias D., Kettrup A., 1997. Product analysis of the gas-phase reaction of β-caryophyllene with ozone. Atmospheric Environment 31, 283-285.

Cao X.-L., Hewitt C.N., 1994. Study of the degradation by ozone of adsorbents and hydrocarbons adsorbed during the passive sampling of air. Environmental Science and Technology 28, 757-762.

Cardenas L.M., Austin J.F., Burgess R.A., Clemitshaw K.C., Dorling S., Penkett S.A., Harrison A.R.M., 1998. Correlations between CO, NOy, O-3, and non- methane hydrocarbons and their relationship with meteorology during winter 1993 on the North Norfolk Coast, UK. Atmospheric Environment, 32, 3339-3351.

Christensen C.S., Skov H., Palmgren F., 1999. C-5-C-8 non-methane hydrocarbon measurements in Copenhagen: concentrations, sources and emission estimates. Science of the Total Environment, 236, 163-171.

Ciccioli P., Brancaleoni E., Frattoni M., Di Palo V., Valentini R., Tirone G., Seufert G., Bertin N., Hansen U., Csiky O., Lenz R., Sharma M., 1999. Emission of reactive terpene compounds from orange orchards and their removal by within canopy processes. Journal of Geophysical Research, 104, 8077-8094.

Clemitshaw K.C., 2004. A review of instrumentation and measurement techniques for ground-based and airborne field studies of gas-phase tropospheric chemistry. Critical Reviews in Environmental Science and Technology, 34, 1-108.

Conway T., Tans P.P., Waterman L.S., Thoning K.W., 1994. Evidence for interannual variability of the carbon-cycle from the National-Oceanic-and-Atmospheric-Administration Climate-Monitoring-and-Diagnostics-Laboratory global-air-sampling-network. Journal of Geophysical Research, 99, 22831-22855.

Creasey D.J., Heard D.E., Lee J.D., 2001. OH and HO2 measurements in a forested region of north-western Greece. Atmospheric Environment, 35, 4713-4724.

Creasey D.J., Evans G.E., Heard D.E., Lee J.D., 2003. Measurements of OH and HO2 concentrations in the Southern Ocean marine boundary layer. Journal of Geophysical Research, 108, Art. No. 4475.

Derwent R.G., Davies T.J., Delaney M., Dollard G.J., Field R.A., Dumitrean P., Nason P.D., Jones B.M.R., Pepler S.A., 2000. Analysis and interpretations of the continuous hourly monitoring data for 26 C-2-C-8 hydrocarbons at 12 United Kingdom sites during 1996. Atmospheric Environment, 34, 297-312.

Dettmer K., Engewald W., 2002. Adsorbent materials commonly used in air analysis for adsorptive enrichment and thermal desorption of volatile organic compounds. Analytical and Bioanalytical Chemistry, 373, 490-500.

Dewulf J., van Langenhove H., 1999. Anthropogenic volatile organic compounds in ambient air and natural waters: a review on recent developments of analytical methodology, performance and interpretation of field measurements. Journal of Chromatography A, 843, 163-177.

Dlugokencky E.J., Masarie K.A., Lang P.M., Tans P.P., Steele L.P., Nisbet E.G., 1994. A dramatic decrease in the growth-rate of atmospheric methane in the northern hemisphere during 1992. Geophysical Research Letters, 21, 45-48.

Ehhalt D.H., Dorn H.P., Poppe D., 1991. The chemistry of the hydroxyl radical in the troposphere. Proceedings of the Royal Society Edinburgh B, 95, 9857-9571.

Ehhalt D.H., Rohrer F., Wahner A., Prather M.J., Blake D.R., 1998. On the use of hydrocarbons for the determination of tropospheric OH concentrations. Journal of Geophysical Research, 103, 18981-18997.

Eisele F.L., Mauldin R.L., Tanner D.J., Cantrell C., Kosciuch E., Nowak J.B., Brune B., Faloona I., Tan D., Davis D.D., Wang L., Chen G., 2001. Relationship between OH measurements on two different NASA aircraft during PEM Tropics B. Journal of Geophysical Research, 106, 32683-32689.

Engelberth J., Alborn H. T., Schmelz E.A., Tumlinson J.H., 2004. Airborne signals prime plants against herbivore attack. Proceedings of the National Academy of Science of the USA 101, 1781-1785.

Fabbri A., Crescentini G., Mangani F., Mastrogiacomo A.R., Bruner F., 1987. Advances in the determination of volatile organic-solvents and other organic pollutants by gas-chromatography with thermal desorption sampling and injection. Chromatographia, 23, 856-860.

Faloona I., Tan D., Brune W., Hurst J., Barket D., Couch T.L., Shepson P., Apel E., Riemer D., Thornberry T., Carroll M.A., Sillman S., Keeler G.J., Sagady J., Hooper D., Paterson K., 2001. Nighttime observation of anomalously high levels of hydroxyl radicals above a deciduous forest canopy. Journal of Geophysical Research, 106, 24315-24333.

Fastyn P., Kornacki W., Kardas M., Gawlowski J., Niedzielski J., 2003. Adsorption of water vapour from humid air in carbon molecular sieves: Carbosieve S-III and Carboxens 569, 1000 and 1001. Analyst, 128, 198- 203.

Ferretti D.F., Miller J.B., White J.W.C., Lassey K.R., Lowe D.C., Etheridge D.M., 2007. Stable isotopes provide global limits of aerobic methane emission from plants. Atmospheric Chemistry and Physics, 7, 237-241.

Fick J., Pommer L., Andersson B., Nilsson C., 2001, Ozone removal in the sampling of parts per billion levels of terpenoid compounds: An evaluation of different scrubber materials. Environmental Science and Technology, 35, 1458-1462.

Forberich O., Pfeiffer T., Spiekermann M., Walter J., Comes F.J., Grigonis R., Clemitshaw K.C., Burgess R.A., 1999. Measurement of the diurnal variation of the OH radical concentration and analysis of the data by modelling. Journal of Atmospheric Chemistry, 33, 155-181.

Fruekilde P., Hjorth J., Jensen N.R., Kotzias D., Larsen B., 1998. Ozonolysis at vegetation surfaces: A source of acetone, 4-oxopentanal, 6-methyl-5-hepten-2-one and geranylacetone in the troposphere. Atmospheric Environment, 32, 11, 1893-1998.

Gautrois M., Brauers T., Koppmann R., Rohrer F., Stein O., Rudolph J., 2003. Seasonal variability and trends of volatile organic compounds in the polar tropsphere. Journal of Geophysical Research, 108, Art. No. 4393.

Gawlowski J., Gierczak T., Jezo A., Niedzielski J., 1999. Adsorption of water vapour in the solid sorbents used for the sampling of volatile organic compounds. Analyst, 124, 1553-1558.

Gawrys M., Fastyn P., Gawlowski J., Gierczak T., Niedzielski J., 2001. Prevention of water vapour adsorption by carbon molecular sieves in sampling humid gases. Journal of Chromatography A, 933, 107-116.

George L.A., Hard T.M., O'Brien R.J., 1999. Measurement of free radicals OH and HO2 in Los Angeles smog. Journal of Geophysical Research, 104, 11643-11655.

Goldan P.D., Kuster W.C., Fehsenfeld F.C., 1997. Nonmethane hydrocarbon measurements during the Tropospheric OH Photochemistry Experiment. Journal of Geophysical Research, 102, 6315-6324.

Goldan P.D., Kuster W.C., Williams E., Murphy P.C., Fehsenfeld F.C., Meagher J., 2004. Nonmethane hydrocarbon and oxy hydrocarbon measurements during the 2002 New England air quality study. Journal of Geophysical Research, 109, Art. No. D21309.

Goldstein A.H., Wofsy S.C., Spivakovsky C.M., 1995. Seasonal variations of nonmethane hydrocarbons in rural New England: Constraints on OH concentrations in northern midlatitudes. Journal of Geophysical Research, 100, 21023-21033.

Goldstein A.H., Millet D.B., McKay M., Jaegle L., Horowitz L., Cooper O., Hudman R., Jacob D.J., Oltmans S., Clarke A., 2004. Impact of Asian emissions on observation at Trinidad Head, California during ITCT 2k2. Journal of Geophysical Research, 109, Art. No. D23S17.

Gros V., Williams J., van Aardenne J.A., Salisbury G., Hofmann R., Lawrence M.G., von Kuhlmann R., Lelieveld J., Krol M., Berresheim H., Lobert J.M., Atlas E., 2003. Origin of anthropogenic hydrocarbons and halocarbons measured in the summertime European outflow (on Crete in 2001). Atmospheric Chemistry and Physics, 3, 1223-1235.

Gros V., Williams J., Lawrence M.G., von Kuhlmann R., van Aardenne J., Atlas E., Chuck A., Edwards D.P., Stroud V., Krol M., 2004. Tracing the origin and ages of interlaced atmospheric pollution events over the tropical Atlantic Ocean with in situ measurements, satellites, trajectories, emission inventories and global models. Journal of Geophysical Research, 109, Art. No. 22306.

Grosjean D., Williams E.L., Grosjean E., Andino J.M., Seinfeld J.H., 1993. Atmospheric oxidation of biogenic hydrocarbons: Reaction of ozone with α-pinene, d-limonene and trans-caryophyllene. Environmental Science and Technology, 27, 2754-2758.

Guenther A., Archer S., Greenberg J., Harley P., Helmig D., Klinger L., Vierling L., Wildermuth M., Zimmerman P., Zitzer S., 1999. Biogenic hydrocarbon emissions and landcover/climate change in a subtropical savanna. Physics and Chemistry of the Earth Part B, 24, 659-667.

Hakola H., Laurila T., Lindfors V., Hellen H., Gaman A., Rinne J., 2001. Variation of the VOC emission rates of birch species during the growing season. Boreal Environment Research, 6, 237-249.

Hakola H., Hellen H., Laurila T., 2006. Ten years of light hydrocarbons (C-2-C6) concentration measurements in background air in Finland. Atmospheric Environment, 40, 3621-3630

Hamrud M., 1983. Residence time and spatial variability for gases in the atmosphere. Tellus B, 35, 295-303.

Handisides G.M., Plass Dülmer C., Gilge S., Bingemer H., Berresheim H., 2003. Hohenpeissenberg photochemical experiment (HOPE 2000): measurements and photostationary state calculations of OH and peroxy radicals. Atmospheric Chemistry and Physics, 3, 1565-1588.

Hansen U., Seufert G, 1999. Terpenoid Emission from citrus sinensis (L.) OSBECK under drought stress. Physics and Chemistry of the Earth Part B, 26, 681-687.

Heard D.E., Pilling M.J., 2003. Measurement of OH and HO2 in the troposphere. Chemical Reviews, 103, 5163-5198.

Heiden A.C., Hoffmann T., Kahl J., Kley D., Klockow D., Langebartels C., Mehlhorn H., Sandermann jr. H., Schraudner M., Schuh G., Wildt J., 1999. Emission of volatile organic compounds from ozone exposed plants. Ecological Applications 9, 1160-1167.

Helmig D., Schwarzer N., Steinhanses J., 1990. Flame control accessory for GC-FID operation with autosampler injection. HRC&CC, 13, 849-851.

Helmig D., Arey J., 1992. Organic chemicals in the air at Whitaker's forests/Sierra Nevada Mountains, California. Science of the Total Environment, 112, 233-250.

Helmig, D., Greenberg J., 1994. Automated in-situ gas chromatographic mass spectrometric (GC/MS) analysis of ppt level volatile organic trace gases using multistage solid adsorbent trapping. Journal of Chromatography A, 677, 123-132.

Helmig D., Vierling L., 1995. Water-adsorption capacity of the solid adsorbents Tenax TA, Tenax GR, Carbotrap, Carbotrap C, Carbosieve SIII, and Carboxen-569 and water management-techniques for the atmospheric sampling of volatile organic trace gases. Analytical Chemistry, 67, 4380-4386.

Helmig D., 1997. Ozone removal techniques in the sampling of atmospheric volatile organic trace gases. Atmospheric Environment, 31, 3635-3651.

Helmig D., Greenberg J., Guenther A., Zimmerman P., Geron C., 1997. Observation of biogenic emissions and their oxidation products at a forest side in Oak Ridge/TN. Proceesings of the 3rd Conference on Atmospheric Chemistry, 2-7 February, Long Beach, CA, Preprint Volume 141-142. American Meteorological Society.

Helmig, D., 1999. Air Analysis by Gas Chromatography. Journal of Chromatography A, 843, 129-146.

Helmig D., Klinger L.F., Guenther A., Vierling L., Zimmerman P., Geron C., 1999, Biogenic volatile organic compound emissions. I. Identifications from three sites in the U.S. Chemosphere, 38, 2163-2187.

Helmig D., Revermann T, Pollmann J., Kaltschmidt O., Jiménez Hernández A., Bocquet F. David D., 2003. Calibration system and analytical considerations for sesquiterpene determination in air. Journal of Chromatography A, 1002, 193-211.

Helmig D., Bocquet F., Pollmann J. Revermann T., 2004. Analytical techniques for sesquiterpene emission rate studies in vegetation enclosure experiments. Atmospheric Environment, 38, 557-572.

Hewitt, C.N. (editor), 1999. Reactive Hydrocarbons in the Atmosphere, Academic Press, London, ISBN 0123462401.

Hoffmann T., Jacop B., Linscheid M., Klockow D., 1993. Measurements of biogenic hydrocarbons and their atmospheric degradation in forests. International Journal of Environmental Analytical Chemistry, 52, 29-37.

Hoffmann T., 1995. Adsorptive preconcentration technique including oxidant scavenging for the measurement of reactive natural hydrocarbons in ambient air. Fresenius Journal of Analytical Chemistry, 351, 41-47.

Hoffmann T., Odum J.R., Bowman F., Collins D., Klockow D., Flagan R.C., Seinfeld J.H., 1997. Formation of organic aerosol from the oxidation of biogenic hydrocarbons. Journal of Atmospheric Chemistry, 26, 189-222.

Hooshiyar P.A., Niki H., 1995. Rate constants for the gas-phase reactions of Cl-atoms with C-2-C-8 alkanes at T=296+/-2 K. International Journal of Chemical Kinetics, 27, 1197-1206.

Huang J., Cardoza Y. J., Schmelz E. A., Raina R., Engelberth J., Tumlinson J.H., 2003. Differential volatile emissions and salicylic acid levels from tobacco plants in response to different strains of Pseudomonas syringae. Planta, 217, 767-775.

Jaenicke R., 1982. Physical aspects of the atmospheric aerosol in Chemistry of the Polluted and Unpolluted Troposphere, H.W. Georgi, W. Jaeschke (editors), 341-373, D. Reidek, Norwekk, MA, USA.

Janson R., Kristensson J., 1991. Sampling and analysis of atmospheric monoterpenes. In: *Report CM-79*, Department of Meteorology, Stockholm University, International Meteorological Institute in Stockholm, Stockholm, Sweden, Distribution by Library, Dept. of Meteorology, Stockholm University, Arrhenius Laboratory, S-10691.

Jefferson A., Tanner D.J., Eisele F.L., Davis D.D., Chen G., Huey J.W., Torres A.L., Berresheim H., 1998. OH photochemistry and methane sulfonic acid formation in the coastal Antarctic boundary layer. Journal of Geophysical Research, 103, 1647-1656.

Jobson B.T., Niki H., Yokouchi Y., Bottenheim J., Hopper F., Leaitch R., 1994. Measurements of C2-C6 hydrocarbons during the Polar Sunrise 1992 Experiment: Evidence for Cl atom and Br atom chemistry. Journal of Geophysical Research, 99, 25355-25368.

Jobson B.T., Wu Z., Niki H., Barrie L.A., 1994. Seasonal Trends of Isoprene, C-2-C-5 Alkanes, and Acetylene at a remote boreal site in Canada. Journal of Geophysical Research, 99, 1589-1599.

Jobson B.T., Parrish D.D., Goldan P., Kuster W. Fehsenfeld F.C., Blake D.R., Blake N.J., Niki H.,1998 Spatial and temporal variability of nonmethane hydrocarbon mixing ratios and their relation to photochemical lifetime. Journal of Geophysical Research, 103, 13557-13567.

Jobson B.T., McKeen S.A., Parrish D.D., Fehsenfeld F.C., Blake D.R., Goldstein A.H., Schauffler S.M., Elkins J.C.,1999. Journal of Geophysical Research, 104, 16091-16113.

Jorgensen A.D., Picel K.C., Stamoudis V.C., 1990. Prediction of gas-chromatography flame ionization detector response factors from molecular - structures. Analytical Chemistry, 62, 683-689.

Junge C.E., 1974. Residence time and variability of tropospheric trace gases. Tellus, 26, 477-488.

Jüttner F., 1988. A cryotrap technique for the quantification of monoterpenes in humid and ozone rich forest air. Journal of Chromatography, 442, 157-162.

Kanaya Y., Sadanaga Y., Nakamura K., Akimoto H., 2001. Behavior of OH and HO2 radicals during the observations at a remote island of Okinawa (ORION99) field campaign 1. Observations using laser-induced fluorescence instrument. Journal of Geophysical Research, 106, 24197-24208.

Karbiwnyk C.M., Mills C.S., Helmig D., Birks J.W., 2002. Minimization of water vapor interference in the analysis of non methane volatile organic compounds by solid adsorbent sampling. Journal of Chromatography A, 958, 219-229.

Karl T., Crutzen P.J., Mandl M., Staudinger M., Guenther A., Jordan A., Fall R., Lindinger W., 2001. Atmospheric Environment, 35, 5287 – 5300.

Karst U., Binding N., Cammann K., Witting U., 1993. Interferences of nitrogen dioxide in the determination of aldehydes and ketones by sampling on 1,4-dinitrophenyl-hydrazine-coated solid adsorbent. Fresenius Journal of Analytical Chemistry, 345, 48-52.

Keppler F., Hamilton J.T.G., Brass M., Rockmann T., 2006. Methane emissions from terrestrial plants under aerobic conditions. Nature, 439, 187-191.

Kim H.J., Kim K., Kim N.S., Lee D.S., 2000. Determination of floral fragrances of Rosa hybrida using solid-phase trapping-solvent extraction and gas chromatography-mass spectrometry. Journal of Chromatography, 902, 389-404.

Kim E., Brown S.G., Hafner H.R., Hopke P.K., 2005. Characterization of non-methane volatile organic compounds in Houston during 2001 using positive matrix factorization. Atmospheric Environment, 39, 5934-5946.

Klenø J.G., Wolkoff P., Clausen P.A., Wilkins C.K., Pedersen T., 2002. Degradation of the adsorbent Tenax TA by Nitrogen Oxides, Ozone, Hydrogen Peroxide, OH Radical and Limonene Oxidation Products. Environmental Science and Technology, 36, 4121-4126.

Köllner T.G., Schnee C., Gershenzon J., Degenhardt J., 2004. The sesquiterpene hydrocarbons of maize (Zea Mays) from five groups with distinctive developmental and organ-specific distribution. Phytochemistry, 65, 1895-1902.

Komenda M., Parusel E., Wedel A., Koppmann R., 2001. Measurements of biogenic VOC emissions: sampling, analysis and calibration. Atmospheric Environment 35, 2069-2080.

Komenda M., Schaub A., Koppmann R., 2003. Description and characterization of an on-line system for long-term measurements of isoprene, methyl vinyl ketone and methacrolein in ambient air, Journal of Chromatography A, 995, 185-201.

König G., Brunda M., Puxbaum H., Hewitt C.N., Duckham S.C., 1995. Relative contribution of oxygenated hydrocarbons to the total biogenic VOC emissions of selected mid-European agricultural and natural plant species. Atmospheric Environment, 29, 861-874.

Konrad S., Schmitz T., Buers H.-J., Houben N., Mannschreck K., Mihelcic D., Musgen P. Patz H.W., Holland F., Hofzumahaus A., Schafer H.J., Schroder S., Volz-Thomas A., Bachmann K., Schlomski S., Moortgat G., Grossmann D., 2003. Hydrocarbon measurements at Pabstthum during the BERLIOZ campaign and modeling of free radicals. Journal of Geophysical Research 108, D4, doi10.1029/2001JD000866.

Krol M., van Leeuwen P.J., Lelieveld J., 1998. Global OH trend inferred from methylchloroform measurements. Journal of Geophysical Research, 103, 10697-10711.

Krol M., Lelieveld J., Oram D.E., Sturrock G.A., Penkett S.A., Brenninkmeijer C.A.M., Gros V., Williams J., Scheeren H.A., 2003. Continuing emissions of methyl chloroform from Europe. Nature, 421, 131 – 135.

Krol M., Lelieveld J., 2003. Can the variability in tropospheric OH be deduced from measurements of 1,1,1-trichloroethane (methyl chloroform)? Journal of Geophysical Research, 108, Art. No. 4125.

Kurdziel M., 1998. The effect of different drying agents in the analytical data for non methane hydrocarbon concentrations in ambient air samples. Chemia Analityczna, 43, 387-397.

Kuster W.C., Goldan P.D., Albritton D.L.,1986. Ozone interferences with ambient dimethyl sulfide measurements: the problem and a solution. Eos Transactions AGU, 67, 882.

Larsen B., Bomboi-Minagro T., Brancaleoni E., Calogirou A., Cecinato A., Coeur C., Chatzianestis I., Duane M., Frattoni M., Fugit J.L., Hansen U., Jacob V., Mimikos N.,

Hoffmann T., Owen S., Perez-Pastor R., Reichmann A., Seufert G., Staudt M., Steinbrecher R., 1997. Sampling and analysis of terpenes in air. An interlaboratory comparison. Atmospheric Environment, 31, 35-49.

Leach J., Blanch A., Bianchi A.C., 1999. Volatile organic compounds in an urban airborne environment adjacent to a municipal incinerator, waste collection centre and sewage treatment plant. Atmospheric Environment, 33, 4309-4325.

Lee B.H., Munger J.W., Wofsy S.C., Goldstein A.H., 2006. Anthropogenic emissions of nonmethane hydrocarbons in the northeastern United States: Measured seasonal variations from 1992-1996 and 1999-2001. Journal of Geophysical Research, 111, Art. No. D20307.

Lehmpuhl D.W., Birks J.W., 1996. New gas chromatographic-electron-capture detection method for the detemination of atmospheric aldehydes and ketones based on cartridge sampling and derivatization with 2,4,6-trichlorophenylhydrazine. Journal of Chromatography, 740, 71-81.

Lelieveld J., Dentener F.J., Peters W., Krol M.C., 2004. On the role of hydroxyl radicals in the self-cleansing capacity of the troposphere. Atmospheric Chemistry and Physics, 4, 2337-2344.

Lelieveld J., 2006. New Directions: Watching over tropospheric hydroxyl (OH), Atmospheric Environment, 40, 5741-5743.

Levy H., 1971. Normal atmosphere – large radical and formaldehyde concentrations predicted. Science, 173, 141.

Lewis A.C., Carpenter L.J., Pilling M.J., 2001. Nonmethane hydrocarbons in Southern Ocean boundary layer air. Journal of Geophysical Research, 106, 4987-4994.

Llusia J., Penuelas J., 1998. Changes in terpene content and emission in potted Mediterranean woody plants under severe drought. Canadian Journal of Botany, 76, 1366-1373.

Logan J.A., 1981. Tropospheric chemistry – a global perspective. Journal of Geophysical Research, 86, 7210-7254.

Maiss M., Brenninkmeijer C.A.M., 1998. Atmospheric SF6: Trends sources and prospects. Environmental Science & Technology, 32, 3077-3086.

Mauldin R.L., Eisele F.L., Tanner D.J., Kosciuch E., Shetter R., Lefer B., Hall S.R., Nowak J.B., Buhr M., Chen G., Wang P., Davis D., 2001. Measurements of OH, H2SO4, and MSA at the South Pole during ISCAT. Geophysical Research Letters, 28, 3629-3632.

Mauldin R.L., Kosciuch E., Henry B., Eisele F.L., Shetter R., Lefer B., Chen G., Davis D., Huey G., Tanner D., 2004. Measurement of OH, HO2+RO2, H2SO4, and MSA at the South Pole during ISCAT 2000. Atmospheric Environment, 38, 5423-5437.

McKeen S.A., Liu S.C. (1993) Hydrocarbon ratios and photochemical history of air masses. Geophysical Research Letters, 20, 2363-2366.

Millet D.B., Goldstein A.H., Allan J.D., Bates T.S., Boudries H., Bower K.N., Coe H., Ma Y.L., McKay M., Quinn P.K., Sullivan A., Weber R.J., Worsnop D.R., 2004. Volatile organic compound measurements at Trinidad Head, California, during ITCT 2k2: Analysis of sources, atmospheric composition and aerosol residence times. Journal of Geophysical Research, 109, Art. No. D23S16.

Millet D.B., Donahue N.M., Pandis S.N., Polidori A., Stanier C.O., Turpin B.J., Goldstein A.H., 2005. Atmospheric volatile organic compound measurements during the Pittsburgh Air Quality Study: Results, interpretation, and quantification of primary and secondary contributions. Journal of Geophysical Research, 110, Art. No. D07S07.

Mochida M., Matsunage S., Kawamura K., 2003. A model evaluation of the NO titration technique to remove atmospheric oxidants for the determination of atmospheric organic compounds. Environmental Science and Technology, 37, 1589-1597.

Mount G.H., Williams E.J., 1997. An overview of the tropospheric OH photochemistry experiment, Fritz Peak Idaho Hill, Colorado fall 1993. Journal of Geophysical Research, 102, 6171-6186.

Mugica V., Vega E., Chow J., Reyes E., Sanchez G., Arriaga J., Egame R., Watson J., 2001. Speciated non-methane organic compounds emissions from food cooking in Mexico. Atmospheric Environment, 35, 1729-1734.

Na K., Kim Y.P., 2001. Seasonal characteristics of ambient volatile organic compounds in Seoul, Korea. Atmospheric Environment, 35, 2603-2614.

Namiesnik J., Wardencki W., 1999. Water vapour removal from gaseous samples used for analytical purposes. A review. International Journal of Environmental Analytical Chemistry, 73, 269-280.

Novelli P.C., Lang P.M., Masarie K.A., Hurst D.F., Myers R., Elkins J.W., 1999. Molecular hydrogen in the troposphere: Global distribution and budget. Journal of Geophysical Research, 104, 30427-30444.

O'Doherty S.J., Simmonds P.G., Nickless G., 1992. Analysis of replacement chlorofluorocarbons using Carboxen microtrap for isolation and preconcentration in gas-chromatography mass-spectrometry. Journal of Chromatography A, 657, 123-129.

Olivier M.G., Bougard J., Jadot R., 1996. Adsorption of propane, propylene and propadiene on activated carbon. Applied Thermal Engineering, 16, 383-387.

Omata A., Nakamura S., Yomogida K., Moriai K., Ichikawa Y., Watanabe I., 1990. Volatile components of TO-YO-RAN flowers (*Cymbidium faberi* and *Cymbidium virscens*). Agricultural and Biological Chemistry, 54, 1029-1033.

Panshin S.Y., Hites R.A., 1994. Atmospheric concentrations of polychlorinated biphenyls in Bermuda, Environmental Science and Technology, 28, 2001-2007.

Parrish D.D., Hahn C.J., Williams E.J., Norton R.B., Fehsenfeld F.C., Singh H.B., Shetter J.D., Gandrud B.W., Ridley B.A., 1992. Indications of photochemical histories of pacific air masses from measurements of atmospheric trace species at Point Arena, California. Journal of Geophysical Research, 97, 15883-15901.

Parrish D.D., Trainer M., Young V., Goldan P.D., Kuster W.C., Jobson B.T., Fehsenfeld F.C., Lonneman W.A., Zika R.D., Farmer C.T., Riemer D.D., Rodgers M.O., 1998. Internal consistency tests for evaluation of measurements of anthropogenic hydrocarbons in the troposphere. Journal of Geophysical Research, 103, 22339-22359.

Parrish D.D., FehsenfeldF.C., 2000. Methods for gas-phase measurement of ozone, ozone precursors and aerosol precursors. Atmospheric Environment, 34, 1921-1957.

Parrish D.D., Dunlea E.J., Atlas E.L., Schauffler S., Donnelly S., Stroud V., Goldstein A.H., Millet D.B., McKay M., Jaffe D.A., Price H.U., Hess P.G., Flocke F., Roberts J.M., 2004. Changes in the photochemical environment of the temperate North Pacific troposphere in response to increased Asian emissions. Journal of Geophysical Research, 109, Art.No. D23S18.

Plass C., Koppmann R., Rudolph J., 1993. Light-hydrocarbons in the surface-water of the mid-Atlantic. Journal of Atmospheric Chemistry, 15, 235-251.

Plass Dülmer C., Brauers T., Rudolph J., 1998. POPCORN: A field study of photochemistry in North Eastern Germany. Journal of Atmospheric Chemistry, 31, 5-31.

Plass-Dülmer C., Michl K., Ruf R., Berresheim H., 2002. C-2-C-8 hydrocarbon measurement and quality control procedures at the Global Atmospheric Watch Observatory Hohenpeissenberg. Journal of Chromatography A, 953, 175-197.

Platt U., Heintz F., 1994. Nitrate radicals in tropospheric chemistry. Israel Journal of Chemistry, 34, 289-300

Pollmann J., Helmig D., Hueber J., Tanner D., Tans P.P., 2006. Evaluation of solid adsorbent materials for cryogen- free trapping – gas chromatographic analysis of atmospheric C2-C6 non-methane hydrocarbons. Journal of Chromatography A, 1134, 1-15.

Pollmann J., Helmig D., Hueber J., Plass-Dülmer C., 2007. Sampling, storage, and analysis of C2-C7 non-methane hydrocarbons from whole air glass sampling flasks. In preparation.

Prinn R.G., Weiss R.F., Miller B.R., Huang J., Alyea F.N., Cunnold D.M., Fraser P.J., Hartley D.E., Simmonds P.G., 1995. Atmospheric trends and lifetime of CH3CCl3 and global OH concentrations. Science, 269, 187-192.

Prinn R.G., Huang J., Weiss R.F., Cunnold D.M., Fraser P.J., Simmonds P.G., McCulloch A., Harth C., Salameh P., O'Doherty S, Wang R.H.J., Porter L., Miller B.R., 2001. Evidence for substantial variations of atmospheric hydroxyl radicals in the past two decades. Science, 292, 1882-1888.

Prinn R.G., 2003. The cleansing capacity of the atmosphere. Annual Review of Environment and Resources, 28, 29-57.

Prinn R.G., Huang J., Weiss R.F., Cunnold D.M., Fraser P.J., Simmonds P.G., McCulloch A., Harth C., Reimann S., Salameh P., O'Doherty S., Wang R.H.J, Porter L.W., Miller B.R., Krummel P.B., 2005. Geophysical Research Letters, 32, Art. No. L07809.

Pszenny A.A.P., Fischer E.V., Russo R.S., Sive B.C., Varner R.K., 2007. Estimates of Cl atom concentrations and hydrocarbon kinetic reactivity in surface air at Appledore Island, Maine (USA), during International Consortium for Atmospheric Research on

Transport and Transformation/Chemistry of Halogens at the Isles of Shoals. Journal of Geophysical Research, 112, Art. No. D10S13.

Ramacher B., Rudolph J., Koppmann R., 1999. Hydrocarbon measurements in the spring arctic troposphere during the ARCTOC 95 campaign. Tellus B, 49, 592-601.

Rappenglück B., Apel A., Bauerfeind M., Bottenheim C., Brickell P., Čavolka P., Cech J., Gatti L., Hakola H., Honzak J., Junek R., Martin D., Noone C., Plass-Dülmer C., Travers D., Wang D., 2006. The first VOC intercomparison exercise within the Global Atmosphere Watch (GAW). Atmospheric Environment, 40, 7508-7527.

Ren X.R., Brune W.H., Mao J.Q., Mitchell M.J., Lesher R.L., Simpas J.B., Metcalf A.R., Schwab J.J., Cai C.X., Li Y.Q., Demerjian K.L., Felton H.D., Boynton G., Adams A., Perry J., He Y., Zhou X.L., Hou J., 2006. The behavior of OH and HO2 in the winter atmosphere in New York city. Atmospheric Environment, 40, S252-S263.

Ren X.R., Brune W.H., Cantrell C.A., Edwards G.D., Shirley T., Metcalf A.R., Lesher R.L., 2005. Hydroxy and peroxy radical chemistry in a rural area of Central Pennsylvania: observations and model comparisons. Journal of Atmospheric Chemistry, 52, 231-257.

Rhee T.S., Brenninkmeijer C.A.M., Rockmann T., 2006. The overwhelming role of soils in the global atmospheric hydrogen cycle. Atmospheric Chemistry and Physics, 6, 1611-1625.

Riano D., Ruiz J.A.M., Isidoro D., Ustin S.L., 2007. Global spatial patterns and temporal trends of burned are between 1981 and 2000 using NOAA-NASA Pathfinder. Global Change Biology, 13, 40-50.

Rohrer F., Berresheim H., 2006. Strong correlation between levels of tropospheric hydroxyl radicals and solar ultraviolet radiation. Nature, 442, 184-187.

Rudolph J., 1995. The tropospheric distribution and budget of ethane. Journal of Geophysical Research, 100, 11369-11381.

Rudolph J., Wedel A., Schuh G., Heiden A., Wildt J., 1997. Emissions of volatile organic compounds from agriculturally used vegetation: ambient measurements, field studies of emissions and laboratory investigations. Workshop on Biogenic Hydrocarbons in the Atmospheric Boundary Layer, University of Virginia, Charlottesville, pp. 22-25.

Sahu L.K., Lal S., 2006. Characterization of C-2-C5NMHCs and related gases at a tropical urban site in India. Atmospheric Environment, 40, 880-891

Sanchez J.M., Sacks R.D., 2005. On-line multi-bed sorption trap for VOC analysis of large-volume vapor samples: injection plug width, effects of water vapor and sample decomposition. Journal of Separation Science, 28, 22-30.

Schuh G., Heiden A.C., Hoffmann T., Kahl J., Rocke, P., Rudolph J., Wildt J., 1997. Emissions of volatile organic compounds from sunflower and beech: dependence on temperature and light intensity. Journal of Atmospheric Chemistry, 27, 291-318.

Shu Y., Atkinson R., 1994. Rate constants for the gas-phase reactions of O_3 with a series of terpenes and OH radical formation from the O_3 reactions with Sesquiterpenes at 296 +/- 2K. Journal of Chemical Kinetics, 26, 1193-1204.

Shu Y., Atkinson R., 1995. Atmospheric lifetimes and fate of a series of Sesquiterpenes. Journal of Geophysical Research, 100, 7275-7281.

Singh H.B., Viezee W., Chen Y., Bradshaw J., Sandholm S., Blake D., Blake N., Heikes B., Snow J., Talbot R., Browell E., Gregory G., Sachse G., Vay S., 2000. Biomass burning influences on the composition of the remote South Pacific troposphere : analysis based on observations from PEM-Tropics-A. Atmospheric Environment, 34, 635-644.

Sinha V., Williams J., Meyerhofer M., Riebesell U., Paulino A.I., Larsen A.I., 2007. Air-sea fluxes of methanol, acetone, acetaldehyde, isoprene and DMS from a Norwegian fjord following a phytoplankton bloom in a mesocosm experiment. Atmospheric Chemistry and Physics, 7, 739-755.

Sirgu A. P., Shepson P.B., 1995. Laboratory and field investigation of the DNPH cartridge technique for the measurement of atmospheric carbonyl compounds. Environmental Science and Technology, 29, 384-392.

Slinn W.G.N., 1988. A simple model for Junge's relationship between concentration fluctuations and residence time for tropospheric trace gases. Tellus B, 40, 229-232.

Smith S.C., Lee J.D., Bloss W.J., Johnson G.P., Ingham T., Heard D.E., 2006. Concentrations of OH and HO2 radicals during NAMBLEX: measurements and steady state analysis. Atmospheric Chemistry and Physics, 6, 1435-1453.

Solberg S., Derwent R.G., Hov o., Langner J., Lindskog A., 2005. European abatement of surface ozone in a global perspective. Ambio, 34, 47-53.

Spivakovsky C.M., Logan J.A., Montzka S.A., Balkanski Y.J., Foreman-Fowler M., Jones D.B.A., Horowitz L.W., Fusco A.C., Brenninkmeijer C.A.M., Prather M.J., Wofsy S.C., McElroy M.B., 2000. Three-dimensional climatological distribution of tropospheric OH: Update and evaluation. Journal of Geophysical Research, 105, 8931-8980.

Stockwel, W.R., Kirchner F., Kuhn M., Seefeld S., 1997. A new mechanism for regional atmospheric chemistry modelling. Journal of Geophysical Research, 102, 25,847-25,879.

Strömvall, A.M., Peterson, G., 1992. Protection of terpenes against oxidative and acid decomposition on adsorbent cartridges. Journal of Chromatography, 589, 385-389.

Sturges W.T., Elkins J.W., 1993. Use of adsorbents to collect selected halocarbons and hydrohalocarbons of environmental interest from large air volumes. Journal of Chromatography A, 642, 123-134.

Swanson A.L., Blake N.J., Atlas E., Flocke F., Blake D.R., Rowland F.S., 2003. Seasonal variations of C-2-C-4 nonmethane hydrocarbons and C-1-C-4 alkyl nitrates at the Summit research station in Greenland. Journal of Geophysical Research, 108, Art. No. 4065.

Tan D., Faloona I., Simpas J.B., Brune W, Olson J., Crawford J., Avery M., Sachse G., Vay S., Sandholm S., Guan H.W., Vaughn T., Mastromarino J., Heikes B., Snow J., Podolske J., Singh H., 2001a. OH and HO2 in the tropical Pacific: Results from PEM-Tropics B. Journal of Geophysical Research, 106, 32667-32681.

Tan D., Faloona I., Simpas J.B., Brune W., Shepson P.B., Couch T.L., Sumner A.L., Carroll M.A., Thornberry T., Apel E., Riemer D., Stockwell W., 2001b. HOx budgets in a deciduous forest: Results from the PROPHET summer 1998 campaign. Journal of Geophysical Research, 106, 24407-24427.

Tang Y.Z., Cheng W.K., Fellin P., Tran Q., Drummond I., 1996. Laboratory evaluation of sampling methods for C-1 to C-4 hydrocarbons. American Industrial Hygiene Journal, 57, 245-250.

Tanner D., Helmig D., Hueber J., Goldan P., 2006. A gas chromatography system for the automated, unattended, and cryogen-free monitoring of C2 to C6 non-methane hydrocarbons in the remote troposphere. Journal of Chromatography A, 1111, 76-88.

Thornton D.C., Bandy A.J., Blomquist B.W., Anderson B.E., 1995. Impact of anthropogenic and biogenic sources and sinks on carbonyl sulfide in the North Pacific troposphere. Journal of Geophysical Research, 101, 1873-1881.

Trolier M., White J.W.C., Tans P.P., Masarie K.A., Gemery P.A., 1996. Monitoring the isotopic composition of atmospheric CO2: Measurements from the NOAA Global Air Sampling Network. Journal of Geophysical Research, 101, 25897-25916.

Tsai W.Y., Chan L.Y., Blake D.R., Chu K.W., 2006. Vehicular fuel composition and atmospheric emissions in South China: Hong Kong, Macau, Guangzhou, and Zhuhai. Atmospheric Chemistry and Physics, 6, 3281-3288.

Velasco E., 2003. Estimates for biogenic non-methane hydrocarbons and nitric oxide emissions in the Valley of Mexico. Atmospheric Environment, 37, 625-637.

Vrekoussis M., Kanakidou M., Mihalopoulos N., Crutzen P.J., Lelieveld J., Perner D., Berresheim H., Baboukas E., 2004. Role of the NO3 radicals in oxidation processes in the eastern Mediterranean troposphere during the MINOS campaign. Atmospheric Chemistry and Physics, 4, 169-182.

Wedel A., Müller K.-P., Ratte M., Rudolph J., 1998. Measurements of Volatile Organic Compounds (VOC) During POPCORN 1994: Applying a New On-Line GC-MS-Technique. Journal of Atmospheric Chemistry, 31, 73-103.

Williams J., Fischer H., Harris, G.W., Crutzen P.J., Hoor, P., Hansel A., Holzinger R., Warneke C., Lindinger W., Scheeren B., Lelieveld J., 2000. Variability-lifetime relationship for organic trace gases: A novel aid to compound identification and estimation of HO concentrations. Journal of Geophysical Research, 105, 20473-20486.

Williams J., Gros V., Bonsang B., Kazan, V., 2001. HO cycle in 1997 and 1998 over the southern Indian Ocean derived from CO, radon, and hydrocarbon measurements made at Amsterdam Island. Journal of Geophysical Research, 106, 12719-12725.

Williams J., de Reus M., Krejci R., Fischer H., Strom J., 2002. Application of the variability-size relationship to atmospheric aerosol studies: estimating aerosol lifetimes and ages. Atmospheric Chemistry and Physics, 2, 133-145.

Williams J., 2004 Organic trace gases: An overview. Environmental Chemistry, 1, 125-136.

Winter A., Arey J., Atkinson R., Achman S., Long W., Morrison L., Olszyk D., 1992. Emission rates of organics from vegetation in California's Central Valley. Atmospheric Environment, 26, 2647-2659.

WMO GAW Report No. 111, WMO-BMBF workshop on VOC establishment of a "World calibration/instrument intercomparison facility for VOC" to serve the WMO global atmospheric watch (GAW) programme, Garmisch-Partenkirchen, Germany, 1995.

WMO GAW Report No. 171, A WMO/GAW expert workshop on global long-term measurements of volatile organic compounds (VOCs), Geneva, Switzerland, 2006.

Yang K.L., Ting C.:, Wang J.L., Wingenter O.W., Chan C.C., 2005. Diurnal and seasonal cycles of ozone precursors observed from continuous measurement at an urban site in Taiwan. Atmospheric Environment, 39, 2829-2838.

Zhang Q.H., Birgersson G., Zhu J.W., Lofstedt C., Lofqvist J., Schlyter F., 1999. Leaf volatiles from nonhost deciduous trees: Variation by tree species, season and temperature and electrophysical activity in Ips Typographus. Journal of Chemical Ecology, 25, 1923-1943.